THE UNIVERSITY OF HULL

Development of environmental water monitors based on hydrostatic and fluorescence detection techniques

being the Thesis submitted for the
Degree of Doctor of Philosophy

by

Robin M Scott BSc (Hons) MSc

September 2009

Acknowledgement

I would like to thank all those who assisted me in the work for my PhD. Particularly my supervisors Professor Gillian Greenway and Dr Howard Snelling for their guidance throughout my research and in the preparation of my thesis. Also, to Gordon Sowersby for his technical help in making the electronic equipment and in setting up some of the experiments and his general advice throughout my research. To the glass technicians in the Chemistry department for making the specialist parts required. Above all, my peers in the Physics department who made my time here most enjoyable and arriving each morning was something to look forward to, especially afternoon tea with Rozalina Zakaria, Manea Al Khalifah and Adam Law.

Abstract

The research for this thesis led to the development of two environmental detectors, whose function was to identify predetermined threshold levels of the analyte. The research centred onto two types of analyte; immiscible and dissolved, both occurring in water based locations.

The first detector was developed to detect the accumulation of oil within an oil/water interceptor. Pollution from oil spillages is a major contaminate of water systems and the control of this potentially hazardous material has legal obligations. This liquid, which naturally separates from water, accumulates within the interceptor enclosure and can be removed once the quantity of oil reaches the desired level. However, the often unpredictable nature of oil leaks and spillages means that the accumulation of oil within an interceptor is an irregular occurrence. Interceptor detectors based upon electrical techniques already exist. This research specifically developed a detection system that operated without any electrical devices within the interceptor. The research explored several possible avenues, eventually pursuing a technique based upon pressure change, based on the density differential between water and oil. The final system was capable of identifying when the oil had reached a depth of 200 to 250 mm within the interceptor.

The second detection system, a portable microfluidic fluorimeter, was intended for placement in locations for the direct analysis of water. Glutathione was chosen as a model analyte, associated with a sex pheromone and prior to the onset of spawning may be found in high concentrations. The system that has been developed is capable of selectively sensing glutathione to below 10 µM. However, the threshold concentration in the proximity of its release as a pheromone is greater than 100 µM and within this range the fluorimeter produced a linear response. The fluorimeter used an LED light source with a PMT detector. An analysis could be made every seven minutes, using 150 µL each of analyte and reagent for every cycle. Through assessment of a pre-made standard, the viability of the microfluidic system could be assured with regards to blockages or other malfunctions of the system.

Table of contents

1. Introduction

Environmental analysis has become a part of life and the techniques used are as varied as the analytes themselves. The purpose for such examinations may be for no other reason than curiosity, although for a larger number the purpose will usually be for economic, safety or legal requirements. For both the determination of a trend or simply to substantiate a stable condition, a number of analyses must take place over a period of time. An analysis may be performed in a laboratory and, in particular cases, this may be the only technique available but where continuous or regular periodical analyses are required laboratory testing is not always practical or cost effective. In these instances, the use of automated in-field monitoring, suitably located, along with appropriate analytical equipment, can provide an efficient alternative data collection system.

This thesis presents the work undertaken to develop two automated monitors that are to be employed in two different environments, which for their own purposes required observation. In both cases the concentrations of the particular analyte are analysed to determine whether they have increased to an amount where they have exceeded a predetermined level, subsequently triggering a response.

1.1 Background to environmental monitoring

Throughout time people have been aware of the weather and of seasonal fluctuations but without a means to measure or test these variables, comparisons could not easily be made and it was harder still to truly record events or findings. The 17th century developments saw the first thermometers where accurate and comparable temperature measurements could be observed and recorded. Using methods such as the Beaufort scale, wind speed could be recorded more accurately but until reliable clocks were developed, more precise measurements that required a time-scale could not be made.

The 19th and 20th centuries brought accurate measuring equipment capable of analysing physical and chemical quantities over a range of magnitudes. With an awareness of the effects of industrialisation and an increasing human population, the last fifty years have seen an increase in environmental monitoring. With more

techniques available and a greater awareness of chemical and biological interactions, a greater number of chemicals and their effects are being assessed, all of which require someone and something to monitor and record them.

Important repercussions that can effect the health of humans or have been caused by human activity such as lead in water, acid rain and the persistence of DDT [1] are well known. As technology is further developed, the opportunity to examine more substances in a greater number of locations is ever increasing. The advances in electronics and the use of micro-fluidics have extended the ability for monitoring to occur in a greater number of places.

1.2 Applications for environmental analysis

There are, at times, requirements for physical and chemical conditions to be met for the safety and well-being of people, structures and the environment. These are often implemented through local, national and international laws or guidelines. However, before any decision or judgement can be made as to what is a safe or reasonable limit, knowledge of the present and maybe historic circumstances would be required.

The presence of pollutants, their source and tractability is an important issue, which concerns governments and individuals. The European Community's Drinking Water Directive 98/83EC for instance, dictates to the member countries maximum permissible levels of undesirable substances in drinking water; this is a list of chemical and biological material that for the safety of people are considered to be detrimental in excess. Nitrates (NO_3^-) for example, must not exceed concentrations of 50 mg L^{-1} [2]. However, before such a law is implemented, the substance has to be associated with being a problem. Following this, the extent of any material must be monitored in a variety of locations for a period of time to find the extent of any problem, legislation, if required is then set in place. After any problem has been identified, monitoring may need to continue to check upon compliance

For the assessment of any parameter, the method of analysis has to be standardised. Without this, results would possibly vary and the analytical values diminish or become worthless. Determination of the moisture content of grain, for instance, has industrial standards, set out by the National Institute of Standards and Technology, whereby the grain's moisture is extracted and expressed as a percentage of the mass. There are only

certain accepted methods for giving this reproducible standard. These methods are not practical for everyday use and as in this case, as with many other measurements, everyday analyses are undertaken using different instruments which are calibrated directly or indirectly against known standards.

With advances in technology there is an increasing number of environmental locations and events that may be monitored, principally, they can be categorised into three main groups; air, land and aquatic.

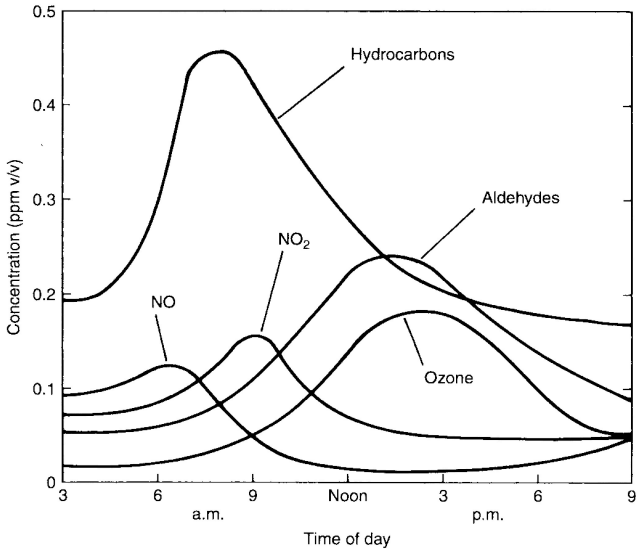

Figure 1.1. *Variation of atmospheric concentrations during a photochemical smog incident [2].*

The air can be analysed for gases, particulates or its physical state. The air may be contained within structures or be part of the open atmosphere. Gases can mix through diffusion, convection and mass movement through air currents, the latter two being particularly important in the open atmosphere. Gas in the atmosphere has the opportunity to mix naturally through the weather systems, an analysis of the major constituents of air, nitrogen, oxygen, argon and carbon dioxide and for the majority of the time analogous at most locations throughout the world. There are exceptions to this, where locally, due to human or natural activities there will be local variations even if only on a temporary basis. It is these variations that create the opportunity for environmental monitoring to take place. Figure 1.1 is a graph that shows the variation of the chemical constituents of air within a city and how the concentrations may vary over a relatively short period of time, before ultimately being incorporated into the

atmosphere as a whole [2]. These gases and any particles can then be transported and deposited or be integrated into other non atmospheric systems.

The land, through its more static nature, is more complex and diverse than air and consists of a far greater content of organic material. The opportunities for environmental monitoring are less than for the other two media, as once a particular location has been analysed, there is little need for reassessment as change will occur far more slowly. Any modification will have had to be brought about through the interaction of biological activity, deposits from the air or water, or through human activity. It will be mainly due to human activities with particular regard to pollution that will see the requirement to monitor an area [3].

Aquatic locations, which are the main interest of this research, include the sea, fresh water including rivers and drainage channels, are similar to air insomuch as each location will have the opportunity to mix over time. Here, as with the air, local variations can occur, these may be fluctuations varying from daily to seasonal periods. Water contaminants can be physical or chemical and this can have a diverse effect upon the ecology. Pollutants may directly kill the wildlife or distort the balance within a locality through the increase of a particular species at the expense of others. It is possible that no effect is directly noticed, for example, the bioaccumulation of mercury can have a harmful effect further down the food chain [4]. So depending upon the particular contaminant, the techniques that are useful to determine one type of pollutant may be quite unsuitable to evaluate another. Pollution caused by humans that enters water systems can, to some extent, be controlled and here environmental monitoring plays an important role. The well being of a particular ecosystem may not necessarily be an indicator to the state of the aquatic environment as a whole.

As with the variation of the chemical status of the air, as discussed above, the physical and chemical status of an aquatic system may also vary through a short period of time. The importance of a high sampling frequency can be seen in figure 1.2 [5], here, temporal resolution reveals information that would otherwise be lost through lower sampling frequencies. Automated field deployed analysis, like that shown above, is able to capture data over long spans of time that in the past was only available for less intense analytical methods. The two types of monitor that are examined in this research consider contrasting aquatic locations; the first is an enclosed body of liquid, an oil

interceptor, where the analyte only varies insomuch as it increases in total. The first monitor is required to examine a situation where the analyte would be expected to increase over time. The second monitor is designed to assess samples from an open body of water where the quantity of analyte may vary by increasing or decreasing in concentration over time.

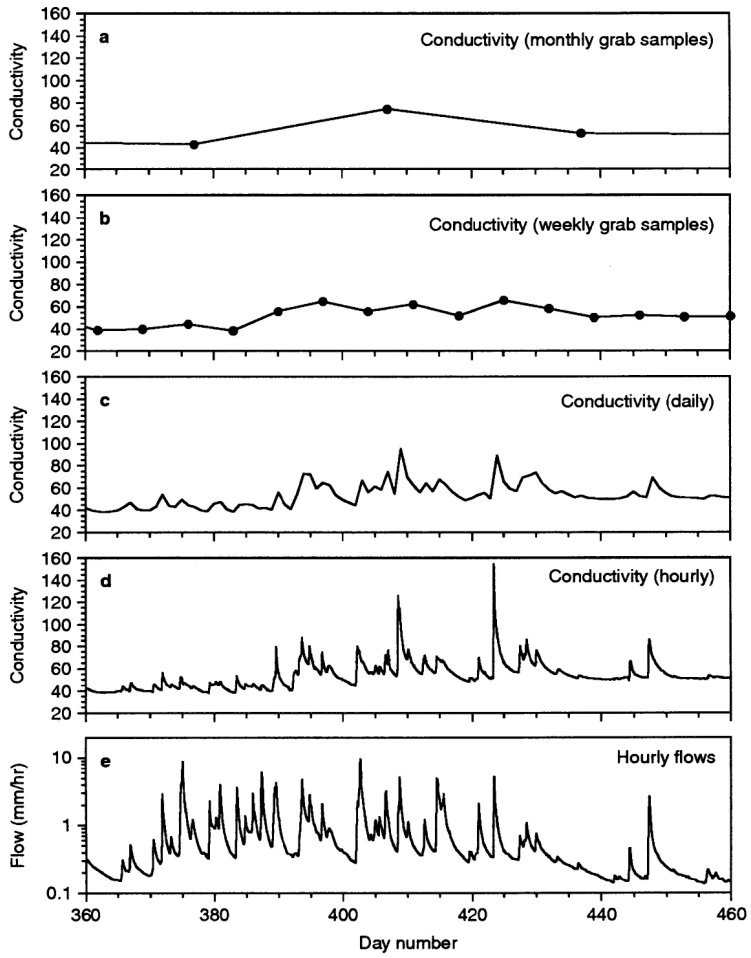

Figure 1.2. *Electrical conductivity measured monthly, weekly, daily and hourly in a Welsh stream, the variations are shown against the water flow rate [5].*

It is not just for the assessment of pollutants that environmental monitoring is important. Biological and other natural activities are also of concern, as these can have economic consequences, such as industrial and food production. Monitoring any system can help in the evaluation of environmental risk.

1.3 Sampling

Good reliable data must be a fair representation of the area being analysed. A sample is only a portion of the whole and the careful collection of this portion is imperative for a

representative analysis. The greater the number of samples gathered, the higher the likelihood the analysis will be to represent the mass as a whole. The area sampled may be homogenous or vary to a greater or lesser extent and as such there should be reasoning behind the chosen sampling points.

Analysis of the sample can take place in situ, the results of which could be instantaneous for a pH measurement or up to several minutes for a chemical reaction, alternatively, the sample or samples may be stored for later retrieval and analysis. When samples are to be examined either off site or at a later time, storage procedures must be consistent; standard protocols may exist within a trade, nationally or internationally [6]. Sample storage for one particular site may not necessarily be suitable for another, due to chemical differences in the water matrix [7]. The management of the sample whether it be as pre-treatment, conditions for storage, time between sample and testing should be to enhance the reliability of the final result.

The format of the results may represent an average reading where appropriate, alternatively there may be requirements to show the range of the results. The goals of any study should be clear as this will ultimately be the driver for the analysis.

1.4 Monitoring systems

The types of environmental monitors range from the simplest liquid filled thermometer to the most sophisticated satellite monitoring systems. Whatever category a monitor fits into, the basic task is to provide data that is reasonably accurate in characterising a place or particular point over a period of time. This time period may be a single instance or it may be for a prolonged period. Similarly, the data gathered may be a collection of separate pieces of information or may be an average of several data points. Results can either be gathered manually or recorded. Traditionally the commonest way of automatic recording was by tracing with ink onto paper, this being interpreted at a later date. Today most results are kept electronically, however, before the collected data can be stored, this data has to be converted into electrical signals.

The information required will greatly influence the mode of data collection. For instance, if air speed or a river flow rate is required, a physical measurement would be the most appropriate and this could well be achieved through a mechanical movement of a turbine or through a pressure variation. For a chemical analysis, the system of

producing an electronic readout may not be as direct, this may be made more complicated by the need to draw a sample into a reaction chamber.

The frequency of analysis will vary depending upon the circumstances. For example, an incinerator temperature may well be an indicator of the dioxin emission into the atmosphere and continuous monitoring would be appropriate, followed up by direct testing on periodic basis [3], whereas average daily temperatures could be represented by a mean of regular discrete samples.

Environmental monitors investigating the levels of chemical species within a body of water, whether it is a confined volume or an open system, requires establishing the frequency of analysis. Continuous analysis may be desired but this may be restricted by the duration of the analytical measurement, if for instance each test takes a period of time to perform. The expense of each analysis may be prohibitive and a compromise between cost and information would need to be reached. Large amounts of data will not always be required and reducing the sample frequency will limit a waste of resources. Occasional assessment may be sufficient if the expected change of the analyte or condition is gradual.

Field deployment of chemical analytical systems has been used for several decades. Flow injection analysis (FIA) uses the continuous flow of the analyte or the medium in which the analyte would be found. Here, the reagent is injected into the flow and after allowing time for any reaction, detection occurs further along the flow line. This methods allows high resolution monitoring and is particularly useful for water based environments [8]. For analytical techniques that require less frequent sampling, sequential injection analysis (SIA) has advantages over FIA due to a less complex mechanical arrangement and also because less reagent volume is used, resulting in the need for smaller waste storage [9, 10]. Through the use of modern electronic devices, the development of micro FIA makes use of micro pumping and detection systems [11] allowing more efficient usage of reagents. Micro-fluidic devices introduced in the early 1990s [12], operating at μL/minute flow rates [13] permit automated environmental monitoring with not only low chemical consumption but also importantly low power expenditure, increasing the lifetime of the device between services.

1.5 Requirements for self contained monitors

The size and shape of the monitor will principally be determined by its particular application and location. Monitors for environmental assessment will predominantly be situated in locations exposed to the weather or at least part open to the elements. Other factors such as whether there is a need for the data to be constantly relayed or if the data may be stored for later use, the time period between sampling, the duration of the sample period, the type of analysis and access to a power supply, will all help to establish the type of equipment needed inside the unit. The time required between supervision and servicing will all contribute to the design of the monitor.

The power requirements of the monitor will be determined by several factors. Firstly, the method of analysis, this may require motors and other equipment, together with the frequency of sampling. Secondly, the length of time that the monitor will be expected to run unsupervised. Monitors that only check the temperature for instance, will require smaller amounts of power. Battery power is convenient and allows flexibility in remote regions, these can be easily replaced when necessary or be recharged through solar panels or wind turbines if the monitor is on a more permanent site. Mains electricity may well be suitable where the location allows.

Analysis requiring chemical reactions needs storage for several substances, such as reagents and flushing liquids, as well as waste storage. The use of micro-reactors reduces these volumes but nevertheless the access and storage is another consideration of the monitor contents and interior design.

As most analysis is ultimately interpreted electronically, data storage can be held digitally on a memory card. Retrieval of information may later be down loaded or the memory card can be removed and replaced. The ability to self test and give a failure warning are important attributes in a monitor. A testing strategy may be required in an active monitor where chemicals or the testing equipment requires to be checked prior to each analysis or periodically to make sure that the chemicals are still suitable or that power is adequate.

Any monitor, whilst having access ports for sampling and communication, still needs to be protected against the ingress of unwanted outside material. The degree of which will depend upon the type of the location to where it is placed. It is preferable that the

interface is user friendly, functionality is not always sufficient as ease of use is important. This is particularly helpful if the monitor requires readjustment of the sampling parameters, chemical or general servicing.

In later chapters, two types of monitoring systems are investigated. The first one, monitors whether a predetermined threshold has been passed, this could be reached in a short period of time or may not be reached for many years. For this type of monitoring, a constant real time feedback of information may be required. The second type of monitor captures data that only later will be used. For this form of data collection, no continuous outside communication is necessary, the data needs to be stored for later retrieval.

1.6 Signal evaluation

For the measurement of most analytes, the resulting reaction is at some stage of the process converted into an electrical signal. The value of collecting results in an electrical form are several, they can be quantified, readily compared and easily stored in an electronic form. The down-side is that is that these electrical signals can, or more likely, will carry an unwanted additional electrical component; this extra part is known as noise.

1.6.1 Noise and limits of detection

The noise may come from several sources, the most common being the natural, environmental and instrumental. Natural noise arises from atmospheric and cosmic radiation and through arrangement of components, referred to as pick-up and can be significantly reduced by not having a high input impedance and by providing sufficient shielding and a good earth.

Environmental noise which comes from man-made sources, such as power lines, electrical wiring and switches, vehicle ignition systems, TV and radio, may appear as periodic or random pluses, these will vary in intensity depending upon the location of the detector [14]. Figure 1.3 shows relative power and frequency of environmental noise for a typical location [15]. Instrument noise is attributed to the electrical components within the detection system (including amplifiers etc.), these can be further subdivided; circuit noise, shot noise, flicker noise, thermal and other types. The result of which is

the unwanted random movement of electrons around the electrical circuits which give rise to a false signal, and due to its nature this cannot be eliminated but can be minimised by cooling and reducing bandwidth.

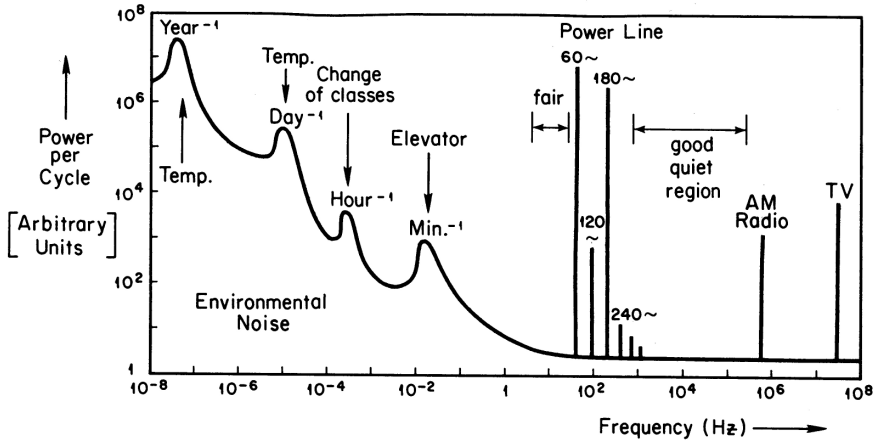

Figure 1.3. *Graph showing environmental noise as a function of frequency, for a typical location [15].*

Although not strictly noise, any background signal that is produced from a blank/control for various reasons that cannot be removed will all be part of a residual background signal. This background will tend to produce a continuous signal as opposed to the fluctuations of the electronic noise. The background plus any noise will form the baseline over which the analytical signal should be seen.

For much analytical analysis, noise is not particularly an issue, either the instrument being used has been designed to sufficiently reduce its effect or the range that the instrument can accurately examine has been predetermined. Noise only starts to have a significant effect towards the lower limit of detection (LOD). As the analyte concentration decreases and the signal lessens, the signal to noise ratio (S/N), where N is the mean of the noise, as shown in equation (1.1).

$$\text{Signal to noise ratio} = \frac{\text{Signal}}{\text{Noise}} \qquad (1.1)$$

As the S/N ratio decreases, the recovery of the signal becomes difficult to impossible as the signal is embedded within the fluctuations of the noise and may well be the limiting factor for particular analytical systems. There are several methods used to derive the lower LOD. One method is based around the S/N being equal to 2 or 3 [16]. This method may have limitations particularly if the noise varies over a large range. A

second method is based upon the standard deviation (σ) of the background signal/noise, then the LOD is determined to be the signal having a value greater than 2.5σ [17] to 3σ [6, 18] of the mean, giving a > 99 % confidence level that the analyte has been detected. Whereby any signal below 3σ will be classified as an undetected assay.

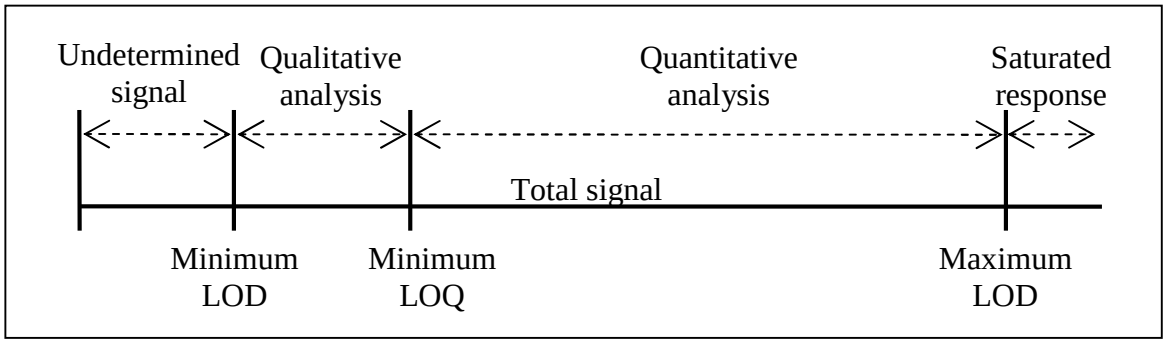

Figure 1.4. *The regions where the analytical signal may fall.*

Once above the minimum criteria for the lower LOD the analyte can confidently be detected but not necessarily be quantified. As the detected analyte concentration is raised, the signal may not significantly or detectably increase and as such the level of quantification (LOQ) may not as yet be reached. For particular analyses a value greater than 10σ may be preferred for a reliable LOQ [6, 19].

As well as lower LOD most instruments will have an upper limit for detection or for quantification. This may be due to the size or weight that can be accommodated or, as with optical instruments, the detectors may be saturated as the maximum signal has been reached. With some detectors, such as a pressure transducer, beyond its maximum detection limit damage may occur to the components, such as electrical or physical. These regions of analysis are shown in figure 1.4. Laboratory instruments may have inbuilt safeguards but when building detectors from individual parts, knowledge of safe working limits of the components is important.

1.6.2 Signal handling

Once the analysis has been performed and the results are in an electrical format, there are several processes that can be performed upon the signal, although it is important that the actual data is not distorted in any way that may give a false analysis.

It is probable that when analysing micro quantities of a material, results will vary around a particular mean figure [20], then averaging these results over a period of time

will give a more meaningful assessment of the analyte. Alternatively the acquisition time for each analysis can be taken over a longer period.

With most instruments, the electrical response will need to be amplified to a higher level for the information to be assessed. It is unfortunate that along with the signal, the noise is also amplified and once the lower LOD is reached, amplification alone cannot increase this limit any further. The use of a lock-in amplifier or phase sensitive detector, as they are also known, has the ability to recover a signal that appears to be swamped by noise or background readings. For this type of instrument to work, the signal from the analyte needs to be capable of being pulsed (modulated), fluorescence analysis is particularly suited as the excitation source can be electronically pulsed or mechanically chopped. This in turn will produce an oscillating fluorescence emission signal at the frequency of the excitation light, giving the wanted part of the electronic response a signature. The phase sensitive part of the detector also receives a reference signal that matches that of the pulsed light source and from this the noise can be separated from the signal, thereby increasing the S/N several fold, lowering the LOD. By choosing a pulse frequency in the quiet region, see figure 1.3, the effect of environmental noise can be reduced. The lock-in amplifier can also diminish the signal swamping effects of small amounts of ambient light falling onto the analyte [21], although the total light is required to be within the range of the light detector. This system will not be able to reduce any effect of the excitation light falling upon the detector as it will be in phase with the emission light, hence the need for optical filtering.

1.7 Optical methods of analysis

Detection through optical analysis allows the examination of a number of chemical and physical properties of the analyte. For most optical systems, an artificial light source is required, accompanied with a suitable detector. The light source and detector are discussed in chapter 6. Chemiluminescence is the exception as it does not require a light source, for this, the analyte and a reagent are mixed and a chemical reaction creates its own emitted light.

For an automated optical portable detector, analysis of the chemical properties (absorption, transmission and fluorescence), along with the physical properties of reflection and total internal reflection, TIR, are further discussed.

1.7.1 Absorption and transmission

Photons directed towards an object are either reflected, absorbed or transmitted (including refraction and scattering). When the radiation passes through matter, the discrete quantum energy of each individual photon may be selectively absorbed by the atom or molecule. The discretion of the matter to absorb the photon is dependant upon whether the photon energy can match the vibrational, rotational or electronic energy band structure of the atomic and molecular systems through which it passes. The different energy values of the photons affect their interactions with the absorbing material, lower energy photons excite the atomic bonds, whereas higher energy photons may induce electronic transitions. The higher energy photons, mainly from the visible to the UV part of the spectrum, that are able to excite electrons are absorbed in 10^{-14} to 10^{-15} seconds. This incorporation of energy occurs so rapidly that inertia free electrons become excited before any vibration of the much heavier nucleus has time to take place, being known as the Franck-Condon Principle [22].

The absorption spectrum of a particular material can be assessed in the laboratory using a spectrophotometer, here, the absorption is indirectly measured. Using a light source suitable for the specific spectra, the intensity of the transmitted light, I, is compared to the original intensity, I_o. The transmittance, T, is defined in equation (1.2).

$$T = \frac{I}{I_o} \tag{1.2}$$

The transmittance can also be expressed as a percentage (%T being % transmission), as shown in equation (1.3).

$$\%T = T \times 100 \tag{1.3}$$

From T the absorbance, A, in equation (1.4).

$$A = -\log T = \log \frac{I_o}{I} \tag{1.4}$$

The comparison to transmittance can be seen in figure 1.5 [23]. Then for a straightforward reference A = 2 –log %T (%T ≠ 0). A has a logarithmic value but is plotted as a linear scale. Here it must be noted that reflection has not been accounted for

(deducted), and in this case is classed as external absorption. Where reflection has been accounted for, the remaining light loss is termed internal absorption.

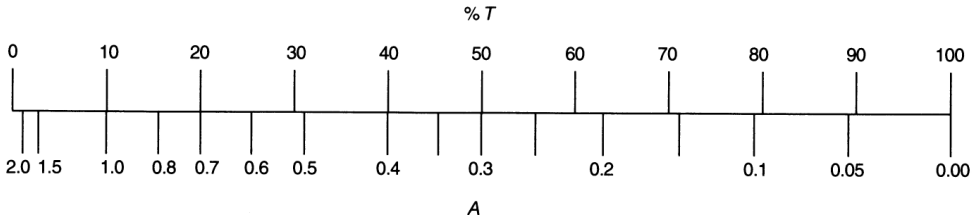

Figure 1.5 *Comparison of the readout for the transmittance and absorbance graphs [23]*

The molecular concentration and the optical path length can affect the absorption of light, the greater the concentration the higher the absorption and also the longer the path length the larger the reduction in light intensity, this is represented by Beer's Law, equation (1.5).

$$A = \varepsilon bc \qquad (1.5)$$

Where the molecular absorbance, A, is directly proportional to the path length, b, through the solution, with a concentration, c, and the absorptivity, called the molar absorptivity, ε. Generally, b, is in centimetres and c, in mol dm^{-3} and ε in dm^3 mol^{-1} cm^{-1} (also given in m^2 mol^{-1}) and A is a dimensionless number.

This research examined the transmittance and absorbance of the four oils and pure water, as shown later in table 2.1, through UV/visible to the mid-IR wavelengths. This investigation was not only to look at the characteristics of the samples but also to seek for differences between the hydrocarbons and water. The UV/visible range traverses 195 to 800nm the NIR was from 0.8 μm to 2.5 μm and the Mid IR range was from 2.5 to ~16 μm (shown in wavenumbers 4000 to ~600 cm^{-1}). Absorption peaks associated with UV and visible light tend to be quite broad in comparison with those from the IR region which are distinctively narrow. It is the absorption spectra from the IR that can be related to bond types and from here chemical structures can be identified.

The wavenumber is the number of wavelengths per unit distance, typically per cm. For example a wavelength of 1μm, has a wavenumber of 10×10^3 cm^{-1}, as the wavelength measurement become larger, the wavenumber becomes smaller, in this way, the wavenumber is proportional to the photon energy.

The photon energy, which depends upon incident wavelength, is absorbed or transmitted depending upon whether that particular energy quantum interacts with the molecules or particles of the samples being investigated. The photon energy may be capable of stimulating reactions and depending upon the molecule type present within the sample these photons may then be absorbed. Reflection and internal scattering losses can occur, although the latter is quite limited (unless enhanced by contaminants, particularly in the case of the used motor oil). In the IR range the photon energy spans from ~ 1.13 to 0.08 eV, this affects molecules through vibrational excitation. The photons associated with the UV and visible wavelengths have a higher energy, with a range from ~ 1.13 to 6.36 eV. The absorption of this higher photon energy enables electronic excitation to take place.

1.7.2 Fluorescence

The emission of electromagnetic radiation from a substance whether it be a gas, liquid or solid as a result of non thermal processes is known as luminescence. There are several types of luminescence, such as; chemiluminescence, a product of a chemical change, triboluminescence which is created through the physical movement or destruction of solids and photoluminescence caused by the absorption of photons. It is photoluminescence that is considered here.

Luminescence, where possible, is an important tool for analytical purposes. As well as having several advantages over other methods, it can achieve sensitivity several orders of magnitude greater than absorption techniques, typically into the ppb range. This sensitivity advantage is achieved through being able to enhance the analyte response by increasing the intensity of the excitation light, whereas for absorption detection a greater intensity of the incident light would not enhance the degree of absorption. The emitted light can be analysed off axis to the excitation light thereby minimising the background signal and emission spectra are linear for limited concentration ranges. Analysis through luminescence can be used for gaseous, liquid and solid phases. As not all chemicals exhibit luminescence, this means this method is quite selective for these materials.

The absorbed energy produces different effects, dependent upon the recipient material, its energy state and importantly the photon energy absorbed. The most frequent result of electro-magnetic absorption is ultimately the conversion of photon energy into heat. For fluorescence to occur, the incident photons must be from the shorter wavelengths of the

visible light to the UV, with a photon energy greater than ~ 2 to 3 eV. This is sufficient energy to raise electrons into a higher electronic energy level. Radiation at wavelengths shorter than 250 nm, ~ 5 eV, may start to damage the material through the disassociation of bonds. Figure 1.6 shows a typical Jablonski diagram [23] describing the various energy levels for a photoluminescence system. In the ground state, S_0, electron pairs are in an unexcited singlet state, after absorbing the energy from a photon electrons are raised to an excited singlet state, S_1 or S_2. The excited triplet state, T_1, can only be achieved through intersystem crossing, this is less likely to occur than other relaxation forms.

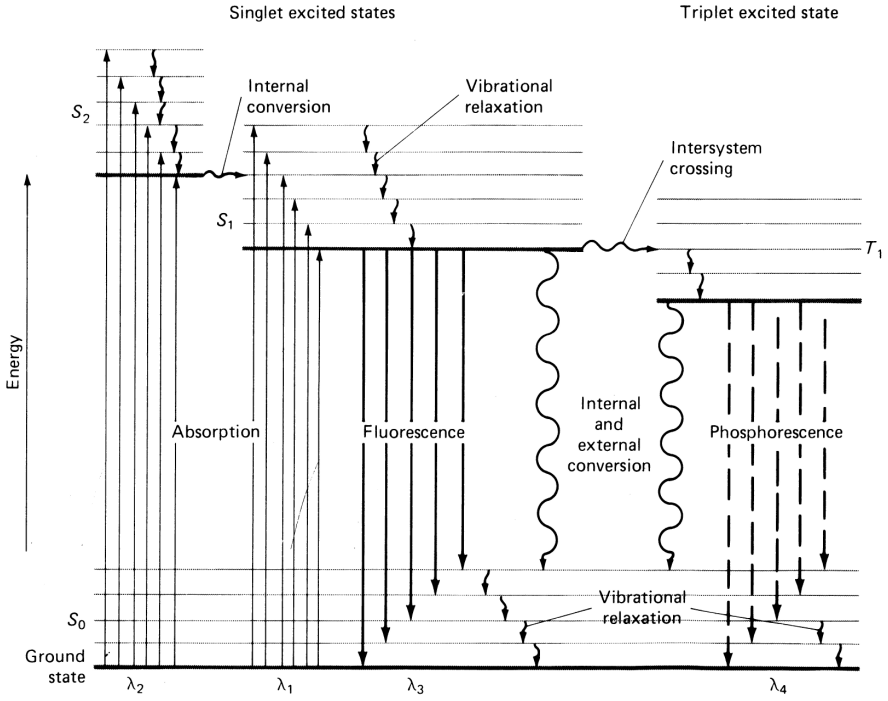

Figure 1.6. *Jablonski diagram showing partial energy levels for a photoluminescence system* [23].

This newly acquired energy promotes the recipient material into a less stable higher energy state. The energy can dissipate via several possible routes, allowing the excited electrons to return to their ground state. Although within this ground state there are also a number of discrete vibrational energy states. The timescale of this relaxation may vary depending upon the material and its state, along with other outside factors. The energy of the electrons may be given up by vibrational relaxation to the rest of the atom or molecule, occurring in $\leq 10^{-12}$ seconds in metals but slower in polymers, or via external conversion to a solute for example. Internal conversion may occur, whereby electrons in

a singlet state lose energy by exciting other electrons which in turn may themselves lose energy by vibrational relaxation. Intersystem crossing of singlet state to triplet state may further transfer energy to other electrons.

Deactivation of both singlet and triplet electrons may result in the emission of photons, whereby a specific quantum of energy is lost and so light is emitted. The lifetime of excited singlet state electrons is ~ 10^{-8} to 10^{-5} seconds, this being the time when fluorescence, if occurring, will take place, whereas the lifetime of the excited triplet state can be much longer lasting, from ~ 10^{-5} to several seconds and beyond [24]. The emitted light is always at longer wavelengths than the excitation light, having lost some energy in the deactivation process. The excited triplet state is less energetic than the excited singlet state and as such this light emission tends to be at longer wavelengths. It is this timescale of emission that divides photoluminescence into fluorescence and phosphorescence, the latter being the emission from the triplet state, occurring beyond 10^{-5} seconds. The time that the molecule remains in the excited state prior to returning to the ground state is known as the fluorescent lifetime. Further re-absorption of photons can occur as long as the excitation source is available and that the process has not been halted through other conditions.

Most materials do not exhibit fluorescence, the molecular structure or bonding arrangement plays a crucial role in how the electrons once excited convert their energy as they return to the ground state. Rigid bonding structures, such as those found in aromatic systems, compounds with conjugated double bonds, carbonyl linkages and condensed heterocyclic compounds are less able to loose energy through vibrational relaxation and are typically the molecular types where fluorescence will occur. These structures are present in the hydrocarbons that are intercepted in the oil/water separators. In investigations into materials where no fluorescence occurs, it may be possible to combine or tag these chemicals with a known fluorophore, thereby making assessment through fluorescence achievable.

The intensities of the different wavelengths emitted during fluorescence give rise to an emission spectrum and this will vary to some degree depending upon the excitation wavelengths. Similarly the excitation wavelengths that can produce fluorescence are collectively known as an excitation spectrum. These excitation and emission spectra are distinctive to particular fluorophores and it is these that can be used to identify different

materials. The difference between the peak excitation and emission wavelength is known as the Stokes shift and is shown in equation (1.6).

$$\text{Stokes shift} = h\nu_{ex} - h\nu_{em} \tag{1.6}$$

Where $h\nu_{ex}$ is the excitation λ peak and $h\nu_{em}$ is the emission λ peak.

The fluorescence quantum yield, Q, is the measure of the photon emission to photon absorption efficiency of the fluorophore and is shown in equation (1.7) [25].

$$Q = \frac{\text{Photons Emitted}}{\text{Photons Absorbed}} \tag{1.7}$$

The values of Q fall into the range from 0 to 1. When the radiationless decay is small, Q will be close to unity, rhodamine dyes are particularly efficient [22]. The possibility that emitted photons may be sequentially reabsorbed by the medium, thereby going undetected, would decrease Q.

Materials can also be characterised through their fluorescence lifetime. Differences can be significant where two molecules are similar but their non-radiative decay rates differ. The fluorescence lifetime is defined as the time it which the fluorescence intensity decays to 1/e of the initial intensity (37% of I_0), shown in equation (1.8) [25].

$$I(t) = I_0 \, e^{(-t/\tau)} \tag{1.8}$$

Where I(t) is the intensity at time t, I_0 is the intensity immediately after the end of the excitation pulse and τ is the fluorescence lifetime.

Even in the presence of an excitation light source, a decrease of fluorescence intensity may occur, this is referred to as quenching. Quenching can occur through several different processes, where the fluorophore may or may not be chemically altered. Collisional quenching occurs when the excited fluorophore is deactivated through a collision with another molecule in the solution, this being concentration dependant, here neither molecule is chemically altered. Fluorophores can be altered whilst in the ground state, thereby deactivating them chemically, this being known as static quenching. Photobleaching chemically alters the fluorophore through the activity of the photon energy effecting the bonding of the chemicals. Attenuation of the excitation light may also stop the fluorescence process.

There are several factors that can affect the performance of the fluorescence process, either marginally or quite profoundly. An increase in temperature of the solvent can decrease the efficiency as this will raise collisional and external conversions. The effect of pH which alters the ionized and non ionized forms of the fluorophore may have quite marked changes with some fluorophores but little effect upon others. Dissolved oxygen in the solvent encourages intersystem crossing, acting as a quenching agent and oxidation of the solvent may be increased through photon activity itself. Through a given range of fluorophore concentrations, the increase in fluorescence may be linear but as the concentration reaches a particular level, self-absorption may occur, particularly if the wavelengths of excitation and emission are close. Another occurrence that may arise through high fluorophore concentration is that self quenching due to the increase of collisions of excited molecules.

Fluorescence can occur naturally, for instance through sun light upon a suitable material, but for fluorescence analysis the necessary excitation light needs to be provided artificially. The excitation and resultant photon emission from the fluorophore increases with increased absorption of light, an appropriate light source is therefore important. The range of light sources available is discussed later in this report.

Whilst in micro-fluidics short path lengths and small quantities of analyte have limitations when measuring absorbance, fluorescence, with a suitable fluorophore and optical system, can be a superior analytical method. There are two significant factors that have a bearing on fluorescence analysis which have little effect on the absorbance analytical method in a micro-fluidic system. Firstly, an increase in the strength of the excitation light source may be matched by an increase in the emission and although this may be small, the result will lead to a stronger fluorescence signal. Secondly, as the molarity is raised, so proportionally, the fluorescence signal will become more intence, however quenching may also be increased.

1.7.3 The function of light filters

Analysis by fluorescence operates with light from two sources, the excitation light and the emitted light. It would be to the disadvantage of any detected fluorescent signal that whilst efficiently collecting the fluorescent light, the light from the excitation source was also detected. Light from the excitation source would increase any background noise which if large enough would mask the fluorescence, leaving no detectable signal.

In fact any excitation light entering the detector would reduce the lower limit of detection. To avoid or at least reduce the excitation light from reaching the light detector several strategies can be adopted. The use of an appropriate optical arrangement (this is discussed later), will reduce the light from directly or indirectly entering the detector, however, light filters, will greatly reduce unwanted light from entering the detector. The larger the Stokes shift, the greater the choice of filters systems available. Whereas when these peaks are closer together, filters with sharp cut-offs would be required. Similarly, the light source, whether it be a LED with a broad spectrum or a laser with a narrow emission, influences the filter choice.

There are many different types of filters, varying in transmission characteristics, blocking method, efficiency and price. The specific task will dictate which parts of the spectrum will need to be transmitted or blocked. The ideal filter would have total transmission where required and block the rest of the spectrum, with the transition from one to the other being immediate.

The transmission and blocking by the filters can be broadly placed them into three groups; long pass, allowing transmission of light longer than a particular wavelength, short pass, these transmit below a certain wavelength, band pass, which only transmits light over a small range of the wavelengths. The change from transmission to blocking and vice versa, known as the slope factor, may be quite steep, occurring over a few nm to a more gradual change spanning over a hundred nm.

The method of filtering light is normally through either interference or a coloured substrate which may be glass or plastic. Interference filters are formed through multiple thin layers of film of precise thickness upon a suitable glass substrate, which through different refractive indices exhibit destructive interference for specific wavelengths but allow other wavelengths to pass. These types of filter have steep slope factors but are sensitive to the angle of incidence. Coloured substrate filters acquire their properties through absorbing or transmitting light across the spectrum. These are much less dependant upon the angle of incidence and generally are cheaper than the interference filters. Coloured glass filters are inclined to have less abrupt changes, i.e. poorer slope factors.

The blocked light is either absorbed or reflected, both of these modes have their advantages and disadvantages. Absorbed light with low powered light sources will pose

no problems but from a high powered source the filter may become hot and will be damaged. Whereas filtering through reflection may cause damage to the light source unless redirected and when diverted the light may have to be rendered safe (normally by absorption).

The efficiency of the filters can vary with peak transmission ranging from < 25% to > 90%. Similarly, in the stop band, transmission of < 0.1% can still be present. Filters with good blocking but poorer transmission may be unsuitable if the light source does not provide ample power for the task, and choosing the filters for any particular scheme may be a compromise.

1.7.4 Reflection, transmission and TIR

How light reacts when reaching interfaces may be significant for the performance of optical systems, from improving the light collection for detection, to being the basis for a detection system. Transmission and total internal reflection, TIR, can be used as a detection technique, where the necessary optical properties of an analyte differ from that of its surroundings, and the monitoring of a situation is merely looking for a presence or an absence of a particular material.

The degree of reflection and transmission of non polarised light at the dielectric interface between two transparent materials depends upon the angle of incidence and the respective refractive indices. TIR can only occur when the light travelling from a higher refractive index medium to a lower refractive index medium exceeds the critical angle, θ_C, defined in equation (1.10), which is derived from Snell's law of refraction, equation (1.9).

$$n_1 \sin\theta_1 = n_2 \sin\theta_2 \tag{1.9}$$

$$\theta_C \geq \sin^{-1}\left(\frac{n_2}{n_1}\right) \tag{1.10}$$

Where n_1 and n_2, refers to the refractive indices of the respective media and θ_1, θ_2 and θ_R the angles of incidence, transmission and reflection respectively and are shown in figure 1.7.

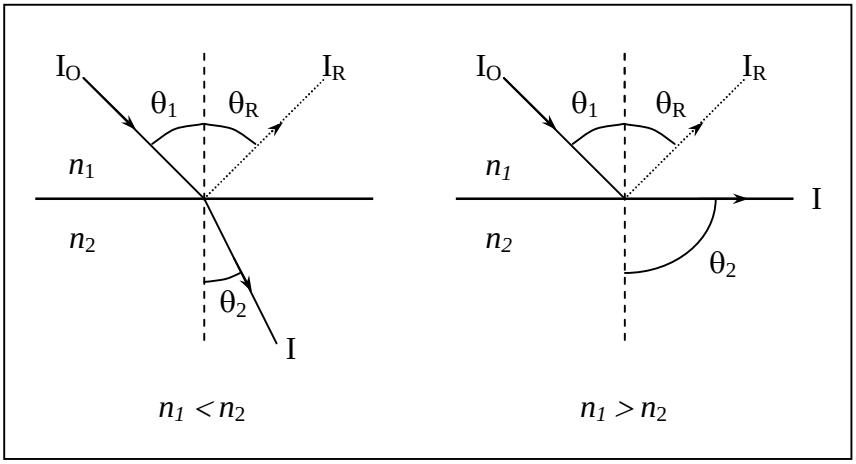

Figure 1.7. Light ray, I_O, travelling from one medium into another. Refraction only (left) and the occurrence of TIR (right). I_R are reflected rays.

The level of reflected light, R, when the incident rays are normal to the interface is defined by the Fresnel formulae, equation (1.11).

$$R = \frac{(n_1 - n_2)^2}{(n_1 + n_2)^2} \tag{1.11}$$

As the angle of the incidence increases away from the normal, at any interface, the absolute magnitude of reflection of non polarised light increases, although not at a linear rate. The absolute magnitude for the reflection coefficient (R_A), equation (1.12), is the mean value for the reflection coefficient of p polarised light (R_P), equation (1.13) and the reflection of s polarized light (R_S), equation (1.14) [26].

$$R_A = ½(R_P + R_S) \tag{1.12}$$

$$R_P = \frac{\tan(\theta_1 - \theta_2)}{\tan(\theta_1 + \theta_2)} \tag{1.13}$$

$$R_S = \frac{\sin(\theta_1 - \theta_2)}{\sin(\theta_1 + \theta_2)} \tag{1.14}$$

Unwanted reflection can not only create unwanted light and false readings but scattering from such as a UV light source may create an unsafe local environment.

1.7.5 Light sources

A range of light sources are available for analytical systems based on fluorescence, the three main types are; lamps (gas discharge and filament), lasers and LEDs. Illustrated in figure 1.8 [17] is a chart of light sources that are available for particular wavelengths. The gas discharge lamps tend to be continuum sources, emitting over a large wavelength range, the output varying greatly across the spectrum. Lasers produce line source emissions, each particular output wavelength being specific to the laser. Not shown in figure 1.8 are LEDs, these are available from the middle UV through to IR, the spectral output is wider than a line but not a continuous broad spectrum as would be expected from the first category. The wavelengths emitted from the LEDs depend upon the basic material from which the semiconductors are made and their characteristics. Typical spectral widths are; ≤ 1 nm for lasers, 10s nm for LEDs and up to several 100s nm for high pressure discharge lamps.

For fluorescence excitation, the choice of which light source to use depends on several factors. One of the major factors would be the required spectrum of the excitation light which would in turn be dependant upon the analyte and the particular reagent being used. Where there is a clear separation between the excitation and emission spectra there is the possibility to use a light source with a broad emission, whereas if the excitation and emission are close together, or overlap to some degree, then a narrowband excitation light or sharp cut off filters would be necessary. Restricting the excitation light to a narrow band would mean that the required excitation power has to be delivered within those particular wavelengths. A xenon gas arc lamp has a broad emission predominantly in the visible spectrum tailing off into the UV (see figure 1.8). Using this lamp to deliver excitation light between 300 to 380 nm would require greater than 90% of the power to be blocked by filters, whereas deuterium and mercury lamps have higher emission power in the UV spectrum.

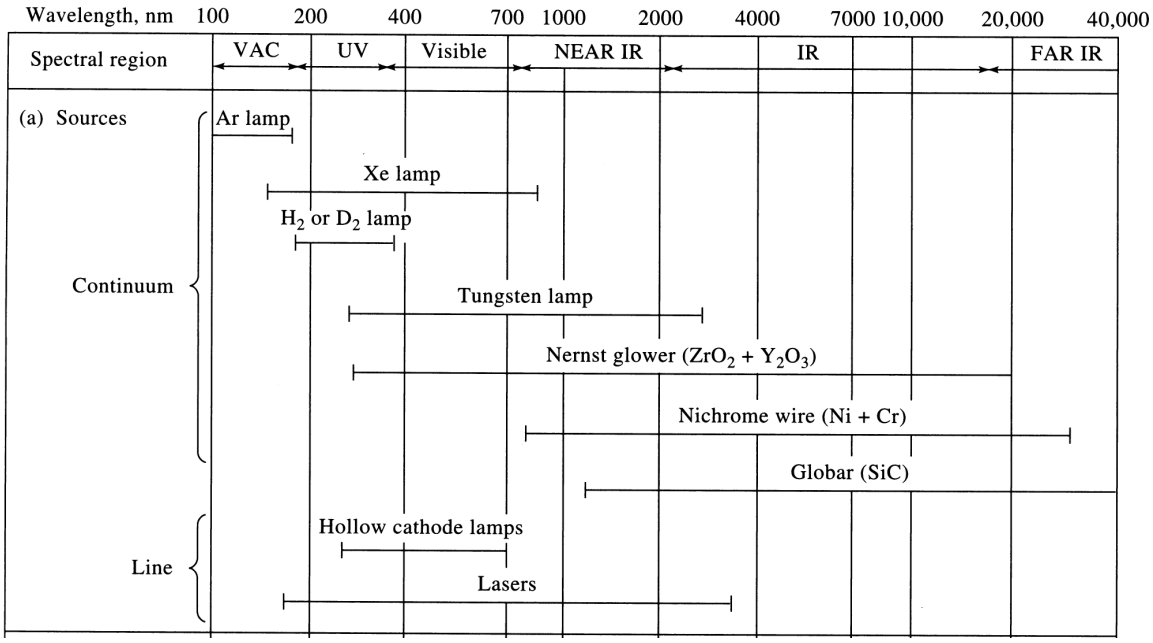

Figure 1.8. *Emission wavelengths from various light sources [17].*

With a bench top fluorimeter, a light source requiring a constant power input may be used along with a grating or filter system or for more specific use a laser. In a portable system, that is expected to operate unattended for several days with only a low voltage source available the power supply becomes a significant consideration when choosing a suitable light source. Other factors to be considered when choosing a light source are; size of appliance, cost, lifetime and durability, stability of output (drift and power output) and power consumption.

The spectral output required for the fluorimeter used in this research, a light source emitting from 320 to 360 nm was needed. Filament or gas discharge lamps are either too large in size with large power requirements or inefficient in this UV region. Lasers would also exceed these parameters and diode lasers are not available for these wavelengths. LEDs have more recently become available within this wavelength range and are able to produce an optical power output of up to several hundred μW.

The advantages of using LEDs are many; they are relatively low in cost, low power consumption, long lifetime, small in dimension, they are quicker than conventional bulbs to stabilise [27] and have the ability to be continually modulated or pulsed. The disadvantages are that the output power may drift with temperature, voltage and ageing [28] and that the peak spectrum and output power may vary from LED to LED. This may be overcome by calibration before readings are made. The beam from an LED is

divergent and can typically vary from around 15 - 60º, dependent upon the particular type and integrated lens. The data for these are given by manufacturers who may supply various lenses already incorporated, alternatively correcting lenses can be integrated into the system.

1.7.6 Light detection

A photodetector detects electromagnetic radiation from γ rays to beyond radio waves. Photodetectors discussed here cover a smaller part of the spectrum, from UV-B through visible to NIR (280 to 1000 nm), this will be collectively referred to as light. For most optical analytical measurements the light collected is required to be quantified, not merely whether it is a present or not. The human eye which can detect not only the existence of light but may also discriminate different parts of the visible spectrum is only able to give a subjective analysis of intensity. For a meaningful analysis whilst monitoring a series of events comparable measurements are required to be consistent.

The name photodetector generally refers to a transducer, in this case an instrument that can transform the light (photon energy) into an electrical signal that can be translated into a quantifiable signal of whatever is being examined. There are several ways to characterise photodetectors, but they can mainly be placed into two groups, thermal photodetectors and photon photodetectors [29].

Thermal photodetectors, as the name suggests, utilises the photon energy to heat a black or non reflective screen which absorbs the radiation. The resultant rise in temperature is then measured via a transducer, typically a thermocouple or pyroelectric device although there are several others. These have a low responsivity but have constant calibration factors over a wide range of wavelengths.

Photon photodetectors use the photon energy directly to either excite or liberate electrons. This mode of operation makes their calibration wavelength dependent. The effect only occurs when the photon energy of the incident radiation is equal or greater than the bandy gap or the work function. There are three main groups of photon detectors; photovoltaic, photoconductive and photoemmisive, the first two being solid state detectors.

Photovoltaic detectors are similar to photoconductive devices, containing a *p*-*n* junction, but producing a current when light falls upon its surface, this type is also known as a

self generator. The small output efficiency at low light levels makes this type unsuitable for the detection required.

Photoconductive detectors contain semiconductor material and when reversed biased allows a current to flow as light reaches the interface surface. Responses to different photon energies may be achieved through using differently doped material to achieve different energy band gaps. Here, doped silicon being the most suited semiconductor materials for the shorter wavelengths within the visible spectrum. This type of detector, as with the previous type, requires amplification of the output signal when used with low light levels. The small fluorescence output expected from using micro litre quantities of solution with low concentration of analyte would put this type of detector at operating levels below a reliable signal to noise ratio. Avalanche photodiodes (APDs) are silicon photodiodes with an internal gain mechanism and, as with conventional photodiodes, incident photons excite electrons from the conduction band. Here, the difference is that a higher reverse bias voltage creates a strong internal electric field that promotes electron acceleration leading to collisional ionization and a cascade of electrons follows an avalanche effect is created. A gain factor of several hundred to several thousand is achieved, producing an internal amplification exceeding that from equivalent external amplification where noise would be equally amplified.

Photoemmisive detectors absorb photons and emit electrons, the best known photoemmisive detector is the photomultiplier tube, PMT, and is suitable for low light detection. Figure 1.9 shows a cross section through a typical end-on type PMT. The mode of action starts with the incident light falling upon the photocathode from where photoelectrons are emitted and accelerated by an electric field. These electrons subsequently strike the surface of the first dynode, which emits a number of electrons for each incident electron, these in turn are accelerated by the electric field to strike the second dynode and from here the process is repeated from dynode to dynode. Eventually, the large number of electrons emitted from the last dynode, are collected by the anode as the output pulse. The gain of the PMT is the ratio of the anode output current to the photoelectric current from the photocathode. A gain from 10^5 to 10^6 can be expected, the advantage is that amplification occurs prior to load resistance resulting in a high signal to noise ratio. The choice of material of the photocathode determines the peak sensitivity of the PMT. This system is suitable for extremely low light levels and

current models are smaller and can run from lower input voltages more suitable to portable systems.

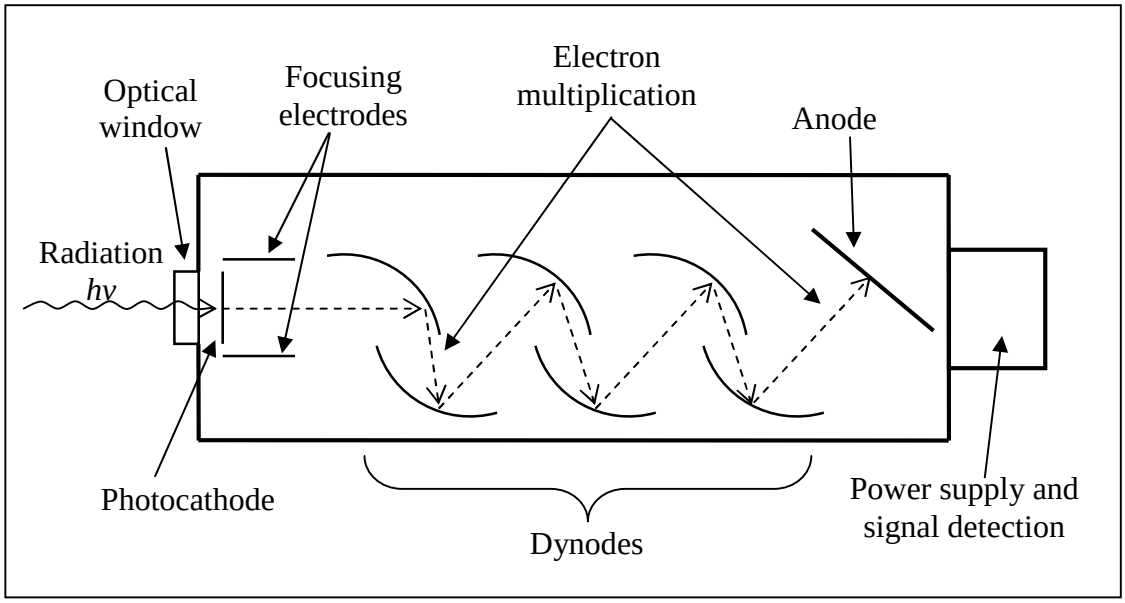

Figure 1.9. *Cross section though a typical end-on type PMT. The number of dynode may vary depending upon the desired sensitivity of the model.*

As with most systems there is a trade off between performance and other factors. Where the PMT is the most efficient it is more bulky than the photodiode or the APD, also more fragile and expensive. Nevertheless, for low light levels expected with low molarities and micro litre quantities this particular detector will be used.

For the detection of the fluorescence emission from the GSH and OPA isoindole, a detector that is particularly sensitive within 400 to 500 nm wavelength is required. Although emission occurs over a larger part of the spectrum, this range contains the most intense part of the emission.

1.7.7 Applications of fibre optics

Light has been used to transfer signals for thousands of years and with the exception of mirrors or refraction, transmission was limited to straight lines. The transfer of light along a non linear path is possible through the use of optical fibres, developed over 150 years ago. Not only has the telecommunications industry been revolutionised through the use of this technology but applications also have been found in science, engineering and industry. This discussion centres upon the area of fibre optics when used in conjunction to sensors.

The light transfer along a fibre optic cable relies primarily upon the property of TIR, where the refractive index of the core, n_1, of the cable is greater than the cladding, n_2, which surrounds this core. The outer sheath is there to protect the cladding and core from abrasion or other damage, as shown in figure 1.10. The core can be made from any material that will allow light to pass but is generally made from a glass or polymer that allows a degree of flexibility of the cable. The receiving cone of light by the fibre optic cable is dictated by the maximum acceptance angle of the light that once refracted inside the optic fibre cable will undergo multiple internal refractions. This in turn, is dictated by the refractive indices of the core and the cladding. The acceptance angle, shown in Figure 1.10 as θ_0, is derived from Snell's law and this maximum angle is known as the numerical aperture, NA, of the fibre optic. The NA is the sine of θ_0 and is shown in equation (1.15).

$$NA = \sin \theta_0 = \sqrt{n_1^{\,2} - n_2^{\,2}} \qquad (1.15)$$

The fibre can be characterised into three different types; single mode, multimode and graded index. The core of single mode fibre is smaller in diameter than the other two, typically less than 10 μm and with a small NA. This type of fibre is less dispersive of light pulses, producing sharp output pulses, however with a continuous wave this is not an issue. Multimode fibre has a larger diameter, up to 1 mm or more, and has the advantage of a much larger NA. This type of cable is suited for sensor purposes if the light intensity is the object of the investigation rather than a phase modulated signal. Graded index core fibres fall between the previous two types, allowing a large NA whilst still producing a relatively sharp output pulse. The price and application will often dictate the type of fibre that is used.

Not all of the light entering the fibre optic system is transmitted to the detector, losses may arise through several ways, the most significant occurring due to couplings and connections, attenuation within the fibre and through bends along the route of the fibre. When the fibre optic is interrupted with a connection or is coupled to an actuator, there is always the possibility of signal loss through light scattering. These losses can be reduced if the face of the core is polished or by using joining compound. Attenuation within the fibre may be associated with the quality of the optical fibre cable, as impurities within the fibre can increase light absorption. Any bending of the cable will increase the losses into the cladding, the light rays at the maximum acceptable angle

will be degraded first as bending occurs. The data sheet from optical fibre manufacturers will recommend the minimum bend radius that should not be exceeded before significant losses or breakages start to occur.

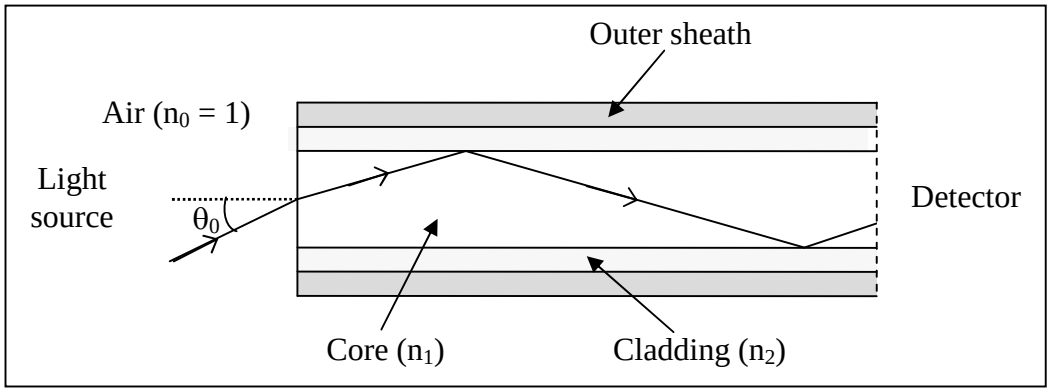

Figure 1.10. *Diagram showing the light transferred along a multimode fibre optic cable and θ_0, the acceptance angle.*

Attenuation loss is defined as decibels (dB) per unit length, in fibre optics this is typically expressed as dB/km. This is shown in equation (1.16), where A is the attenuation, and P_i and P_o is the input and output power respectively. Depending upon the core material, losses of several to hundreds dB/km can occur. At the same time losses can be wavelength dependent, with some wavelengths being more suitable for some applications, telecommunications preferring infrared wavelengths from 1100 nm to 1500 nm [30].

$$A = -10 \log \frac{P_i}{P_o} \tag{1.16}$$

As the use and application of fibre optics has expanded, particularly driven by the telecommunications industry, the range of available components has also increased along with their improved reliability and reduction in cost [31]. The advantages of fibre optics for the use of data or information carrying are many; the cable is light-weight and small in comparison to electrical cable, it is immune to electromagnetic interference and cross talk between cables is absent meaning that shielding is not necessary. Importantly for environmental applications, fibre optic cables are relatively rugged against vibration and shock. There are several limiting drawbacks of fibre optics, the main ones for sensors are; the interference of ambient light overriding any generated signal, attenuation of light within the optical fibre and couplings (this being common to both

sensors and telecommunications). This can limit the length or type of cable unless the complication of amplification or a repeater is added to the system. There may be a limited availability of specialist accessories mass produced for specific applications [32].

Fibre optics may be used as chemical or physical sensors, and these can be further subdivided into intrinsic and extrinsic sensors. Intrinsic sensors rely upon the property of the fibre itself being modified, thus, the signal carried is affected, whereas an extrinsic sensor detects a change that takes place outside of the fibre and the fibre itself merely transfers information about the change back to the detector. The extrinsic sensor can be further subdivided into phase modulated or intensity modulated. The former requires a reference signal whereby a relative change in the phase is detected. This makes it very sensitive but more expensive than the intensity modulated sensor. The majority of extrinsic sensors fall into the intensity modulated category [30].

For chemical sensors, the detection system may monitor changes of the chemical state that affects the light transmission or measure luminescence where light intensity is measured [28]. Whereas, for a physical sensor, a physical change is monitored, this may include a displacement, a change in level or pressure, a flow or rotational speed. A change in pressure can be monitored through some form of attenuation of the light along the fibre. This may be through a shutter obscuring the light as it travels through a gap between two cables, or by a movement of a reflective surface, to a pressure exerted directly upon the optic fibre, extrinsically bending it to increase losses or intrinsically affecting the refractive properties of the fibre [30].

The ability of fibre optics to penetrate into the area for investigation is advantageous, as this can be less intrusive and damaging than other methods. The effect of this can allow for a real time analysis to take place.

1.8 Physical methods of analysis

In locations where optical detection is not a suitable option and electrical or mechanical methods cannot be used, the presence of different liquids or materials in an aqueous location then requires an analysis through other means. Detection through changes of physical properties may provide an alternative technique.

Determining the presence of dissolved material may change the viscosity, density or other mechanical properties but as the quantity of the analyte is reduced, detecting or quantifying its existence will become more difficult. In detecting the presence of a non dissolving material in a controlled location, such as an interceptor, assessing the presence of a limited amount of material would be possible due to its localised accumulation. Detecting not for milli-litre quantities but for volumes of several hundred litres or more opens up techniques of different types of analysis. Methods for detecting the presence of oil are discussed in Chapter 2.

1.9 Performance testing

For results to be worthwhile or acceptable by a third party, verification of the ability of the monitor to analyse correctly is essential [6]. Several validation methods can be used, the fundamental one being to scrutinise the results to confirm whether any of the analysed samples are outside the range expected for the system, although this will not identify failings that fall within the expected range. Checks against known samples, if possible, should be undertaken periodically. In automated systems it is not always feasible (due to deterioration of the reagent or a spiked sample) to be able to carry definitive standards by which to compare the newly sampled analyte. The ability to self test preferably before each analysis is made or at least on a regular basis is preferred. Checking against a standard will confirm that all parts of the monitoring system are functioning correctly as faults can potentially occur in all parts of the system; the chemicals, the electronics, the detectors, the pumps, power supply as well as blockages to the tubing and filters. Embedded electrical sensors within a system can detect faults, alerting the operator or annotating on the data [33].

1.10 Limitations and safety of materials and equipment

The sampling requirements will differ for each application, affecting the frequency between each analysis. The quantity of the chemicals as well as their shelf life (this may be influenced by the location conditions) can limit the monitoring period. Similarly, the power supply or the life of some components (such as filters) may limit the length of time that a monitor can produce acceptable analyses before attention is required.

1.10.1 Chemicals reagents and waste material

Whilst some monitors will gather data through physical or electrical analysis, those whose examination methods require chemical reactions will need extra precautions to be taken. Many of the chemical reagents and the waste products have the potential to be harmful to some part of the environment as well as the operator. As such, safely retaining these chemical needs to be considered in the design of the analytical system.

1.10.2 Electrical system

With electrical devices and particularly in situations when monitoring liquid, safety for personnel is important. With any research project the equipment may be individually made for a single application. Here it is essential to assess eventualities that such a monitor may encounter. Battery operated devices, although limited in power, are inherently safer than those with mains supplies.

1.10.3 UV light

With UV LEDs available at higher powers than were available several years ago, care needs to be taken to avoid excessive cornea and skin exposure. Data for levels of maximum permissible exposure (MPE) for radiation were taken from directive PD IEC TR 60825-14:2004 [34], this literature, although promoted for laser safety, provides information regarding extended sources (LEDs are not collimated but divergent). LED data sheets provide figures for typical output, however the maximum output would be the cautionary emission level to use. However, the emission from LEDs cannot be assured to conform to Lambert's emission law and as such the intensity may be greater from the centre of the emission cone. For each LED used, a safe working distance should be calculated and a mechanical guard should be placed to prevent close contact

1.11 Aims and objectives

The agenda for this research is to develop two different automated environmental monitors, both of which can qualitatively analyse the liquid in a specific location. Each type of monitor being able to; report their analyses, identifying when a predetermined threshold has been reached or surpassed and function unattended for defined period of time.

The first of these monitors, the progress of which is reported in chapters 2 to 6, has been developed for the commercial application of detecting the presence of oil in an oil/water interceptor. This monitor has to be able to function within the harsh environment of an interceptor for periods of up to six months between services. The second monitor, which is reported in chapters 7 and 8, shows the methods investigated in the development of an automated portable fluorimeter, which through the use of micro fluidics can analyse samples of water from an aquatic system. This particular monitor uses the detection of the pheromone glutathione as a model analyte, which when mixed with a reagent will fluoresce in the presence of a suitable excitation light.

This first chapter generally discusses different types of environmental monitoring, their need and applications. It further examines the requirements for self contained monitors, their durability and limitations. The latter part of the chapter discusses the optical and physical properties that are significant for the detection methods chosen for the environmental monitors.

Chapter 2 assesses the development of an oil level detector and discusses the type of monitor that can be used. Later in this chapter, existing optical and physical detection methods are described and discussed. Chapter 3 examines both theoretical and experimental techniques which were eventually discounted due to failures in their ability to comprehensively function in all conditions. Chapters 4, 5 and 6 presents two detection techniques based upon pressure analysis, both of these systems relying upon the density difference between water and oil. These detectors are taken out of the laboratory for further analysis.

Chapters 7 and 8 present the development of an automated portable fluorimeter. This self contained stand alone unit would be capable of sampling, analysing and data storage.

2. Development of an oil/water interceptor monitor

This chapter and the four following describe the development of a monitor capable of indicating the oil level in an oil/water interceptor. This chapter examines how an interceptor works, the requirements and purpose for a monitor and the types of material that are likely to be encountered. The current technology that already exists for oil detection is reviewed, including other methods that may also have some relevance to monitoring oil levels in an oil/water interceptor. These findings and their relative applications are discussed and a program of research is laid out. Analyses of several oil types and the initial experimental studies are presented in the chapter 3. The following three chapters follow the development of the oil detection method which was ultimately chosen.

2.1 Introduction

An automated monitoring system of any process or event can have advantages over manual methods, in addition, practices which may be deemed to be too expensive or inaccessible may not be observed at all. Automated monitoring can reduce the costs of manual supervision, produce data giving round the clock observation and an addition advantage of automation comes when the site that requires observation may produce harmful vapours. The use of an oil/water interceptor monitor includes all these benefits but in addition automated monitoring has now become a legal requirement for all newly installed interceptors [35]. Andel Ltd [36], a company with an interest in pollution prevention have requested a new and novel method to detect and ultimately alert when the oil level within an interceptor has reached a particular critical level.

The specifications from Andel Ltd., laid down five key requirements for this monitoring system; the first, is that there must not be any electrical components within the interceptor or immediate vicinity, the second, there must not be any moving part within the interceptor that may come into contact with the liquid, thirdly, the monitor must be able to function unattended for a minimum of six months between servicing, fourthly, there must be some system that indicates whether or not the oil level has reached the

notifiable level and fifthly, the unit must be competitively priced. It is within these constraints that the final monitoring system must fall.

References to oils in this text includes mineral oils and petroleum products, these may also be referred to as hydrocarbons. The terms oil separator and oil interceptor are found in different literature, both have the same meaning, although within some interceptors different chambers are used for separating solids (such as grit) and separating oils.

2.2 Environmental need for the control of oil pollution

Water contamination caused by oils and in particular fresh water is predominantly through the results of human activity. Detrimental effects of this type of pollution can produce particular risks to animals and plant life in the aquatic environment and to human health. For if no unfavourable reactions resulted from oil pollution, then there would be no need for this type of pollution control. As modern society has increasingly used oil and oil products for so many applications, it is inevitable that the opportunity for spillage in one form or another will occur and that this will, over time, enter into the environment.

The direct effect of oil pollution upon humans is mainly a health issue, through absorption by skin contact or from drinking water. Drinking water is sourced through both surface water and ground water and of the two, surface water is the most likely to be contaminated [4] and it is regarded by the Economic Union (EU) that 20% of all the surface water in the EU is seriously threatened with pollution (this includes all pollutants, not just oil) [37]. It is the metals and carcinogenic products present in many refined and waste oils that are the main cause of concern.

Oil pollution has become major issue, not only for the crude oil spillages at sea that can make headline news but also diffuse oil pollution on land that can find its way into fresh water systems. This second type of pollution receives less public attention but can be far more damaging to humans and the environment alike. It is estimated that around three million tonnes per year of oil and its by-product contaminates the world’s water, with 92% of the causes directly related to humans [38].

Pollution of the freshwater system is widespread and the effect upon the ecosystem can be considered to be in many forms. The dispersive nature of oil, coupled with natural

forces (wind and water movement) can lead to rapid spreading over the water surface, this in turn allows the natural environmental mechanisms further processing of the oil. Figure 2.1 shows the fate and breakdown process for oil pollution in a water system, where not just the water itself is affected but also the sediment at the bottom of the waterway. Photodegradation, particularly UV solar radiation, through a combination due to the higher photon energy and the greater photon absorption by the oils at these wavelengths leads to oxidation of some of the compounds within the oil matrix. This has a greater oxidative effect upon the aromatic compounds and the smaller polar molecules than the alkanes and other saturates which are relatively unaffected [39, 40]. The speed of this photooxidation is dependant upon several factors but greatly upon radiation intensity, temperature and molecular components of the oil. In particular instances several hours to several days is sufficient to be destructive for most of the polycyclic aromatic hydrocarbon (PAH) molecules [41]. Evaporation is generally restricted to molecules with <15 carbon atoms, occasionally extending up to ~30 [42]. Similarly the fate of lighter fractions of oil and aromatics are biodegraded more rapidly than the heavier ones [43].

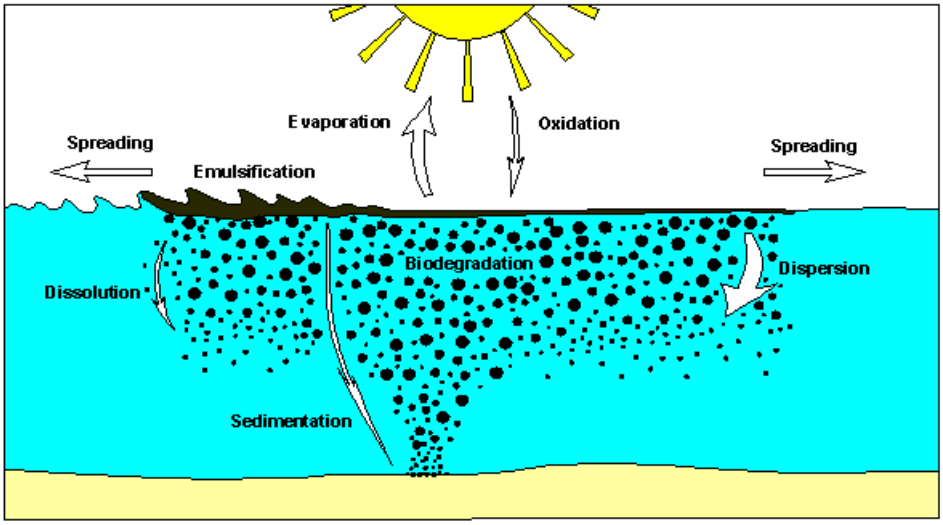

Figure 2.1. *Fate of oil spilled into water, showing the main weathering processes that may occur* [44].

The resultant toxic effect of oils works through several routes. If they are water soluble, they can directly kill wildlife. Those that carry lead or other heavy metals can lead to an accumulation in the body tissue effecting health and their ability to breed successfully. The oil whilst being broken down through biodegration may compete directly for the oxygen within the water, such oxygen demanding pollutants are especially known to kill

the higher life forms and is often the cause when dead fish are seen [45]. The population increase of one species, such forms as algal bloom, is brought on through an upset in the available nutrients and this may affect the rest of the ecosystem in a particular locality. Even if no direct effect of oil in fresh water is noted, the presence of the oil upon the water may alter the penetration of sunlight which in turn affects water temperatures and have an impact upon photosynthesis due to attenuation of the incident light. The physical properties of the oil floating upon the water surface can threaten aquatic birds and other surface vertebrates due to buoyancy and heat insulation. The resulting impact brought on through oil pollution of fresh water is vast, affecting the whole ecosystem. Where possible, it is far more economic and logistically easier to intercept the spillages of oil at source than it is to retrospectively collect oil once it has escaped into the environment

2.3 Legal requirements for pollution prevention

The importance of environmental issues inevitably led to legislation and with the ubiquitous presence of oil, pollution control became an important part of such laws. The Water Resources Act 1991 regulated discharges within England and Wales but in 2000, all the countries within the EU were collectively expected to abide by the Water Framework Directive (WFD). The WFD 2000/60/EC [46] sets out objectives for now and the future to protect all waters from the problems of pollution and to ultimately assure that the water resources are secure and in good chemical status for present and future generations. A further directive was issued in the year 2006, Groundwater Directive 2006/118/EC, to expand control of groundwater and additional daughter directives have been proposed to control the emission and discharges of substances.

In the UK, EU and British laws are under the control of the Department of Food and Rural Affairs (DEFRA), in England and Wales this is carried out by the Environment Agency, with Scotland and Northern Ireland having their own similar bodies.

Encompassed within the legal requirements are Pollution Prevention Guidelines (PPG) that draw attention to obligations and also provide recommendations for relevant businesses and individuals. PPG1 is a general guidance for pollution prevention covering all aspects of oil storage and use as well as site drainage, spillage prevention and security [47]. PPG2 and PPG8 provide more details for safe storage and disposal

with recommendations for tank types and other related containers [35, 48]. Specifically for oil/water separators and drainage systems, PPG3 provides guidelines and how to comply with current legislation.

There are several different standards and types of oil separator, each one being dependant upon the needs of the location and the type of use. A threshold for oily hazardous waste is set at varying levels depending upon the type of oil, with a generic threshold for oil at 0.1% w/w (1000 mg/kg) [49]. Legislation requires that separators that discharge into a foul sewer are expected to have an oil concentration of less than 100mg/litre, whereas separators that discharge into surface water drains and the water environment should not exceed 5 mg/litre [35].

Oil/water separators once correctly installed are required to be regularly maintained and accessible at all times. The accumulation of silt must not reduce the oil storage volume and the removal of oil and silt must be undertaken by a registered waste removal company. An automatic warning device must be fitted (this is only advisory for existing separators) to provide a visual and audible alarm when the oil level reaches 90 % of the oil storage volume [35]. Electrical devices used as monitor sensors must be intrinsically safe and conform to the requirements of BS EN 60079-10 and regular maintenance of such equipment is essential. Furthermore, visual inspection can have hazardous consequences to health, as certain volatile organic compounds can be emitted when removing inspection covers [50], inspection requires safety precaution to be undertaken. For a separator to work correctly it is important that a routine inspection is undertaken at least every six months. A log must be kept of inspection, maintenance and silt and oil removal. When oils are kept on any premises it is obligatory to have a pollution incident response plan and this must be kept updated.

2.4 Oil/water separators – how they work and where they are located

The technique of separating oil from water by effectively floating off the oil has been known for as long as oil has been used. It is due to the property of most oils being less dense than water, coupled with the immiscible nature of the oil and water that is the key behind this approach, allowing this method to be used successfully. Due to its simplicity, it is this method that is employed in most oil/water separators that are commonly found in the majority of locations, not only in this country but also around

the world. For some more specialised situations, inline scrubbers are required to separate the incoming liquids from particles or to break up emulsions.

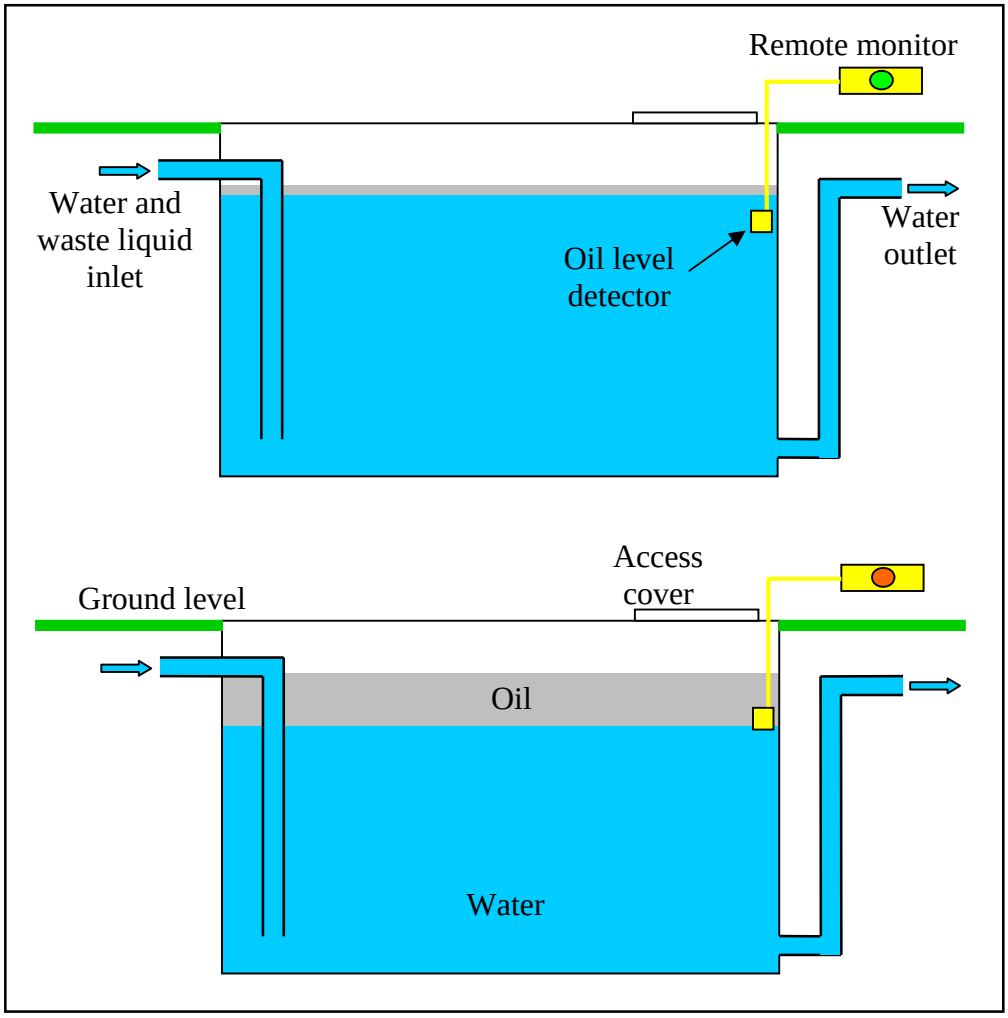

Figure 2.2. *Diagrams of the general layout for an oil/water interceptor. The upper diagram shows the separator tank containing a thin layer of oil. In the lower diagram, the oil has displaced the water and activated the oil indicator.*

The oil and water enters the separator via a surface drainage system, shown in figure 2.2, and goes into the main chamber, it is here that the separation occurs. The oil then floats to the surface of the water. As more liquid enters the separator, the oil free water at the bottom of the chamber is displaced, being forced out through the water outlet. As more oil is separated over a period of time, the main chamber stores an increasing amount of oil. Once the level of the oil in the main tank reaches a predetermined height/volume, a detector, if fitted, would trigger an alarm indicating that the separator requires emptying, and after being emptied the process would then start again. Depending upon the requirements of the separation storage tank, such an alarm is usually triggered from 10 to 90% of the oil holding capacity. This range of oil capacities

is due to the particular requirement of the interceptor. In a mechanical workshop for instance, the interceptor would be in place to catch small incidental spillages and it would be reasonable to allow the separation tank to fill to 90% capacity before emptying, whereas in a transport refuelling bay the interceptor would be emptied of oil when 10% full, thus allowing for a catastrophic spillage from the main fuel tank.

The class and size of the tanks is laid out in the Environment Agency's PPG3, here, the likely inflow of spilt oil, area draining into the separator and other factors are taken into consideration and the type and capacity of separator would then be recommended. The minimum capacity starts at 1,000 litres and for a typical petrol station forecourt this would be ~ 7,500 litres.

The amount of oil and water entering a separator from each catchment area will depend upon the location of the site, the individual circumstances at any point in time and the current weather conditions. To intercept mineral oils these would need to be immiscible in water; oils held in an emulsion or dispersed through the use of detergents do not readily separate from the water. The separation time will depend upon variables such as: oil type, separator design and premixing with water prior to entry into the separator. The incoming water may also be carrying gravel and silts in suspension along with other material that may be dissolved. A trap positioned prior to the separator should remove the larger or heavier materials, other impurities contained within the water are outside the scope of this research.

Oil may be accidentally or deliberately discharged and it is the responsibility of the business or individual to prevent the oil from reaching the water course or environment and breach of the pollution prevention regulations may lead to a prosecution where such laws have been disregarded. Therefore it is the responsibility of the potential polluter to make adequate provisions to entrap potential spillages and importantly have facilities to control or the loss of any oil that may be stored on site. This includes all waste oils, as they are considered hazardous wastes regardless of their composition or biodegradability, the only exception to this are edible oils. Edible oils do not contain the metals or other additives that are found in mineral oil products.

Oil separators should be situated where any oil may pollute surface water drainage. These locations are most likely to be garages, vehicle service stations and other urban settings where spillages can occur [51]. Although oil spillages can be intercepted from

any surface where run-off occurs, these may be roads, motorways and car parks or indeed any impervious areas where oils may be used.

Current legislation does not require oil/water separators that are already in service to be fitted with an oil level alarm, although this is recommended by the Environment Agency. Where no oil level indicator is in place, either the separator has to be inspected to ascertain the height of the oil within the holding tank or the tank is emptied on a regular basis regardless of the amount of oil therein. The first option requires both regular and competent level readings so that the separator does not become full to excess and consequently overflow into the drainage system. The second option creates an expense of emptying a tank that may contain no significant oil.

Oil level monitors used in separators have to be able to cope with an unfavourable environment and still function correctly over a period of time, with a nominal amount of maintenance. Detrimental effects upon a detector may take the form of a build up of dirt or oily deposit upon surfaces or moving parts. The safety aspect of any detecting equipment is important, as any spark or excessive heat could create an explosive condition. The ATEX regulations [52] categorise areas into zones, each with their own degree of safety requirements. Zone 0 has gas or vapour hazards continuously present and this refers to the area within the separator. Any electrical device used in the separator should be intrinsically safe and be certified to Zone 0 requirements [35]. Zone 1 has hazards present intermittently and would be the immediate area surrounding the tank. Zone 2, refers to the area where any hazard would be infrequent and if any, be of short duration and most likely to be within the near locality of the separator.

2.5 Oil and other material found in interceptors

As mentioned previously, the interceptor will contain solids (settled or in suspension), gases and liquids. The solids, such as silts, that have settled will only be of concern if they accumulate to any great extent and start to occupy an excessively large volume of the storage capacity of the separator. Any non dissolved gas will reside above the liquid, being made up of air that has entered during maintenance or emptying, along with any gas that has evaporated from the liquid contained within the separator. The gases found within an interceptor may be of an explosive nature or they may be hazardous to health so that care must be taken during maintenance of the interceptor

Any liquid that falls or is spilt within the catchment area will either, evaporate, become absorbed by the ground, be recovered or will eventually flow into the separator. As such, it is not only rainwater or oils entering the separator but anything that may be spilt or discarded. On a roadway it will be unpredictable which materials may be present, some of the rubber debris from tyres for instance (an estimated 53×10^6 kg per year in the UK [53]) may also be washed into the separator.

2.6 Assessment of current technology used for oil/water detection

The following discussion groups together the different technologies that have been reported or used in industry to detect oil. Not all the following techniques reviewed relate directly to oil/water separators. Many of these methods detect the presence of oils either in open water or within contained areas. For each of the different systems discussed a basic outline of the technology is provided, followed by a review of its practicality for this research. Frequently manufacturers have been cited with commercial examples.

2.6.1 Mechanical

The types of mechanical detector that employ a system of physical movement, detect the oil/water interface by relying on the density differential between that of oil and water. Thus a float is designed to be within a density that falls between that of the water and the oil, this then works on a principal similar to that of a ballcock float. This float is connected to an electric switch, which itself must comply with requirements for Zone 0. Figure 2.3 shows a typical float switch, Afriso Eurogauge Ltd. [54] produce this particular example.

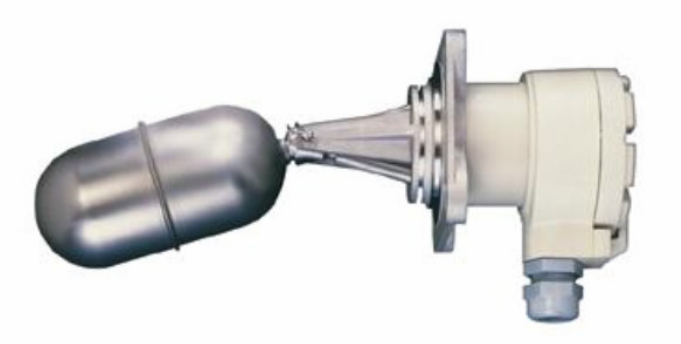

Figure 2.3. *Float switch produced by Afriso Eurogauge Ltd*. [54]

The suitability of this type of detector can be compromised over a period of time in particular environment due to a build up of substances adhering upon the float, thereby altering the overall density of the float itself. The consequences of which, are to affect the long-term accuracy of the buoyancy device.

2.6.2 Optical

Optical detection of hydrocarbons encompasses a variety of methods, some used in the laboratory other methods being used in the field. The differences in optical properties between oil and water have enabled several different routes of detection to be explored. The techniques are grouped as follows; detection through different refractive indices, detection through transmission/absorption and light scatter, and detection by fluorescence.

The majority of oil detectors require, at some position within their system, the use of electrical equipment, which is generally in close proximity if not actually integral to the detector itself. An optical detection system has the possibility of using fibre optics, whereby the detector if the equipment allows may be located some distance from the electrical components. A second advantage of fibre optics is that by the very nature of these thin flexible cables they can be placed in small or relatively inaccessible locations.

(i) Detection through different refractive indices

The refractive indices for various oils and water can be seen in Appendix A, Optical and physical properties of water and various oils. There is a consistent difference between the oils and water and through this a distinction between the collective groups of hydrocarbons can be identified from that of water. Figure 2.4 shows a technique for

such measurements through using TIR (total internal reflection). Here a sensor element of known refractive index acts as the interface between itself and the medium being investigated. The respective refractive index will either allow transmission of the light into the medium or produce conditions for TIR. The resultant signal at the receiver will then indicate the type of medium present. The effective shape of the sensor element will need to be tailored for the particular media. Problems can occur with this type of sensor if a drop of liquid or a thin film adheres to the sensor element as this will effectively alter the shape of the sensing element thus effecting the refractive properties of the sensor, thus, severely compromising the system [55].

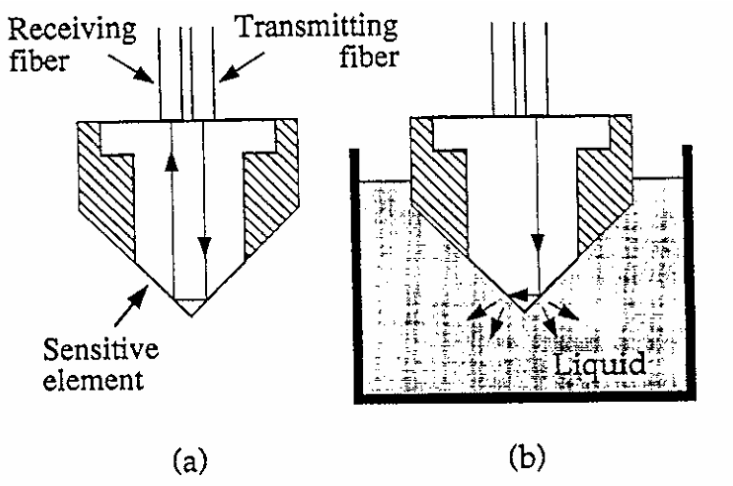

Figure 2.4. *Diagram of the sensor head which uses TIR to detect when in air (a) and light loss through transmission to detect the presence of liquid (b). [55]*

Kobold Instruments [56], see figure 2.5, have successfully used TIR in a liquid/air interface sensor, they have reported that through creating a hemispherical shape to the optical window (shown in the figure) droplets of liquid are less likely to adhere.

A technique for measurement over a large volume (as opposed to measurement at discrete positions) uses TIR within fibre optics, relying upon gradual light loss along the fibre optic cable. Here, the cladding and jacket of the cable is removed in the region of the medium being analysed. Depending upon the relative refractive indices between the fibre optic core and the medium, light will be transmitted or lost [50, 57]. The sensitivity of this method is responsive enough to determine if kerosene has been added to petrol or diesel [58]. This type of detection can suffer from the effects of thin films of material residing upon the optic fibre core but when cleaned between use is not problematic.

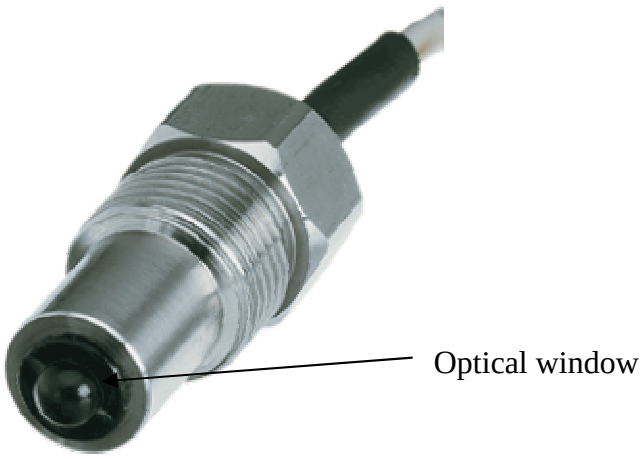

Figure 2.5. *Kobold Instruments sensor, using total internal reflection to detect a liquid/air interface [56].*

Accumulation of liquids or other debris can compromise the ability of detectors that use TIR to function correctly without a higher degree of complexity or manual intervention. Such drawbacks can, in less than ideal conditions, render this type of detector unreliable particularly if expected to function unsupervised for long periods of time whilst still trying to keep to a low cost simplistic detection technique.

(ii) Detection through transmission/absorption and light scatter

The attenuation of light at a specific wavelength varies from one medium to another and by exploiting this fact the possibility of determining the presence or absence as well as concentrations of different materials. Different methods can be used with this system of detection, which can be used for a range of functions; discrete single point position detection, level detection for a continuous flow of liquid and determination of concentrations. Each of these techniques requires some prior knowledge of the materials or likely materials that are to be determined, as their optical properties are the crux. As with all detectors, it is preferable that the system has been optimised for the particular role that it will be undertaking.

A simple two point liquid level detector as shown in figure 2.6 [59], can indicate a maximum and minimum level using a transmitter (T_1 and T_2) and receiver (R_1 and R_2). This particular sensor has been designed to determine between air and a liquid using a system of LEDs and photodiodes. Using a larger number of transmitters and receivers, the liquid level can be determined to a more exact position. This system of transmission can be customized to ascertain between different immiscible liquids by choosing a

suitable emission wavelengths. Systems based upon this arrangement have been used within the oil industry by Heron Instruments [60] and Solinst [61].

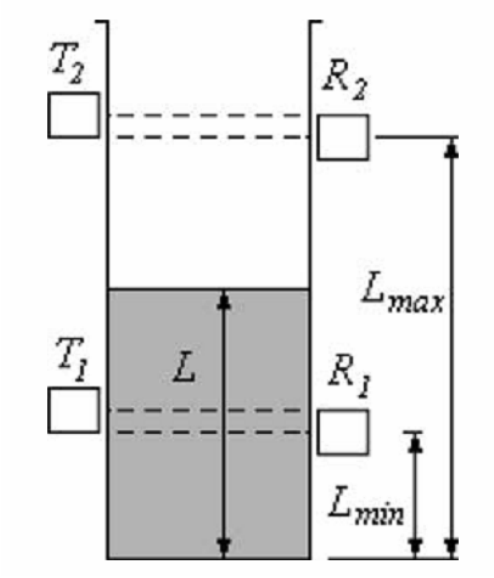

Figure 2.6. *Diagram showing the location of the light transmitters (T) and receivers (R) for the determination of liquid levels (L).* [59]

A method tried by Sandia National Laboratories [62] for use in crude oil storage tanks to determine the quantity of water to oil, was based upon the absorbance of light by the crude oil. This used two optical fibres, one with light going down and being outwardly transmitted whilst the second received light from the first. The absence of the jacket and cladding at the position where the monitoring takes place allows the light to escape from the optical fibre. The strength of the signal would then depend upon the water level, the water transmitting the light and the oil absorbing the light. A similar scheme is shown in figure 2.7 [28] where the refractive index of the surrounding medium effects the angle of the light as it enters the second fibre optic cable. Such a technique would require a system to maintain an unobscured surface for both the transmitting and receiving fibres to sustain the integrity of the detector.

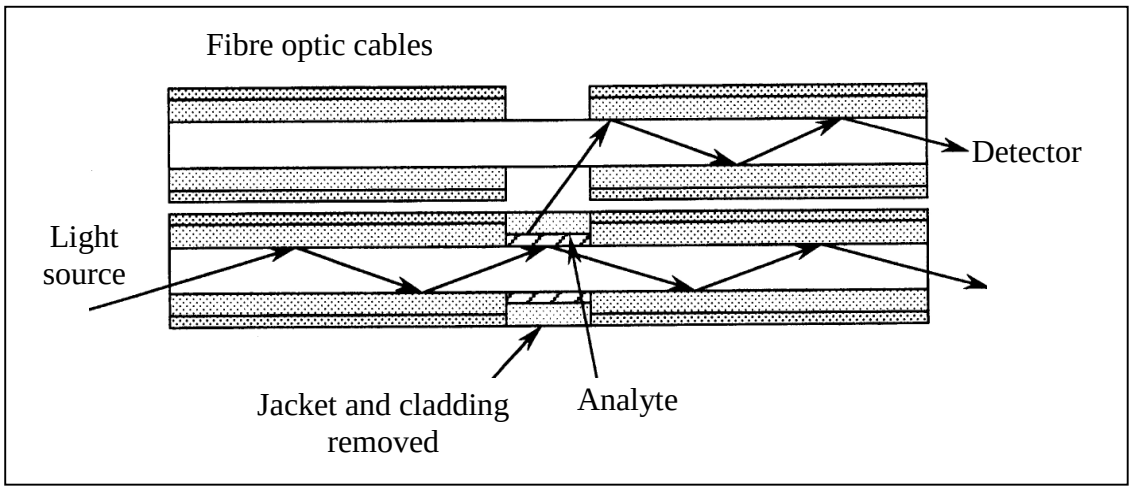

Figure 2.7. *Schematic diagram showing the use of optical fibres and the transmittance and absorbance of light in the presence of oil and water. [28]*

Another method for determining the position of the liquid/liquid or liquid/air interface uses the interface to reflect light from a transmitter to an array of receivers [59] similar to figure 2.8. The position of the reflected light would thereby determine the location of the interface. For this method to successfully work, however, the interface would require to be relatively smooth from ripples and debris, both of which would affect the results.

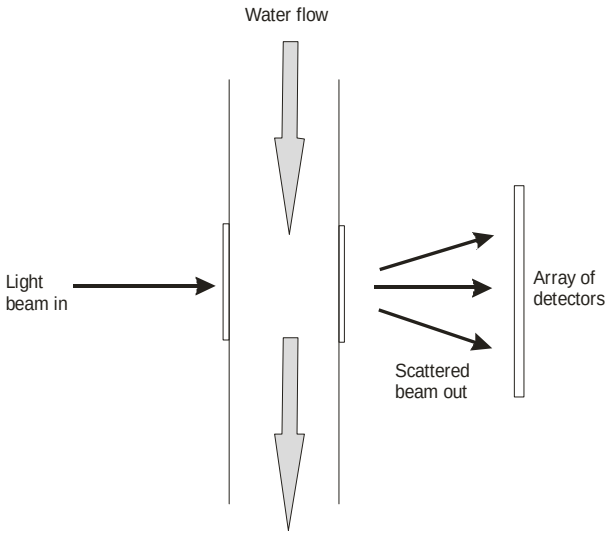

Figure 2.8. *Diagram of a light sensor instrument that detects the presence of solid impurities in flowing water through the use of light scatter. [63]*

A light based detection technique that does not have to rely upon transmission or absorption to assess the purity of a liquid. Impurities in a liquid can disrupt the transmission of light not only through absorption but also light scatter. A system using

light scatter produced by the effect of impurities in water is shown in figure 2.8 [63]. Here the use an array of detectors determines the degree of scattered light. This method has the advantage of being able to assess a continuous flow of liquid which could be a selected sample of a larger quantity. This system of assessment could be affected by flow speed or flow irregularity (i.e. creating air bubbles) which may artificially disturb the light path. This technique could be more useful in assessing the presence of oil droplets in the liquid flowing into the interceptor rather than in the bulk container itself.

(iii) Detection by fluorescence

Fluorescence has many applications for oil detection, polycyclic aromatic hydrocarbons (PAHs) which are present in oil, have with the correct excitation source the ability to fluoresce. The non fluorescent nature of water has allowed for this method to be successfully used for distinguishing between these two substances in many circumstances. It is possible to detect small quantities of oil in water (moving or still) with this process and through using lifetime induced fluorescence (LIF) to distinguish the type of oil and in the case of crude oil its source [64, 65]. Dissolved organic matter may however in some circumstances create difficulties [66]. Biological organic matter, such as algae, can fluoresce but with an excitation peak at around 685 nm for chlorophyll, this can be distinguished from mineral oil having an excitation ranging from 400 to 600 nm [67]. Fluorescence cannot only be utilised for near field detection but also from much larger distances such as from aeroplanes when detecting oil slicks [68, 69]. Unlike the methods used in other optical detection systems, detection through fluorescence does not require the oil medium to be able to transmit light but merely respond to it, although penetration to excite sufficient volume may be required, with for example, the use of laser induced fluorescence for a high powered excitation source [70]. Systems using this technique vary in size from stationary continuous flow monitors to small portable hand held detectors.

Continuous flow fluorescence monitoring of watercourses and treatment plants is employed in a variety of situations. These types of constant assessment equipment predominantly use a non-contact technique, with the optical windows being positioned marginally away from the flowing water, thereby avoiding contamination of the optical surfaces. There are several of these systems available commercially [71, 72], figure 2.9 shows a typical diagram of the system. Such a system could be used for oil detection providing a sufficient fluorescence signal could be obtained from all oils encountered.

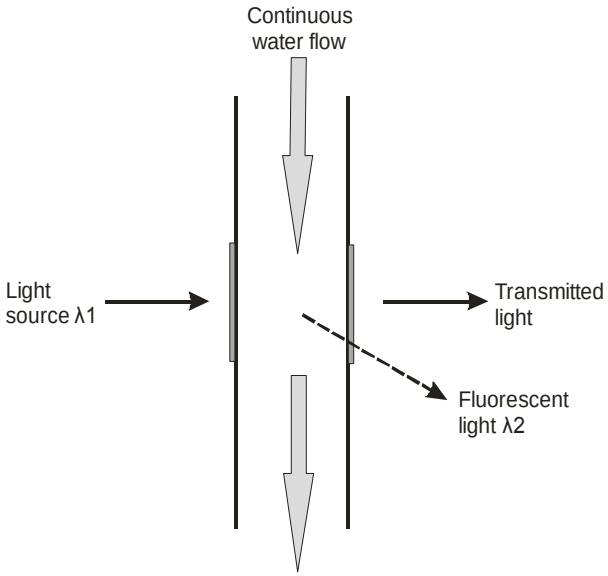

Figure 2.9. *Schematic diagram of a continuous flow fluorescent monitor, here λ_1 is UV light and λ_2 is the fluorescent light. [72]*

Portable hand-held apparatus that can determine the presence of oil pollution through laser induced fluorescence are generally light weight and capable of producing immediate assessments [70, 73]. The general design of these consists of an excitation source and detector with a separate probe connected through a flexible fibre optic cable or a more rigid system if used close to the operator. LaserLaboratorium Göttingen [74] produce a sophisticated system that can analyses both the type and concentration of oil in water.

More complicated and expensive systems for examining hydrocarbons work by producing a fluorescence excitation-emission matrix (EEM). Here the three dimensional graphs that are produced can not only distinguish between different types of liquid hydrocarbon fuels but also determine whether these fuels have been illegally contaminated by kerosene or other lower taxed fuel [75, 76]. The use of a pulsed UV-laser to induce fluorescence followed by the measurement of decay times has been used for the detection of crude oil pollution in open seas, to trace sources of these pollutants [77]. These technique can be used both in field and laboratory [70] but would probably be too expensive to be used for oil detection within an interceptor

The use of fluorescence for oil detection can require quite expensive and sophisticated equipment. Nevertheless, moderately priced detection techniques could be used for what would be the simpler task of determining the presence of oil a particular position within

an oil interceptor. Again as with the other optical techniques discussed the obstacle of maintaining transparency for the optical windows over an extended period of time would be possibly the part that posed the main challenge. The delivery of a light source as well as receiving any response whether it be for fluorescence or transmission /absorption detection could be served through fibre optics, whereby any associated electrical system would be sited at an appropriate safe distance.

2.6.3 Ultrasonic

Ultrasonic level detectors (or distance detector) offer a non-contact system, which can identify interfaces between air and liquids or solids or between two liquids where the liquids are immiscible. Through using the speed of sound (acoustic velocity), the level is detected by measuring the time of flight from the emitter to the detector, via the sound echoing (reflected) from the surface or interface being detected. The available ultrasound range of frequencies varies from just above human detection at around 20 kHz to 15MHz. The most common form of emitter and detector is a piezoelectric crystal that vibrates with an alternating voltage or step voltage excitation, producing the ultrasound and a piezoelectric transducer for receiving it.

Medium	Velocity (m s^{-1})
Air	331.3
Oxygen	316
Water	1498
Mercury	1452
Various oils [78]	~ 1300 - 1500
Glass	5000

Table 2.1. *Ultrasonic velocity through different media. [79]*

The temperature of the medium affects the velocity of the sound, this can be compensated by factoring in the temperature or measuring the time of flight over known distances through having two systems, humidity of air has a lesser effect but can also be adjusted in the same way. Table 2.1 shows the relative ultrasonic velocities through different media at room temperature [79]. The acoustic velocity of oil is dependant upon the type of oil, this range reflects the diversity of oil that may be encountered within an interceptor, making detection by a direct comparison not possible.

The minimum distance of detection is dependant upon the wavelength between each pressure front, the shorter the wavelength the more accurate the distance that can be determined. The shorter wavelength (higher frequency) ultrasounds have a reduced range due to higher attenuation and hence tend to be used over shorter distances, for larger ranges the longer wavelengths are more suited.

Ultrasound is used for many applications, in liquid level gauges in oil tanks, over a distance of several metres they can have accuracy of ± 10 mm [80]. Ultrasound can also be used for single point level sensors, where the emitter and receiver are placed opposite to one another in close proximity, here they are not some much detecting an interface but rather the presence of different media [81].

The necessity of an electrical system to produce and receive the ultrasound and without the option of an alternative method of delivering this non contact sensor into the interceptor, this reasonably priced ultra sonic technique was not pursued.

2.6.4 Radar and nuclear

The radar like the ultrasonic based level gauges can use the interface of the materials to reflect or absorb the signal. The main advantages of radar, being similar to optical electromagnetic radiation except using longer wavelengths, are that there are no moving parts and most of these systems do not come into contact with the material. Situations with flammable, hazardous or dirty working conditions will not affect the mechanisms.

For non-contact radar, the transmitter/receiver is positioned above the target and from there the position of the interface for the materials is detected. In the less sensitive radar techniques, the difference of the dielectric constant (ε) for the two liquids must be > 10 to create a significant reflected signal and the material with the greater ε must be the lower of the two materials [82]. Water has $\varepsilon \approx 80$ whilst hydrocarbons have $\varepsilon \approx 1.8\text{-}2.5$, the air/hydrocarbon interface has no significant signal and as such is not detected.

Whilst these methods can be accurate down to a few millimetres the current commercial units are quite highly priced (from £2000 and above [83]) and so this type of system may leave little scope to produce an inexpensive detector. The depth of material to be measured must also have known and predictable properties. The types of hydrocarbon that could be found in practice in the oil/water separators will no doubt be from various

origins and thus having varying properties, possibly making detection of the interface difficult to determine.

2.6.5 Electrical

Methods directly based on electrical measurement use conductivity, capacitance and inductance. Liquids and solids (powdered or granulated) can be monitored, however, contaminates in solids and in particular moisture, can produce inaccurate results, but in homogenous liquids consistent results can be achieved. These types of monitors can work in extreme environments and are suitable for many chemical processes.

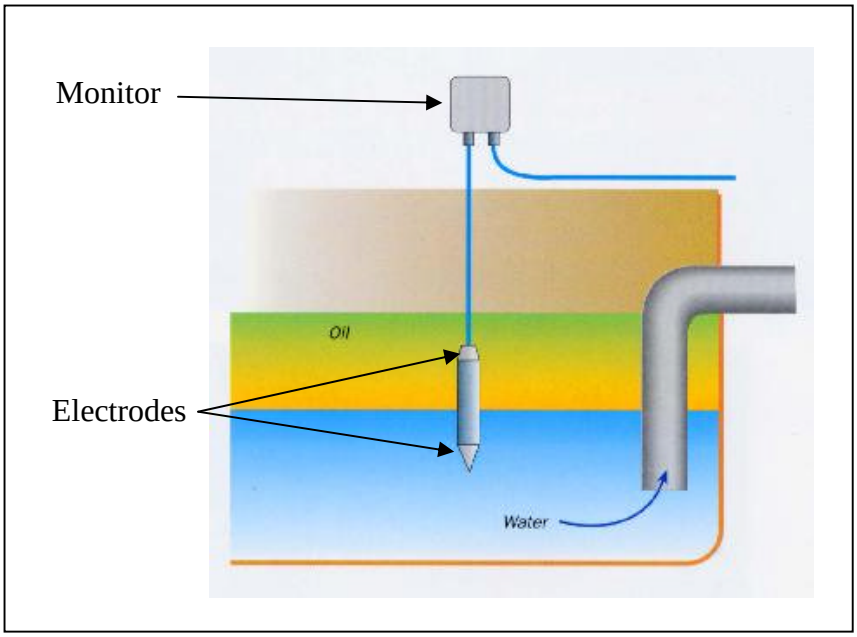

Figure 2.10. *Diagrammatic layout of the Afriso Eurogauge Ltd. oil detector, showing the electrodes positioned in the liquid. [54]*

Through measuring the electrical conductivity (or the resistance) different materials may be identified. The difference between the electrical conductivity of oil and water, which is low and high respectively, has made this method suitable for use in an interceptor. By using a probe (with two electrodes) that is positioned at the critical height within the separator, then determination that the oil had displaced the water is through the electrical resistance of the oil. A commercial example of this type is produced by Afriso Euroguage Ltd. [54] and is shown in figure 2.10. This detector is suspended into the interceptor, being positioned in the liquid.

The effect of material build up upon the electrodes over time may possibly interfere with the performance. This system produced a simple detector with no moving parts but

would contravene the brief from Andel Ltd. that there shall be no electrical components within the interceptor.

A capacitance sensor uses the dielectric constant of the substance, the higher the dielectric constant, the higher the capacitance. These monitors can be used as detectors in two ways; determining a presence of different substances, or as a capacitance level sensor, where the level of the liquid or solid rises between the two plates, thus, the substance behaves as a dielectric between the two plates as the depth increases, similar to the principle used for a car fuel tank. This arrangement does not require any moving parts or the direct contact of the material being assessed. An example of commercial applications of these detectors are produced by Arjay Engineering Ltd. [84] and is depicted in figure 2.11, (a) shows probe A in a tank, where the distance from the walls (D) is fixed. As the different levels of two materials vary within the tank their relative ratios can be indicated, here K=1 for air and K=80 for water (where K is the dielectric constant). Petroleum products have a typical K value from 1.5 to 4 [85]. Figure 2.11 (b), is a picture of a typical appliance that can be placed within a tank. Arjay Engineering Ltd has several variants of this system, including oil/water separator monitors.

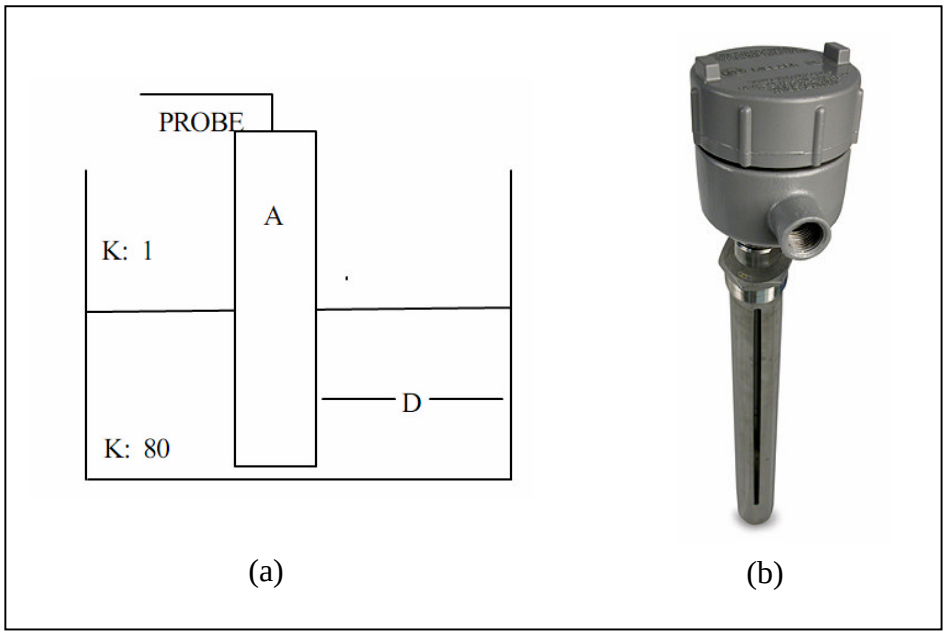

Figure 2.11. *Capacitance sensor by Arjay Engineering Ltd., (a) shows a diagram of position of the sensor and (b) is a picture of a probe [84].*

Whilst all electrical components need to comply with safety standards, these electrical methods have an absence of moving parts which makes them suitable when working

with abrasive materials and are capable of working in harsh environments but again require electrical components within the region of the interceptor.

2.6.6 Hydrostatic

Hydrostatic pressure created by a liquid at any particular point is related its depth and density of that liquid and hence, as the depth varies, so does the pressure. Using a measurement of pressure, then allows the level of liquid above the sensor to be indirectly assessed. There are several types of systems available to measure pressure; from mechanical diaphragm gauges and pressure transducers (electrical) to systems using light deflection and fibre optics.

The SI unit for pressure is the Pascal (Pa) which is equal to one N m^{-2}, other units often quoted are pounds per square inch (PSI), atmosphere (atm), bar and millibar (mbar or mb). Appendix A shows the conversion for the commonly found units. Commercially available systems can detect small pressure changes required in altimeters to high pressure systems found in industry. Most gauges are intended to operate only through a small range of pressures, these usually offering the most accuracy. Subjecting a gauge to a pressure greater than which it was originally designed to measure may cause permanent damage.

All the different types of pressure measurement systems operate in one of three ways, each one being suited to particular applications, these are listed below:

(i) Absolute pressure; A gauge with one inlet going to the environment to be measured and the other inlet is connected to a vacuum chamber. This type is used for atmospheric barometric pressures.

(ii) Sealed gauge pressure; A gauge with one inlet going to a measuring port, whilst the other is connected to a sealed chamber pressured to the average atmospheric pressure. Vehicle tyre pressures are measured this way and are referred to as gauge pressure.

(iii) Differential pressure; A gauge with two inlets (ports), each port is in a different environment. The difference between the two ports is the pressure indicated. This type of gauge can be seen on liquid tanks and pressure sprayers.

Determining liquids density by volume has been practiced for many years where allowances may be made for temperature and pressure [86]. Accurate electronic pressure transducers have allowed density to be determined through pressure [87]. In figure 2.12 [82] are three different pressure transducer gauges, (a) is an open tank measuring at a single point, making no allowance of atmospheric pressure, measuring absolute pressure. The tank in (b) has a differential pressure gauge in a sealed tank, whereas in (c) is a more involved arrangement, where a gas is pumped in under pressure, the pressure required by the gas to create bubbles is related to the depth of the liquid, this pressure is then relayed to the differential pressure transducer.

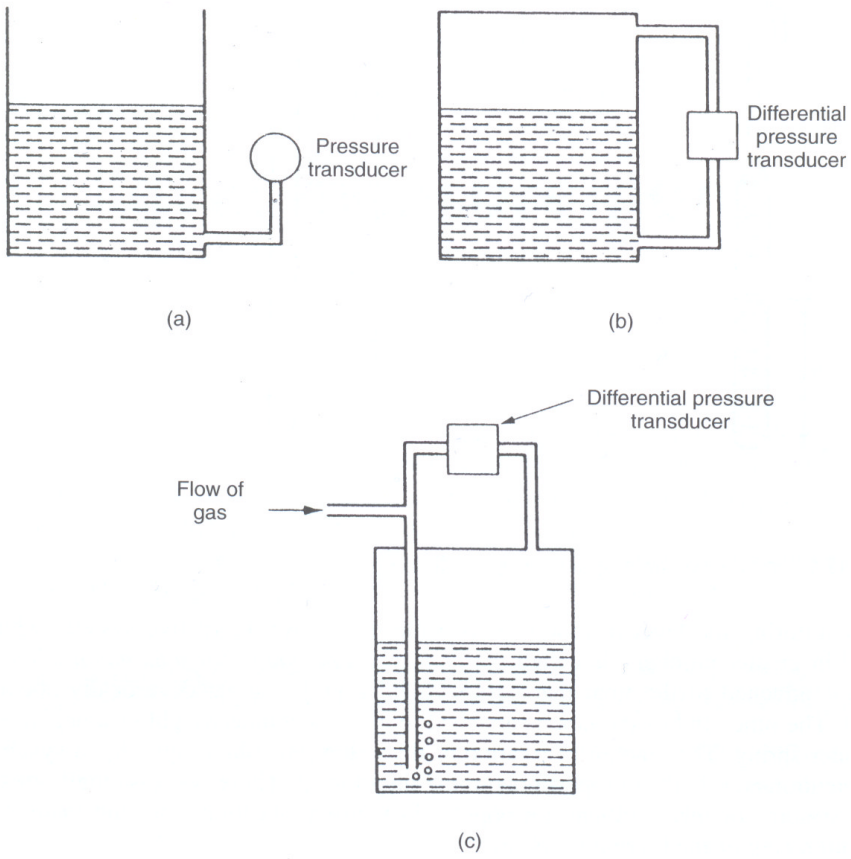

Figure 2.12. *Three different hydrostatic pressure measurement systems each one is using a pressure transducer, (a) measures the differential pressure of the liquid and the atmosphere, (b) measures a sealed system and (c) measures the differential pressure of a gas flow. [82]*

2.6.7 Air bubble rise times

The different viscosity between liquids has been studied and through the use of bubble rise times, information has been determined about the fluids [88]. A gas flow through the liquid and a detection technique based upon fibre optics would potentially form a detection system without the use of electrical systems within the interceptor.

2.6.8 Fibre optics

Methods of pressure measurement using fibre optics involve variation of light loss caused through some mechanical movement. Figure 2.13 [89] shows a method when a fibre optic is placed between two profiled plates, as pressure is applied to one of the plates the fibre optic cable is distorted, creating micro-bending, producing light loss from the fibre. The resulting reduction in light transmission along the fibre thus indicates a pressure change. There are several variations of this type of fibre optic bending loss.

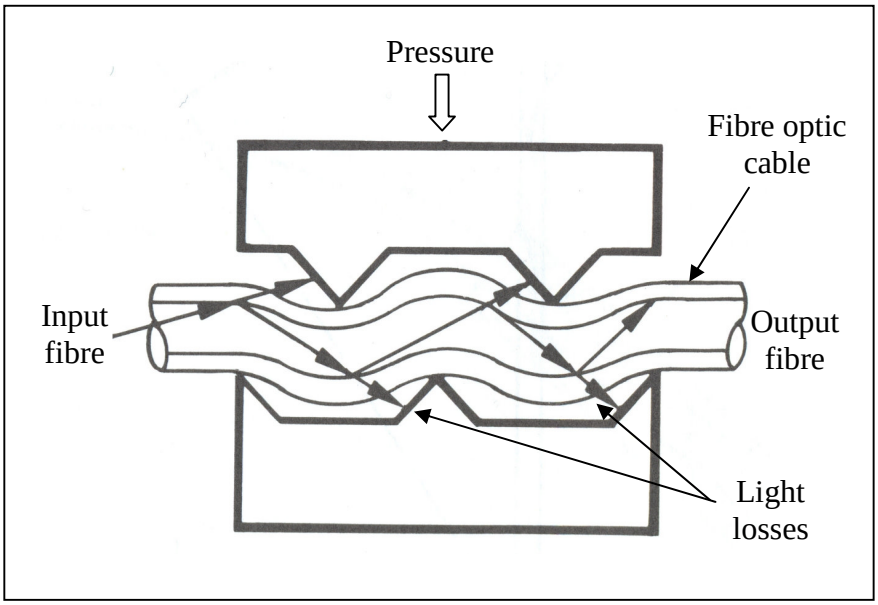

Figure 2.13. *Light loss from a fibre optic cable due to micro-bending as pressure is applied to the fibre. [89]*

Various other techniques involving fibre optics rely upon movement of a piston or diaphragm to distort a mirror or some other reflective surface. Figure 2.14 [90], shows a reflective diaphragm whose movement effects the returning light intensity.

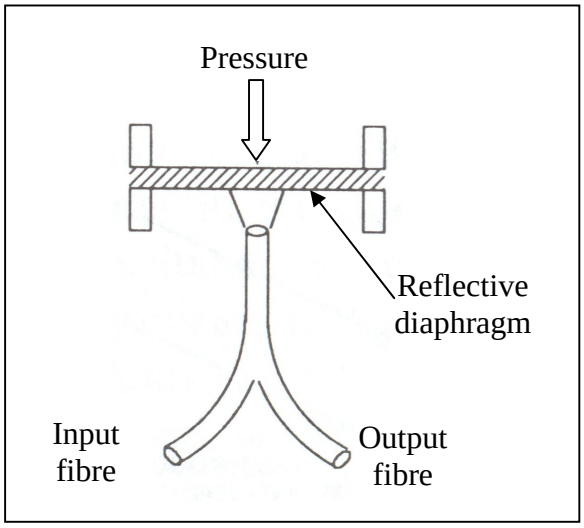

Figure 2.14. *Light scatter due to the movement of a reflective diaphragm resulting from pressure change. [90]*

The use of fibre optics to measure a pressure change would allow a non electrical signal to be carried to and from the interceptor. The micro bending technique which requires direct physical contact with the fibres would involve a pressure force that may be beyond that experienced through the change from water to oil. Systems which require the use of reflective areas need to be kept free from deposits or corrosion which may reduce the reflectivity of the surface and so the continuous reliability of this technique, however such systems have the advantage that they do not effect or retard the diaphragm/piston movement but merely respond to its change.

2.6.9 Other methods

There are a number of other techniques for assessing the presence of oil in water that are laboratory procedures and as such would probably be unsuitable for use in a separator or too intricate to economically adapt i.e. gravimetric (involving precipitation) and nephelometry analysis (light scattering of a precipitate), produced by Arjay Engineering Ltd [84].

2.6.10 Summary of existing oil and level detection techniques

It has been shown that there is a range of techniques available for detection of both oil/water presence and level of the interface, for in-field and laboratory assessment. Some of these are always going to be inherently too expensive or not practical to be used in an interceptor, for example radar, although many of the other methods initially

show an economic and reasonable possibility. Ideally, a detector that has no moving parts and is free from fouling or is non-contact would produce a suitable solution, such as ultrasound, but in the conditions of an interceptor debris, from incoming materials will undoubtedly create problems. With the type of oil and other material entering interceptors varying at different locations, fouling of the optical windows as with any other parts may be problematic due to its unpredictable nature. The opportunity to periodically service any detector or at least the sensor that lies in the vicinity of the liquid, allows the scope for several detection techniques to be further investigated.

Mechanical methods of detection, where moving parts are in contact with the liquid are not suitable due to possible fouling of the mechanics. Similarly, systems using electrical parts within the vicinity of the detectors are also inappropriate. The non-contact method of ultrasonic wave propagation would also require electrical components to be placed within the interceptor.

Optical or hydrostatic detection methods offer the scope for further research for use within an interceptor. Fluorescence and other optical techniques have been widely used, for detecting oil and in distinguishing oil types, both in-field and in laboratories. Here for the use within an interceptor, light could be transferred via fibre optics. Similarly, for hydrostatic analysis, tubing could relay pressure to a sensor. Both of these systems would allow electrical components to be located some distance away from the interceptor. With these methods, any moving parts if required would not need to be in contact with any liquid from the interceptor.

2.7 Methods of oil level detection to be investigated

Following the review of detection techniques, there are a number of areas which show potential research routes through which a solution for producing a detector or detectors that will fit the criteria, demanded by Andel Ltd, may be found. These five directives are; non electrical devices within the area of the interceptor, no moving parts to come into contact with the liquids, to be capable of operating unattended for up to six months, to be able to detect oil at a particular level and to be competitively priced. Outlined below are five key areas of investigation areas to be pursued:

1. Viscosity, air bubble rise

Based upon the various viscosities of the oils and water, assessment of air bubble rise

times should indicate the type of liquid present, thereby identifying oil or water. Gas (possibly air) can be pumped to the base of a tube and small volumes released, optical sensors directed through fibre optics could measure the rise times and as such no electrical components would be required within the interceptor.

2. Reflection at the interface

The immiscible nature of oil and water results in the oil lying above the water. Ideally this will produce an interface that should be detectable. With the use of light, the position of this interface should be detectable. The light emitter and collector can be conveyed through fibre optics.

3. Transmission and TIR

Light transmission through various media varies with wavelength this line of investigation will examine the oils and water to find a suitable waveband that will be suitable for oil and water distinction. Similarly, through the difference in refractive indices of oil and water a system using TIR may well be suitable for use in an interceptor.

4. Fluorescence

The detection of hydrocarbons through fluorescence has been widely used. This research will examine techniques to transfer fluorescence detection into an automated system capable of working in an interceptor.

5. Hydrostatic detection through density and pressure

The small but significant density difference between oil and water allows an approach for a detection method that is different from that of using an optical system. This technique does not rely upon the non-fouling of optical widows or moving parts within the interceptor gives a system that should be free from many of the drawbacks of other detection methods.

Each of the five areas of research is further explained and the theoretical and experimental results of each are presented and discussed in the following four chapters.

3. Oil/water interceptor: Analysis and detection methods

This chapter follows the development for an oil/water monitor. In the first part of this chapter, several oil samples have been analysed and appropriate comparisons with water have been made to determine whether any distinctive physical or optical differences found could be feasibly used to produce an oil level monitor. In the second part several detection methods have been appraised, either experimentally or theoretically.

3.1 Analysis of the properties of oil samples and water

The oil samples were examined with regards to their optical and physical properties in order to substantiate their differences with regards to the monitoring techniques described in the previous chapter. Included in this analysis are mixing and separation experiments for the oils and water, and a theoretical assessment of how oil droplet sizes can affect the speed of separation.

3.1.1 Oils and water used in this research

In the laboratory experiments several different oils were used, all of these were refined mineral oils and had been chosen to be a representative of the type of oils that could be encountered in different locations where interceptors have been placed. Data for many of their physical properties of the oils were available from the manufacturers and their range would be sufficient to test a monitor in a variety of conditions. The used motor engine oil and the sample from Andel Ltd were exceptions to the other oil samples, although mineral oil based, both of these samples represented what would be more a challenging representation for oil detection as some of their properties were in contrast to the other samples, such in their viscosity and light attenuation.

For the majority of the experiments in the laboratory ordinary tap water was used. Purified water was used in the absorption and fluorescence assessments.

Oil samples used in the experiments and theoretical analysis were:

(i) Motor engine oil;

The samples used were Castrol GTX Magnatec 10W-40 and is referred to in this text as new motor oil.

(ii) Road diesel;

This is also known as DERV (Diesel Engine Road Vehicles). The samples used were obtained from a petrol station.

(iii) Rebated diesel;

This is similar to DERV except that the rebated diesel is higher in sulphur and is used for off-road vehicles such as plant and agricultural machinery and commercial river craft. This rebated diesel is taxed at a lower rate than DERV and as such is distinguished by having a diazo dye added, this readily dissolved compound [91] and in the UK is usually in the form of Sudan IV.

(iv) Used motor oil;

The sample used was recovered sump oil from a diesel engine vehicle. Although all used engine oil will vary, not only from vehicle to vehicle but also from the length of time it has been in the engine. Used engine oil contains many other substances apart from the original oil. There will be water from condensation, metal particles from engine wear, unburnt fuel, particles of soot from burnt fuel and burnt engine oil and other substances which have been drawn into the engine or been produced from combustion. The dark or black appearance comes from the denatured oil and particles of soot.

(v) Petrol;

This was not used in the laboratory experiments but its performance with the monitors was assessed theoretically.

(vi) Oil samples provided by Andel Ltd.

This had been recovered randomly from an interceptor.

3.1.2 Optical and physical properties of oils and water

Several of the optical and physical properties for the oils and water are available from data sheets and other references. Other properties not found but considered to be of value for the oil/water detector were measured in the laboratory. This section presents and discusses the results of the optical and physical properties of air, water and various oils. An overall summary can be found in Appendix A.

(i) Assessment of refractive index

To determine the refractive index, the liquid samples were placed in an Abbe Refractometer and assessed at the average Sodium D line wavelength of 589.3 nm. In this refractometer, the liquid is sandwiched into a thin layer between two prisms both of which have a known refractive index of around 1.7, this being the upper limit of the refractometer. Light is then shone across the sample, the region between the light and dark region can be noted against a scale, this then being the refractive index

Oil sample	Refractive index
New motor oil	1.477 ± 0.005
DERV	1.460 ± 0.005
Red diesel	1.478 ± 0.005
Used motor oil	Not determined
Sample from Andel Ltd.	Not determined
* Petrol	1.430 ± 0.005 [92]
* Water (20°C)	1.333 [78]

Table 3.1. *Refractive index of samples assessed in the laboratory, * the data for petrol and water were from other sources.*

The results shown below table 3.1 were determined at room temperature (~ 20°C). Due to the highly scattering nature of the used motor oil and the sample from Andel Ltd., it was not possible to determine the refractive index for these materials.

The findings for the refractive indices for all the oils vary from ~ 1.430 ± 0.005 for Petrol [92] to ~ 1.478 ± 0.005 for red diesel, in comparison, refractive index for pure water at 20°C is 1.333 [78]. A clear distinction can be seen between the refractive indices for the oil samples and that of water.

(ii) Assessment of absorption and transmission

For any optical approach, some knowledge is required of the absorption and transmission of light at different wavelengths for the different media. The analysis presented in this section examines the transmission and absorption of the four oil samples and pure water, from UV/visible to the Mid-IR wavelengths. The UV/visible range traverses 195 to 700nm, the NIR from 0.7µm to 2.5 µm and the Mid IR range was from 2.5 to ~16 µm.

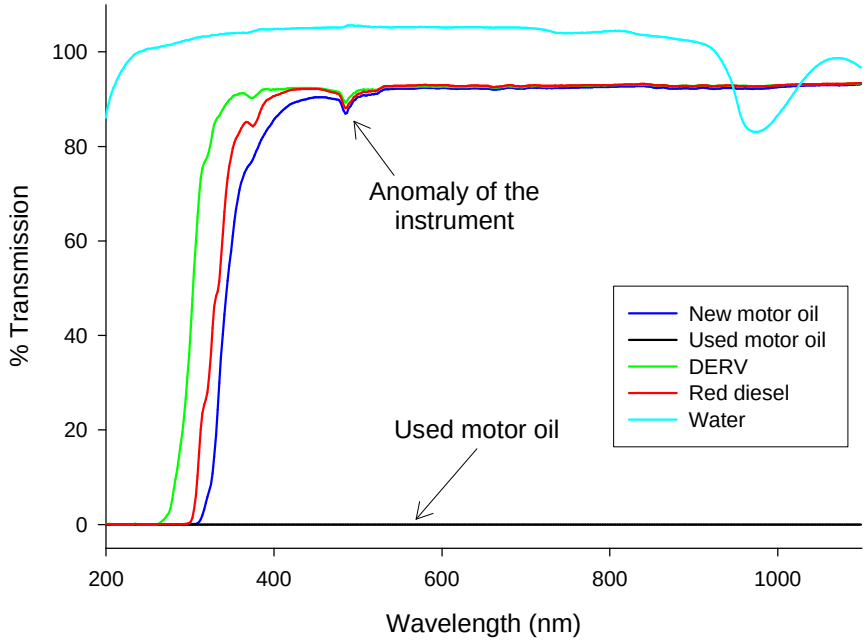

Figure 3.1. *UV/VIS % transmission for oil samples and water using a 5 mm optical path length fused silica cuvette.*

As discussed in chapter 1, the UV part of the spectrum has higher photon energy than that of the IR and this light absorbed by the molecule changes the electronic state, whereas the IR light affects the vibrational and rotational states of the molecule. When the UV to visible light is used to measure the absorption or transmission of the material, characteristic broad absorption was seen. In contrast, the absorption peaks of the IR light have sharp peaks providing information about the materials structure itself. The IR spectrum is usually given in wavenumbers as opposed to wavelengths. The three spectrometers used are as follows:

(i) UV/visible; Unicam 5625 UV/VIS Spectrometer, range 195 to 1100 nm.

(ii) NIR to Mid IR; Bruker IFS 66/S, range 0.8 to 5 µm

(iii) NIR; Perkins Elmer Spectrum RX1, range 4000 to 600 cm^{-1} (1 to 16 µm)

For the UV/visible spectrum a fused silica cuvette with a 5 mm path length was used. The advantage of the fused silica is that it has low absorption in the UV region. The results are shown in figure 3.1, a base line using an empty cuvette had been used and no correction for reflection has been made, hence, the pure water shows a transmission of over 100% for part of the spectrum.

Water has low absorption through the near UV to visible spectrum. The new motor oil, DERV and the red diesel displayed similar transmission spectra, the major transition from absorption to transmission occurring from 300 to 400 nm. The used motor oil in contrast to the other oils displays a low transmission through the whole of this spectrum.

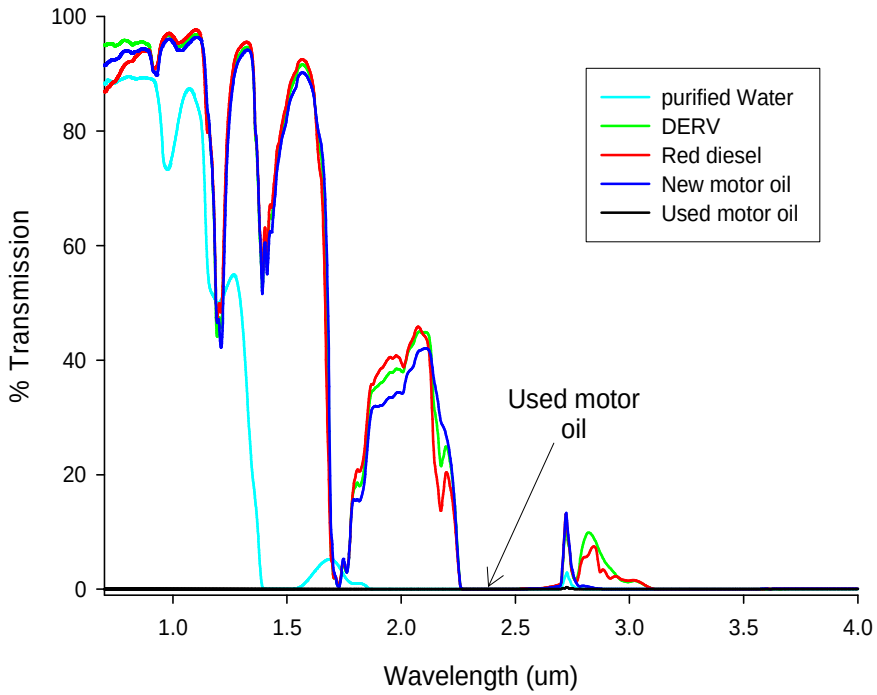

Figure 3.2. *NIR to Mid IR % transmission for oil samples and water using 5 mm fused silica cuvette.*

The significance of the oils' absorption of the light in the UV region becomes important with regard to fluorescence detection. The small differences in their absorption in this part of the spectrum affect their fluorescence emission, as will be discussed later.

The NIR to Mid IR transmission analysis also used the 5 mm path length fused silica cuvette, the new motor oil, DERV and red diesel produced results where these oils were similar to each other and again no transmission was detectable for the used motor oil. As expected, the purified water was highly absorbent of all light at wavelengths longer than ~ 1.4μm, this can be seen in figure 3.2.

The fused silica cuvette had low transmission at ~ 2.7 μm due to absorption by the O-H bonds due to the presence of H_2O within the fused silica itself. The cuvette started to show increasing absorption from ~ 4 μm to 5 μm and beyond this region there was total cut off.

For the Mid-IR assessment instead of a cuvette a small amount of oil was placed between two optical windows made from NaCl. This created a film of oil, which was then positioned into the Perkins Elmer Spectrum RX1 spectrometer. The percentage transmission was then plotted through the wavenumbers 4000 to 600 cm^{-1} (1 to 16 μm). At wavenumbers less than 600 cm^{-1} the NaCl window starts to absorb the light and hence is the upper limit for this technique.

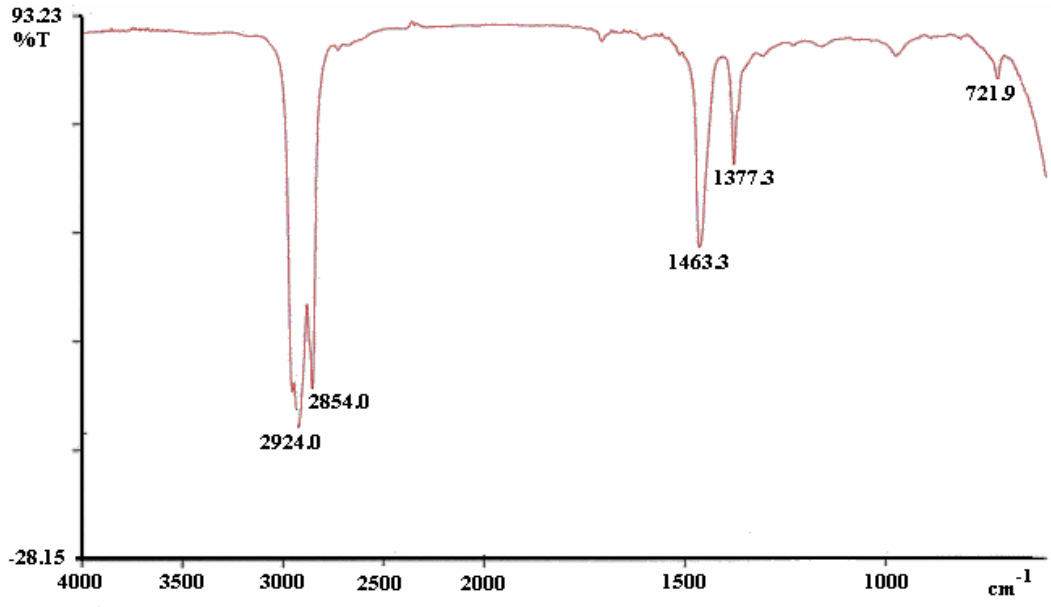

Figure 3.3. *Mid IR spectra for new motor oil, for wavenumbers 4000 to ~600 cm^{-1} showing absorption peaks.*

The plotted results from two of these experiments are represented in figure 3.3 to figure 3.4. Similar percent transmission peaks were seen in with these carbon based oils, strong absorption occurred from 2800 to 3000 cm^{-1}, due to the characteristic C-H bond stretching and again two sharp absorption peaks at 1460 and 1377 cm^{-1} from C-C stretching [93]. The red diesel, which normally has Sudan IV added, showed greater absorption in the 1000 to 600 cm^{-1} region of the spectra. Sudan IV has a molecular structure containing aromatic rings which absorb in this region.

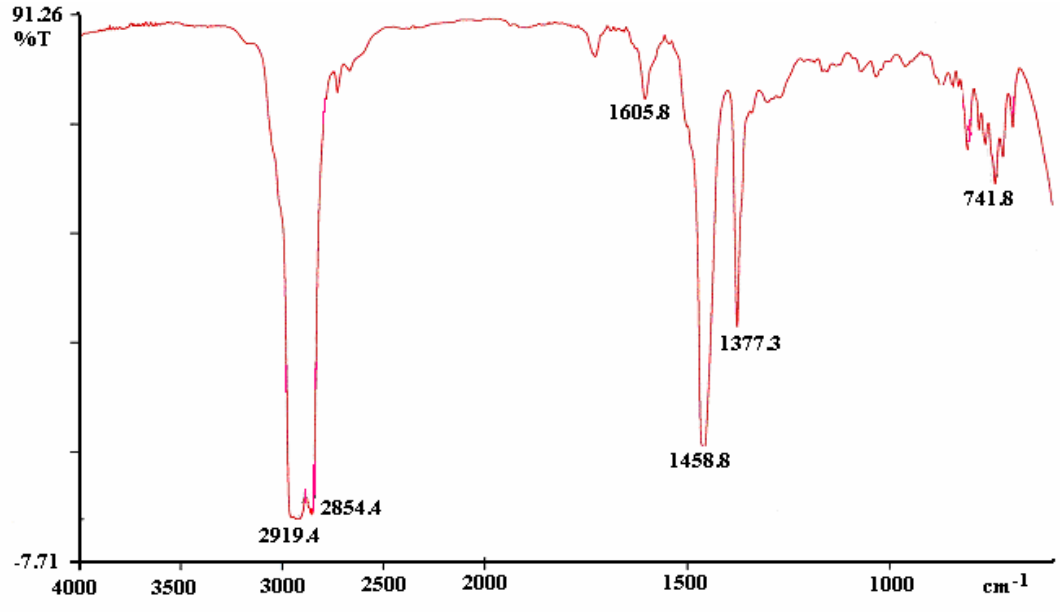

Figure 3.4. *Mid IR spectra for red diesel, for wavenumbers 4000 to ~600 cm^{-1} showing absorption peaks.*

The short path length of this Mid-IR spectrometer technique allowed light to be transmitted through the used motor engine oil, showing the characteristic aromatic absorption peaks seen in the other oils but with an overall lower transmission across the spectra. The used motor engine oil through both internal and external conditions will have had other particles and contaminates contained within it, such as, soot, water, fuel, oxidized and degraded oil.

The smaller peaks found in the area of the spectrum from 700 to 1500 cm^{-1} are known as the fingerprint region, these peaks are characteristic absorption patterns resulting from interacting vibration modes. This region is complex and usually difficult to interpret, although different compounds have their own unique absorption pattern and consequently this region allows compounds to be identified through matching with known samples. Here similarities were seen in the DERV to red diesel samples and the new motor oil to the used motor oil, however the used motor oil contains a collection of other products.

(iii) Assessment of the absorption coefficient of oils from UV to NIR

The light transmission for the oils and water has been seen to be wavelength dependant, similarly the fluorescence response of the oils produced an emission response that depended upon both the type of oil and the excitation wavelength. As with all analysis which requires an optical response, a comparison of the absorption coefficients of the different analytes can give a clearer understanding to the efficiency of different analytical techniques. This section takes a quantitative examination of the oils with regard to their absorption coefficient across the UV to NIR spectrum

The absorption coefficient was assessed for four oils samples by using a Unicam 5625 UV/VIS spectrophotometer from the UV to the NIR (300 -1100 nm), set to a resolution of 2 nm. One main obstacle limiting such a determination was the low transmission of optical radiation by the used motor oil, this may be a function of both light absorption and scatting. When measuring light transmission, the problem of light reflection at the cuvette interfaces, albeit small (generally less than 4% per interface for air to glass), needed to be taken into account. As can be seen in figure 3.1, the percentage transmission for the purified water through a part of the spectrum examined appeared to be greater than 100%, although it would be reasonable to expect that optical transmission for this liquid through a 5.0 mm path length be high, this phenomenon, however, was caused by the water altering the reflection coefficient of the two interfaces of the cuvette after first using an empty cuvette as a baseline (to counter the absorption of the cuvette itself). This reduction in reflection had the effect of increasing the total light transmission beyond that seen by the base line. Whilst the above technique would often be suitable for a general transmission assessment for a material, a more comprehensive appraisal would be required to allow calculation of the absorption coefficients of these oils. Here, techniques to counter both low transmission and interface reflection have been addressed.

To determine the absorption coefficient for the used motor oil, a cuvette was required that had a sufficiently short path length to allow a sufficient proportion of light to be transmitted. For highly absorbent liquids such as crude oils, other researchers have used specially made cuvettes from 1 to 10 μm [94], although these had proved to be difficult to uniformly fill. For this work, three cuvettes were used, the smallest cuvette having a path length 200 μm. This cuvette comprised of two fused silica glass slides, which acted as the optical windows, separated by two spacers, once assembled these produced an

optical path length through the liquid of 200 μm ± 10 μm, see figure 3.5. The top fused silica slide was made so that it could be lifted to allow the cuvette to be filled with oil and after several practices this cuvette could be filled uniformly and be free from air bubbles. The other two cuvettes were standard purchased fused silica cuvettes filling from the top, with path lengths through the liquid of 5 and 10 mm.

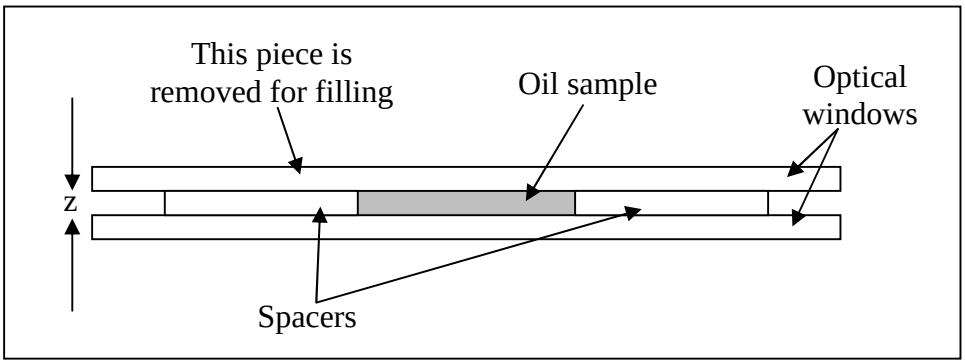

Figure 3.5. *Diagram of the 200 μm fused silica cuvette, showing the optical path length z and the removable optical window.*

The three empty different sized cuvettes were compared for their % transmission. Figure 3.6 shows that there was a small difference at the shorter wavelengths (~ 7%) but towards the NIR part of the spectrum the cuvettes exhibited a near comparable transmission (≤ 3%).

The reflection of light from the four interfaces of the cuvette needed to be corrected when calculating the transmission. The reflection coefficient, R, ranges from R = 1 for total reflection to R = 0 for entire transmission. Figure 3.7 shows a diagram of a typical cuvette, the four interfaces where R possibly will occur are indicated, also shown is the path length, z, and the incident, I_0, and transmitted light, I_1. Each interface creates the possibility for a reduction in the transmitted light and a baseline from using an empty cuvette would correct for the reflection coefficients for the outer interfaces, R_1 and R_4 however, when the cuvette was filled with liquid (in this case oil), the reflection at the interfaces R_2 and R_3 would be reduced due to the relative similarity of the refractive indices between the cuvette and the oil compared to that of cuvette and the air. Two methods were used to counter the effect of the reflection at the two inner interfaces.

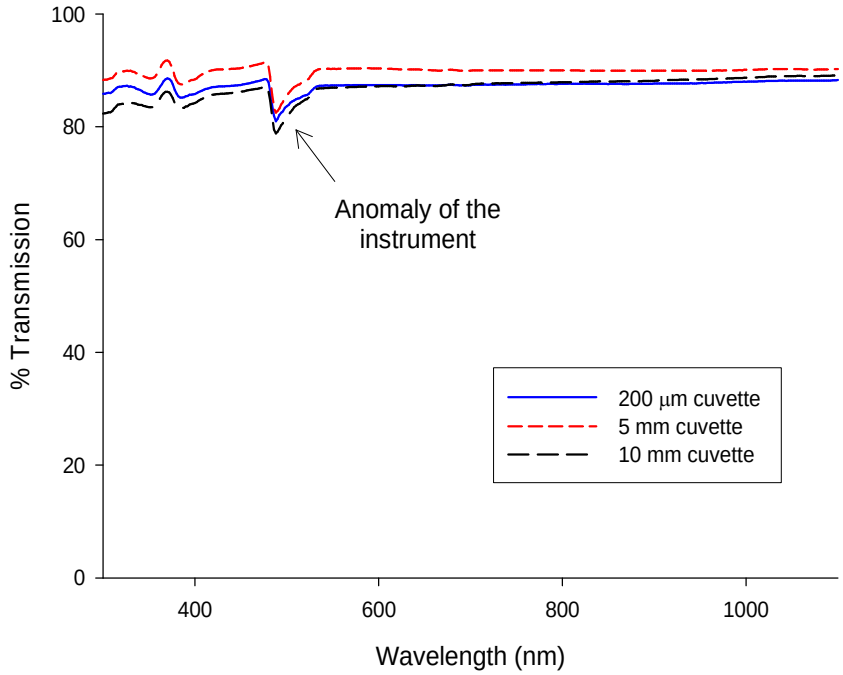

Figure 3.6. *Graph showing the % transmission for the three empty different sized fused silica cuvettes.*

The first method made use of the three cuvettes by deducting the transmission of one cuvette from that of a larger cuvette. Here for example, transmission from the 5 mm cuvette was used as a baseline for the larger 10 mm cuvette, this produced an optical transmission for a path length of 5 mm, and so forth with combinations using the other cuvettes. This resulted in a transmission values through known path lengths for the various liquids. Here, the effect of the change in interface reflection coefficients between fused silica to air and fused silica to oil was avoided.

The second method used the transmission for oil within a cuvette and adjusted this figure to allow for the reflection at the different interfaces. Here for each different sized cuvette, a base line was established with the empty cuvette, this cuvette was then filled with oil and the transmission spectrum recorded, this was repeated for each of the oils. This process was then repeated using the other cuvettes.

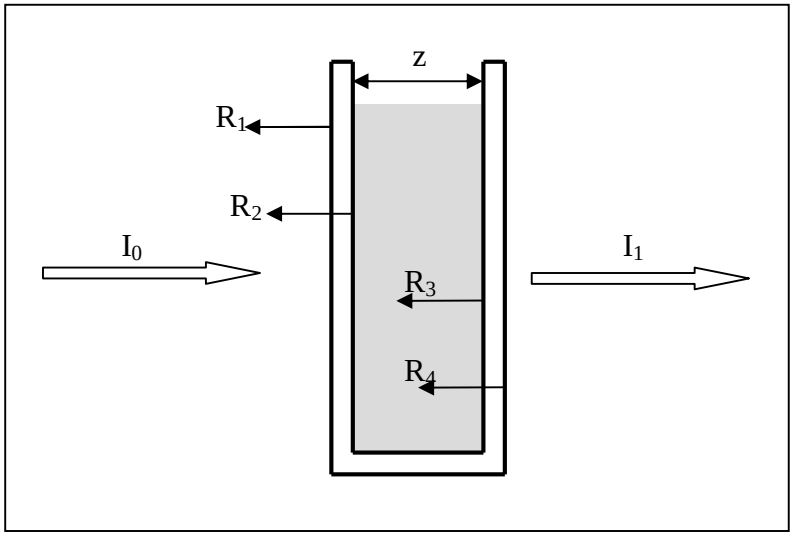

Figure 3.7. *Schematic* d*iagram showing a cuvette indicating the reflection at the interfaces, R, the path length through the liquid, z, and the incident, I_0, and transmitted light intensity, I_1.*

The reflection at the interfaces changes depending upon the refractive index of the media and the cuvette, which is dependant upon the incident transmission wavelength. A change in wavelength from 300 nm to 1000 nm is accompanied with a change in refractive index from 1.486 to 1.453 for fused silica [78]. From previous experiments it was found that the refractive indices at 589.3 nm ranges from 1.460 to 1.478 for DERV and red diesel respectively, with the new motor oil falling between these figures. As no data was available for the refractive index of used motor oil the figure for new motor oil was used. As the incident light from the spectrophotometer was perpendicular upon the cuvette, equation (3.1) [26] was used to establish the reflection at each interface, where n_1 and n_2 refers to the refractive indices for fused silica, oil or air where appropriate.

$$R = \left(\frac{n_1 - n_2}{n_1 + n_2} \right)^2 \qquad (3.1)$$

The range of the calculated reflection for the maximum to the minimum refractive indices for fused silica (300 to 1000 nm) and the known refractive indices for the oil samples at 589.3 nm (due to limited data this was the only figure used) was less than 0.01%, as the mean value for $R < 0.0001$ for the oils, it was reasonable to assume a figure of $R = 0$ at the these interfaces (R_2 and R_3) over the wavelength range considered.

Similar calculations for the fused silica to air interfaces produced a figure varying of less than 0.2%, where the value for R = 0.034 to 0.036 (3dp). With a negligible dispersion ($\Delta n/\Delta\lambda$), a mean value of R = 0.035 was used in the calculations where the reflection would change (R_2 and R_3) as the oil was added.

Once R was established for the cuvette/air and the cuvette/oil, then by using equation (3.2) the light transmission for each cuvette and oil type could be corrected, to produce the corrected transmission, I_Z.

$$I_Z = I_1 \times (1-R_2) \times (1-R_3) \tag{3.2}$$

Once the light intensity after passing through a depth of oil I_Z has been derived, then, from Lambert's law, equation (3.3), the absorption coefficient (α) could be found.

$$I_Z = I_0 \exp(-\alpha z) \tag{3.3}$$

Rearrangement of Lambert's law giving the form in equation (3.4) is more practical, and z is given in metres. Where $\frac{I_O}{I_Z}$ was found from the percentage transmission.

$$\alpha = z^{-1} \ln \frac{I_0}{I_z} \tag{3.4}$$

As only limited data was available for the refractive indices for the oil and that the different cuvettes were not identical in their transmission, coupled with the signal to noise limit of the detector, then when the transmission reached less than ~ 1% or greater than ~99%, these results were not used to determine an absorption coefficient. High absorption occurred for all the oils at wavelengths shorter than 350 nm, resulting in a transmission below 1%, this occurred even when the 200 µm cuvette was used. As was expected, transmission greater than 99% occurred when using the 200 µm cuvette with all oils apart from the new and used engine oil once the wavelength became longer than ~ 650 nm. The path length of the 200 µm cuvette was too short to produce meaningful results for the least absorbing DERV and also only useful for the New motor oil and the red diesel below 500 and 600 nm wavelength respectfully. The results from the 200 µm cuvette did allow for the calculation techniques using the interface reflection deductions to be used.

The abbreviations detailed in table 3.2 show how the different results have been derived, these results are plotted and shown in figure 3.8 and detailed in table 3.3. The results have been calculated in steps of 50 nm on the graph in figure 3.8, a straight line connector between points has been added to aid clarification of the trend.

Abbreviation	Method of calculation
Used(0.2+R)	Used motor oil in the 0.2 mm cuvette, reflections corrected
New(10-0.2)	New motor oil in 10 mm cuvette, less 0.2 mm cuvette. z = 9.8
New(10-5)	New motor oil in 10 mm cuvette, less 5 mm cuvette. z = 5
New(0.2+R)	New motor oil in the 0.2 mm cuvette, reflections corrected
New(10+R)	New motor oil in the 10 mm cuvette, reflections corrected
DERV(10-5)	DERV in the 10 mm cuvette, less 5 mm cuvette. z = 5 mm
DERV(10+R)	DERV in the 10 mm cuvette, reflections corrected
Red(10-5)	Red diesel in the 10 mm cuvette, less the 5 mm cuvette. z = 5 mm
Red(0.2+R)	Red diesel in the 0.2 mm cuvette, reflections corrected
Red(10+R)	Red diesel in the 10 mm cuvette, reflections corrected

Table 3.2. *Abbreviations for the methods of calculations used for the absorption coefficients, with their meanings.*

It can be seen (and was expected) that the used motor oil produced by far the least transmission, this liquid contained suspended particles and many other impurities which could account for the high absorption and possible scattering. Whereas in contrast the transmission for DERV new motor oil and the red diesel was much higher. Pure water is also given in table 3.3 for comparative purposes [95].. The absorption coefficient of DERV tends to that of water at the longer wavelengths.

The two methods used for calculating the absorption coefficient produced similar results to each other. The short path length of the 200 μm cuvette proved useful for assessing the used motor oil, as the 5 mm and 10 mm cuvettes allowed insufficient light transmission. Conversely, for DERV, this cuvette with the short path length had a high transmission of light, (greater than 99 %) this was beyond what was considered reliable and as such these results were not used. In order to measure small absorption coefficients, reliable results were only obtained with long optical path lengths and this was particularly the case with DERV. The other two oils, the new motor oil and the red

diesel, were between the two extremes allowing all three of the cuvettes to be used. The use of the 200 μm cuvette was limited to when the new motor oil and the red diesel had an absorption coefficient greater than 80 m^{-1}, once the wavelength was longer than ~ 600 nm the absorption for these two oils became too low.

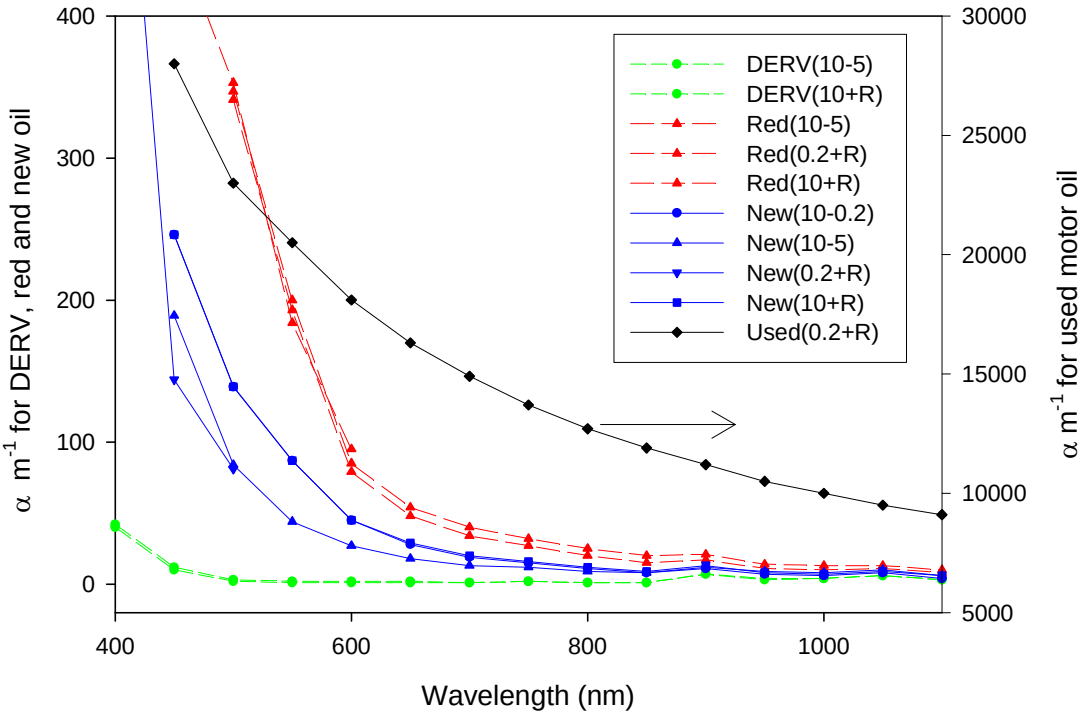

Figure 3.8. *Graph showing the absorption coefficient (m^{-1}) for the four oil samples from the different methods of analysis.*

The absorption coefficient results quantify what had been seen in the spectroscopic analysis in other experiments. In particular for fluorescence, the new motor oil and the red diesel are highly absorbent for UV light, whereas the DERV is less so. The used motor oil was highly absorbing at all the wavelengths examined which resulted in a low to nil fluorescence from the Shimadzu spectrofluorophotmeter.

λ (nm)	Used (0.2+R)	New (10-0.2)	New (10-5)	New (0.2+R)	New (10+R)	DERV (10-5)	DERV (10+R)	Red (10-5)	Red (0.2+R)	Red (10+R)	Pure water [95]
300	>28000	>460	>460	>6100	>460	>460	>460	>460	>1700	>460	0.141
350	>28000	>460	>460	6100	>460	>460	>460	>460	>1700	>460	0.0463
400	>28000	>460	>460	655	>460	42	40	>460	1700	>460	0.0171
450	28000	246	189	144	246	12	10	>460	460	>460	0.0145
500	23000	139	84	81	139	3	2	347	353	341	0.0257
550	20500	87	44		87	2	1	200	184	193	0.0638
600	18100	45	27		45	2	1	85	95	79	0.244
650	16300	28	18		29	2	1	54		48	0.349
700	14900	19	13		20	1	1	40		34	0.650
750	13700	15	12		16	2	2	32		27	2.47
800	12700	11	9		12	1	1	25		20	2.07
850	11900	8	8		9	1	1	20		15	
900	11200	11	12		13	7	7	21		17	
950	10500	7	9		8	3	4	14		11	
1000	10000	6	8		7	4	4	13		10	
1050	9500	8	10		9	6	6	13		11	
1100	9100	4	6		6	3	3	10		8	

Table 3.3. *Calculated absorption coefficients (α m^{-1}) for four oils, from 300 to 1100 nm. Data for pure water [95] has been added for comparison.*

(iv) Assessment of fluorescence

The ability of hydrocarbons to fluoresce whilst pure water does not, has led to many different specialised techniques in identifying the presence or absence of oil in water. This section examines the optimum excitation wavelengths for the oil samples using a Shimadzu Spectrofluorophotometer RF-1501. This fluorimeter allows the excitation wavelength to be fixed whilst recording the emission spectrum intensity, alternatively the emission wavelength can be selected whilst the excitation spectrum is scanned. By collectively optimising the excitation wavelengths for the oils, a suitable wavelength for a fluorescence light source may be identified. It was known that diesel produced a fluorescence spectrum from ~ 400 to 550 nm whilst using a laser excitation sources at 355 nm [68], remote aerial laser induced fluorescence techniques for crude oil often use UV wavelengths 300 – 355 nm, taking advantage of the laser high pulse energy and narrow beam [64, 65, 70].

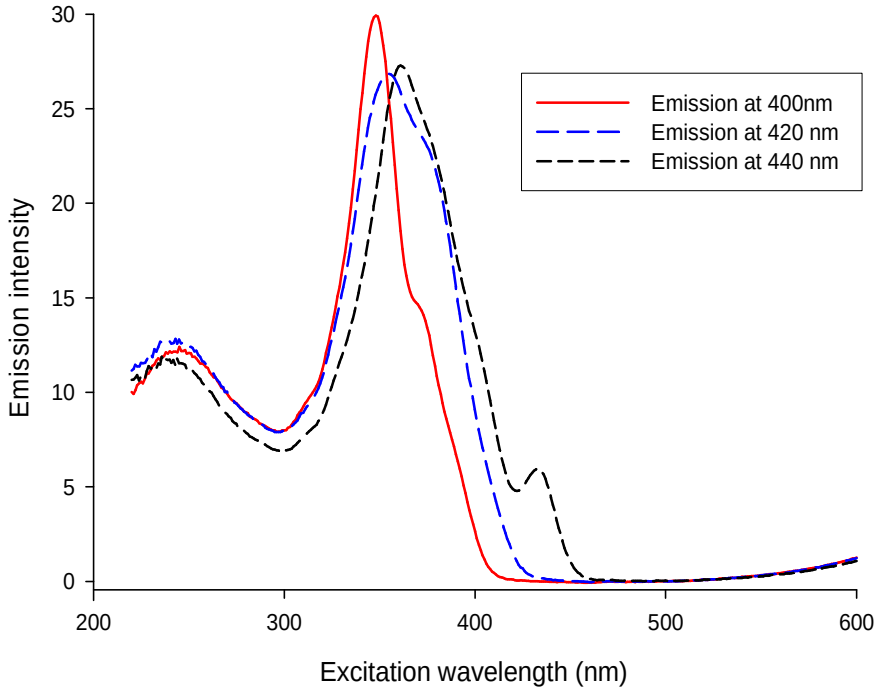

Figure 3.9. *Emission intensity for DERV for three fixed emission wavelengths.*

Examining DERV as the initial sample, three experiments were run with the fluorescence emission wavelengths fixed at 400, 420 and 440 nm whilst the excitation spectrum was set to scan from 220 to 600 nm. The results in figure 3.9 show the emission intensity at these fixed wavelengths as a function of the excitation wavelength. The three fixed emission wavelengths peaked differently at 348, 354 and 361 nm

respectively, within the spectral range previously reported. The excitation wavelength that caused the highest level of output depended on which emission wavelength was monitored. Excitation wavelengths from ~320 to 380 nm produced the greater response. However, excitation up to ~ 430nm produced a fluorescence response with the emission wavelength fixed at 440 nm.

In the following experiments the excitation wavelengths were then fixed at 350 and 380 nm and the emission spectra investigated. Figure 3.10 shows the emission peaks and the emission intensities for DERV and new motor oil. The results obtained using DERV showed a small difference in the intensities from the two separate excitation sources but these are dwarfed by the emission intensities from the new motor oil. The two excitation wavelengths produced a pronounced difference in the two emission intensities of the new motor oil, the greater one being produced from an excitation at 380 nm.

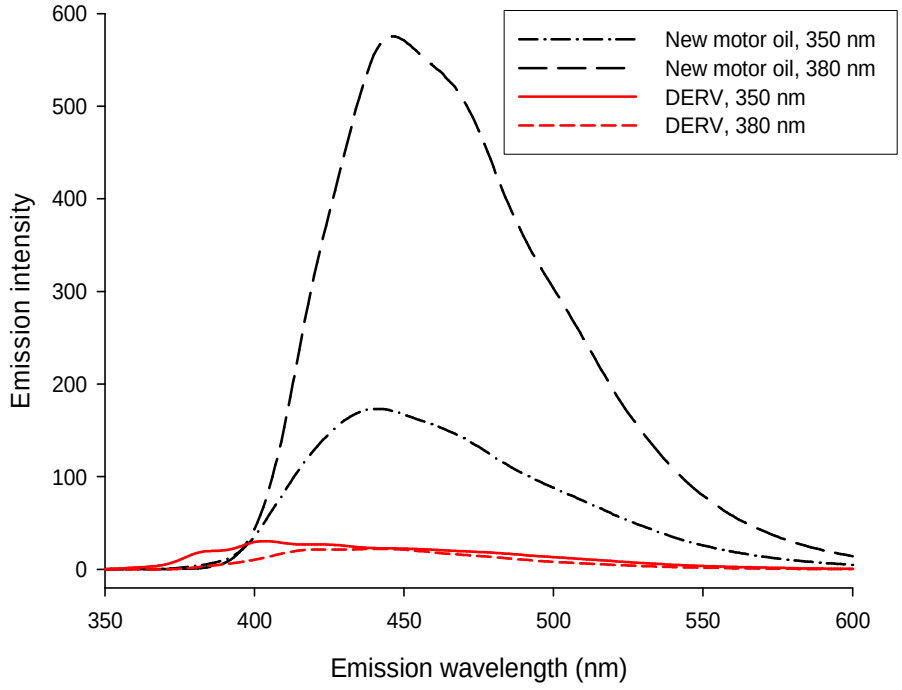

Figure 3.10. *Fluorescence emission intensities for DERV and the new motor oil at excitation wavelengths 350 and 380 nm.*

The different emission intensities between the two oils were possibly representative of the differences in the two oils ability to absorb the light at thes wavelengths and noted in figure 3.1.

Four oil samples were placed in the fluorimeter and excited at 370 nm, this being a compromise between the DERV and the new motor oil, the results are shown in figure 3.11. The two diesel samples, DERV and the red diesel showed similar results, again the new motor oil had the greatest intensity. The used motor oil showed virtually no fluorescence, the highly absorbent nature of this oil for both excitation and emission allowed very little light to reach the emission detector.

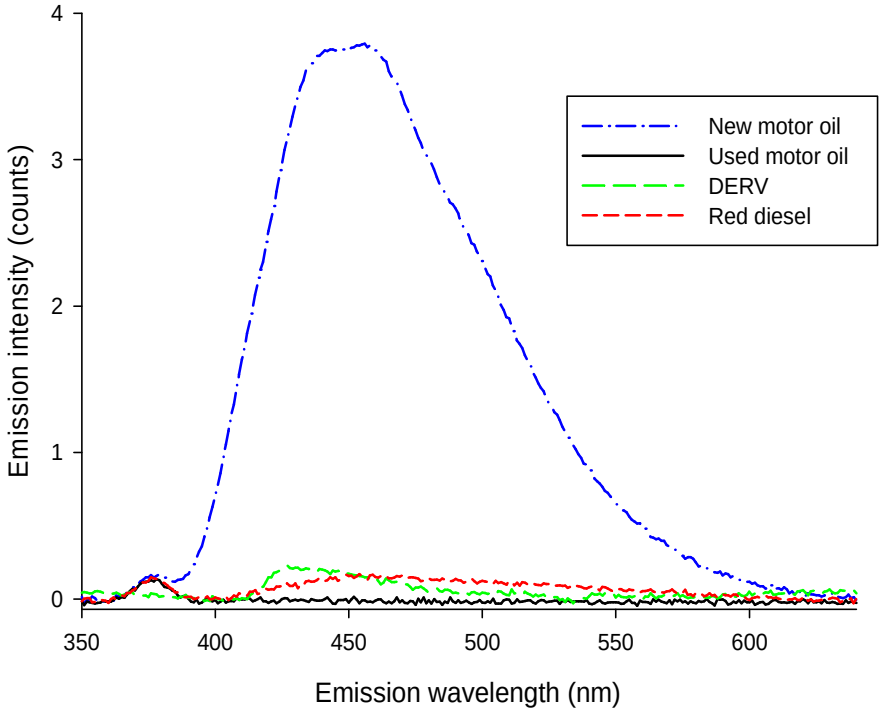

Figure 3.11. *Fluorescence emission intensity for the four oils with excitation wavelength fixed at 370 nm.*

The results from this fluorescence analysis have shown that excitation wavelengths of 340 to 400 nm produce the main fluorescence response for most of the oil samples, with 350 to 380 nm being the most suitable for the collection of oils studied here. The excitation light in the Shimadzu fluorimeter was positioned orthogonal to the emission detector, however this would not necessarily need to be the arrangement for any experimental set up in the laboratory.

(v) Assessment of density

The densities for the purchased oil samples were obtained from the appropriate data sheets and similar data could be found for water. The used motor oil and that for the oil sample provided by Andel Ltd. were established through weighing a known volume (0.5 L) of the oil in the laboratory and factoring these results to give a density in kg m^{-3}.

The results for these oils were 870 and 845 kg m^{-3} respectively and are summarised in Appendix A. Both of these oils, as expected, were shown to have a density less than that of water.

The density of the used motor oil will depend in general upon several factors, such as the category of the original oil (this being the major factor), the condition and type of engine and the time that the oil has been within the engine.

(vi) Mixing and separation

The oils and water were examined to investigate whether the liquids, if added separately into a test tube, would remain divided or combine. It was expected that the water would remain separate but whether the different oils would spontaneously mix was uncertain.

To observe mixing and separation, two experiments were carried out. Samples, 10 ml each of water and two oils were carefully placed into a test tube using a pipette. The water and oils were added with the densest first and the least dense last. In tube A, water, new motor oil and red diesel, and in tube B, water, used motor oil and DERV were placed and are shown in figure 3.12. It was noticed that whilst adding the DERV on top of the used motor oil, that if it was not added slowly and carefully to the upper surface of the used motor oil these two oils immediately mixed, this had not been the case for the new motor oil and the DERV. These two tubes were then left for 24 hours and re-examined. In both cases all three of the liquids had remained separate. Both these tubes were then mixed vigorously, through shaking by hand and then left.

After a period of 7 days the two tubes were then re-examined. As shown in figure 3.12, the oil and water had separated, with the more dense water lying beneath the oil. In both experiments the two oils in each tube remained mixed. In tube A, the interface between the water and the oil was not clearly defined having a white frothy appearance a few millimetres deep, although the water was relatively clear. In tube B, again the water separated from the oil and was at the bottom and the two oils remained mixed but here a grey material remained at the side of the glass tube. This possibly was a constituent of the used motor oil, and was later to prove problematic for some of the optical detection techniques. The water in tube B, where it could be observed was again relatively clear. The oil/water interface in tube B was difficult to see due to the grey material on the surface of the glass tube, although it was more clearly defined than for tube A.

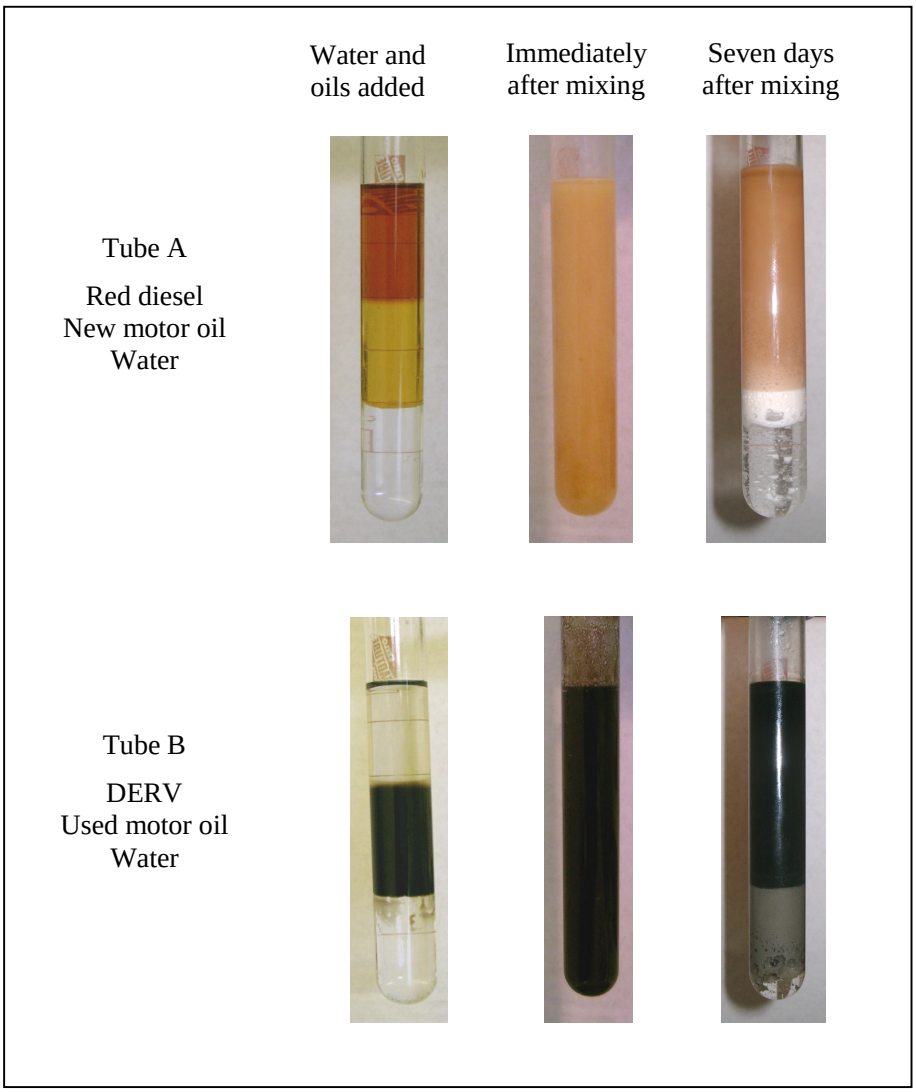

Figure 3.12. *Two test tubes containing water and two oils, showing mixing and separation.*

The rate of separation depends upon several factors and can be modelled through using Stokes' law of Terminal Settling Velocity [96] shown in equation (3.5).

$$V_T = \frac{gD^2(\rho_p - \rho_L)}{18\mu_L} \tag{3.5}$$

where, V_T is terminal velocity of a particle or droplet, g is acceleration due to gravity, D is the diameter of the droplet or particle, ρ_p is the density of the droplet or particle, ρ_L is the density of the surrounding medium and μ_L is the dynamic viscosity of the surrounding medium.

Equation (3.5) does have certain limits of applicability, the most significant are: the droplet has to be spherical at all times and must not deform, the sphere must be smooth,

each particle or droplet must not be affected from interactions by crowding, the surrounding liquid must be a Newtonian liquid, the flow around the sphere must be laminar and the liquids immiscible. As the droplet alters its shape its speed due to buoyancy is likely to increase depending upon its new form [97].

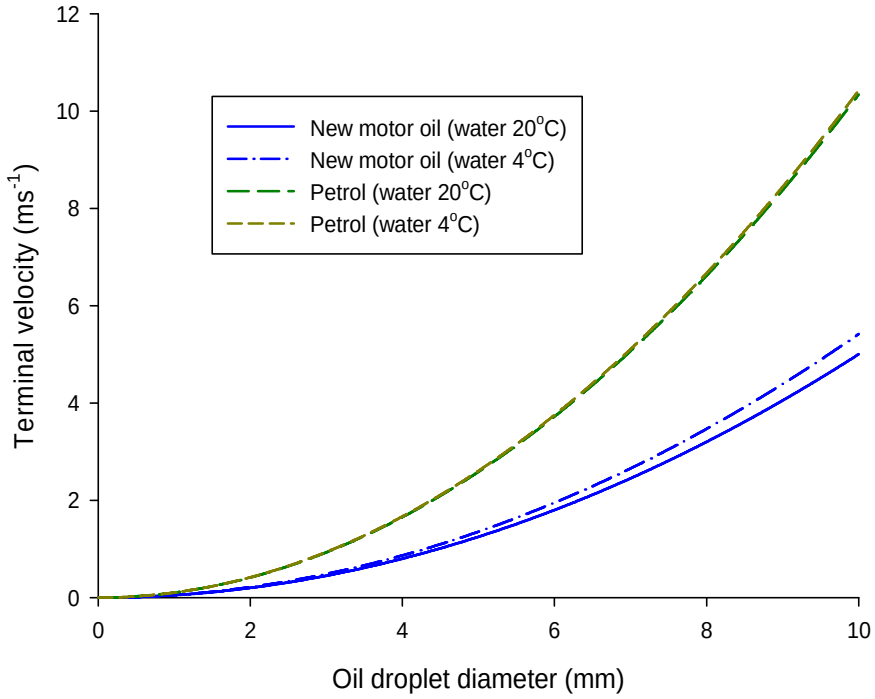

Figure 3.13. *Calculations showing the terminal velocity rise times for different sized droplets of new motor oil and petrol at two water temperatures. The temperature difference has little effect upon the petrol viscosity.*

The terminal velocity shown in figure 3.13 will not be reached immediately. The velocity, V, at time (t), can be derived from equation (3.6) [98]

$$V(t) = V_T \tanh\left(\sqrt{\frac{\alpha g}{m}} \times t\right) \qquad (3.6)$$

where $\alpha = \frac{gm}{V_T^2}$ and m is the mass of the droplet. When (t) becomes large, $\tanh\left(\sqrt{\frac{\alpha g}{m}} \times t\right)$ approaches 1, and $V(t) \rightarrow V_T$. The droplet velocity as a function of size and time can be seen in figure 3.14, showing the rise time for different sized droplets of new motor oil and petrol in water at 4˚C and 20˚C. The density difference between the type of oil and water and the droplet size plays the major role in separation speed, whereas the viscosity of the water from 4° to 20°C has a smaller effect.

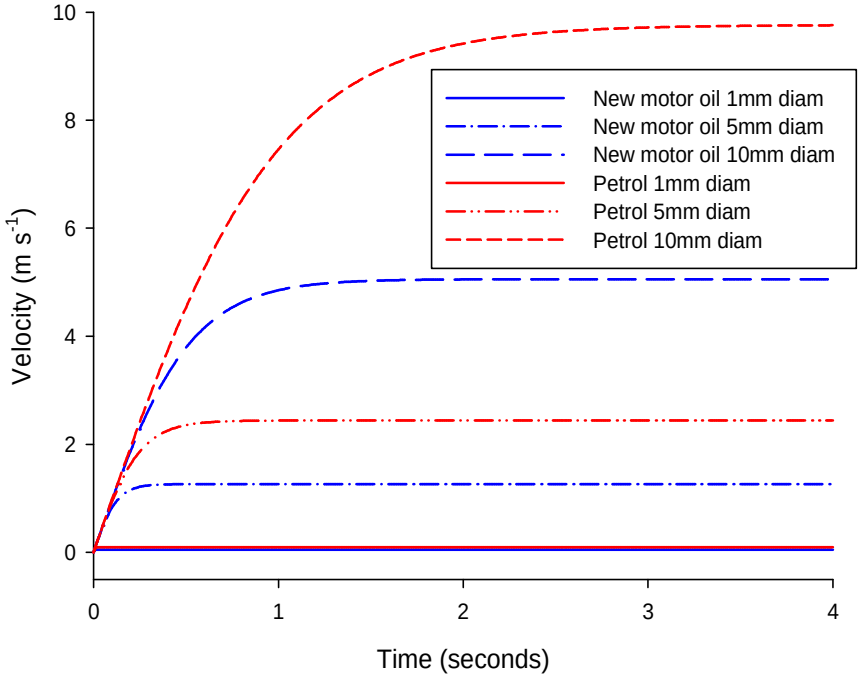

Figure 3.14. *Calculated droplet velocity as a function of time, for three sizes of droplet in new motor oil and petrol. The 1 mm diameter droplet shows a similar velocity for both new motor oil and petrol over the period.*

Oil type	Droplet diameter (mm)	Time to rise 1 m (seconds)
New motor oil	0.5	79.1
New motor oil	1	19.61
New motor oil	5	0.88
New motor oil	10	0.48
Petrol	0.5	41.0
Petrol	1	10.2
Petrol	5	0.58
Petrol	10	0.46

Table 3.4. *Table showing theoretical times for different sized oil droplets to travel 1 metre.*

The time taken for different droplets of oil to rise through one metre of water is summarised in table 3.4. As would be expected, the smaller droplets take much longer to rise one metre, whereas the 10 mm diameter droplets from both oil types travel this distance before they reach their terminal velocity, although it is unlikely that these droplets would retain their spherical shape. Consequently the capacity of the separation

chamber needs to be sufficient to allow enough time for the more dispersed oil to separate out from the water before the oil free water leaves the interceptor.

3.1.3 Summary of sample analysis

From the analysis of the chosen oil samples, it could be seen that throughout all of the physical investigations particular correlations prevailed, their carbon based MIR spectra analysis their displayed marked similarities, as too their densities and their immiscible nature set them apart from water. Exception to the similarities for most of their physical properties was a large variation in their viscosities but as these mineral oils had been purposely produced from crude oils for particular roles this would have been expected. However, the optical analysis demonstrated a marked difference, inasmuch as one of the oil samples repeatedly stood out throughout each of the analyses. The used motor oil which repeatedly through its highly absorbent nature proved difficult to find common heritage with the other carbon based samples. To produce a single detection system capable of functioning in the presence of these oils proved to be challenging.

3.2 Development of the Interceptor Monitor

Section 3.1 examined the oil samples chosen to represent the array of oils likely to be encountered within an oil/water interceptor. In section 3.2, methods based upon the distinctive characteristics of the oils and were investigated. Within this section, four of the five detection methods summarised in the last chapter are examined to establish their merits and durability for all the oil samples.

All of the following methods have been effectively used for other applications albeit within the confines of specialised applications, however, this oil detector is required to function unattended. This demands that any system employed needs to be able to cope with the expected conditions without being compromised. Failure of the system, could lead to potential pollution risks, as such, any detection method that shows weaknesses needs to be re-examined or disregarded. The following research areas pursued needed to comply with the confines set down by Andel Ltd.

3.2.1 Viscosity and air bubble rise sensing

This method of detection uses the various fluid viscosities and examined the theoretical rise times of air bubbles as they travel through a known depth of liquid. As the travel

time of the air bubble will be determined by the liquid's density and viscosity, these differences in the properties of the oils and water will affect the speed of the air bubbles.

Both the density and viscosity is dependent upon the temperature but as shown in figure 3.13 for oil droplets the theoretical effects of the temperature from 4° to 20°C upon droplet rise times was minimal. Table 3.5 shows the density (ρ) and dynamic viscosity (μ) for selected oils, water and air from which the calculations have been based. The dynamic viscosity is given in N s m^{-2}, this being equivalent to the SI unit of one Pascal second (Pa s)

Material type	Density kg m^{-3}	Dynamic Viscosity N s m^{-2}
Air (10˚C) [78]	1.247	1.8×10^{-5} (18˚C)
(15˚C) [78]	1.2256	
Water (10˚C) [78]	999.7	1.307×10^{-3}
(15˚C) [2]	999.1	1.139×10^{-3}
(20˚C) [2]	998.3	1.002×10^{-3}
Diesel oil (15˚C) [99]	820	2.7×10^{-3}
Petrol (20˚C) [92]	750 (15˚)	$0.4 - 1.1 \times 10^{-3}$
New motor oil (15˚C) [99]	870	224×10^{-3} [3]
Used motor oil (15˚C) [99]	870	175×10^{-3} [3]

Table 3.5. *Showing density and viscosity for various oils, water and air.*

The calculated terminal velocity for an air bubble with a 5 mm diameter, for new motor oil, water and petrol is shown in figure 3.15, these speeds were calculated using equation (3.5). For the petrol, two lines are shown, one for the least viscous and one for most viscous petrol samples (as specified in table 3.5). Here it has been assumed that the air bubble has remained spherical throughout.

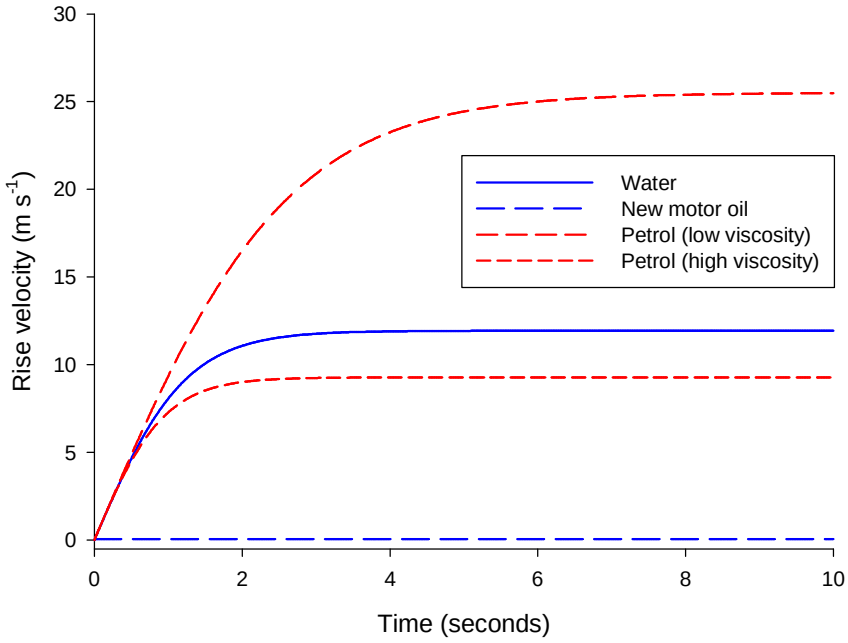

Figure 3.15. *The terminal velocity for a 5 mm diameter air bubble travelling in new motor oil, petrol (at two viscosities) and water.*

The terminal velocity will not be reached immediately and for the least viscous liquid, this will take several seconds. Table 3.6 shows the time taken for an air bubble to travel through 0.5 metre and 1 metre from a stationary position in water. Terminal velocity is reached only by the air bubble travelling through new motor oil. However, the different liquids would not be differentiated within the depth available. For situations when the oil type would be known to be of the more viscous, such as for new motor oil, then the possibility of using this system would exists.

Liquid	Terminal velocity (ms^{-1})	Time (s) to reach 0.5m	Velocity (ms^{-1}) at 0.5 m	Time (s) to reach 1.0m	Velocity (ms^{-1}) at 1.0 m
Water	11.94	0.32	3.07	0.46	4.22
New motor oil	0.053	9.44	0.053	18.87	0.053
Petrol (low μ)	25.51	0.32	3.12	0.45	4.37
Petrol (high μ)	9.28	0.32	3.03	0.46	4.11

Table 3.6. *Rise times for a 5 mm air bubble travelling through 0.5 and 1 metres depths, for new motor oil, petrol and water*

Mixtures of different oils may produce various unpredictable viscosities, with the possibility of matching that for water, further complicating the detection system. This rise time detection system would be reliable for only limited locations, making this technique unsuitable for universal use. Consequently this detection method was not pursued

3.2.2 Reflection at the oil/water interface

As previously discussed, the position of the oil/water interface will signify the level of oil contained within the interceptor. To determine the interface through optical means requires some degree of transmission through the liquid and the ability of the interface to reflect at least a detectable portion of the emitted light. As the light emission and detection can be relayed into the interceptor via fibre optic, this allows the positioning of these to be placed either above or within the liquid.

Light transmission was to be the main problem for this detection method for two main reasons. The first was the absorbent nature of the used motor oil (see 3.1.2 Assessment of absorption and transmission), this would if present, not allow sufficient light to be reflected due to absorption and scatter. Secondly, it can be seen in figure 3.12, that once any used motor oil had been mixed with water, particles from this oil separated out leaving a coating on surfaces in which it came into contact. This would coat any optical surfaces and over time rendering them ineffective, this coupled with what may be a less than well defined oil/water interface, made this method unsuitable and it was not continued.

3.2.3 Transmission and TIR sensing

For a sensing technique that works through transmission and absorption, a part of the UV to IR spectrum requires that transmission can occur for either water or oil. It has been shown in section 3.1.2, which for a region of the IR spectrum, 1.4 to 1.6 μm, transmission in water was low whilst for most of the oils transmission was high, making this suitable for the widely available telecommunications wavelength at 1550 nm. However, as for the entire spectrum investigated, used motor was highly absorbent, attenuating all the detectable light. Using a shorter path length would aid the detection of the used motor oil but this would at the same time make it harder to distinguish the oils from that of water. Such a small chamber would however be more liable to be obstructed from particles and other objects. This oil/water monitor needs to be able to

function for all possible oil types found in different locations and therefore a technique using transmission was not investigated further.

Detecting oil, water and other liquids using their different refractive indices has been successfully used in many different applications. This technique does not rely upon the transmission of light through any of the liquid but travelling along light guides (often fibre optic) into a sensing head before any returning signal goes to the detector via a parallel route. Using TIR for an oil/water application, as discussed in section 2.6.2, would produce a returned light signal if in air or water, but when placed in oil, the light signal would be transmitted, resulting in either a decrease in the return of light or none at all.

Assuming that the sensing element has a refractive index of ~ 1.518 (BK7 Borosilicate crown glass at 589 nm), then TIR would occur when the incident angle reaches:

41.2º for air	n = 1
61.2º for water	n = 1.33
70.4º for paraffin	n = 1.43 (an oil with a low refractive index)

By placing the incident light at an angle of ~ 66.0º, then TIR occurs when the sensing element is placed in either air or water and the light will be transmitted when the sensor is placed in a medium where the refractive index is greater than 1.39, this will include all the oils assessed.

An experiment was set-up, as shown in figure 3.16, using a LED emitter from Infineon SFH756V (peak wavelength 660 nm), with an aperture for connecting a 2 mm multimode jacketed fibre optic cable and a photodiode detector from Centronic OSD 5-5T. The 90° prism was placed in a container so that the base of the prism could be in either air or immersed in a liquid. At the base of this container was placed a black cloth to avoid any inadvertent reflection from the container.

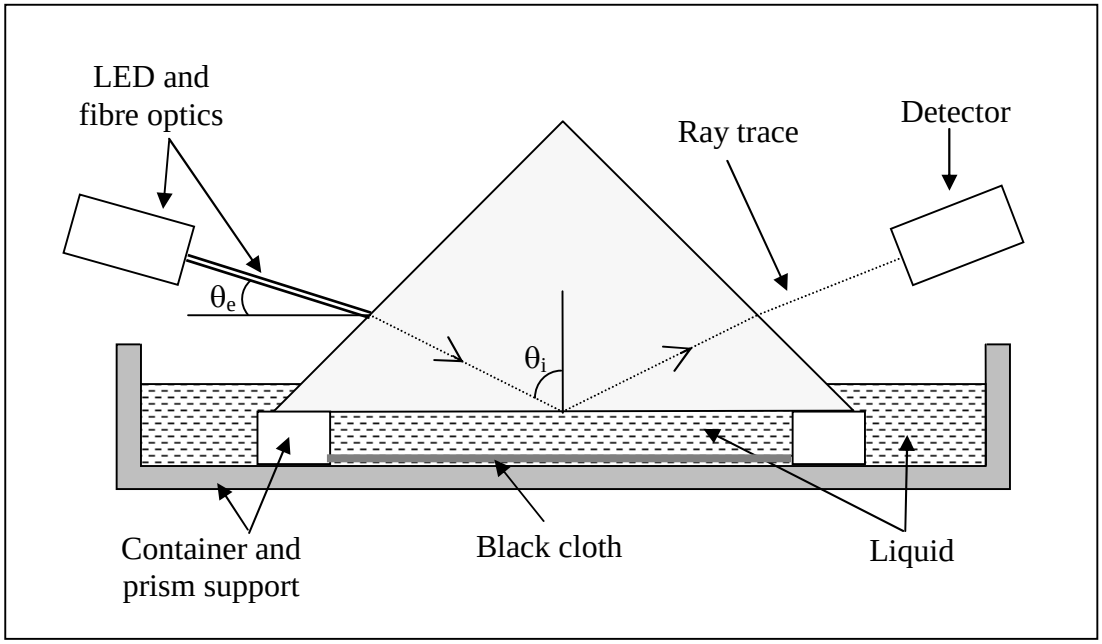

Figure 3.16. *Diagram showing the experimental set-up using a 90° prism, emitter and detector.*

The emitter was placed in two different positions, the first, experiment 1, with θ_e at 30° from the horizontal, (see figure 3.16), creating a calculated angle if incidence at the base of the prism, θ_i, of 55°. In experiment 2, θ_e was angled at 12° from the horizontal, creating an angle if incidence within the prism, θ_i, at 66°. Three tests were undertaken, the first with air only, the second with water and the third using DERV (DERV having the lowest refractive index of the oil samples and the nearest to that of water).

In experiment 1, the position of the light source allowed TIR to occur for air but not for oil or water. Repositioning of the LED for experiment 2 again produced TIR for air, however now TIR occurred when the base of the prism was immersed in water but not in DERV, producing the desired effect. This small but significant adjustment of incident angle was able to discern between the water and the oil. These results were repeatable but only when the prism had been wiped clean of oil using a cloth. The presence of smears of oil and in particular new or used motor, due to their adhesive nature, reducing the intensity of the detected TIR in the presence of water. To further evaluate the effect of oil, the prism was then moved and the base was placed overnight in 2–3 mm of used motor oil. The used motor oil had previously been shown to leave particle as well as oil deposits upon surfaces. The following day, the prism which had not been not wiped clean, was repositioned in the container and reassessed for air, water and oil, this procedure was repeated over several days. The effect of these deposits from the used

motor oil severely reduced the ability of this system to reproduce the TIR which had previously been seen for air and water.

Medium at base of prism	Position 1 (volts)	Position 2 (volts)	
	Prism cleaned	Prism cleaned	Prism smeared
Air	0.44 – 0.46	0.40 – 0.45	0.17 – 0.44
Water	0.05 – 0.06	0.40 – 0.44	0.06 – 0.26
Oil	0.01 – 0.02	0.01 – 0.02	0.02 – 0.03

Table 3.7. *TIR response from the prism with different incident angles as the prism base is placed in air, water and oil.*

The results in table 3.7 show that the range of the detected optical intensity varied from 0.01 to 0.45 volts. With 0.40 to 0.45 volts indicating TIR and a detection below 0.2 volts indicated no internal reflection or merely a small amount of scattered light. In position 2, once the prism had been smeared by the used motor oil, there was a variable response from air but no consistent difference could be detected between the water and the oil. The thickness of the oil smear only becomes significant, with regards to effecting TIR, once it reaches than several 100 nm, approximately one wavelength [100]. With no means to regularly clean the optics, the variation in efficiently would be unsuitable and as such, a system based upon this technique was not pursued.

3.2.4 Fluorescence sensing

For an oil/water sensing system based upon fluorescence, the most suitable point for analysis would be the position where the oil level within the interceptor is nearing or at its desired maximum volume/depth. This would require the excitation light source and any resulting fluorescence emission being transmitted through fibre optics, thus avoiding any electrical components within Zone 0.

Having previously established the optimum excitation spectrum in section 3.1.2 to be 340 to 380 nm, a UV LED was chosen as an excitation source; LEDs being versatile in respect that they are small, quick to reach full power, may be battery powered and are relatively cheap. LEDs in the UV spectrum decrease in maximum output power as the peak wavelength becomes shorter and so choosing the optimum LED becomes a

compromise between wavelength and output power. Two different UV LEDs were used in the following experiments and powered from a 9 volt battery:

1. Toyoda Gosei Optoelectronics E1L5M-4P0A2-01
   peak emission λ 380 nm total output power 1.7 mW viewing angle 15°

2. Hero HUVL370-510
   peak emission λ 370 nm total output power 1.5 mW viewing angle 10°

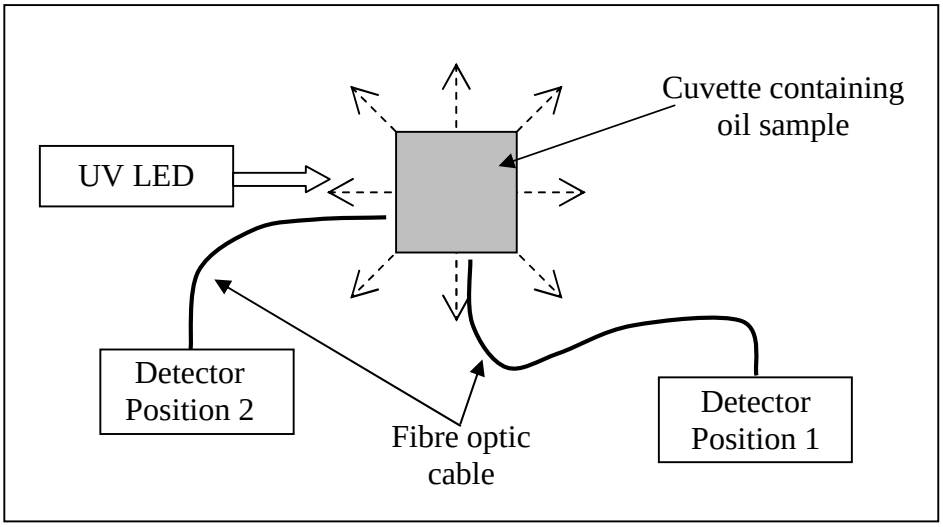

Figure 3.17. *Experimental set-up using a 10 mm fused silica cuvette, a UV LED and a fibre optic coupled detector. Two positions are shown for the fluorescence detection.*

The laboratory experiments were based around fluorescence techniques that would identify the oils samples from that of water. The oil samples were placed into a 10 mm fused silica cuvette and initially using the 380 nm LED for excitation. An Ocean Optics high resolution spectrometer HR2000 CG-UV-NIR with a fibre optic coupling was used for detection. To avoid the detector receiving excessive light from the LED, the end of the detecting fibre optic was placed in one of two positions; position 1, orthogonal to the excitation light and position 2, adjacent to the excitation light. The experiment was set-up as shown in figure 3.17. The emission from the LED, although peaking at a particular wavelength also emits light over a broad spectrum which can mask any fluorescence emitted. Although this can be accounted for as background noise, avoiding this is preferable giving a greater signal to noise ratio. Filtering the excitation light would have avoided masking the emission spectrum but with a reduction of the excitation power. This would also have placed the divergent LED further away from the

cuvette. Through placing the detector away from direct incursion, the need for a filter during these experiments was avoided.

The emission spectra and relative intensity of the fluorescence response for the four oil samples are shown in figure 3.18. The intensity of the fluorescence from the new motor oil, red diesel and DERV was detected from position 1, whereas that for the used motor oil was detected from position 2.

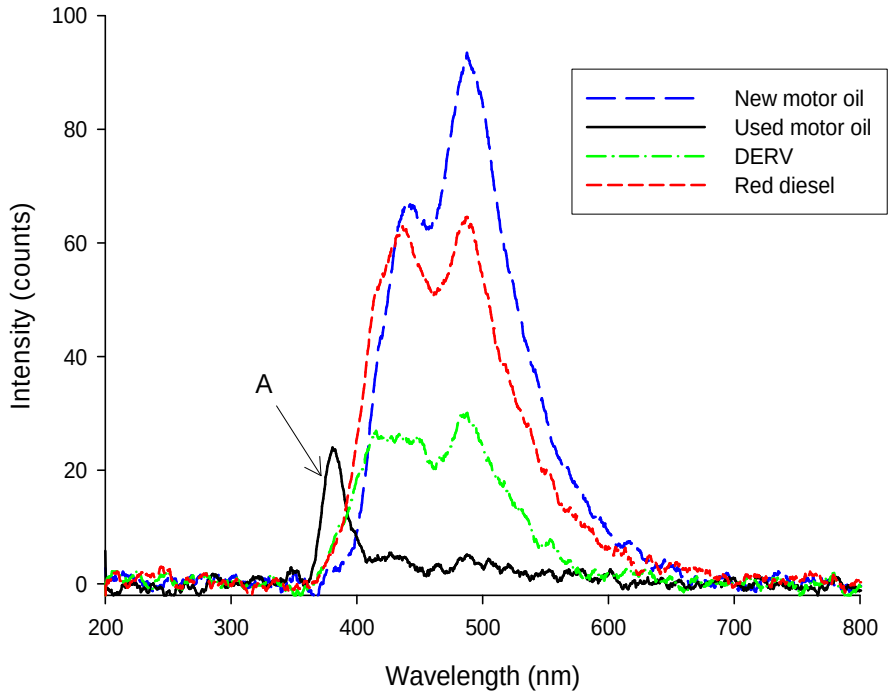

Figure 3.18. *Fluorescence response for four oils, excitation source UV LED at 380 nm. The peak at 380 nm for the used motor oil is from the LED and is indicated by arrow A.*

The ability of the different oils to absorb the excitation light does not only affect the intensity of the fluorescence, but more importantly for this experimental set up, the position of the fibre optic cable could also increase or decrease the detected response. As different oils were placed into the cuvette, the fluorescence emission could be visually seen to vary from one oil type to another, both in intensity and its position within the cuvette. The new motor oil which was previously shown in section 3.1.2 to be more absorbent than DERV or red diesel, displayed a fluorescence emission in a more concentrated area than the other two oils. The fluorescence excitation from the DERV appeared to be emitted equally within the cone of excitation light produced by the LED. Consequentially, the position of the fibre optic cable duly influenced the detected fluorescence.

Due to the highly absorbent nature of the used motor oil, no signal could be detected from position 1, however by placing the fibre optic detector adjacent to the LED a small fluorescence response was detected but due to this position, part of the excitation light appears in the detected spectrum and is denoted by A in the graph. Conversely the detected fluorescence intensity for the other three oils decreased when moved into position 1.

Photodegradation of the oil, as discussed in the previous chapter, has the effect of oxidising the aromatic species. This in turn results in a decrease in the fluorescence from the oil. Circumstances where this could happen may occur when the oil after being spilt has stayed upon the surface, being exposed to sunlight for a period of time before entering the interceptor.

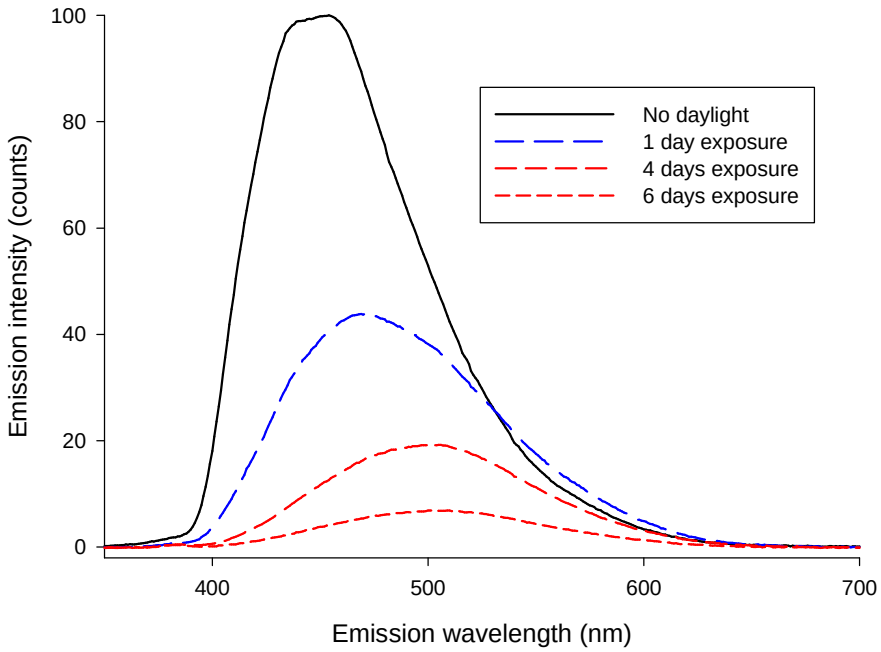

Figure 3.19 *Effect of the fluorescence response of red diesel to different length of daylight. Excitation at 370 nm, emission intensity in counts normalised to no daylight oil.*

To evaluate this effect of photodegradation, several open petri dishes containing red diesel were left outside exposed to sunlight during a period in June. After which, they were individually brought into the dark after specific periods of time. These red diesel samples were then examined for their relative fluorescence intensity and shown in figure 3.19. It can be seen from the graph that the emission intensity of the oil decreased with length of daylight exposure. Within one 24 hour period the peak intensity

decreased by ~ 50% compared to a control that had been placed in the dark. Over a further four and six day time period the other samples showed further reductions to ~20% and ~10% respectively for 4 and 6 days exposure.

Photooxidation and evaporation is more liable to occur when oil is exposed to the outside atmosphere as opposed to oil that has relatively quickly flowed into an interceptor. Nevertheless, any oil detector must be able to cope with all oil entering into the interceptor, this coupled with the weak fluorescence from used motor oil indicates that the method of fluorescence sensing is not suitable for the role demanded.

3.3 Summary of detection methods

The detection methods that have been researched in this chapter have revealed that such techniques would be successful within limited boundaries. These restricted confines generally allowed detection to be achieved for either a limited sample of oil, in the case of the optical systems or that the oils were exclusively of one type, in the case for physical assessment. For the optical systems the principal drawback had been the used motor oil but this could represent any oil that contained a large carbon deposits or other additives. For any detection system, overcoming the requirement for long-term unattended reliability was going to be the major obstacle. The next three chapters are devoted to the analysis of density, which was shown to be a consistent feature of difference between all the oils and water.

4. Oil/water interceptor pressure measurement detector

This chapter investigates the technique of oil detection through sensing a change in pressure. The measurement of pressure at particular locations within the interceptor can be used to determine the density and from this, establish the presence of either water or oil. The theory behind this method and the positioning of the measurement points is discussed in this chapter. Designs for two systems capable of sensing pressure changes are proposed. The development of which, is through modelling and experiments and presented in the following two chapters.

4.1 The effect of adding oil to an interceptor

In general, the densities of oils are usually less than water and this fact coupled with the immiscible nature of these two liquids aids their separation and thus allows the oil to effectively float on top of the water. The separation time, as discussed in the previous chapter, depends upon the properties of the different oil type, the degree of premixing of the oil and water and the relative quantities of each liquid entering the separator. The densities of the oil samples tested are less than that of water by 13% in the case of new motor oil (870 kg m^{-3}) and up to 25% for the lighter petroleum products such as petrol (750 kg m^{-3}). The analyses discussed here are for new motor oil as this represents an oil type which is of a higher density and as such would be more challenging to detect using a density differential system. In later experiments DERV was also used, this was to demonstrate that oils less dense than the new motor oil were also measurable.

Through the design of the oil interceptor, the inverted siphon arrangement (see figure 2.2) allows the separated water or excess water (in the case when only water is entering the interceptor), that resides at the base of the tank to pass through the interceptor and be conducted away. For this process to occur, a pressure is required from inside the tank to force the water through the pipes of the inverted siphon and out of the separator. The liquid inside the separator must produce a pressure sufficient to induce fluid flow up through the extraction pipe and out of the separator into the drainage system. If a less dense liquid is contained within the separator tank (such as oil), then to produce sufficient force, a greater quantity (by volume) of liquid would be required to create the

equivalent pressure at the entrance of the inverted siphon and as such, the liquid level within the separator tank would need to be higher accordingly. This increase in volume is proportional to any reduction in density of the entrapped liquid entering the separation tank. The total weight of the liquid within the interceptor tank would thus remain constant.

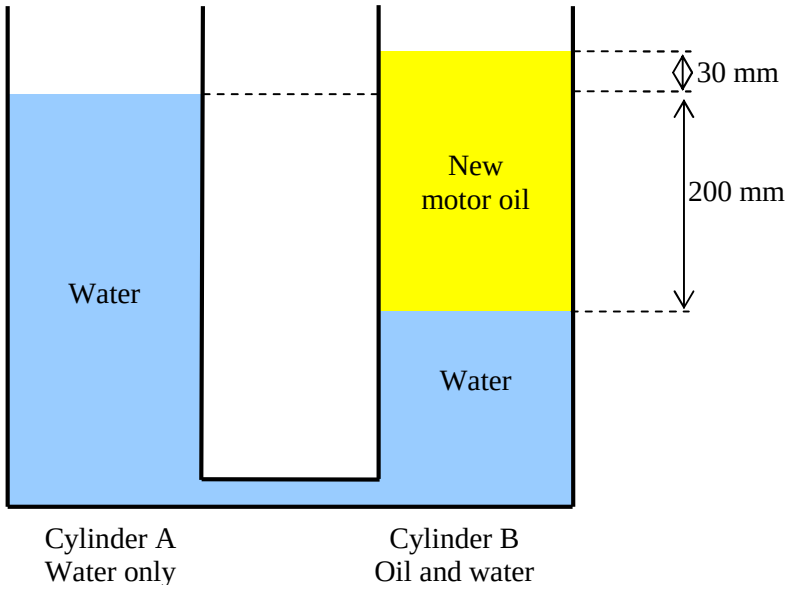

Figure 4.1. *To maintain an equal pressure between both cylinders, a depth of 200 mm of water requires to be replaced by 230 mm of new motor oil.*

Shown in figure 4.1 are two cylinders that are connected at the base. On the left side, cylinder A contains only water whereas on the right, cylinder B has a combination of new motor oil and the water. If the two cylinders contained only water then the depth of the liquid in each cylinder would be equal. In the scenario shown above, cylinder B, in order to maintain the balance of equal pressure, contains the larger volume. Here a depth of 200 mm of water has been replaced by 230 mm of new motor oil, increasing the volume. This rise in the level of the liquid/air interface will create a change in pressure, not at the base of the tank, but in the region above the oil/water interface and the surface of the oil. Thus by placing a probe within this location, the change of pressure created through the addition of oil to the interceptor can be detected. This pressure change forms the basis for the detection methods discussed here.

If the depth of the liquid is being measured via pressure, any variations of the atmospheric pressure will, to an extent, also have an effect. Barometric measurements

recorded at the National Physical Laboratory in Middlesex [101] for the year 2006 recorded highs and lows varying in extremes from 1040.40 hPa to 975.60 hPa respectively, a range of ~ 6.5 %. Similar variations of atmospheric pressure may well be expected for the rest of the UK. Through using a differential pressure gauge variations of the atmospheric pressure will not affect the measured pressure.

The differential pressure gauge, would, when both reference points were placed at different levels, measure only their pressure difference and hence indicate the density of the liquids between them, as shown in figure 4.2.

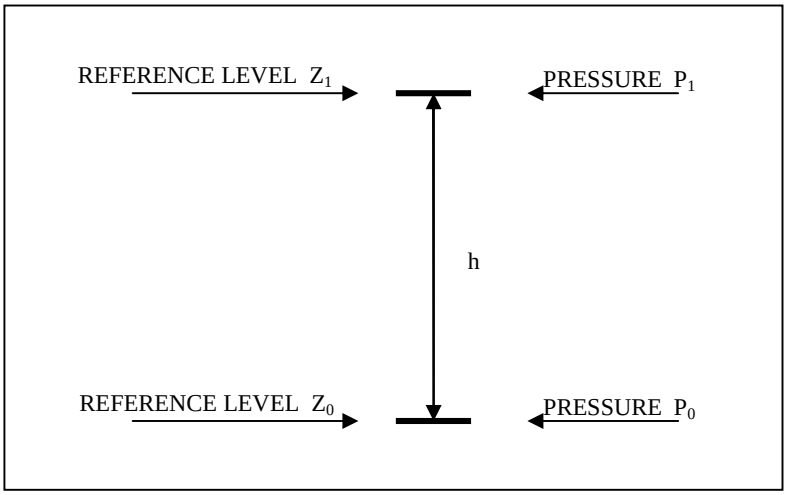

Figure 4.2. *Diagram showing the coordinates of the pressure and reference levels.*

The pressure differential between the two reference levels, Z_1 and Z_0, shown in equation (4.1) [102] will allow the mean density to be calculated. Here ρ is the density, g is acceleration due to gravity and h the vertical difference between the two pressure levels (Z_1 to Z_0)

$$\text{Pressure differential} = P_0 - P_1 = \rho g h \qquad (4.1)$$

The distance that the pressure references are apart and their position within the interceptor are examined in more detail in subsequent sections within this chapter.

4.2 Modelling pressure change within an interceptor

It has been shown that within an interceptor the total volume of liquid will increase (resulting in a rise of the liquid/air interface) as the water is displaced by a less dense liquid. Specific to the request of Andel Ltd. the significant depth of oil to be detected

within the interceptor lies is between 150 to 250 mm. This interface will be located within the upper region of the interceptor provided it was originally full of water.

To identify the significance of the rise of the liquid/air interface upon the change in pressure as oil collects within the interceptor, the effect upon two stationary pressure points has been modelled. The shallower a pressure measurement point is placed below the water surface, the earlier a response to a change in pressure will be detected as the oil is added. The pressure point was chosen such that sufficient liquid covered the probe to ensure that the effect of surface ripples or any evaporation would not leave it out of the liquid, as this may ultimately affect any pre-set pressure differential limits. The other pressure measurement point was placed deeper within the liquid but still within the 250 mm oil depth region.

In the diagrams shown in figure 4.3, the pressure has been assessed at two positions represented by point A and point B. These two points have been fixed at 180 mm apart. When only water is contained within the interceptor, figure (a), they lie at 20 mm and 200 mm below the surface. Point A and point B have a calculated pressure above ambient of 196 Pa and 1960 Pa respectively and thereby through using equation (4.1) a pressure differential of 1764 Pa existed.

As new motor oil was added to the interceptor, the depth of point A and point B increased. When 100 mm of the water was replaced by oil, figure (b), point A now lies beneath 35 mm of oil, the calculated pressure had increased by 103 Pa to 299 Pa. The pressure at point B has remained constant and the pressure differential between points A and B changed to a lower figure of 1661 Pa.

With the addition of further oil, figure (c), 200 mm of water has now been displaced. The oil depth above point A has further increased, raising the pressure to 426 Pa which is 230 Pa greater than the original pressure. Whereas, the pressure at point B, remains the same at 1960 Pa and so the pressure differential is now decreased to 1534 Pa.

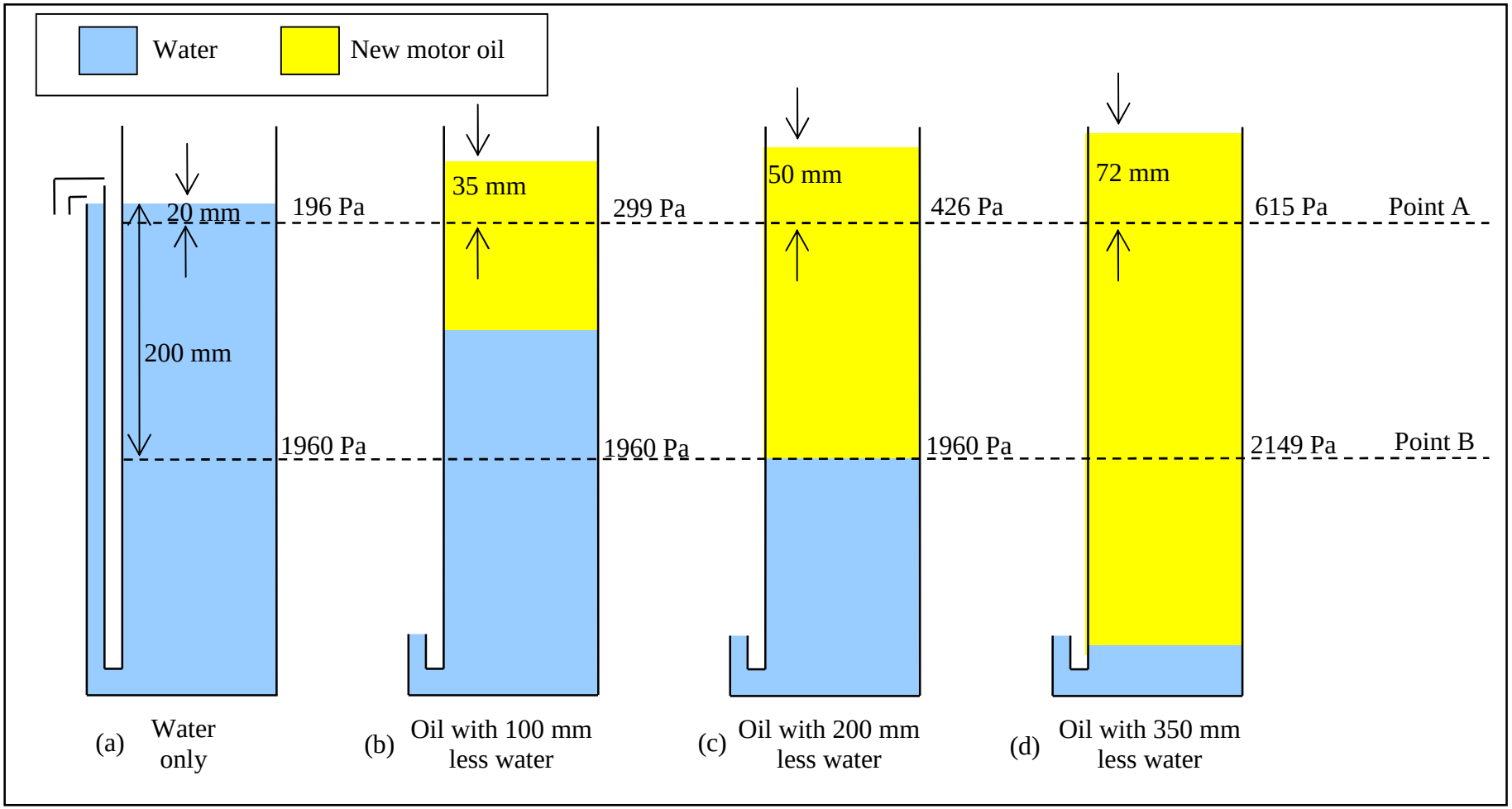

Figure 4.3. *Diagrams (a) to (d) show the displacement of water with new motor oil effects the depth of the measurement points and that the pressure at these measurement points only changes after the oil/water interface has passed.*

As more oil is added to the system, figure (d), the liquid/air interface continues to rise and the pressure at points A and B increase equally as the oil depth above both positions increases uniformly. Thus, the pressure differential from this state on as further oil is added remains constant at 1534 Pa.

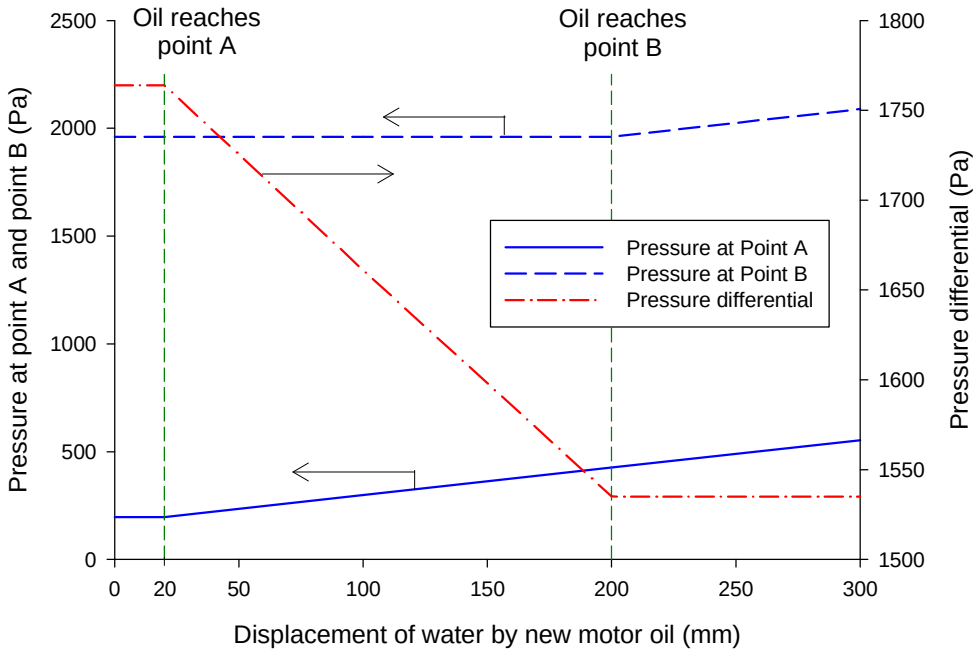

Figure 4.4. *Graph showing the calculated pressure and the differential pressure as oil is added to the interceptor. Points A and B refer to the model previously discussed.*

The calculated pressure changes at points A and B as oil is added to the interceptor (referring to the diagrams in figure 4.3) has been summarised in the graph in figure 4.4. The pressure differential between these two pressures (shown as the broken/dotted line in the graph and scaled to the axis on the right), only changes as the oil/water interface passes between the two reference points A and B. After the oil/water interface passes beyond point B, a similar pressure change is experienced at both pressure points and consequently the pressure differential remains constant.

4.3 Positioning of pressure reference points

For the determination of the presence of oil through pressure change, it has been shown that no pressure change occurred until the oil/water interface passed a particular pressure measurement point, after which, the pressure increases linearly at this point as more oil is added. This section discusses the merits and drawbacks of various positions of the pressure reference points.

4.3.1 A single measurement point in the liquid and one in the air

As oil accumulates within the separator and the air/liquid interface rises (as shown in figure 4.1), it would then appear to be possible to place one measurement point at the initial air/water interface (with no or minimal oil present) and the second pressure point at a position in the air, see figure 4.5 (a), with only water present there would be no pressure differential. Once any oil builds up within the separator, the liquid level would rise, the measurement point once immersed within the liquid would experience a pressure increase and thus create a pressure differential indicating the presence of oil within the separation tank. By still using a differential pressure gauge any change of the atmospheric pressure would affect both ports, which would cancel each other.

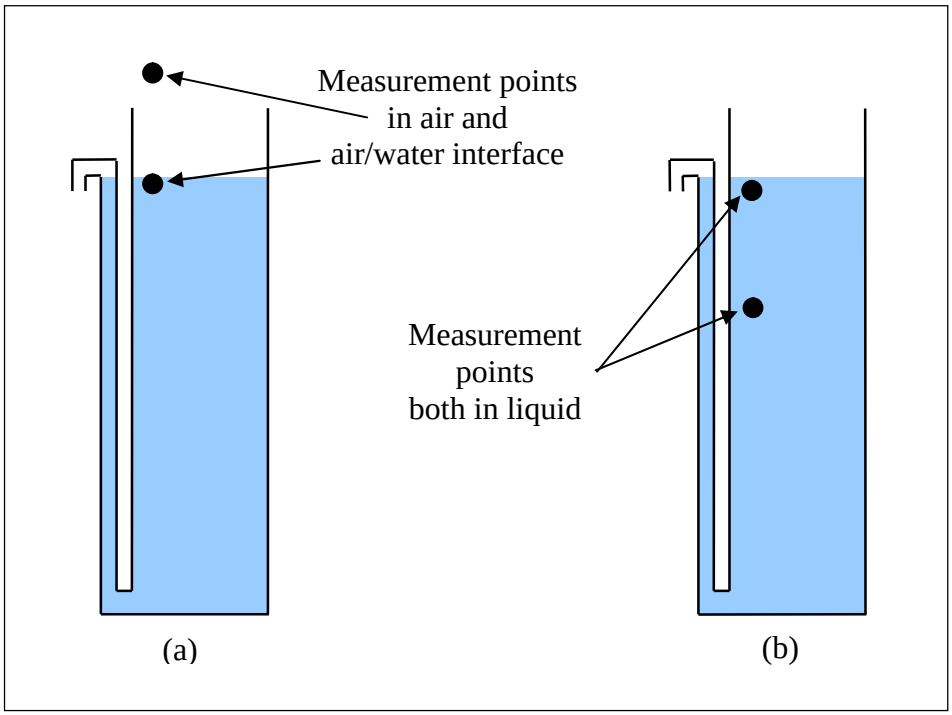

Figure 4.5. *Diagram to show the position of the pressure measurement points; (a) one in air and one at the air/water interface, (b) both within the liquid.*

Any alteration in the pressure differential from this configuration would be a function of the accumulation of oil within the separator. The potential problem with this method would occur if the inflow of water into the interceptor was greater than the outflow, possibly due to a high rate of rainfall or from a poor outflow system. This would result in the interceptor storing the excess water until the drainage system restores equilibrium and the interceptor returns to a stable level. During this time of excess water, a method which uses this single liquid measurement point would indicate the presence of oil through a false pressure reading. Although this method appeared to have limitations in some cases it was investigated further and is reported in the following chapter.

4.3.2 Both measurements point within the liquid

By placing both pressure points in the liquid within the interceptor, see figure 4.5 (b), any temporary increase of the air/liquid interface level due to a large inflow of water would produce the same pressure change for both measurement points and as such, false indication of the presence of oil would be avoided. The position for each pressure measurement point and their distance apart is considered below.

Placing the upper measurement point at or near the surface produces an increase in pressure once oil passes this position. A shallow location at the air/water interface may well be prone to being occasionally exposed to air due to ripples upon the water surface, however, the impact of this would probably be limited and once any oil accumulated this measurement point would effectively become submerged as the liquid/air interface rose. The lower pressure measurement point operates as a reference with which the upper measurement point is compared, nevertheless, its position should not be placed at a random depth within the interceptor. It has previously been shown that once the oil/water interface passes both measurement points, no relative pressure differential occurs. This would infer that the greater the depth of separation between these two points the more effective the system.

Two problems emerged from having the lower measurement point unnecessarily deep. The first became apparent through using tubing to relay the pressure to a pressure transducer. As the measurement point became deeper and the pressure increased, the rate of air leakage due to permeability of the tubing increased, compromising the system. The second complication, which revolved around the pressure differential, was through placing the two measurement points further apart to create a larger pressure

differential. The change in pressure that occurs at the upper measurement point when oil accumulates would represent a smaller overall fractional change in the pressure differential, making it harder to detect. For example, two reference points one metre apart would produce a pressure differential of ~ 9800 Pa, a displacement of 200 mm of water by new motor oil would reduce this differential by ~ 250 Pa, a change of ~ 2.5% to the overall pressure. Placing the lower measurement point within the location of the desired depth of oil to be detected would produce a greater differential change. In the example shown in figure 4.3, the decrease in pressure differential as 200 mm of oil is added is > 12%, creating a more lucid change to be detected. Locating both the measurement points within the region to be detected maximises the fractional change in pressure whilst keeping the air pressure within the system to a minimum.

4.4 Methods chosen for monitoring the pressure

In detection systems that measure pressure, then at some stage in the process this pressure will need to be converted into a secondary force that can be more conveniently monitored. As the remit for this oil detector requires that no electrical devices are placed within the Zone 0, the air pressure from this pressure system has either to be conveyed to a distance away from the interceptor before being assessed or, alternatively, a pressure driven detection system could activate a non electrical control, such as an optical switch. This optical signal may then be relayed to a monitor, thereby avoiding electrical components within the restricted region.

As referred to in the introduction, two methods have been investigated; the first system uses tubing to connect to pressure probes that are located within the separator to an electrical pressure transducer housed some distance away. This monitor is referred to as a pressure tubing detector. The second arrangement was based upon a pressure differential system moving a blade that can obscure a light signal travelling along a fibre optic cable and is referred to as a diaphragm fibre optic detector.

4.4.1 Pressure tubing detector

The pressure tubing detector comprises of three main components and these are shown in figure 4.6; the monitor, the tubing and the sensor head (consisting of the probes).

As the pressure transducer is required to be outside Zone 0, pressure from the two pressure reference points needs to be conveyed from the interceptor to the pressure transducer. The innovative design of this detection device uses two connecting tubes, one to each of the pressure measurement points, with the other ends connected onto the ports of the differential pressure transducer and through the medium contained within the tubes, transfer these individual pressures, and through comparison of the differential pressure measure, the changes in the oil and water status in the interceptor.

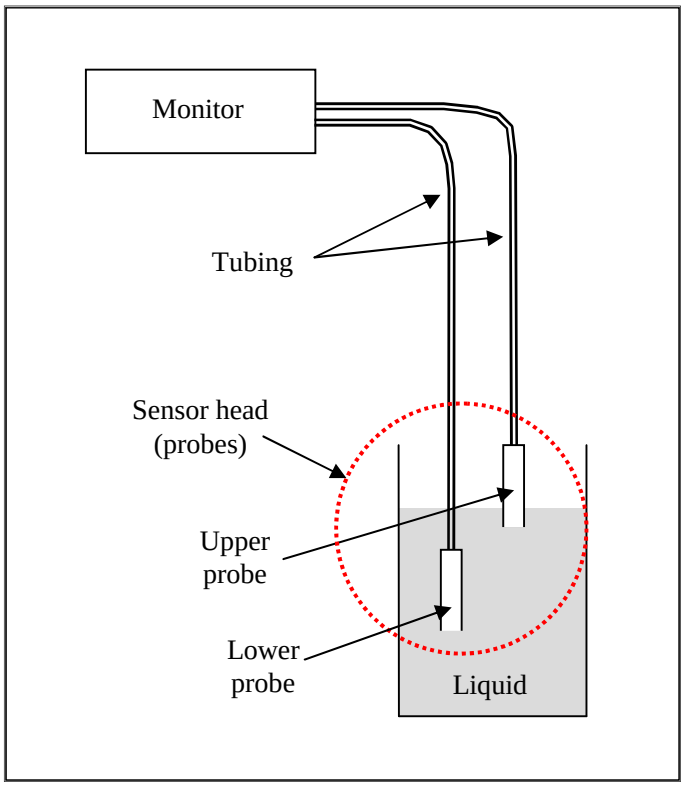

Figure 4.6. *Diagram showing the three main parts of the pressure tubing detector; the monitor, tubing and sensor head (probes).*

The electronic pressure transducer converts pressure into an analogue electrical signal that is related to the pressure imposed, which needs to be suitably sensitive to detect the changes indicated by the pressures modelled. The differential pressure transducers used were compact electrical PCB mounted devices having two ports, suitable for tubing connections. The conversion of pressure into an electrical signal is achieved by the two input pressures entering the transducer and deforming a diaphragm that has a strain

gauge attached, this in turn produces a change to the electrical resistance. Pressure transducers are normally rated to work within designed limits and for this application one that is sensitive to a response within the lower range of 0 to 3 000 Pa was required (often quoted in mbar or inches H_2O).

4.4.2 Diaphragm fibre optic detector

The diaphragm fibre optic detector, similar to the pressure tubing detector, consists of three main components and is shown in Figure 4.7; the optical monitor, the fibre optic cables and the optic sensor (comprising of the diaphragm and probes).

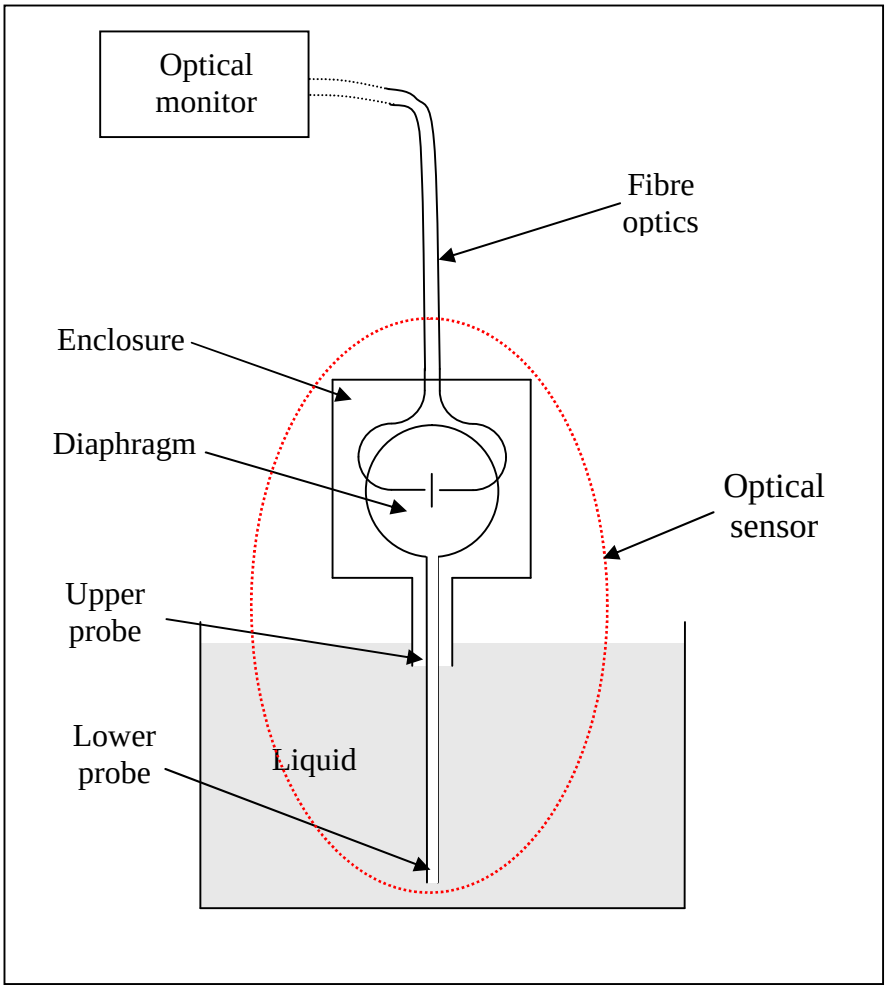

Figure 4.7. *Diagram of the diaphragm fibre optic detector, showing the monitor, the optical sensor and the sensor head (probes).*

By pressurising the interior of the diaphragm from the lower measurement point and the air surrounding the diaphragm from the upper measurement point, the movement of the diaphragm will reflect the pressure difference from these two measurement positions.

The diaphragm was housed within an enclosure capable of containing the pressure supplied by the upper probe, the lower probe being connected to the diaphragm.

To avoid having to convey the pressure through several metres of tubing, the pressure differential from the two reference points may be used to disrupt the light travelling along a fibre optic cable and from there transfer the information of the interceptor oil level via fibre optics to a monitor some distance away. Through using a pressure activated mechanical diaphragm, an attached blade would move according to the pressure differential as it changes. The monitor contains the electronics, including the LED light source and the light detector.

5. Pressure tubing detector

This chapter follows on from the theory of oil detection by pressure change by using a pressure transducer to sense the changes as oil replaces the water. The initial experiments validated this principle for depth measurement through using air filled tubing connected to a pressure transducer. It was found that the dimensions of the probes and their internal volumes affect the measured pressures. As the research progressed, the design and location of the probe was considered. Once optimised in the laboratory, trials were undertaken at Andel Ltd, here, fluctuations in the air temperature produced results that had not been seen in the laboratory. As a result of these trials, monitoring of the air and water temperatures was also incorporated into the logged data. Through analysing the data from these trials, an improved sensor was developed suitable for long term oil detection.

5.1 Components used in oil detection

As the oil detector was developed, various components were used, some of the specialist parts were purchased (pressure transducers and other electronic components) whilst other devices were fabricated. The requirement from Andel Ltd for a competitively priced detector was kept in mind whilst considering the final construction of the detector. As the systems were developed, some of the components were changed or altered as improvements were sought.

5.1.1 Apparatus

Voltmeter and Data logger

During laboratory experiments the outputs from the monitors were connected to a Thurlby 1905a digital multi-meter. For continuous automated recording, data loggers were used. These data loggers converted the analogue signal from the pressure transducer into a digital form suitable for storage on a computer. A Labjack Corporation Labjack-U12 was used in the laboratory. A Pico logger and an Adlink Technologies Inc.

Data acquisition unit were used at Andel Ltd, the latter capable of collecting both pressure and temperature information. The data was date and time stamped whilst being stored on a computer.

Laboratory interceptor

For experiments in the laboratory, an interceptor was made from glass in the department's glass workshop. This had a capacity of ~1.2 litres and reached a working depth of 330 mm before any liquid would flow out of the inverted siphon. With an internal diameter, ID, of 66 mm all the single and double probes could be accommodated except for the large ID 74mm stainless steel probes. These large probes were used in an interceptor in the workshop at Andel Ltd, this interceptor which was made specifically for testing the detector and had a capacity of ~ 100 litres.

Temperature sensor

Daily variations of the monitor output were seen during experiments at Andel Ltd and it was deemed informative to monitor any changes in the temperature. To achieve this, two National Semiconductor LM3342Z integrated circuit temperature sensors in a TO-92 case were used to measure both the liquid and the air temperatures. These produced a linear output voltage over the expected temperature range. They were encapsulated in polyurethane, which gave the sensors protection against liquid damage.

5.1.2 Components of the detector

For clarity, the parts for the pressure transducer detector have been divided into three sections as shown in figure 4.6:

1. Sensor head and probes, these were always situated within the interceptor and positioned at the pressure measurement points.
2. Tubing, these were used to connect the probes to the pressure transducer.
3. Monitor, this contained the pressure transducer, electronic circuits, electrical outputs and LED indicators.

Sensor head

The pressure which was measured at specific positions (pressure measurement points) was conveyed to the transducer through tubing. The parts of the tubing that resided near or within the liquid needed to be made of a more rigid material and are referred to as the

probes. These probes are required to be robust, able to withstand abrasion, be resistant from corrosion, non porous and have an internal diameter sufficiently large to allow liquid to enter without blockages occurring.

Several sets of probes were made, the first two from glass and the others from stainless steel, as a less fragile material was required for durability. Where two measurement points were to be assessed within the liquid, a double probe was used. These were two probes which were either temporarily secured together or more permanently fixed, as shown in figure 5.1.

In the initial experiments glass probes 450 mm long were used, these were straightforward to manufacture, being made in the department's glass workshop, and allowed observation of any liquid entering the probes. The first set of glass probes were glass tubes with an ID of 5.0 mm. The second set of glass tubes had a larger ID of 11.0 mm, increasing their internal volume.

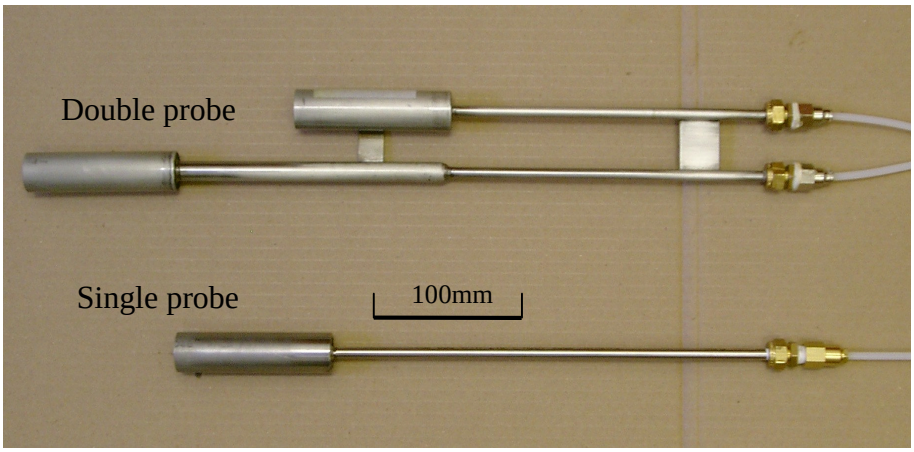

Figure 5.1. *Photograph of the smaller diameter stainless steel double and single probes all with an ID of 20.2 mm. The flexible tubing is attached to one end (right), whilst the other end is open.*

The metal probes, made in the department's machining workshop, were changed in their design inasmuch as the ends of the probes had a large ID with a narrow hollow steel shaft connecting the probe to the tubing. This can be seen in figure 5.1, here there is a double probe (top) and a single probe (bottom) later referred to as probe No.1. The larger ends of these probes were 100 mm long with an ID 20.2 mm. A variation of the single probe was made with the end of the probe 27 mm long with an ID 20.2 mm, reducing the air reservoir but still with the same orifice diameter and will be referred to as probe No.2.

The final set of steel probes were made similar to the previous probes except that the lower parts of the probes were much larger, having an ID 74 mm and are shown in figure 5.2. These larger probes contained a much greater volume of air, the orifice was restricted to an opening with a diameter of 15.0 mm, this was to limit the effect of vertical misalignment and this is discussed later. This device is referred to as probe No.3.

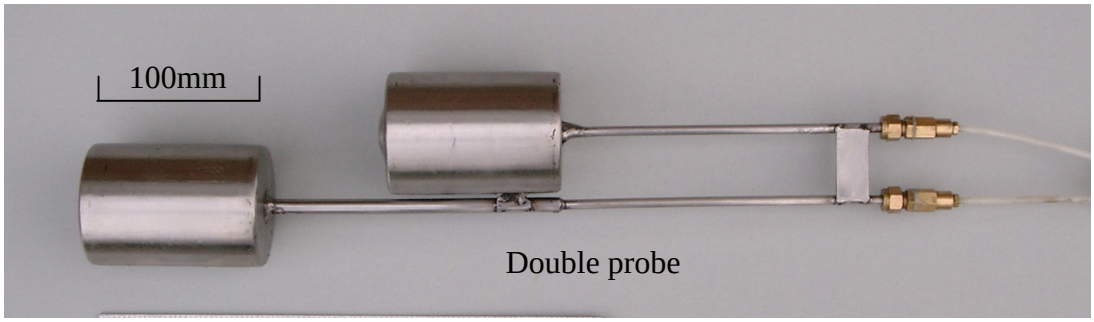

Figure 5.2. *Photograph of the large stainless steel probes with an ID 74.0 mm.*

Tubing and connections

To connect the probes to a pressure transducer, which may be several metres away, some form of tubing was necessary. The tubing is required to be sufficiently flexible for its installation but rigid enough to withstand the internal pressure without deforming, suitably chemically resistant and having low gas permeability. The nylon tubing was manufactured by Norgren and the PTFE tubing was manufactured by Adtech Polymer Engineering UK.

Although the internal pressure of the tubing is relatively low, it is required that it is sustained for several months. Therefore, the permeability of the material needed to be considered. Table 5.1 illustrates the permeability and other properties for several tubing materials. Any tubing used would eventually be wrapped to provide extra protection against abrasion and other environmental effects, offering added shielding. The expected operating temperature for the tubing will be within the range indicated in the table.

The lower the permeability of the material the more suitable it would be and the thicker the tubing wall, the slower the reduction in pressure. As permeability is a function of the internal pressure, a lower pressure created from being closer to the surface would reduce the rate of leakage through the tubing walls. The composition of dry air is

predominantly nitrogen (78.08 %) and oxygen (20.95 %), it follows that these are the most significant gases to be considered. FEP (Tetrafluoroethylene-Perfluoropropylene), nylon and PTFE (Polytetrafluoroethylene) are the most suited, for their chemical resistance and low permeability losses. Polyurethane, which was used as a potting compound, silicone and vinyl have been added for comparison.

Tube material	Operating temperatures °C	Chemical resistance grade	Gas permeability at 25 °C see equation 4.2 ($\times 10^{-10}$ mm sec^{-1})			
			CO_2	H_2	O_2	N_2
FEP	-270 to 205	A	5.9	1.3	14	2.0
Nylon	-51 to 93	A - D	20	19	5.4	1.1
PTFE	-240 to 260	A	6.8	-	-	1.0
Polyurethane	-40 to 82	A – C	395	66	10.5	17.1
Silicone	-51 to 238	A - D	20 132	6 579	7 961	2 763
Vinyl	-43 to 82	A - D	360	-	40	80

Table 5.1. *Properties for tubing. The chemical resistance is from weak to extreme conditions (A, being little damage to D, severe damage for prolonged contact. The D rating of chemical resistance for nylon refers to ozone and weak acids). Not all permeability data is available, as shown by a blank entry.* [103]

The gas permeability data for this tubing material in Table 5.1 provided by the manufacturer was based upon equation (5.1) [103]. The surface area being the internal dimensions of the tube and the pressure is the pressure differential of internal to ambient pressure.

Gas permeability $\times 10^{-10}$ mm sec^{-1} =

$$\frac{\text{diffused gas } (\text{cm}^3) \times \text{tube wall thickness (mm)}}{\text{time (seconds)} \times \text{surface area } (\text{cm}^2) \times \text{pressure (cm of Hg)}} \qquad (5.1)$$

The nylon tubing, at approximately £0.40 per metre, is about half the price of FEP and PTFE, was chosen for the experiments. Tubing of a wall thickness 1.0 mm (OD 4.0 mm and ID 2.0 mm) and lengths of up to 45 metres were used. Typical calculated gas losses (based upon nitrogen and oxygen at 80:20) from a 30 metres length of nylon tubing,

where the probes where placed at 200 mm and 20 mm depth creating internal pressures of 1960 Pa and 196 Pa respectively are as follows:

1.41 cm^3 per month from a probe placed at 200 mm depth.
0.14 cm^3 per month from a probe placed at 20 mm depth.

These figures have been calculated presuming the pressure was constant throughout the time period (though this would not be the case), as such, these figures tend to overestimate the gas loss. However, the figure of 1.41 cm^3 per month would represent a gas loss of less than 2% for this scenario. The effect of gas loss upon the internal pressure and how this has influenced the design of the probes is further discussed later.

To aid in experiments whilst using various lengths of tubing and different probes, the tubing was initially attached to the probes using push-in type fittings manufactured by Norgren, these were quick and convenient to use. Brass compression fittings, also manufactured by Norgren, provided a more permanent and secure coupling and were used later for the longer term experiments.

Monitor indicator/displays

Housed within the monitor enclosure was the pressure transducer and electronic circuitry. Output sockets facilitated a connection to either a voltmeter or data logger. For long term monitoring, the pressure transducers were powered from a 9 volt DC mains adaptor. Mounted on the outside were LEDs, these were connected to the electrical circuit and via potentiometers they could be adjusted to indicate different pressure thresholds within the system. Apart from monitoring the change from water to oil, this pressure system has the means to signify other eventualities, such as the pressure falling outside the normal oil/water range (voltage range), indicating the failure brought on through pressure loss as a result of tube damage, or though a low level of liquid in the interceptor.

Pressure transducers

Two different differential pressure transducers were used, both were PCB mountable. Initially a Honeywell 24PCEFA6D was used, this non-temperature compensated unamplified voltage output transducer had a pressure range 0 to 0.5 PSI (0 to 3450 Pa) with two inlet ports, priced at ~ £8.00. Later, a Sensortechnics HCXM020D6V

temperature compensated transducer with an amplified output and an adjustable off-set built in was used. This transducer had a pressure range 0 to 20 mbar (0 to 2,000 Pa), again with two inlet ports and was priced at ~ £63.00. Both transducers had push-on fittings which were adapted to accept compression connections. With both differential transducers, one inlet port was for the higher pressure whilst the other was to monitor the lower pressure. For continuous monitoring, both pressure transducers were powered from a 9 volt DC mains adaptor.

Two different monitors were made, referred to as Monitor 1 and 2. The main component within these monitors was the pressure transducer; Monitor 1 used a Honeywell 24PCEFA6D non temperature compensated transducer and Monitor 2 the Sensortechnics temperature compensated transducer. For long term pressure monitoring it was important to minimise air leakage, this was partially achieved through using a polyurethane potting compound around the pressure transducer and the connection tubes inside the monitor enclosure. Monitor 2 was potted whilst being assembled but with Monitor 1 this was added later improving gas retention.

5.1.3 Decision to use gas to convey the pressure

Two types of material may be used to transfer the pressure along the tubing, a gas or a liquid. Gas being a compressible medium with some degree of permeability (through the tubing walls) has the advantage of not requiring to be sealed at the interceptor ends of the probes, with the pressure of the liquid within the interceptor trapping and holding it. Whereas liquid, although having the advantage of being a non compressible medium, would require to be contained within a sealed system. In turn this would mean having a form of flexible diaphragm sealing the end of the probe. Some trials showed that such a system unnecessarily complicated the manufacture, but more importantly reduced the sensitivity. Additionally, thermal expansion of the liquid (glycerol was used) impaired the performance. A system of using gas filled tubing was therefore preferred.

5.2 Modelling the effect of using air to convey pressure inside tubing

Using a compressible gas, in this case air, to convey pressure along a tube from the measurement point to the pressure transducer needed to take into account that the gas will vary in volume as the pressure changes. Boyle’s law states that, at a constant

temperature, the volume (V) of a given mass of gas varies inversely with pressure (P), as shown in equation (5.2).

$$P_1 \times V_1 = P_2 \times V_2 \quad (5.2)$$

The consequence of this is that once the probe enters the water, the air under pressure will compress and the water will enter the probe. The deeper the probe goes into the water, the greater the pressure, further reducing the volume of air, resulting in additional water entering into the probe, as depicted in figure 5.3.

The overall effect of volume reduction due to air compression within the tubing will be that the pressure at the transducer will not represent the pressure at the base of the probe (referred to as the pressure measurement point). The pressure at the base of the probe (referring to figure 5.3), created by the surrounding depth of water (P_P), does not equal the air pressure within the probe and tubing. The downward pressure exerted from inside the probe is a combination of both the internal air pressure (P_2) and that from, in this scenario, the water inside the probe (D_W). The pressure added by this compression is dependant upon the liquid depth, density (ρ) and acceleration due to gravity (g), the resultant balance of pressure at the probe base is shown in equation (5.3).

$$P_P = P_2 + \rho g D_W \quad (5.3)$$

This discrepancy between the depth of the probe and the air pressure has been calculated by taking into account several factors; the density of the liquid surrounding the probe, the density of the liquid that had entered the base of the probe (this factor will become significant later as oil is introduced), the combined internal volume of the probe and tubing, the ambient air pressure and the diameter of the lower portion of the probe. The depth of the gas (D_{AIR}) inside the probe when measured against the density of the surrounding liquid is proportional to the true pressure of the gas being measured. This calculated air pressure was used when calibrating the output voltage of the pressure transducer monitors.

As the gas inside the probe and tubing compresses, its volume is reduced and as more liquid enters the probe the effective reference position is compromised. As the monitor may be some distance away from the interceptor, thus requiring a greater length of tubing, this in turn would increase the total volume of gas inside the probe and tubing,

thus reducing D_{AIR}, further restricting the value of any measurement point. This effect may be reduced by the use of a larger diameter probe, through this approach, a given volume of incoming water would occupy less vertical space and a greater D_{AIR} would be maintained.

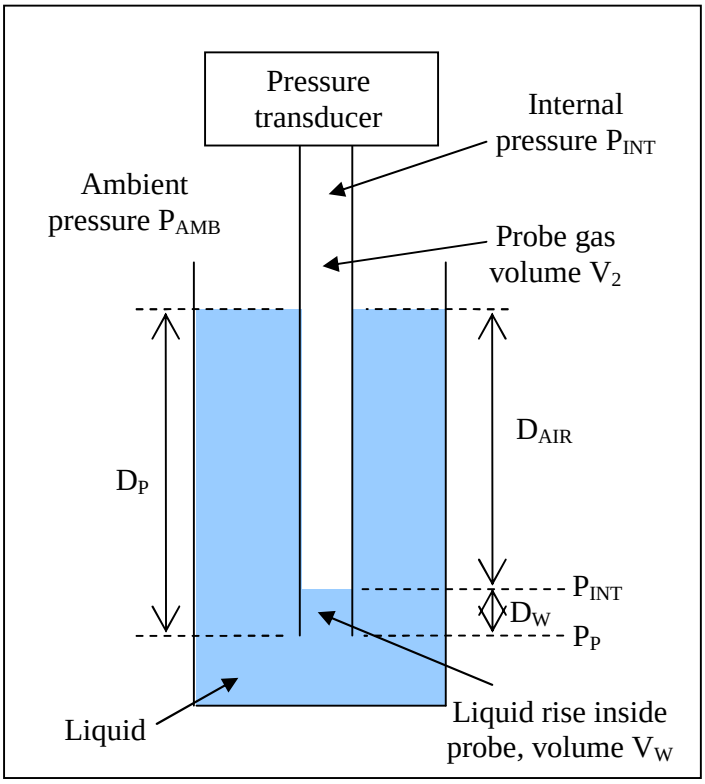

Figure 5.3. *Diagram showing liquid rise inside the probe as the contained air is compressed. D_P is depth of probe, D_{AIR} is the actual depth of the air and D_W is the depth of the inflowing liquid. P_P and P_{INT} are the pressures at these positions.*

In order to calculate the water rise and the air pressure within the probe at a probe depth, D_P, for a probe with a cross sectional area (A) and a probe and tubing volume (V_1), the pressures at the base of the probe, (P_P), are considered thus;

The pressure from the water outside at the base of the probe with a cross section area (A) equals the pressure within the probe, shown below as equation (5.4);

$$\rho g D_P + P_{AMB} = \rho g D_W + P_{INT} \qquad (5.4)$$

Pressure from depth of water (D_P) + Ambient atmospheric pressure (P_{AMB}) =

water pressure from within the probe (P_W) + air pressure from within the probe (P_{INT})

Using Boyle's law; $P_1 \times V_1 = P_2 \times V_2$

rearranging to give; $P_2 = (P_1 \times V_1)/V_2$

where $V_2 = V_1 - V_W$ (V_W = volume of the water rise inside the probe)

$V_W = A \times D_W$

and $P_1 = P_{AMB}$ (P_1 is the original probe pressure equal to atmospheric pressure)

Equation (4.5) may be rewritten as equation (5.5);

$$\rho g D_P + P_{AMB} = \rho g D_W + (V_1 P_{AMB})/(V_1 - A D_W) \quad (5.5)$$

Rearranging equation (4.6) to find the coefficients of D_W^2 and D_W to equation (5.6)

$$D_W^2(A\rho g) - D_W(A\rho g D_P + A P_{AMB} + V_1 \rho g) + V_1 \rho g D_P = 0 \quad (5.6)$$

Using the quadratic formula D_W can be found, the volume of the water in the probe can be determined, followed by V_2 and the gas pressure within the probe (P_{INT}) can be further calculated.

When equation (5.6) is applied to a calculated example probe; having an ID 5.0 mm and an internal volume of 50.0 cm^3, producing a column with a height of 2546 mm (4 sf), the resulting ingress of water as the probe is immersed is shown in figure 5.4. This figure shows an unrealistic depth, however, this graph emphasises that the increase in depth of the inflowing water is not linear with the descent into water by the probe, the ingress of water can never totally occupy the whole volume of the probe, owing to the presence of the air, nor can it ever exceed the probe depth, resulting in an initial steep rate of change, tending to a minimum change with depth. However, as the probe will only be submerged to shallow depths within an oil/water separator (less than one metre), the increase in the depth of the water ingress can be considered to be linear. The pressure differential, also shown in figure 5.4, between the probe pressure and that of the ambient pressure, indicates a near linear increase with probe depth. The small difference in the rate of change within the range of probe depths for this research will be negligible and will also be considered to be linear.

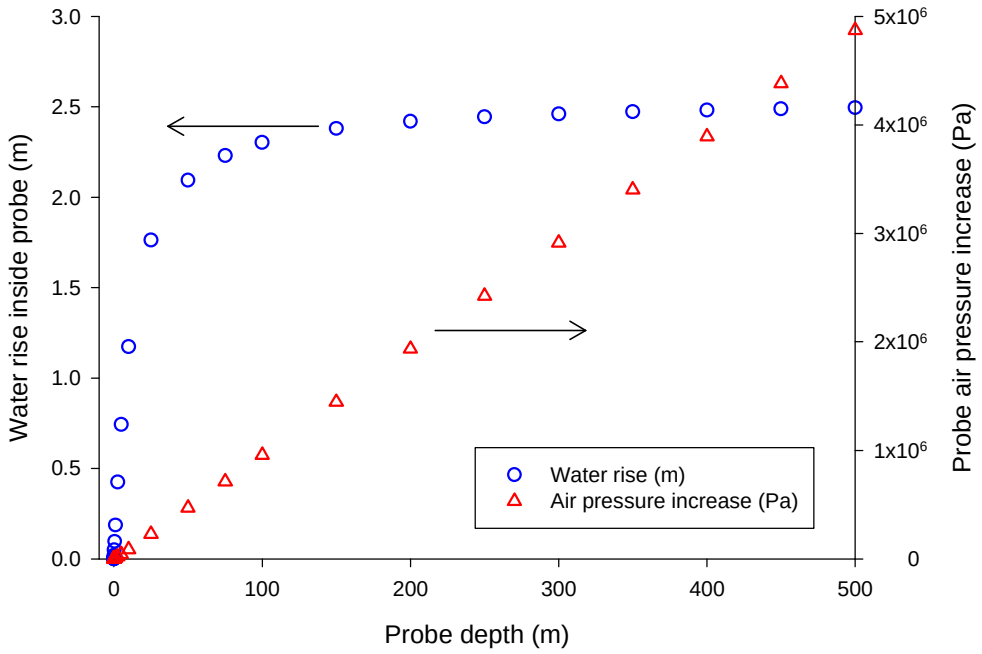

Figure 5.4. *Graph showing the calculated ingress of water and change in differential pressure for a fixed sized probe as it is immersed into water.*

It can be seen from equation (5.6) that apart from the probe depth, the resultant probe internal pressure is influenced by the initial volume and the cross sectional area of the probe at the point where the water is entering and residing. The shape and dimensions of the upper part of the probe and tubing is irrelevant to the probe pressure, apart from their total volumes. It will be shown in the experimental data that by varying the probe shape and collective volume of the probe and tubing, the air pressure inside the probe can be brought near to that of the pressure at the base of the probe.

The effect of the probe dimensions and volume influences both the ingress of water and the probe pressure. The cross sectional area of the probe and its air capacity needs to take into account not only the water ingress but also allow for air losses through permeability, so that the probe air pressure drop is negligible. Probe dimensions and volume, tubing, temperature and air leakage upon air pressure is examined and discussed later in the following section. These factors have an effect upon both the pressure tubing detector and the pressure diaphragm fibre optic detector.

5.3 Development of pressure probe

This section follows the progress of the development of the pressure probes. By using a pressure transducer connected to a simple glass probe via nylon tubing, the relationship between the depth of the probe to the probe air pressure was determined. Later experiments involved using several different sized probes and a range of lengths of tubing, connecting extra lengths of tubing allowed the internal volume to be increased.

5.3.1 A simple glass probe in water

The first experiment investigated how the air pressure of a probe changed as it was lowered into water. This also enabled the pressure transducer to be calibrated. This involved a single glass probe with an ID of 5.0 mm connected to 0.8 metres of nylon tubing, creating a volume for the probe and tubing of 13.5 cm^3. This was joined to the high pressure port of Monitor 1, whilst the lower pressure port was left unconnected, allowing this port to read the ambient pressure, the resulting pressure differential would be that produced from the probe. Glass probes were the first probes to be used, as these were produced relatively easily by the glass workshop. The connecting tube of 0.8 metres was chosen as this provided a convenient length whereby the probe could be manoeuvred into the laboratory interceptor.

The single glass probe was gradually lowered into a column of water and the output voltage was read at 20 mm intervals up to a depth of 300 mm. The other port from the pressure transducer measured the ambient air pressure. Before the glass probe entered the water there was no pressure differential between the two ports, at this point an output voltage of 1.125 volts was shown on the voltmeter and this offset was seen through all experiments whilst using Monitor 1.

As the probe was lowered into the water the voltage increased, this can be seen in figure 5.5. As discussed in the previous section, due to the ingress of water the pressure within the probe differs from the pressure at the probe base. The graph shows the large increase in output voltage from the monitor and also that the output signal appears near linear with the depth of the probe. Through calculating the actual probe pressure the output voltage for Monitor 1 was calibrated as below.

Output voltage (V_O) less Voltage off-set (V_{OFF}) is proportional to Pressure differential (P_D)

then; $V_O - V_{OFF} = P_D \times C_F$

(where V_{OFF} = 1.125 volts and C_F is a correction factor in mV/Pa)

This produced a C_F = 1.07 millivolts/Pa.

The calculated pressure at the probe base and the modelled probe gas pressure are also shown in figure 5.5, it can be seen that the probe air pressure diverges from the probe base pressure as the probe is immersed. However, the measured pressure from the probe closely mirrored that of the model. As previously discussed, maintaining the probe air pressure close to the probe base pressure is important in detecting the liquid density because any discrepancy between these two pressures will erode the sensitivity of the density and pressure sensing system. This discrepancy between the measured probe pressure and calculated pressure at the probe base is further examined in the following experiments.

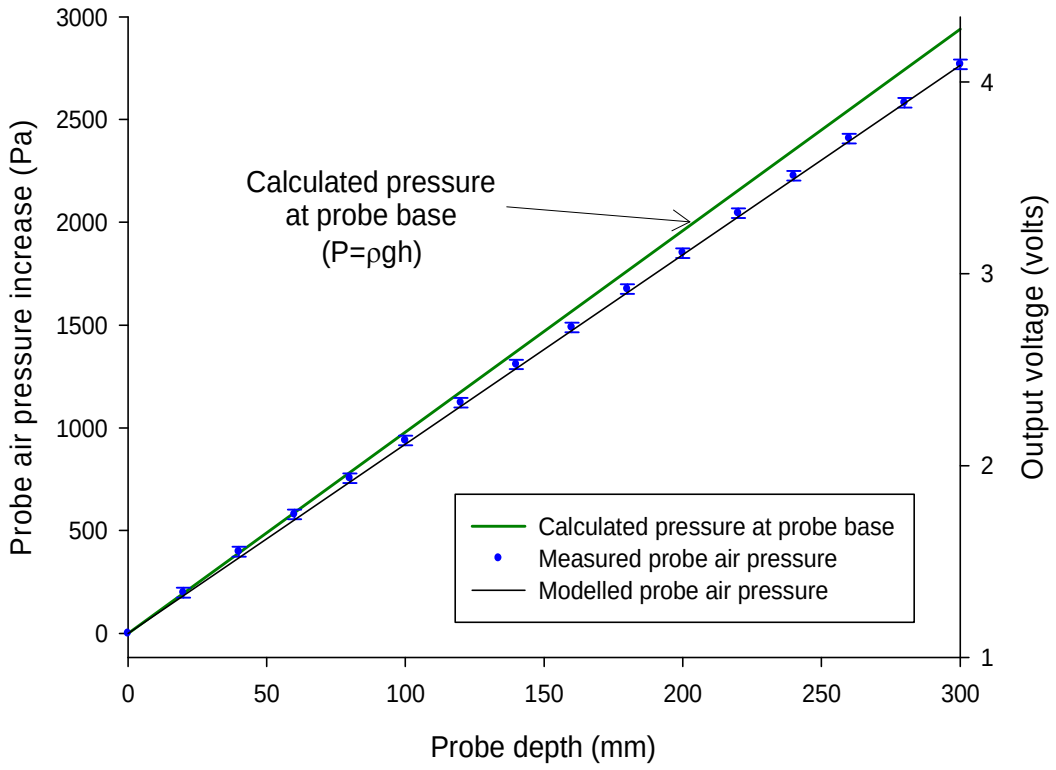

Figure 5.5. *Measured air pressure increase as a glass probe of ID 5.0 mm is lowered into 300 mm of water, this compares favourably to the modelled pressure. The calculated pressure at the probe base is shown for comparison.*

5.3.2 Variation of the probe ID and volume

The data in figure 5.5 shows the effect of depth upon a small diameter probe attached to less than one metre of tubing. The next set of experiments examined the effect of increasing the internal volume, this was achieved through adding a further 27.8 metres of tubing (various lengths of tubing had previously been assembled) to the 0.8 metres, increasing the volume from 13.5 cm^3 to 150 cm^3. In addition to the small diameter probe, a second and larger glass probe with an ID 11.25 mm was also examined with these two lengths of tubing, giving this second probe an internal volume of 50.7 and 187.2 cm^3 respectively. The resulting changes in air pressure for the four combinations of dimensions are shown in figure 5.6.

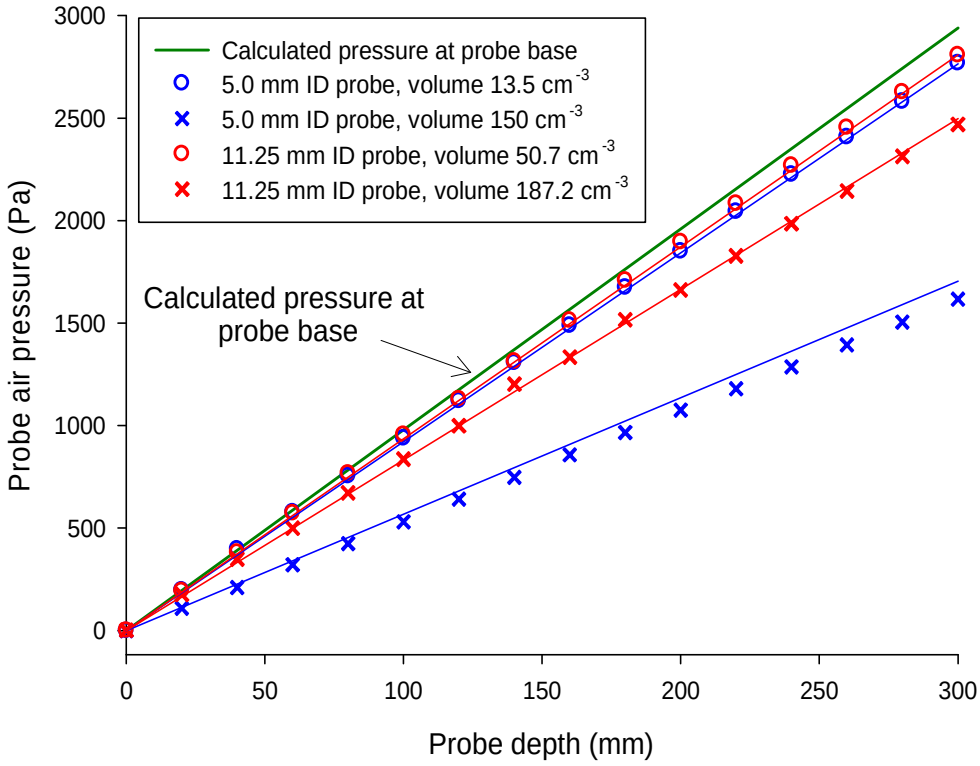

Figure 5.6. Graph *showing the effect of increasing the probe/tubing volume for two different ID probes, whilst lowering the probes into 300 mm of water. The calculated pressure at the probe base is added for comparison. The modelled pressure for the four experiments has also been added (solid lines), indicating the similarity of the results.*

As expected, when the volume for each probe was increased the ratio of the probe base pressure to probe air pressure became more significant. Only a small difference was observed between the ID 5.0 mm and ID 11.25 mm probes when attached to the short tubing but as the tubing was lengthened (effectively increasing their volumes) the smaller diameter probe displayed a greater difference in the probe base pressure to

probe air pressure, whilst for the larger ID probe a smaller deviation away from the probe base pressure was seen. The result of increasing the probe diameter was to limit the water rise inside the probe, thus maintaining the probe air pressure to near that of the probe base. The modelling of the pressure change for the four experiments was similar to the experimental data, varying marginally in the case of the 5.0 mm ID probe for the larger volume. However, these modelled results were shown to reasonably predict the pressure changes that could be expected for different probe IDs and volumes.

5.3.3 Modelling probe dimensions

Through modelling the relationship between the probe diameter and the internal volume, further theoretical assessments were examined. Two internal volumes of 200 cm^3 and 400 cm^3 were studied whilst varying the ID of the probe from 0.5 mm to 100 mm. The probe air pressure for a probe depth of 300 mm was calculated and is shown in figure 5.7. The theoretical probe base pressure is shown on the graph for comparison. These two graph plots may be representative of situations where different lengths of tubing would increase the internal volume. In each case the probe air pressure can be seen to approach the theoretical probe base pressure as the probe diameter increases.

Trying to completely match the probe air pressure to the theoretical probe base pressure would not be realistic, a pragmatic ratio of the two pressures needed to be reached. As discussed in Chapter 4 section 4.3.2, locating the two probes within the upper 200 mm of the interceptor would produce a change to the pressure differential of > 12% as oil is added. To preserve the sensitivity of the sensor, a discrepancy between the probe air pressures and the theoretical pressure of less than 12% would be preferential to retain the ability of oil detection. It could be considered reasonable to use a figure of 5% discrepancy between these two pressures and as such 95% of the theoretical probe base pressure is indicated in figure 5.7, this also proved to be an achievable ratio.

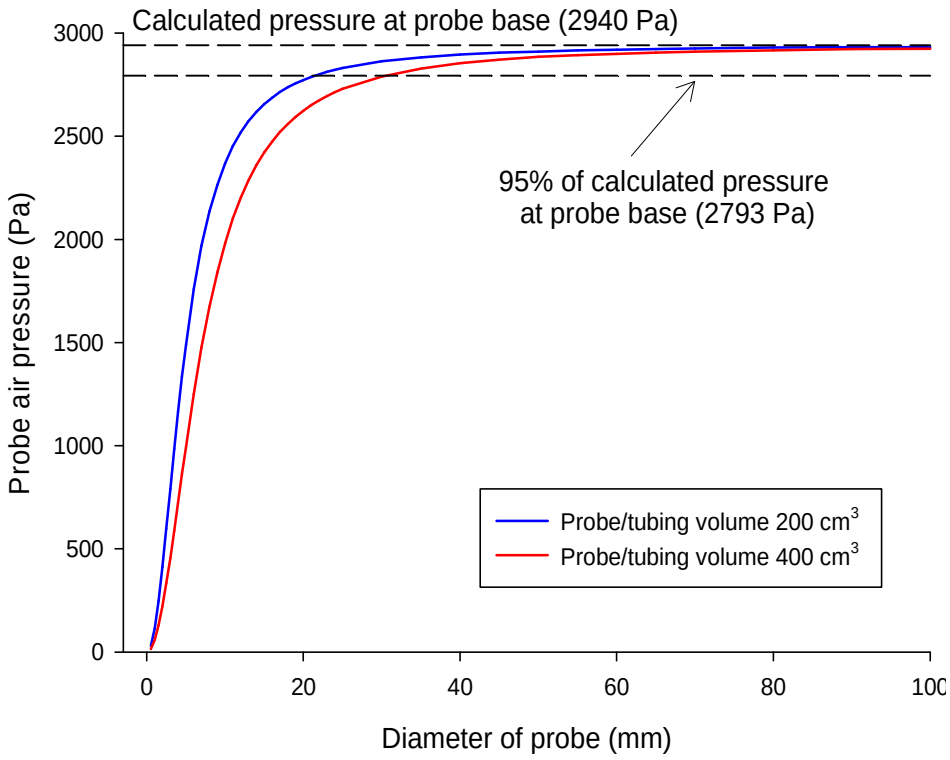

Figure 5.7. *Calculated probe air pressure change as probe diameter is increased to 100 mm, all data for a probe depth of 300 mm in water.*

A calculated example for two different diameter probes for the probe air pressure to achieve 95% of the theoretical probe base pressure shows that a probe of ID 22 mm required an internal volume of not greater than 200 cm^3, whereas a larger a probe of ID 30 mm may have an internal volume up to 400 cm^3. The relationship between probe ID and total probe/tubing volume clearly has an effect upon the indicated probe air pressure and the probe base pressure.

To assess the effect of increasing the tubing length for three different ID probes (10 mm, 30 mm and 70 mm), the pressure change was modelled against the effective increase in internal volume, with an assumed tubing internal volume of 5.0 mL per metre of tubing length. The results are shown in figure 5.8, here the depth of the probe is 200 mm and 95% of the calculated pressure at the probe base is assumed to be the significant pressure change. The 10 mm ID probe reached the 95% pressure change with ~ 10 metres of tubing, whereas the 30 mm ID and 70 mm ID probes required ~ 70 metres and ~ 380 metres respectively. This further indicating, that larger ID probes are more suited to situations requiring larger distances from the pressure transducer.

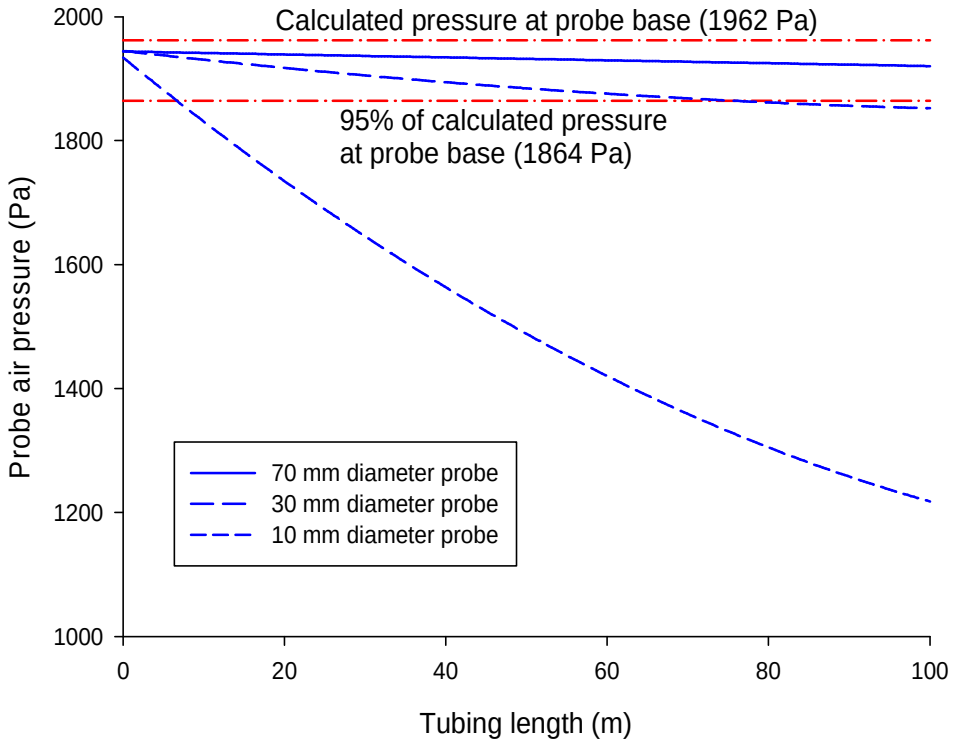

Figure 5.8. *Modelled pressure changes for three different probes (ID of 10 mm, 30 mm and 70 mm) as the internal volume was increased by additional tubing. The calculated pressure for the probe base at a value of 95% is indicated.*

The previous experiments using the probe with an ID of 20.2 mm were repeated with several combinations of tubing lengths. The stainless steel probe was positioned at a depth of 200 mm in water. The tubing length was increased from 0.3 to an extreme of 62 metres. The graph shown in figure 5.9 indicates the calculated probe base pressure of 1960 Pa and also 95% of this pressure. It can be seen on the graph that the probe air pressure decreased as the combined probe and tubing volume increased, and to achieve 95% of the theoretical base pressure the volume needed to be not greater than 135 cm^3. This correlated with the expected calculated results. The error bars were calculated using the uncertainty in the probe depth.

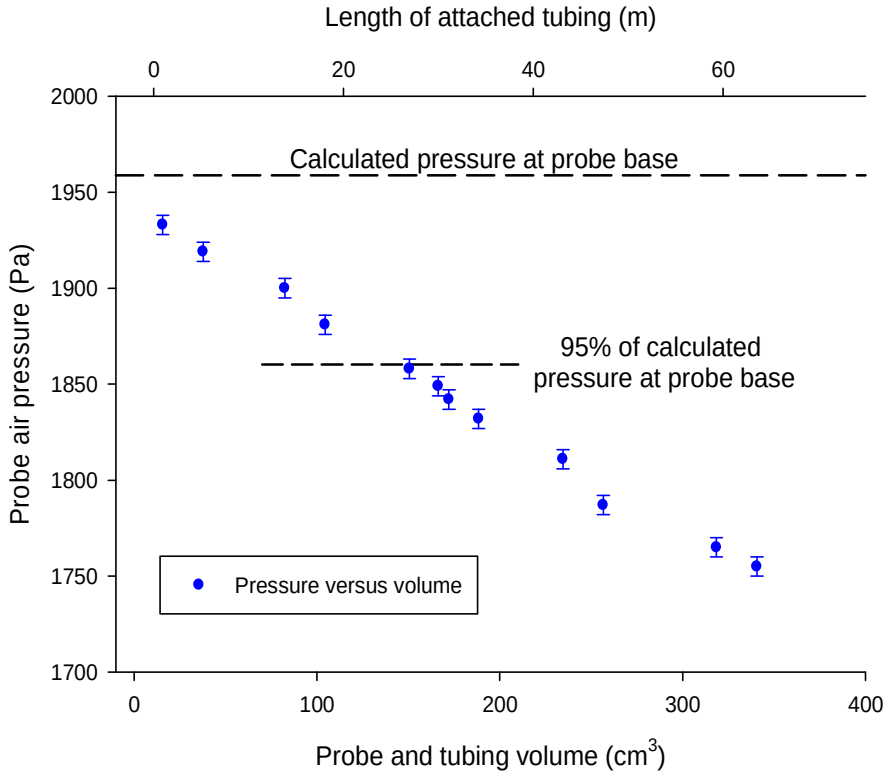

Figure 5.9. *Probe air pressure for the 20.2 mm ID probe, at a depth of 200 mm of water, as the probe/tubing volume was increased. Bottom axis represents the total volume and the upper axis indicates the lengths of attached tubing.*

In order to investigate further the effect of the probe diameter to volume ratio, experiments using five different sized probes were used, each with two different tube lengths. Table 5.2 summarises the results of these experiments where the probe air pressure was measured. The water rise inside the probe and the reduction of internal volume has been calculated. The ratio of the probe/tubing volume to the probe cross sectional area is shown. To reach the significant probe air pressure of ≥ 95% of the probe base pressure, it was found that a ratio of less than 53:1 was needed.

Extending the length of the tubing naturally increased the total internal volume, it can be seen in table 5.2 that through using the two smaller diameter glass probes only the tube with the ID of 11.25 mm and 0.8 m of tubing with a ratio of volume to cross sectional area of 51:1 managed to achieve 95% of the calculated probe base pressure. The steel probe No.1 could only reach this standard when attached to a short tube. Steel probe No.2 maintained a ratio of 48:1 with the long tubing but only the large ID steel probe (steel probe No3) was able to sustain a much lower ratio of 13:1. The final version of the probes would preferably fall within these values.

Probe type	Glass		Glass		Steel No.1		Steel No.2		Steel No.3	
ID (mm) of probe base	5.0		11.25		20.2		20.2		74.0	
Tubing length S = 0.8m L = 28.6m	Short	Long	Short	Long	Short	Long	Short	Long	Short	Long
Volume of probe and tubing (cm^3)	13.5	150.0	50.7	187.2	37.8	174.4	15.7	152.2	434.2	570.7
Ratio of volume to cross section area	69:1	764:1	51:1	188:1	12:1	54:1	5:1	48:1	10:1	13:1
* Water rise inside probe (mm)	18	126	14	45	3	15	1	13	3	4
* Reduction of internal volume (cm^3)	0.36	2.5	1.4	4.5	1.0	4.7	0.4	4.2	12.1	15.9
Difference of probe to depth pressure	179	1237	135	443	32	143	13	120	28	36
Measured probe air pressure (Pa) ±10 Pa	2760	1702	2796	2496	2907	2790	2926	2819	2911	2903
% of theoretical probe base pressure	93.8	57.9	95.0	85.0	98.9	94.8	99.5	95.8	99.0	98.7

Table 5.2. *Probe dimensions, volumes and pressures for a probe at a depth in water of 300 mm (2942 Pa). *Water rise inside probe and reduction of internal volume were calculated. Measured probe air pressures are experimental results.*

5.4 Measurement of oil and water pressure difference

It has been demonstrated that there is a relationship between the depths of the probe in water and the probe air pressure, this section compares the pressure as the probe was immersed 300 mm into new motor oil and DERV.

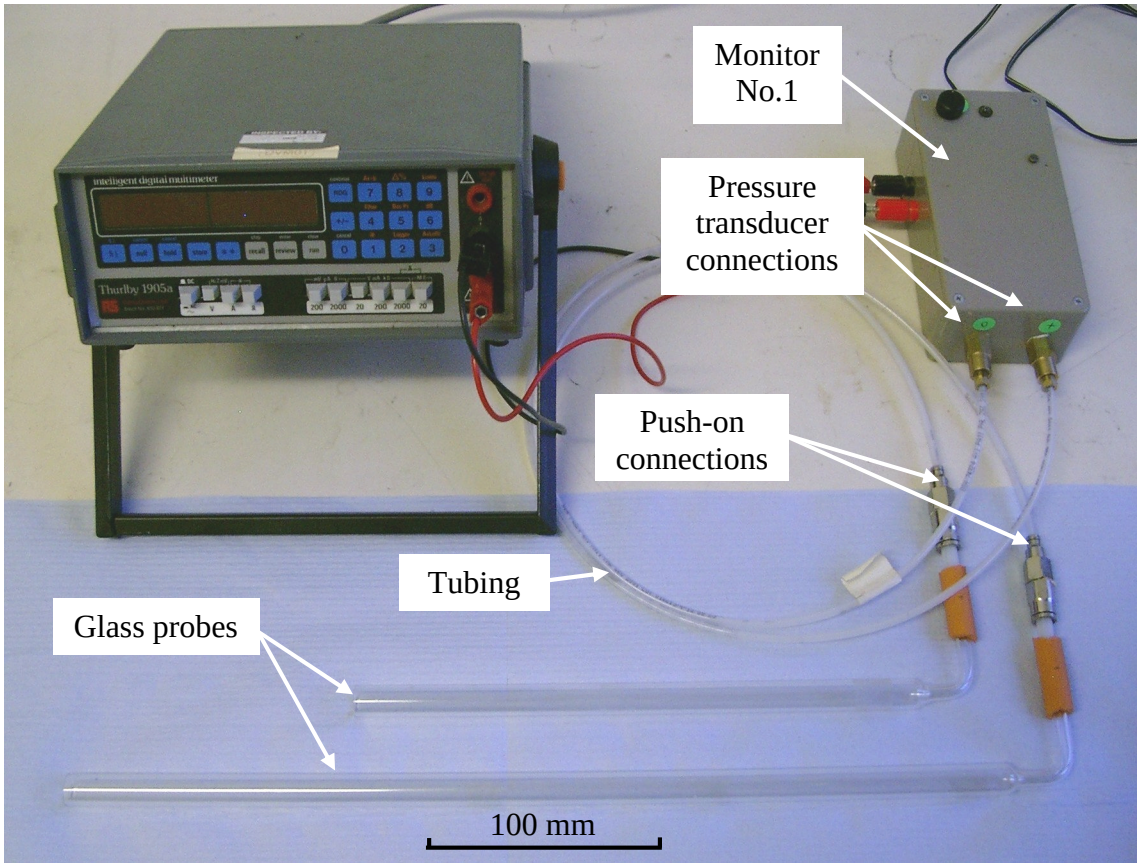

Figure 5.10. *Photograph showing the glass probes of ID 11.25 mm, tubing, push-on connections and Monitor 1 containing the pressure transducer*

Shown in Figure 5.10 are two glass probes (ID 11.25 mm). When using a single probe only the longer one of the two probes was immersed in the liquid, the other probe measuring the ambient air pressure. Through using this probe and 0.8 metres of nylon tubing this system was within 95% of the theoretical probe base pressure.

5.4.1 Comparison between single and double probes

The results in figure 5.11 show that as the probe depth increased the difference in the probe air pressure between the water and the two oil samples became larger, reflecting the density difference of the new motor (870 kg m^{-3}) and DERV (820 kg m^{-3}) to that of

the water. As was expected, the deeper the probe the greater the difference in pressure for these liquids.

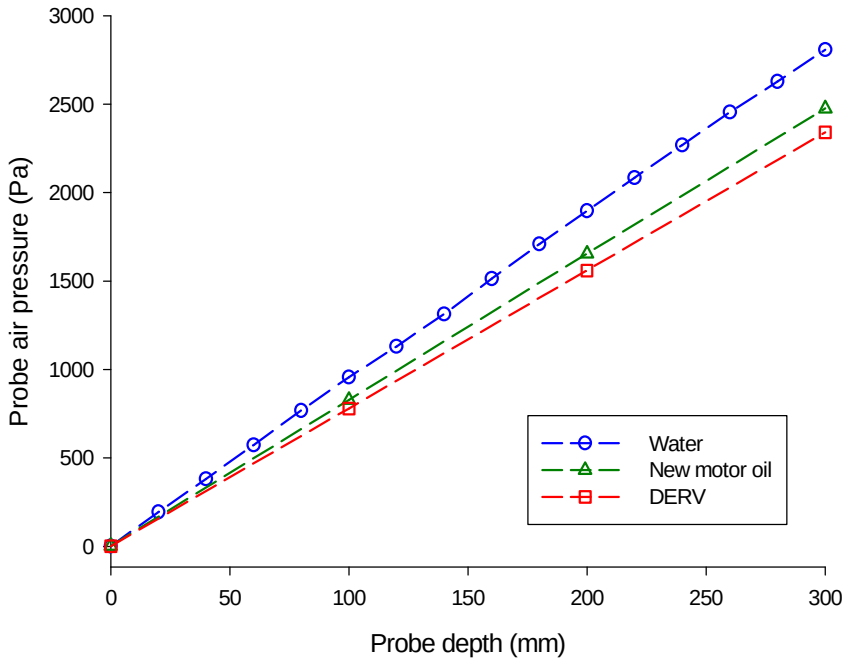

Figure 5.11. *Probe air pressure measurements for a single probe as it is lowered into water, new motor oil and DERV to a depth of 300 mm.*

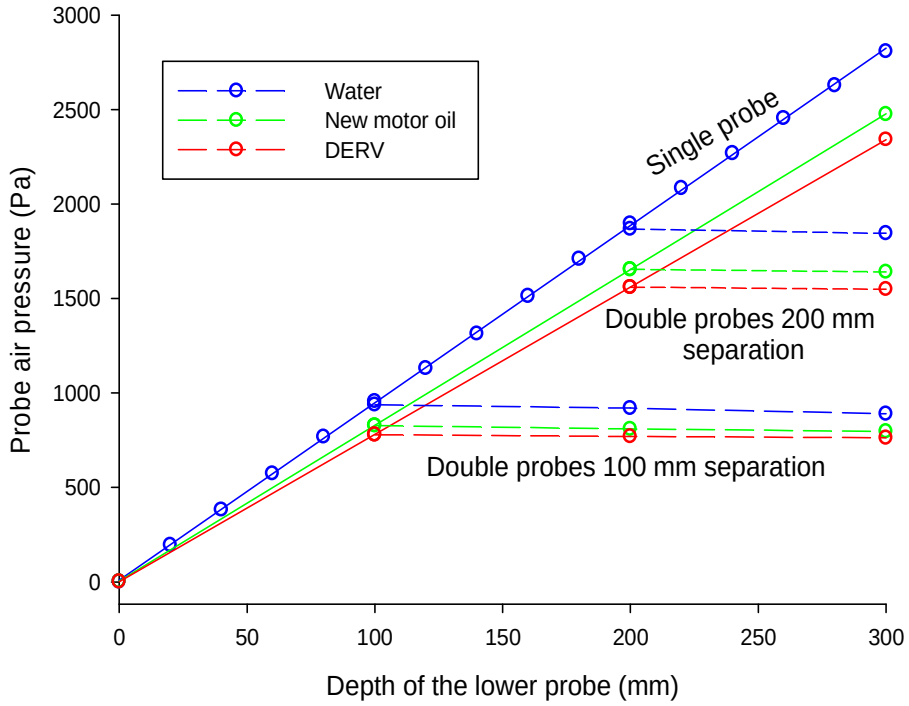

Figure 5.12. *To this graph has been added the pressure differential measurements for the double probes with a vertical separation of 100 mm and 200 mm.*

Following on from experiments using the single probe, both of the two ID 11.25 mm glass probes were attached together forming a double probe. Two double probes were formed, the first with a 100 mm vertical separation and then adjusted to give a 200 mm separation. These double probes were lowered into the different liquids and the pressure differential was measured, the results are shown in figure 5.12. For both of the double probes experiments (100 mm and 200 mm separation) the pressure difference did not become steady until the upper probe also entered the liquid.

As the double probes were further immersed, the pressure differential was not constant but gradually decreased. As previously discussed in section in 5.3.2, the deeper the probes were immersed, the greater the difference between the probe base pressure and the probe air pressure. This resulted in the differential pressure between the water and the new motor oil being compromised to less than 4%. Nevertheless, this effect although detectable was not significant at the depths encountered within these experiments.

Two main points can be noted from the graph in figure 5.12; firstly that the depth of the single probe has a significant bearing upon the pressure reading, for example, a change or inaccurate placement of the probe by 10 mm effects the pressure by 98 to 80 Pa (5% at 200 mm depth) for water and DERV respectively, whereas a difference of 10 mm of the double probes effects the pressure differential by < 3 Pa (< 0.2%). The second prominent aspect is that the larger the separation between the two probes the greater the differential pressure between the water and the oil. The double probes with a 200 mm separation showed, as expected, a pressure differential of ~ 13% between water and the new motor oil (as modelled in section 5.2), whereas the pressure differential for the double probes with 100 mm separation was half this figure.

5.4.2 Using the laboratory interceptor

The laboratory experiments that assessed the pressure sensor for both the single probe and the double probes used a glass oil interceptor as shown in figure 5.13. Illustrated is the double stainless steel probe ID 20.2 mm with a 180 mm separation between the upper and lower probe. The interceptor shown in this picture is empty, the water and oil was poured from above as indicated, with the excess flowing out through the inverted siphon into the excess water collection beaker.

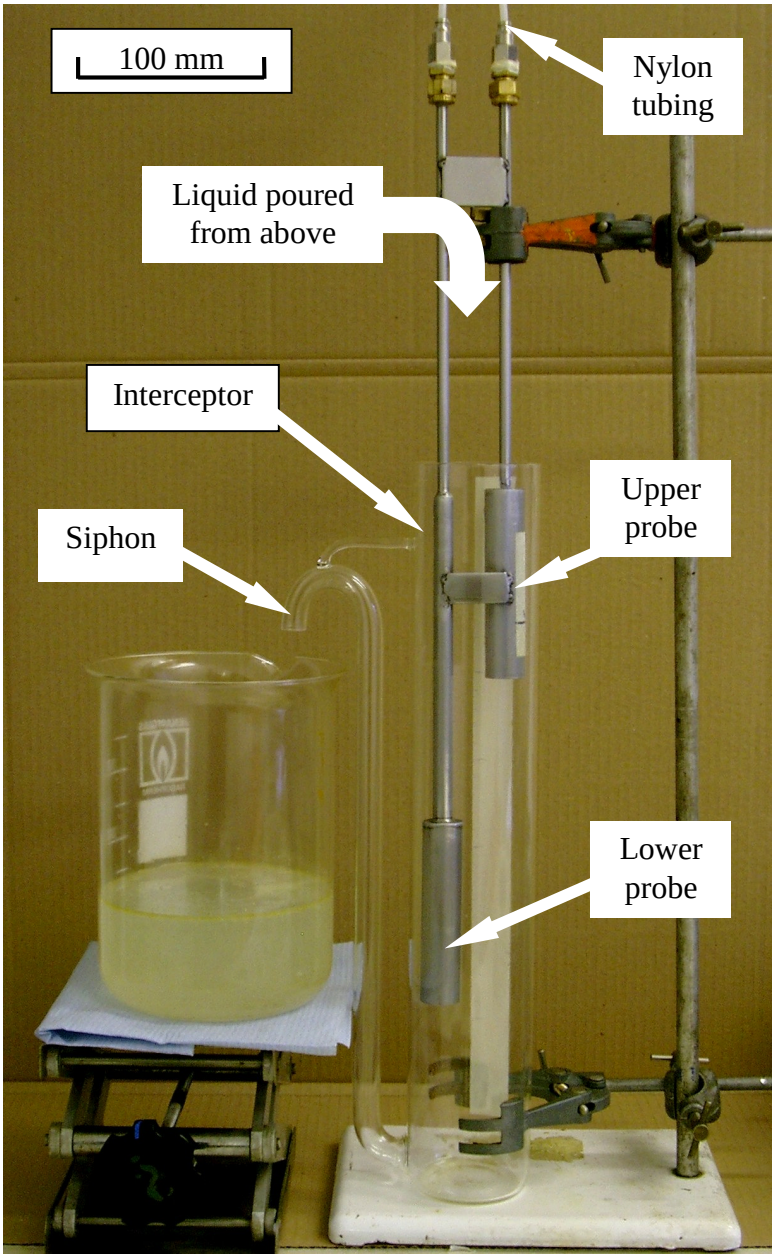

Figure 5.13. *Experimental set up for assessment of the pressure sensor using the laboratory oil interceptor. System shows double metal probes with ID 20.2 mm.*

The experiments in the previous section examined the effect of different densities upon the probe air pressure with the probes at various depths. Here, with the probes positioned at a constant position within an interceptor, any addition of oil has the effect of raising the liquid/air interface and this will as a consequence change the probe depth with respect to the liquid surface. It was the change in probe air pressure due to this depth/density change that was studied here.

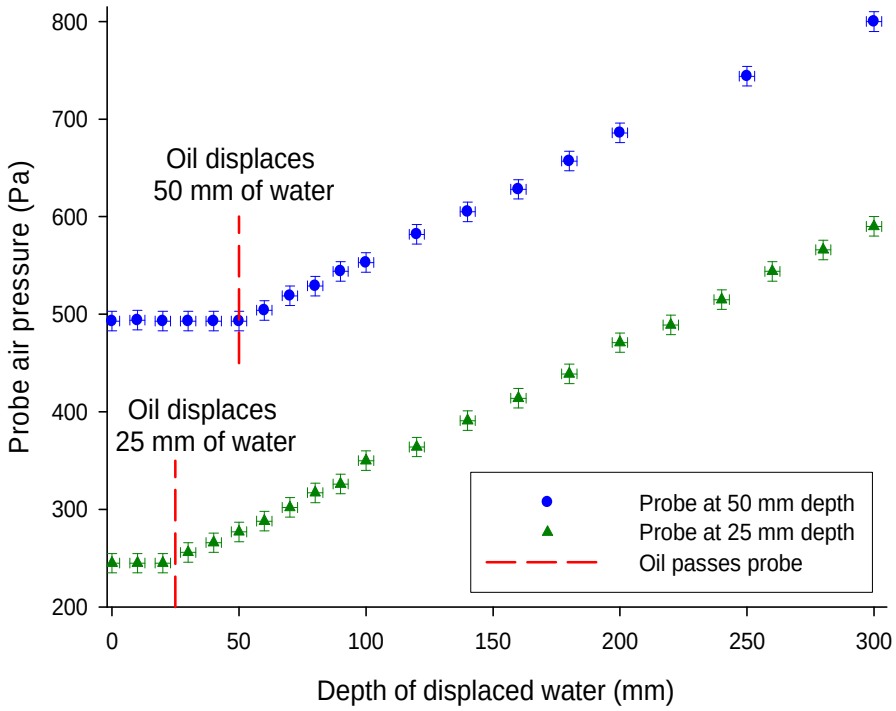

Figure 5.14. *Pressure change upon a single probe at two different positions when new motor oil is added into the interceptor, displacing water.*

A single stainless steel probe ID 20.2 mm connected to 1.5 metres of nylon tubing which produced an internal volume of 33.6 cm^3, was positioned at 25 mm and later at 50 mm below the water surface. New motor oil was poured in discrete quantities into the interceptor displacing the water. The probe air pressure (via the output voltage) was noted between each new addition of oil. Sufficient oil was poured into the interceptor until a 300 mm depth of water was replaced. The results for these experiments can be seen in figure 5.14. As previously discussed in section 5.2, the recorded pressure at any point does not change until the oil/water interface passes the measurement position and this can be noticed for both of the probe positions. The vertical error bars represent the uncertainty of the measurement for the location of the probe's vertical location and the horizontal error bars represent the uncertainty of the measurement of the oil/water depth within the interceptor. A difference of 1 mm in height can affect the pressure by up to 10 Pa.

After the oil/water interface passed the probe, the probe air pressure was seen to increase for both experiments. This increase in pressure of ~ 220 Pa for the 25 mm deep probe and ~ 190 Pa for the 50 mm deep probe from an initial pressure of 242 Pa and 484 Pa respectively, correlates to the theoretical pressure increase of 223 Pa and 192 Pa

respectively. The shallower the probe is positioned, the earlier the probe pressure increases and the greater the pressure change, resulting in a more sensitive system.

By having both probes in the liquid, the effect of variations in the interceptor liquid level or any temperature change, would affect equally each of the probes and tubing entering both ports of the pressure transducer. The following experiments used the double stainless steel probes ID 20.2 mm with 180 mm separation.

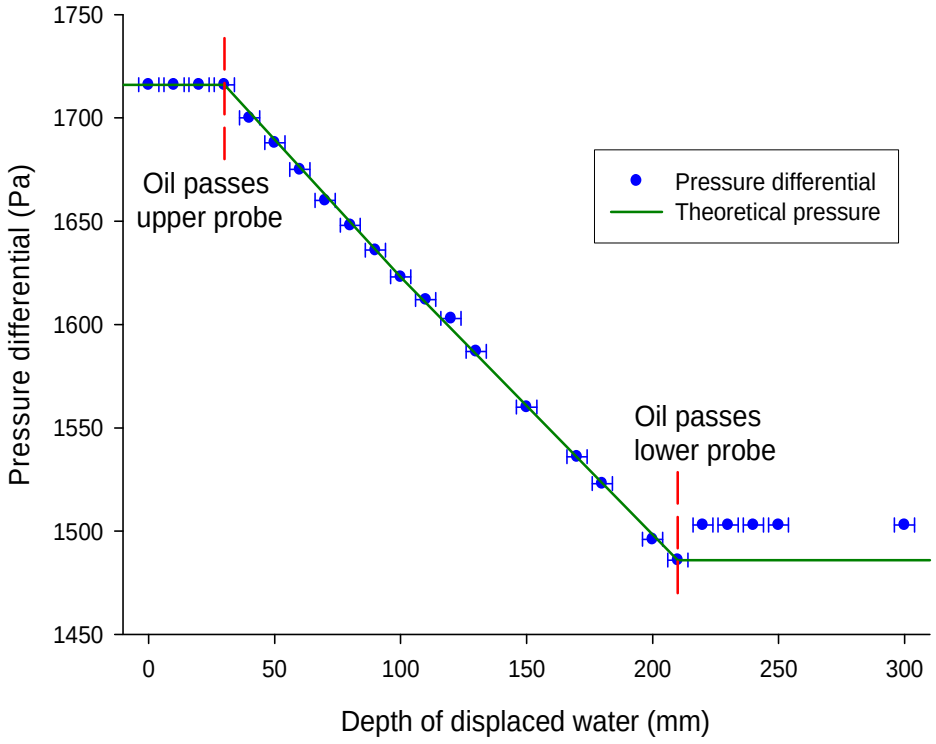

Figure 5.15. *Pressure change for a double probe positioned at 300 and 210 mm, as new motor oil is added into the interceptor.*

The mean results for several experiments are shown in figure 5.15, with the points where the oil passed the positions of the probes indicated. The error bars indicate the uncertainty of reading the oil depth. The results generally follow that which has previously been modelled, however as the oil passed the lower probe a rapid change in the pressure differential was observed. This small increase in the lower probe air pressure was caused when the oil/water interface passed the base of the lower probe. Up to that point, the space created through the compression of the air had been filled by the ingress of the surrounding water but as the oil passed the orifice of the probe the denser water was replaced by the oil and a larger volume of the less dense material was required to balance the probe base pressure to that within the probe. As a result, the

volume of oil was ~ 1% greater than the water previously occupying the space, compressing the air within the probe and so increasing the air pressure.

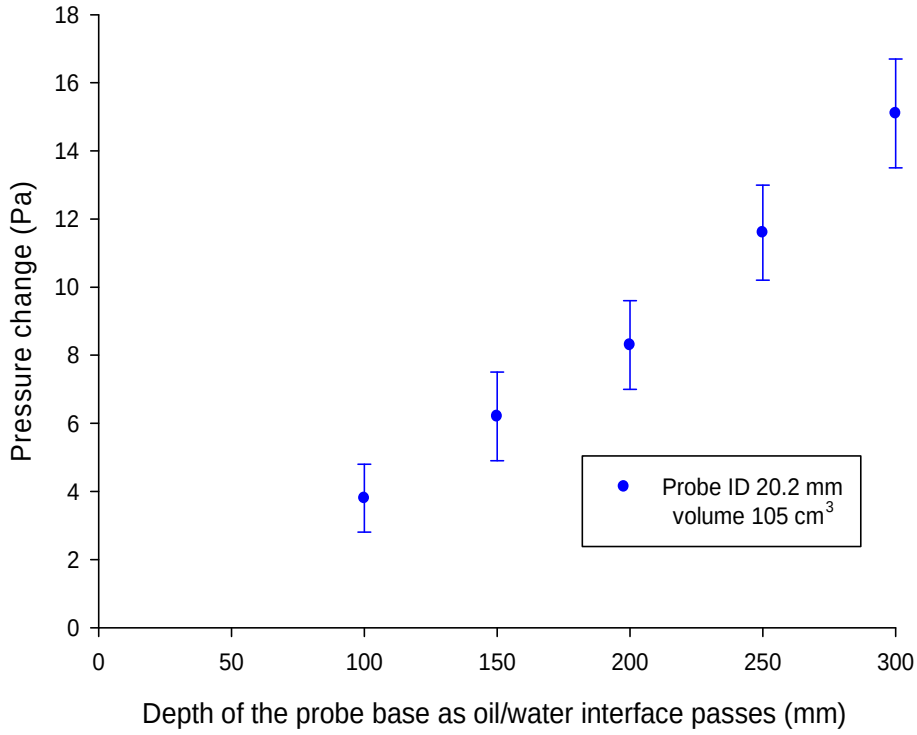

Figure 5.16. *Pressure change for a probe at different depths as oil enters into the probe and displaces the water.*

On further investigation, the magnitude of this increase in pressure was directly related to the depth of the water within the probe at the time the water was replaced by the oil. The depth of water within the probe being a function brought about by the depth of the probe, its ID and probe/tubing volume. Figure 5.16 shows the pressure change for various depths as the oil passed the probe. The single probe used in these experiments had an ID 20.2 mm a probe/tubing volume of 105 cm^3. The pressure change below 100 mm was inconsistent and has not been added to the graph and the error bars show the range of results between experiments.

This change in pressure had not been noticed in earlier experiments when using the glass probes, possibly due to the fact that either the water inside the smaller diameter probes had been trapped as the oil passed the end of the probe or that the water had been gradually replaced by the oil and as such any change in pressure was only gradual and went unnoticed. This pressure change was not significant in comparison to the

differential pressure change as a whole, representing less than 5% of the total water to oil change.

5.4.3 Continuous data acquisition

In the previous experiments, to aid manual recording of the results, the oil had been added to the interceptor in discrete quantities. To simulate a constant flow of oil, the oil was continuously poured into the interceptor and the pressure was monitored using the Labjack data logger. Recording the data at 0.5 second intervals, ~ 1.2 litres of oil was added over a period of approximately two minutes, replacing a depth of 300 mm of water.

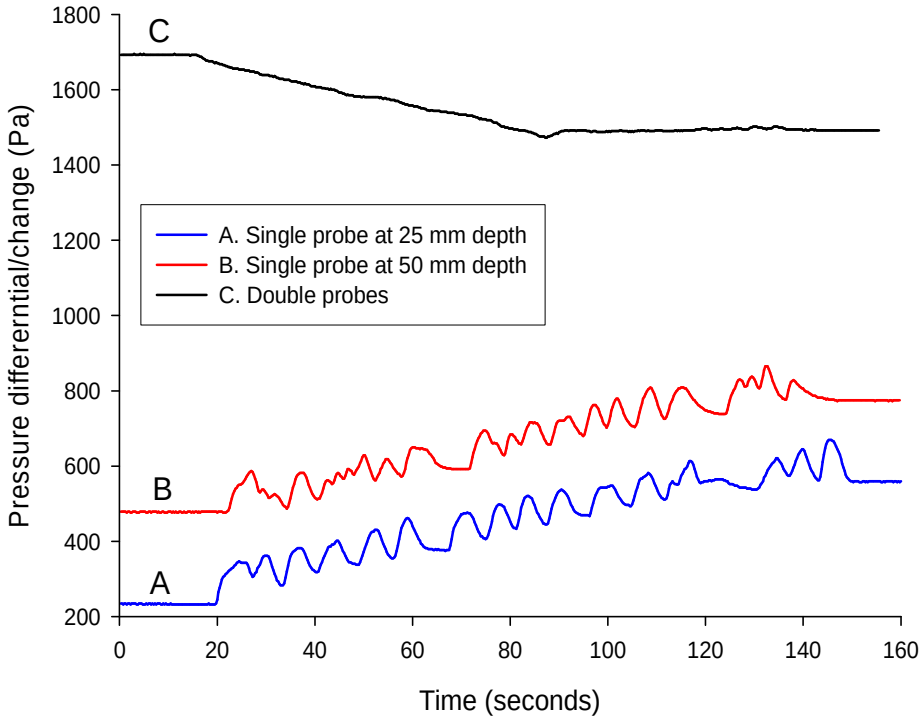

Figure 5.17. *Pressure changes using a data logger as oil is poured into the interceptor. These results are for a single probe at two depths (A and B) and a double probe (C).*

Figure 5.17 shows the results from three experiments; two from single probe and one from the double probe. As would be expected, the change in the differential pressure for the single probe is an increase, whereas for the double probe this is a decrease. The marked difference between the previous experiments and these, where the oil was poured in a continuous but not in an even manner, was that the pressure recorded from the single probe was irregular. This reflected both the uneven way the oil was poured and, more importantly, that there was an inconsistency between the speed of the outflow

of the water and the inflow of the oil. Such events were not significant when the oil had been poured discretely.

Considering the data for the single probe, the nonconformity between the inflow and the outflow created false information about the oil depth. Through the delay in the out flowing water the height of the liquid within the interceptor increased the probe air pressure. The effect of placing the single probe at different heights did not eliminate this effect.

Monitoring the double probe during similar events showed a contrast to that of the single probe. The upper and lower probes were placed at a depth of 30 mm and 210 mm respectively. Here, throughout the time that the oil was poured, a regular change occurred. Although the total liquid levels within the interceptor varied to the same extent as with the single probe, this was countered by the fact that any irregularity was experienced by both the upper probe and the lower probe. Once the oil had replaced 210 mm of oil, the pressure from the double probe remained virtually unchanged, whereas the single probe continued to show an increase in pressure as more oil was added. The overall effect upon the pressure change for both the single and the double system, once a similar quantity of water has been displaced, was the same for when the oil had been added discretely.

These results draw attention to the possibility that events such as high rates of inflowing water could occur where the outflow was unable to keep pace, possibly occurring during periods of high rainfall or where an inadequate drainage system exists. This capacity of the double probe system to manage this showed a robust ability to cope with these temporary variations, compared to the fluctuations shown by the single probe. The use of the single probe was not pursued and the research continued with the double probe system.

5.4.4 Reduction of air loss and further improvements

Prior to long term testing at Andel Ltd, an assessment was needed of the pressure loss from the tubing and couplings. For this, the double stainless steel probes (ID 20.2 mm) were connected to 30 metres of ID 2.5 mm tubing and the probes positioned at 30 mm and 210 mm in water within the interceptor. Experiments were carried out, each for up to seven days, and the output voltage was read each day at approximately the same time.

The temperature within the laboratory was constant at the time of the readings (in later experiments at Andel Ltd. the variations in the daily temperature had a marked effect upon the logged output voltage). The voltmeter and the pressure transducer were switched off, only being turned on 30 minutes before a reading was taken allowing the monitor and voltmeter to stabilise.

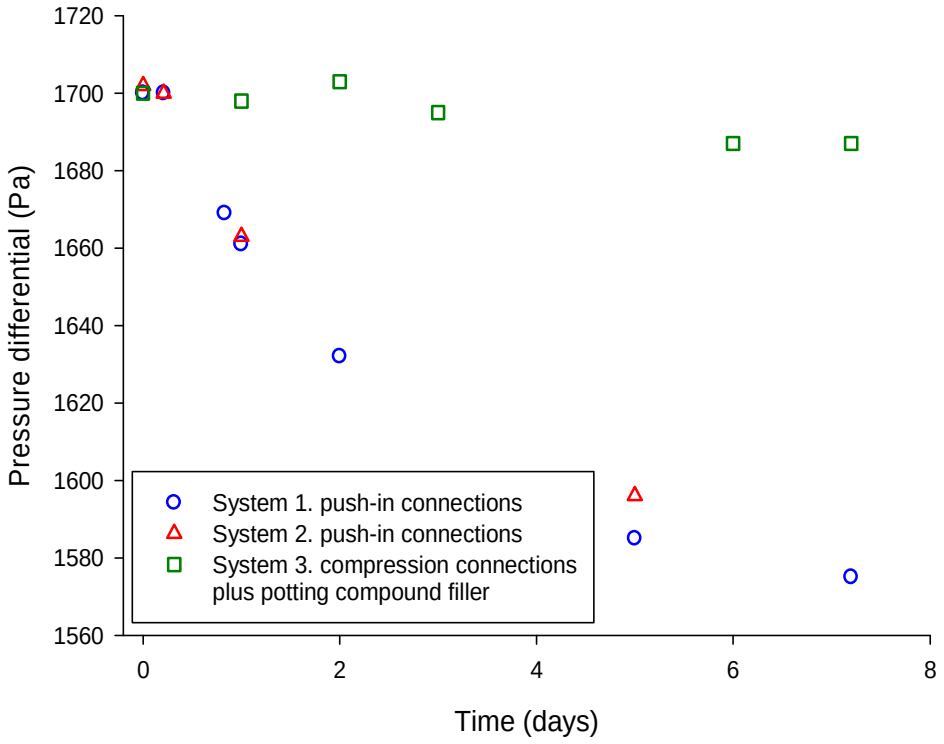

Figure 5.18. *Change in pressure through air leakage from different probe/tubing systems throughout a period of several days.*

Results of the pressure change as a function of time using three connection schemes are shown in figure 5.18. The tubing systems 1 and 2 represent pressure change from the original set-up. In both these systems pressure losses of over 200 Pa were noted, representing a gas loss of ~ 3.5 cm^3. A theoretical loss by gas permeability through the nylon tubing from the lower probe over a month would only be about 1.5 cm^3, indicating that losses were occurring from other sources. The nylon tubing had push-in connections and the outlets from the pressure transducer used tubing which, although fitted tightly over the outlet ports, may have been sufficient to reduce air loss over a short period of time but not efficient enough for tests lasting several days.

System 3 represents an attempt to reduce pressure losses. The push-in connections were replaced with compression joints and the cavity within the monitor that houses the

pressure transducer and connection tubing was filled with a polyurethane potting compound. The permeability properties of polyurethane were shown in table 5.1 and with the thickness of the potting compound this would reduce any gas loss from around the transducer. The pressure loss through a seven day period was considerably reduced, changing by less than 25 Pa, representing a gas loss of ~ 0.8 cm^3. The calculated theoretical gas loss through permeability would be ~ .04 cm^3. However, variations in ambient temperatures were shown have created an effect, albeit small, on the laboratory results.

Through using larger diameter probes, any loss of gas would have a reduced effect upon the pressure fall. The resultant volume of inflowing liquid (replacing the lost gas) would be represented by a smaller rises inside the probe which would maintain the depth of air inside the probe, as discussed in section 5.3. This led to the use of the larger diameter probes in later trials with compression fittings.

5.4.5 Placing the probe into the interceptor

For all experiments there was an assumption that the probes have been positioned vertically in the water. The effect upon the probe air pressures if the probes had been placed at a small angle, or if when immersing the probes they were tilted, has not been considered. Here, the consequence of a misalignment by 5° and 10° is examined.

The effect of positioning the double probes which normally have a vertical separation of 200 mm but having a titled error of 5° and 10° away from the normal would reduce the vertical spacing to 199 and 197 mm respectively, dropping the potential pressure differential of ~1700 Pa by 10 and 30 Pa. The fall of 30 Pa would, as previously discussed, be above that desirable. As such, care in positioning the probe to near vertical is important.

When the probes are to be positioned in water, any tilting away from the vertical as they enter the water prior to being fixed will reduce the volume of air contained within the probe. Any air which escapes at this point in time will effectively reduce the air volume of the probe. This has a greater effect as the probe diameter increases. In practice it tended to be the lower probe which suffered the most as the probes were being positioned, thus reducing the pressure differential. To tilt a probe by 10° would reduce the volume of an ID 20.2 mm and 74.0 mm probe by 1.1 cm^3 and 55 3 cm^3 respectively

and the effect upon the pressure loss of the larger diameter probe would be more acute creating a probe air pressure reduction of ~ 13 Pa.

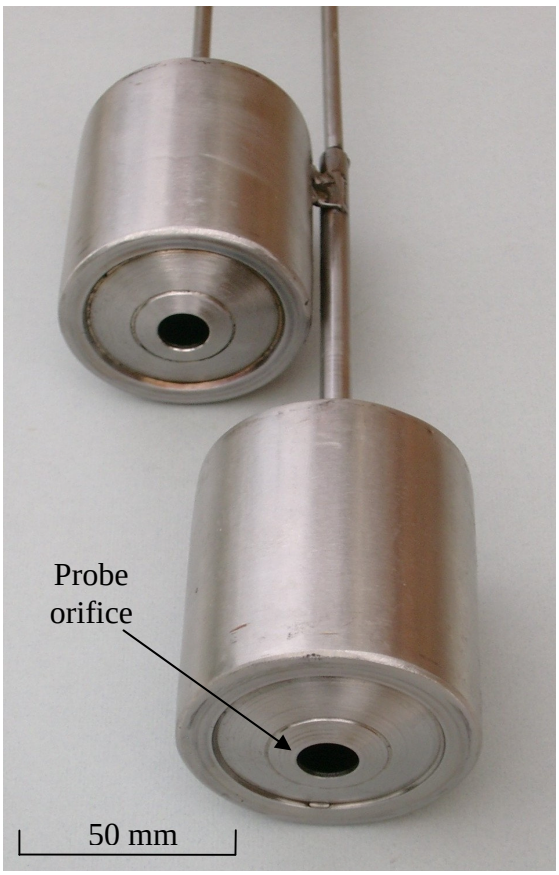

Figure 5.19. *Photograph of the large double probes showing the reduced orifice at the base of the probes.*

To reduce this problem of air loss through tilting, the ends of the larger double probes were partially enclosed. The ends of these probes were slightly tapered and a small orifice with a diameter of 15.0 mm was formed, as shown in figure 5.19. If this probe was tilted by 10°, an air loss would only produce a pressure fall of less than 1 Pa, thus producing a probe that would have a greater tolerance to non perfect conditions.

5.5 Trials at Andel Ltd.

The pressure transducer monitor trials at Andel Ltd were an expansion of the experiments that had been carried out in the laboratory. Here, the larger interceptor which had been made by converting a plastic bin through the addition of an inverted siphon, was used. This interceptor had the capacity to hold just over 100 litres of water before the excess was siphoned off. Oil used in these experiments had previously been taken from an operational interceptor and had a density of 855 to 870 kg m^{-3}. Shown in figure 5.20 is the arrangement of the interceptor, monitor and computer. The probes were connected by two 30 metre lengths of nylon tubing.

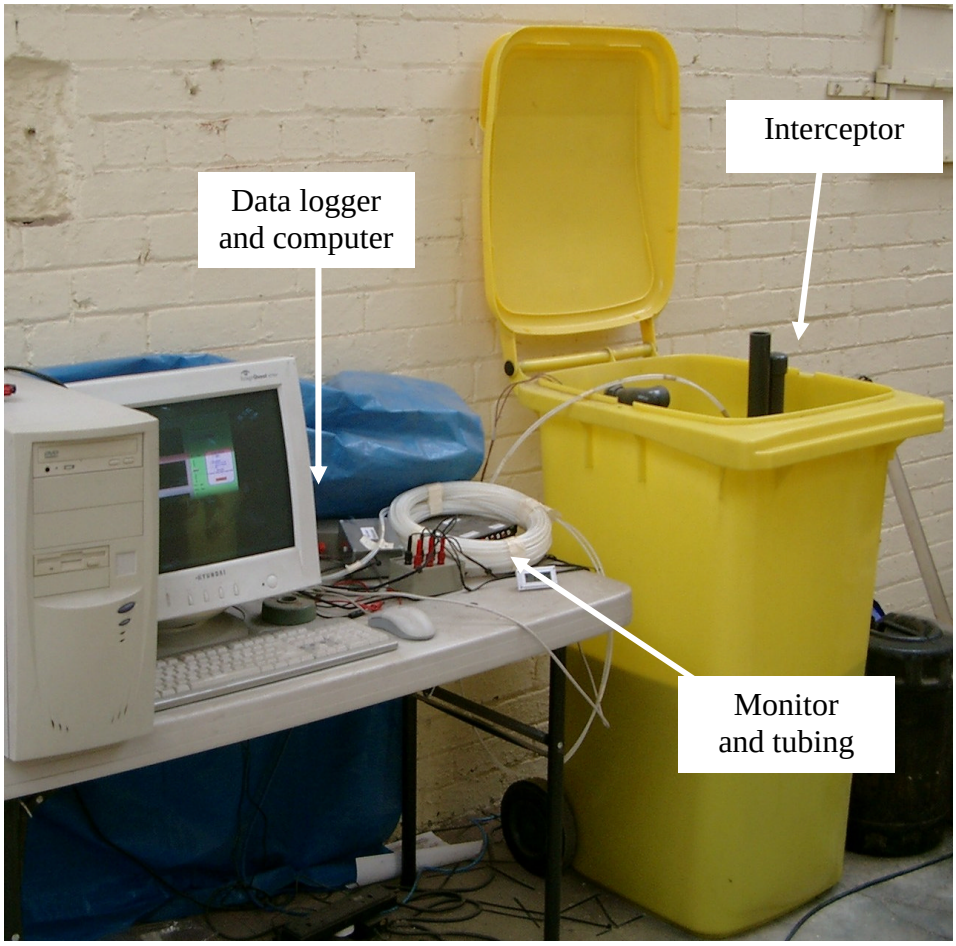

Figure 5.20. *Photograph of interceptor, monitor and data logger set-up at Andel Ltd.*

Within the interceptor the double probe was attached to a vertical support and from here the depth of the probes could be adjusted depending upon the particular experiment. In later experiments the temperatures of the liquid and the air were recorded; these sensors can be seen in figure 5.21

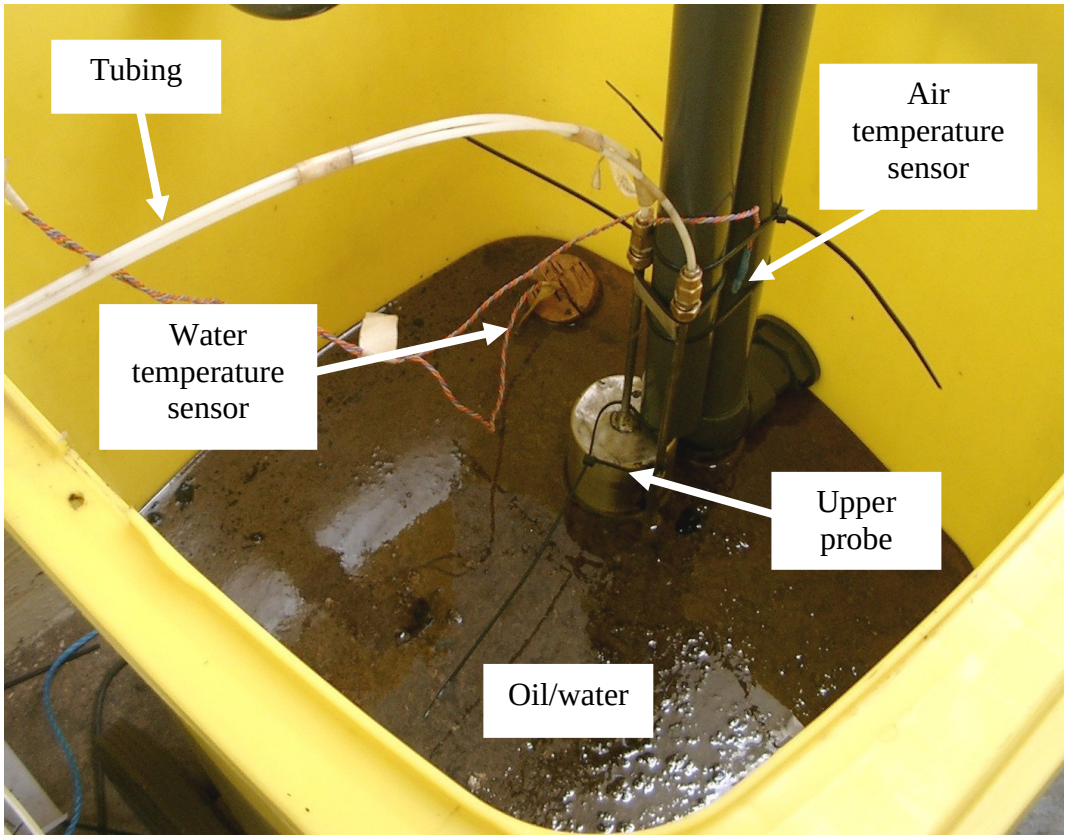

Figure 5.21. *Photograph inside the interceptor showing the upper probe and temperature gauges.*

As previously discussed it was not possible to visually determining the depth of oil floating upon water and the liquid in the interceptor shown in figure 5.21 although appearing to be oil, only contained an oil film of less than one millimetre in depth.

5.5.1 Assessment of monitor in water

The initial experiment was to evaluate Monitor 1 (which used the non temperature compensated pressure transducer) and the large double probes. The probes were placed in water only for a period of 31 days to assess any pressure change over that time. The upper and lower probes were at 30 mm and 210 mm below the surface respectively. The PICO data logger was connected to the computer as shown in figure 5.20 which logged the voltage at 30 minute intervals. The computer, data logger and monitor were left switched on for the entire period and this set-up was then left unattended for the duration of the experiment.

The results in figure 5.22 showed marked changes in the pressure throughout the 31 day period that had not been seen in any of the laboratory experiments. The PICO data logger resolution was 25 millivolts, equal to ~ 15 Pa, but sufficient to show the larger

changes. Through using the large probes in water, the differential pressure was expected to have a continuous pressure of ~ 1740 Pa. Two trends can be seen on the graph; the first is one that has a daily cycle and the second is a more gradual increase and decrease that occurs over several days. This produced a pressure range of 150 Pa through the period of 31 days. The daily cycles show a change of about 40 Pa per day and this occurred invariably every day. Unlike the laboratory, which was situated out of direct sunlight, the trials at Andel Ltd. were in a warehouse that had natural lighting from the sun, resulting in warm daytime temperatures and the possibility for cooler temperatures during the night, which may have been influential on this daily cycle. The gradual pressure change that occurred over several days, shown by the calculated 24 hour mean in figure 5.22, may also have been influenced through longer term temperature changes. Despite the pressure variation throughout the 31 days, the pressure differential remained within a 150 Pa range, not entering into the critical pressure that would indicate the presence of oil.

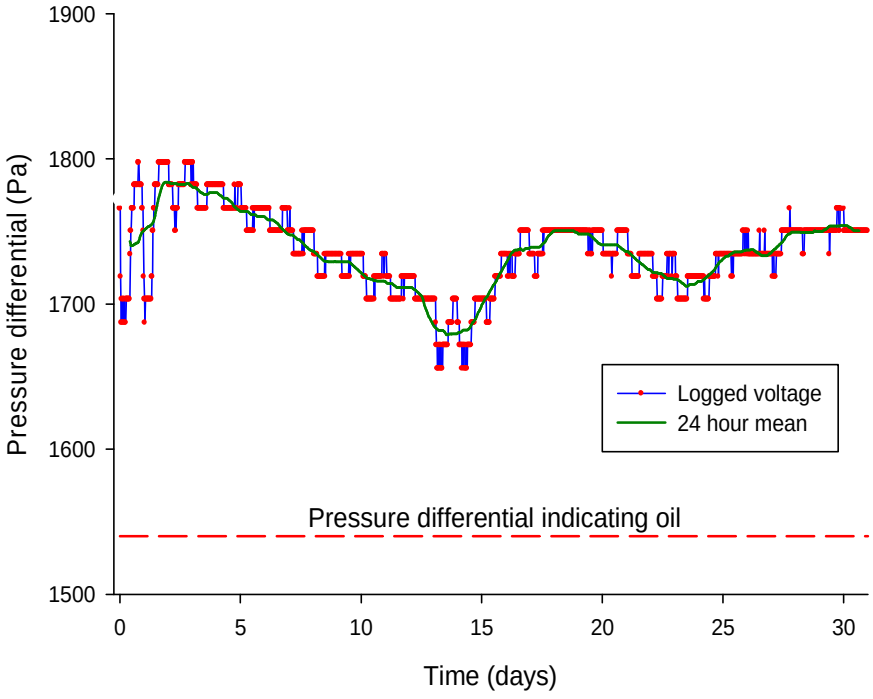

Figure 5.22. *Graph showing differential pressure change for Monitor 1 for the large probes in water over 31 days.*

5.5.2 Monitoring temperature change

The influence of the change in temperature would influence the tubing from each probe evenly but as the air temperature changes at a faster rate than the water temperature, the upper probe situated predominantly in the air may have been influenced by temperature changes greater than the lower probe, located entirely within the water. Any differential in the probe internal air temperatures would cause the probe's air volumes to change disproportionally. An increase or decrease in volume would modify the level of ingression water, thus affecting the depth of air inside the probe, changing the pressure of the probe and the differential pressure. A raise of 10°C of the air temperature within an ID 74 mm probe with a capacity of 420 cm^3 will expand the volume by ~ 15 cm^3 increasing the pressure by 33 Pa. It was possible that the air within the upper probe may not have increased to the ambient air temperature as the effect of being partially immersed in the liquid could have influenced the probe and the air contained within.

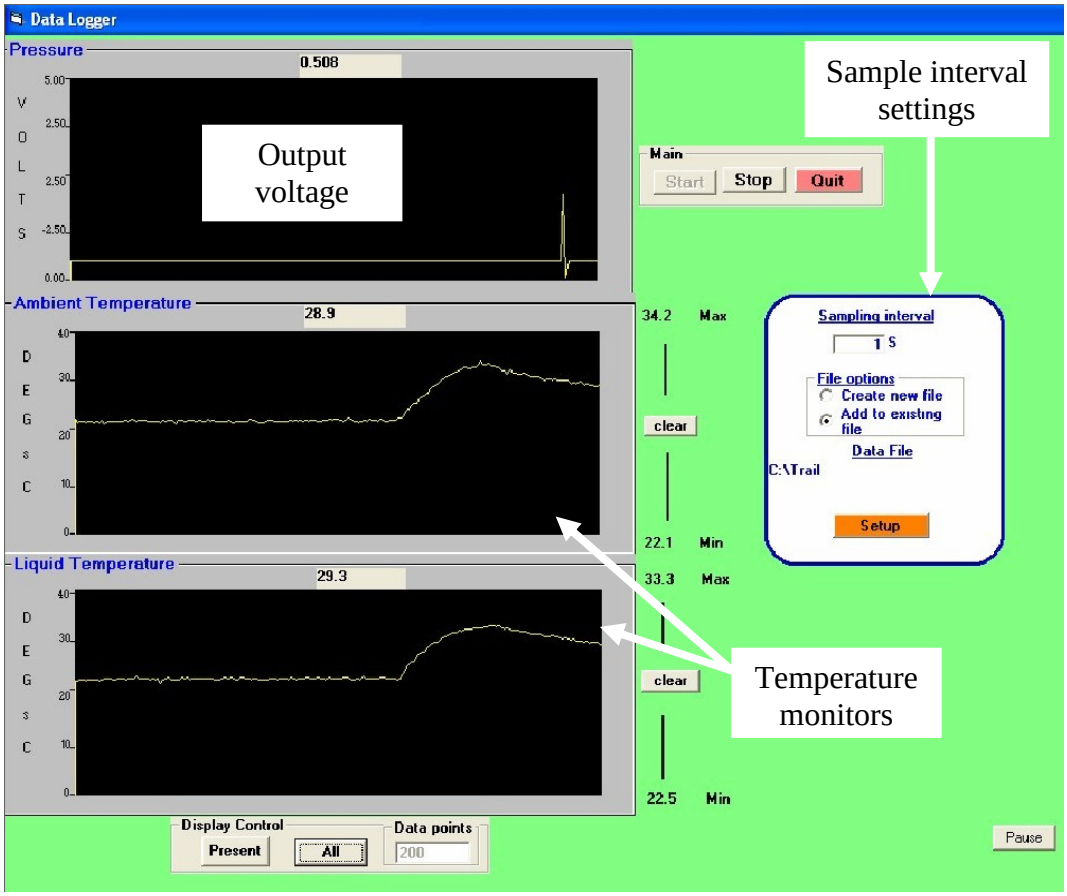

Figure 5.23. *Computer interface and controls for the Adlink data logger, showing the pressure differential voltage and the two temperatures.*

To investigate the effect of the temperature changes, a temperature sensor was placed in the water and another in the air in the vicinity above the probes, as shown in figure 5.21. The Adlink Technologies data logger was used to record the output voltage from the pressure monitor and the two temperature sensors, logging at five minute intervals. In addition the data could be viewed directly on the computer as shown in figure 5.23.

This data logger had a resolution of one millivolt, equivalent to ~ 0.5 Pa and 0.5ºC for the temperatures. Monitor 1 was set-up again with the double probes at 30 mm and 210 mm in water and was left to run for 20 days. The results are shown in figure 5.24 and, as was previously observed, the pressure had a 24 hour cycle of ~ 25 Pa and also the longer term variation. The air temperatures which were monitored, had a daily range of up to 7ºC and varied in its peak day temperature from 8º to 17ºC, which would be normal as this experiment was run through March to April. As the mean air temperature increased so did the water temperature, which had a variation of less than 1.5ºC per day and a mean variation of ~ 7ºC over the recorded period.

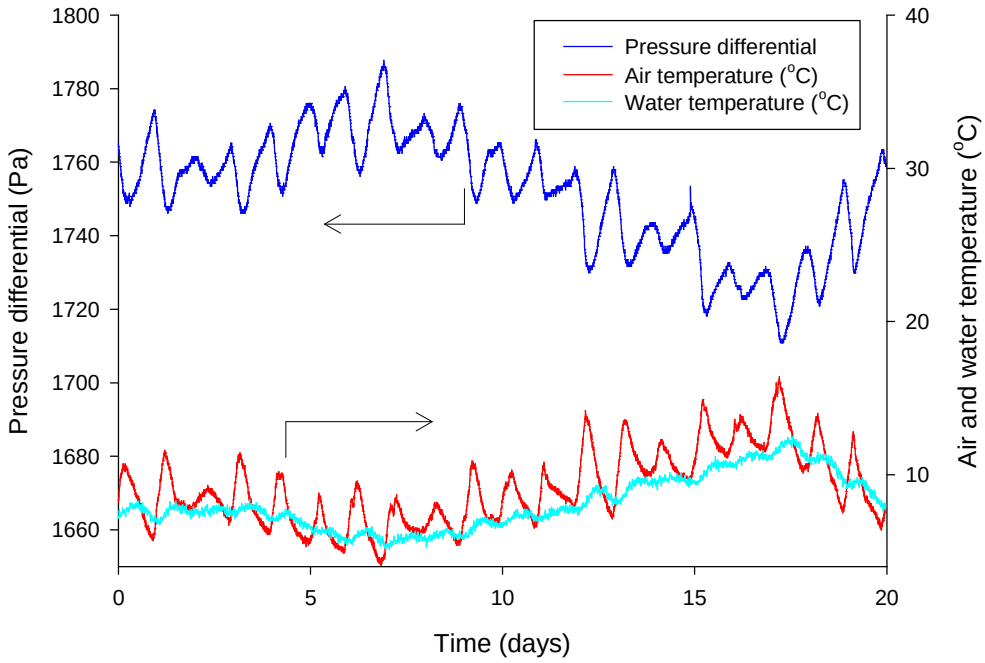

Figure 5.24. *Pressure differential for Monitor 1 where the upper probe is partially immersed. Experiment run in April/May*

Examining the daily pressure cycle, the pressure differential decreased as the air temperature increased, by the degree that may be expected if the upper and lower probes experienced a change in temperature differential. The longer term trend in pressure shows that the pressure increased as the air/water temperatures fall and vice versa,

suggesting that the pressure fluctuations may be influenced not so much by the temperature within the probes but the effect of the temperature upon the electrical components.

To examine whether the variation of the temperature differential of the probes was effecting daily pressure variations, both the probes were fully immersed into the water and the pressure was monitored through a 13 day period. The results are shown in Figure 5.25, this experiment was run in May immediately following the previous one. The daily air temperatures again varied by ~ 7ºC and the water temperature by ~ 1.5ºC, with the daily mean temperatures staying constant over the period of the experiment. The differential pressure also demonstrated a daily cycle, decreasing as the air temperature peaked. From these findings, there is the possibility that the monitor is being affected by the temperature changes and that this non temperature compensated pressure transducer is partially responsible for these cyclic apparent pressure variations.

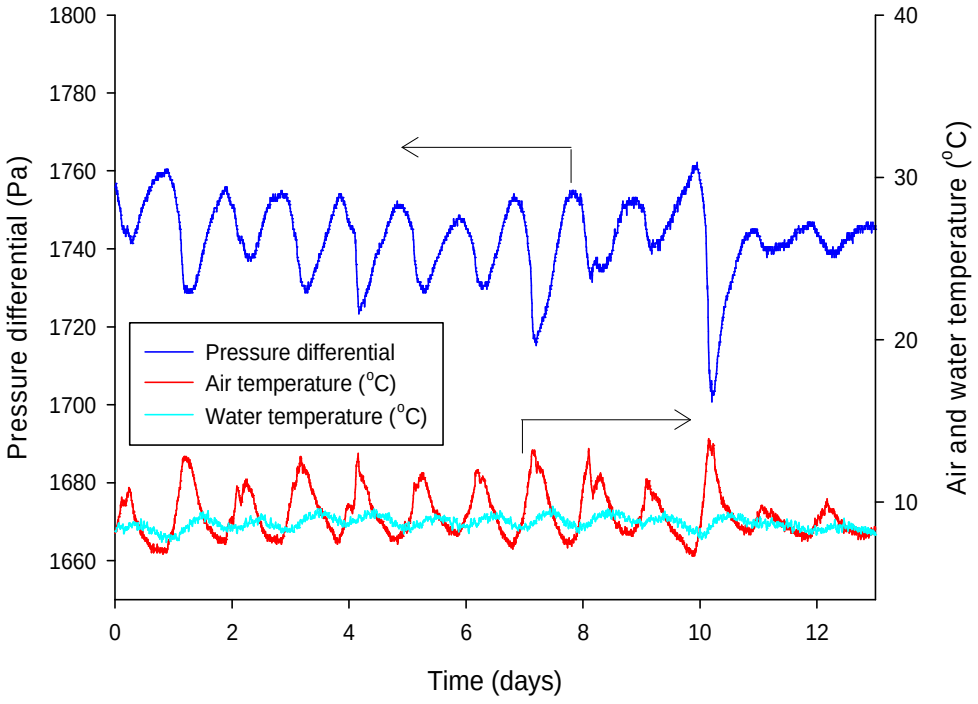

Figure 5.25. *Pressure differential for Monitor 1 where both probes are fully immersed. Experiment run in May*

The previous experiments were repeated using Monitor 2, which incorporated the temperature compensated pressure transducer. This monitor was calibrated using the same method as for Monitor 1. Monitor 2 had a zero pressure differential offset of 0.510

volts and a reading of 0.508 millivolts/Pa. Figure 5.26 shows the results when the upper probe was partially immersed. This 14 day experiment was run in May when the mean temperature was greater, this can be noted from both the air and water temperatures. Variations in daily air temperature reached 16ºC, varying from 12º to 28ºC, the water ranged again over no more than 1.5ºC through a 24 hour period. Despite these large variations in the daily temperatures, the pressure generally varied by less than 15 Pa each day apart from three occasions when large falls in the differential pressure occurred. These were associated with extreme peaks in the daytime temperatures, (when the temperature reached 27-28ºC, here the pressure fell to 1711 Pa). Despite these extremes in pressure spikes, the general variation and range of pressures was less than had been seen when using Monitor 1.

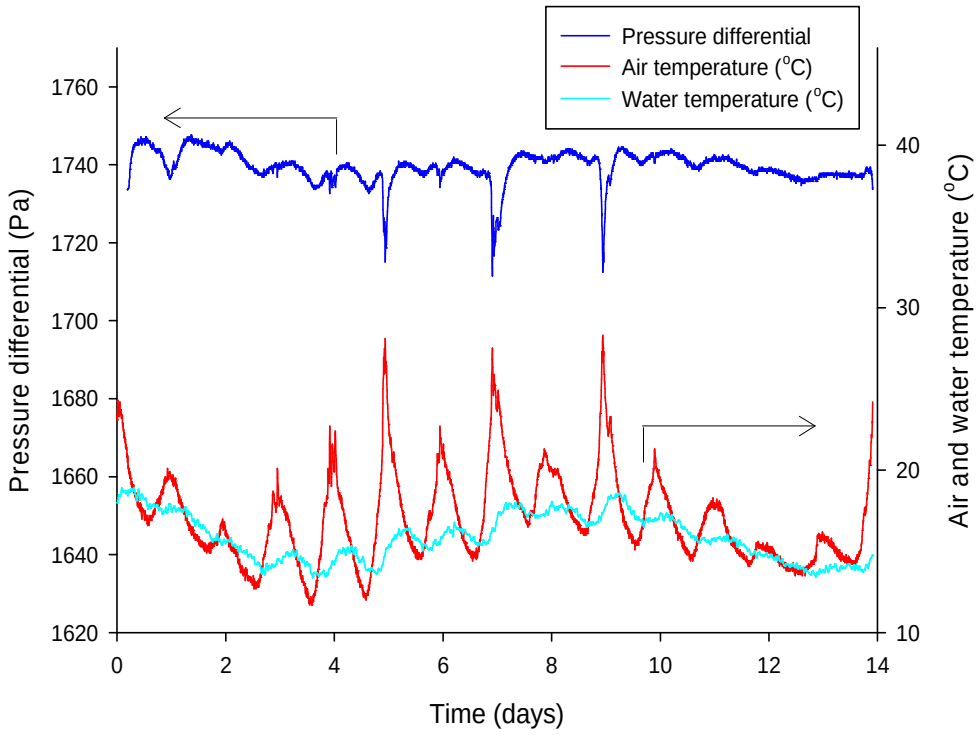

Figure 5.26. *Pressure differential for Monitor 2 where the upper probe is partially immersed (this being the normal position). This experiment was run in May and due to the high air temperatures the Y axes have been adjusted to avoid overlaps of the data differing from the previous two figures.*

Evaluating the two monitors; the temperature compensated pressure transducer produced less daily variation, despite the range of the daily temperatures being greater. Nevertheless, occasional spikes were seen from the voltage output from Monitor 2 regardless of the positioning of the double probes which suggests that the temperature compensated transducer or the electronic circuitry was still affected by large

temperature increases. The total range of the pressures noted from Monitor 2 never exceeded 40 Pa, whereas for Monitor 1 the pressure varied up to 70 Pa over the period of the experiments. An expected stable pressure would have been in the region of 1740 Pa, even so, the recorded differential pressure during these experiments for both monitors, whilst using the Adlink data logger, never fell below 1700 Pa.

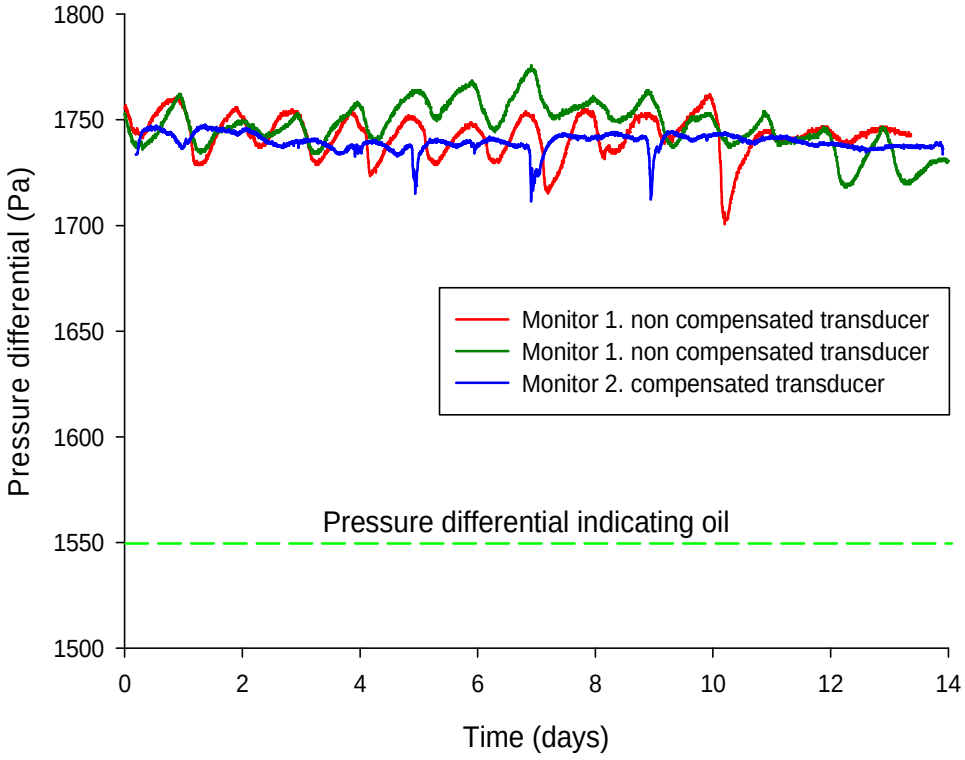

Figure 5.27. *Graph comparing the indicated pressure differential of the two monitors when the probes were in water. The critical pressure indicating oil is included for comparison.*

A comparison of the experimental results for both monitors is shown in figure 5.27, here the pressure differential axis has been enlarged to accommodate the critical pressure indicating the presence of oil. The graph illustrates that the variation of the pressure, although undesirable, was limited in overall impact upon the efficiency of the monitor. These results were obtained when the probes were in water, the critical pressure at ~ 1550 Pa that would have indicated the more dense oil, also shown on the graph, was not reached.

5.5.3 Assessment as oil is added to the interceptor

In the previous experiments at Andel Ltd, the double probes were placed only in water. To assess the capability of Monitor 2 to identify the presence of oil, 25 to 30 litres of oil was poured into the interceptor displacing the water, producing a depth of oil about 250 mm deep and passing the lower probe. The double probes again had been placed at a depth of 30 mm and 210 mm in the water. To simulate a cycle of emptying and refilling the interceptor, an amount of water was initially removed from the interceptor exposing both of the probes and leaving them in air. At this point the pressure differential between the two probes was zero. Water was then transferred into the interceptor until excess water discharged out through the inverted siphon. At this point the oil was added, pouring by hand until the required depth was reached. The output from the monitor was logged and the results for two experiments are shown in figure 5.28.

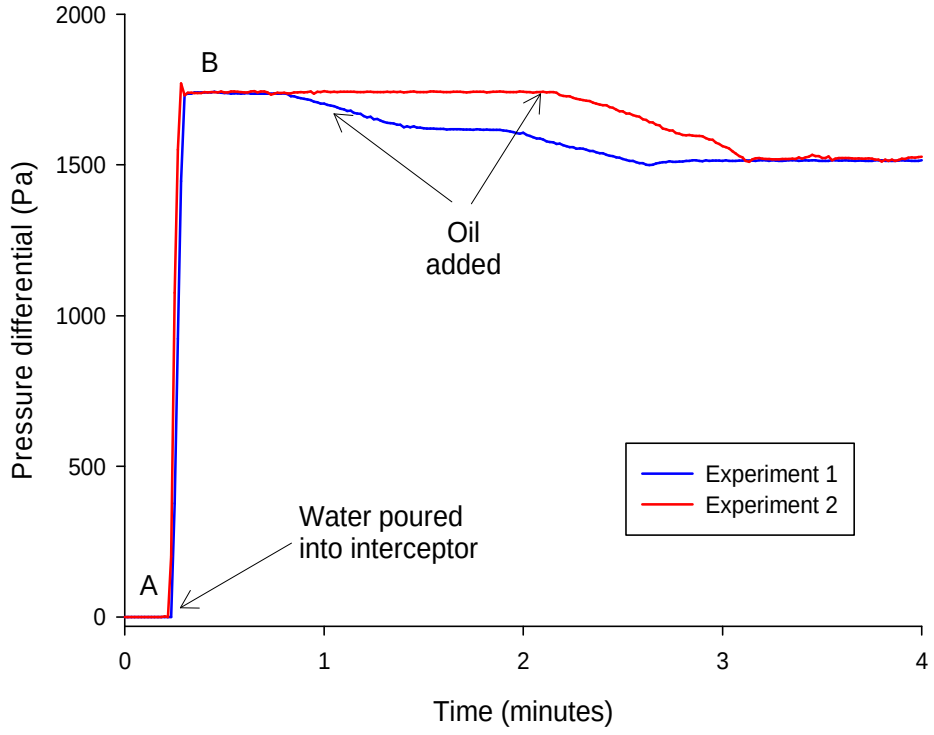

Figure 5.28. *Two experiments showing the change to the pressure differential during a cycle of water and oil being added to the interceptor.*

The results in figure 5.28 show a distinction between the three states of the interceptor cycle. As would be expected, when both of the probes are in ambient air there is no pressure differential. Once the water was added, the pressure differential rises to ~ 1740 Pa. As the oil is introduced, the pressure differential decreases, falling to below

1550 Pa. This differential between water and oil would have increased if less dense oil had been used.

For much of this research the voltage output from the pressure transducer was converted into pressure, by doing this the experimental results could be compared to each other and to the theoretical values. Through this process the air compression and gas leakage could be quantified and modifications to the system made through probe modification. However, the detection system required by Andel Ltd. only needed for there to be a measurable difference for the identification of a predetermined depth of oil within the interceptor. This measurable difference could equally be a voltage variation.

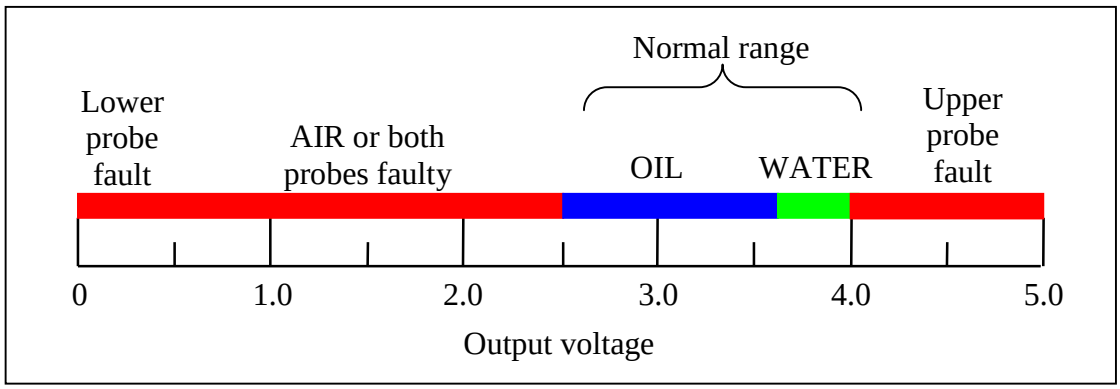

Figure 5.29. *The range of output voltages from Monitor 2 where the double probes are placed 180 mm apart. The different voltages indicate the normal range expected or is fault diagnostic.*

Due to the extensive use of tubing in this detection system, the possibility of damage occurring once the tubes have been installed would be minimal. Nevertheless, this system has the capability to indicate pressure loss in either of the probes. When one of the probes, through damage or parts failure, looses pressure, then the output voltage would fall outside the normal expected range. The initial offset of 0.510 volts for a zero pressure differential allows the failure in the lower probe air pressure (effectively a negative pressure) to show as low as zero volts. If pressure was lost from both probes this would produce the same response as the probes being in air. Pressure loss from the upper probe would result in a higher than normal pressure differential and the output voltage would indicate > 4.0 volts. In these circumstances attention would be required. Shown in figure 5.29 is the range of output voltages that could be expected from Monitor 2.

5.6 Conclusions

The system of oil detection through the use of the pressure tubing detector has been shown to create reliable and reproducible results. The development of the probe design, which led to the larger diameter probes, reproduced pressures that were close to the probe base pressure. Through experimental data backed up by modelling, the ratio of the probe/tubing volume along with the probe internal diameter to tubing length figures provided useful information was where guidelines for a functional system could be given. This created a detection system that could not only reliably represent the pressure at the measurement point but also allowed for the small gas losses which were expected to occur over a six month period.

The monitor, by using the differential pressure transducer, was able to determine the oil/water state of the interceptor with the extra capability to indicate any fault with the tubing through its pressure state. Experiments were run at Andel Ltd, further provided useful evidence that this system would functioned in more than laboratory conditions. The final design of the probes would depend upon the material and system of manufacture. It would be expected that a cage or filter system would be needed to protect the probes from blockage and damage.

6. Diaphragm fibre optic detector

The pressure diaphragm detector, in a similar way to the pressure tubing detector, measures the change in liquid depth as the water in the interceptor is replaced by oil. Unlike the pressure tubing detector which requires tubing to convey the pressure over a distance, the diaphragm fibre optic detector converts, within the interceptor, the pressure differential into a modulated optical signal. This signal is then transmitted via fibre optics to a monitor, thereby avoiding the use of pressurised tubing and its inherent prospect of air leakage.

This chapter examines how the variation of the two pressure points can be used to manipulate the diaphragm and through using this movement, to move an optical blade to modify a light source as it passes along a fibre optic. Through the design of this optical blade, a fail safe system was developed, whereby any failure encountered by the fibre optics or the electronics would indicate a fault. The development of this detector also considered fibre optic mountings and the suitability of various light emitters and detectors.

6.1 Components used in oil detection

This section describes the equipment used in the laboratory and the components used to construct the detector.

6.1.1 Apparatus and equipment

For this detector, as with the previous one, the multi-meter, data loggers and temperature sensors were used. The glass laboratory interceptor and the large interceptor located at Andel Ltd were both used for the oil detection experiments. The optical beam profile was examined using an Ophir Beamstar V-PCI CCD camera in conjunction with a computer. The LED light intensity was measured using a Coherent Fieldmaster power meter fitted with a visible light detection head.

6.1.2 Components of the detector

For clarity the components of this detector have been split into three parts; the optical monitor, fibre optic cables and the optical sensor, these parts are illustrated in the diagram in figure 4.7. The individual parts are described below.

(i) Optical monitor

Two different monitors were produced. The initial monitor, monitor No. 1, used an emitter (HFBR-1524Z) and a detector (HFBR-2524Z) by Agilent Technologies, connected to the optical fibre via a push-in socket. The fibre needed the sheath to be removed before the push-in plug was crimped onto the fibre This photodetector had a built-in integrated circuit that gave a two state output, dependant upon whether the received optical signal was above or below a pre-programmed threshold. This monitor was used for initial demonstrations at Andel Ltd but the pre-programmed threshold was a drawback for further experiments, due to its lack of quantitative output.

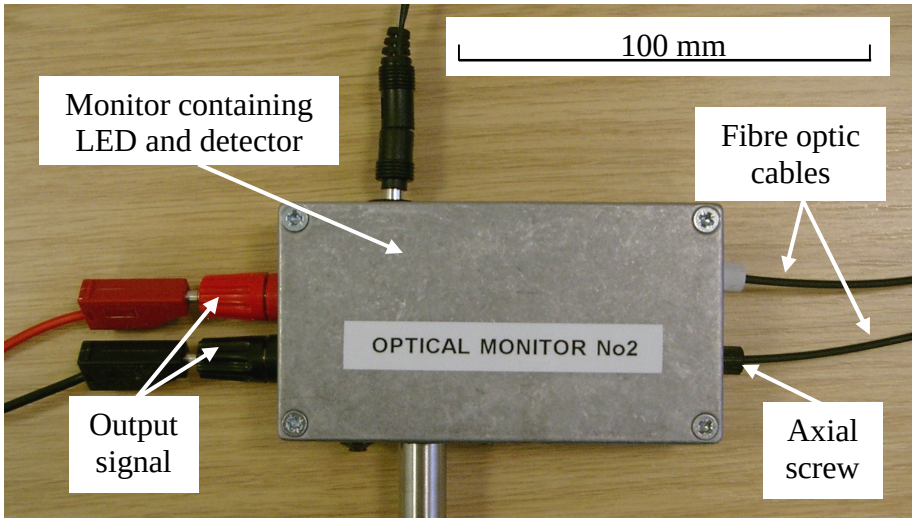

Figure 6.1. *Monitor No.2 showing the fibre optic connections, voltage output connections and power supply.*

This first monitor was later replaced by an improved second monitor, monitor No. 2, which had the Avago Technology higher power LED, SFH756V emitter, and a photodiode SFH250V detector giving an output voltage proportional to the detected optical signal and is shown in figure 6.1. These were attached to the fibre optic by inserting the fibre into an aperture and securing it by means of an axial screw, this could be glued for permanent fixture. This monitor housed the light emitter, detector and circuitry. There was also a power supply socket with an LED to display the power

on/off status and two output sockets at the side that allowed a voltmeter or data logger to be attached to display or record the output.

The two LED emitters (one used in each monitor), having peak output at 660 nm, produced an optical power output of ~ 60 µwatts and ~ 800 µwatts respectively. In later experiments and trials at Andel Ltd, where greater lengths of fibre optic cable were tested, the higher optical power output from the optical monitor No. 2 was required.

(ii) Fibre optic cable

The fibre optic links to and from the optical monitor used a multi-mode step index PMMA fibre, supplied by RS, model number EH4001RLD20M. This 1 mm diameter core had a black poly ethylene, PE, sheathing and a numerical aperture, NA, of 0.47, which is similar in performance to other branded polymer fibres. This fibre had an attenuation at 660nm of 200dB/km and a minimum recommended bend radius of 50 mm. Although a single mode glass fibre has attenuation losses that are far lower (typically less than 10 dB/km), the distances required for this oil detector should not exceed 50 metres. In this case the higher attenuation for the multimode fibre would have a 90% loss each way over 50 metres but this was considered to be tolerable, thus allowing less expensive fittings associated with the multimode fibre to be used. This also reduced the problem of aligning the fibres within the fibre optic guide. Where the fibre optic had been cut, the ends were polished using an Avago Technology polishing kit. Through the use of a fibre optic holder and diamond polishing paper, the finest of which was 3 µm, a good optical finish could be attained.

The major attenuation losses for this type of material are due to; length of fibre, coupling losses and curvature (bending losses). Couplings and bending can be kept to a minimum, whereas the length of fibre required will be dependant on each particular location.

(iii) Fibre optic holder

The fibre optic cables were held in position by placing them into a mechanical holder. This comprised of three 2.0 mm thick sheets of PMMA (polymethylmethacrylate) sandwiched together, with the centre one having grooves in which the fibre optic cable was located and is shown in figure 6.2. This guide catered for several key requirements; that the fibre optic cables were correctly positioned with respect to the blade, that the

cables were led to the enclosure outlet and that the cables could be kept at a regular bending radius. The last feature was important as bending losses could be quite detrimental to the transmitted optical power, this is further examined in section 6.2.5.

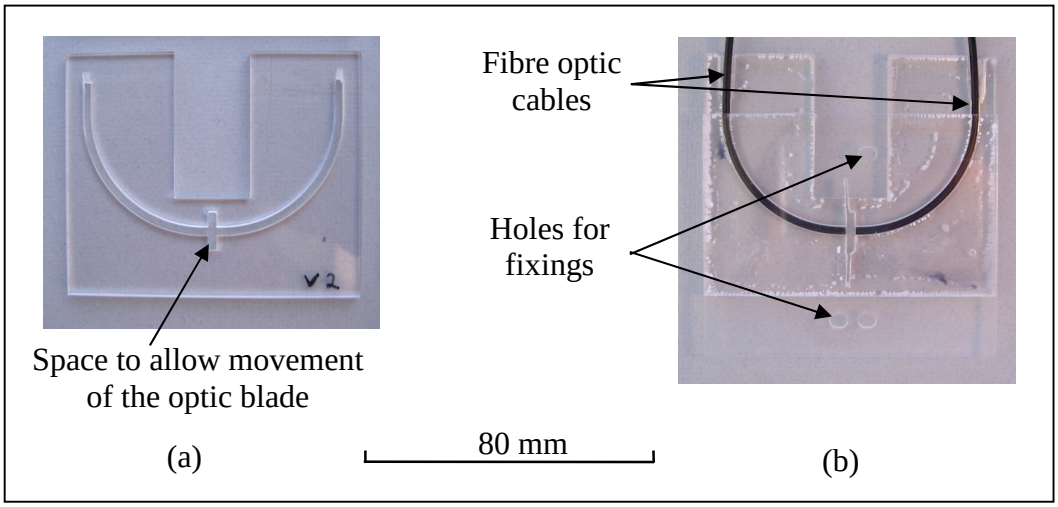

Figure 6.2. *Fibre optic holder,(a) is the centre piece of the PMMA showing the channel for fibre optic cable and (b) the complete guide with fibre optic cable located.*

(iv) Enclosure

The enclosure which houses the diaphragm and the optics guide needed to have an IP (ingress protected) value of 6-7. These two values represent a protection rating against physical abrasive/damaging objects and of the penetration/leakage of liquid respectively. The rating of 6, provides total protection against dust and a rating of 7 protection against liquids for temporary immersion up to 1 metre for 30 minutes, this would allow for any accidental splashing from liquid whilst being installed. It was essential that the enclosure was perfectly air tight as this was crucial to maintaining the pressure from the upper reference probe. This pressure from inside the enclosure counters that from within the diaphragm, creating the pressure differential. The fibre optics exiting from the top of the enclosure, this again is required to be air tight (this was only for optical sensor No.2) The final version of this enclosure used epoxy resin to seal the connecting elements and a silicon sealant to further secure the lid.

(v) Probes

The enclosure and the diaphragm are pressurised from the two probes, these were similar to the pressure tubing detector except that these probes were attached directly to the optical sensor, thus requiring no connecting flexible tubing. Figure 6.3 shows the optical sensor No.1, here this early experimental sensor had an upper and lower probe

with a separation of 210 mm and the fibre optics exiting via the upper probe. Routing the fibre optics in this way produced less opportunity for potential air leakage, it did however create problems through unpredictable and excessive bending of the fibre optics.

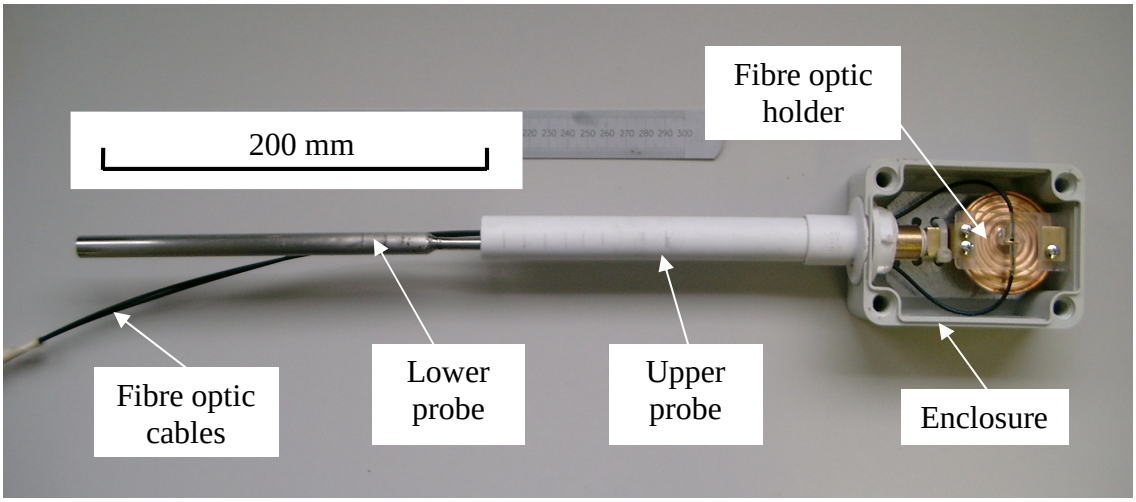

Figure 6.3. *Optical sensor No.1, here the enclosure cover has been removed to show the probes, the diaphragm and fibre optic holder within the enclosure. In this sensor, the fibre optics accessed the enclosure via the upper probe.*

The lower probe, the longer of the two, was made from stainless steel and attached directly onto the diaphragm, whilst the upper probe, made from nylon, was connected to the base of the enclosure and coaxial with the upper probe.

(vi) The pressure diaphragm

The pressure diaphragm was obtained from the internal components of a low pressure mechanical gauge manufactured by Cole-Palmer KC-25-10. This one had a range of 0 to 10 inches of H_2O (0 to 25000 Pa) and the casing, display and the mechanical parts were removed. This resulted in leaving only the diaphragm, ¼" NPT fitting and diaphragm supporting bracket and is shown in figure 6.4.

The pressure diaphragm was connected to a 450 mm long stainless steel tube, this was the lower probe and had an open end ID 10.0 mm, similar to one used in the pressure tubing detector. The internal pressure of the diaphragm was produced from this probe. To counter the internal pressure, an upper probe was connected to an air tight enclosure which housed the diaphragm, as shown in figure 6.3. The pressure change from these two reference levels would produce the pressure differential which would create the movement of the diaphragm as the status of the interceptor changed from water to oil.

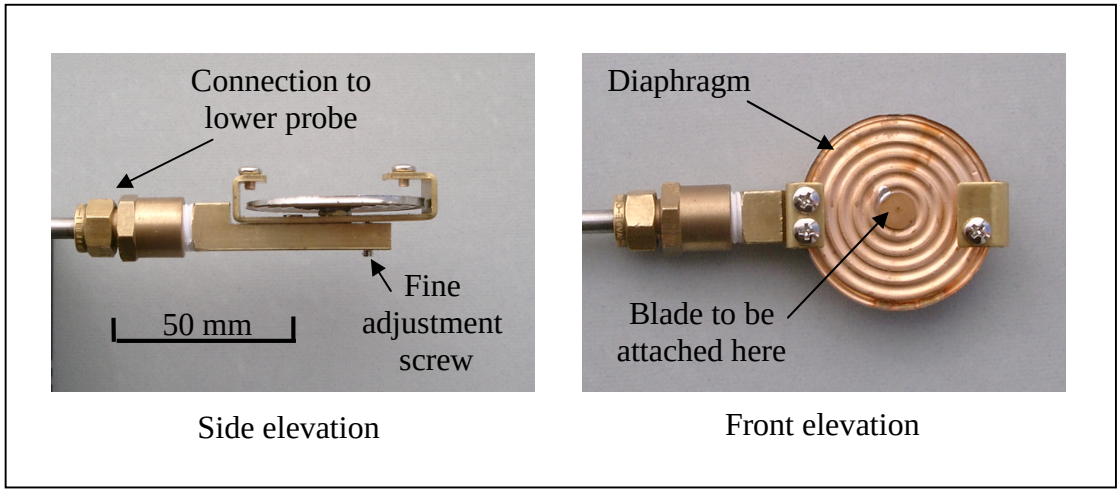

Figure 6.4. *Photograph of the pressure diaphragm from two elevations indicating the position where the blade was to be attached.*

The diagram in figure 6.5 shows the higher pressure, P_1, from the lower probe and the lower pressure P_2, from the upper probe. The airtight enclosure encloses the diaphragm, but importantly, retaining the pressure form the upper probe.

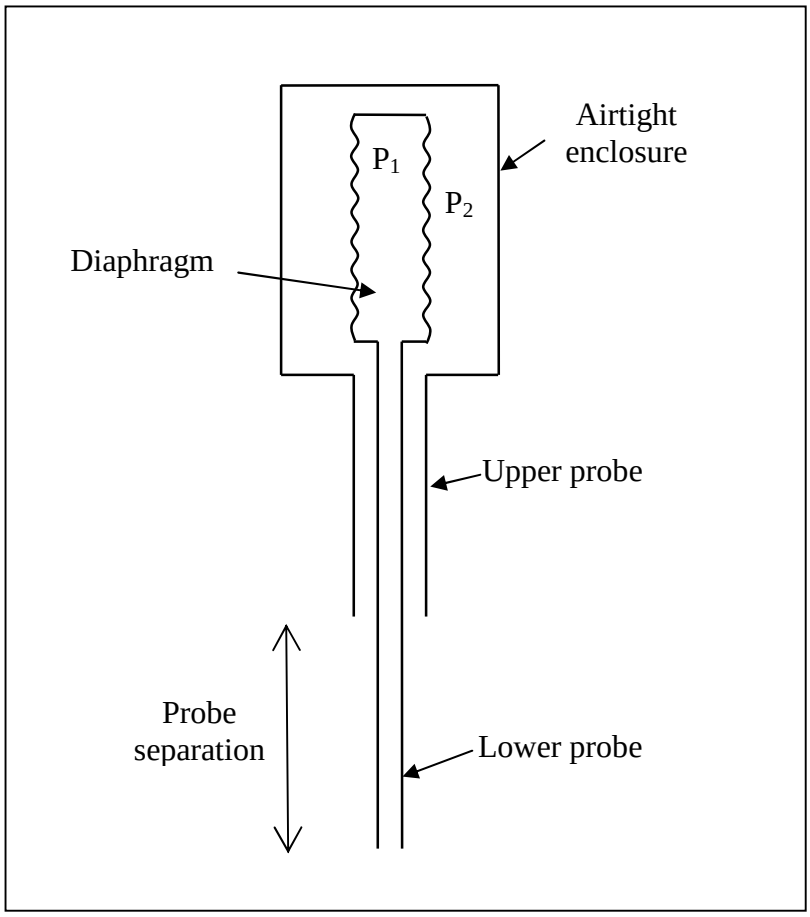

Figure 6.5. *Diagram showing the diaphragm internal pressure, P1, from the lower probe countered by the pressure, P2, from the upper probe.*

This particular diaphragm had a pressure range 0 to 2500 Pa which produced a movement of ~ 2.0 mm by the diaphragm, measured using a travelling microscope. This was equivalent to ~ 0.08 mm of movement of the diagram per 100 Pa. Through creating a larger pressure differential change, a greater movement of the diaphragm would occur, allowing any attached optical blade to travel further. For this reason, the probe separation in optical sensor No.2 was increased, the lower probe was placed at 250mm below the water/air interface and the upper probe at the surface, thereby using the maximum pressure recommended for this diaphragm. Air leakage due to this higher pressure would not be an issue as tubing was not being used in this detection system. With the upper and lower probes ~ 250 mm apart, this would produce ~300 Pa pressure differential as new motor oil accumulated within the interceptor, this in turn would produce a movement by the diaphragm of ~ 0.25 mm. Attaching a blade to the centre of the diaphragm permitted this movement, through expansion or contraction, to interrupt the passage of any suitably placed light source.

6.2 Development of the detector

6.2.1 Positioning of the fibre optic cables within the enclosure

The enclosure as shown in figure 6.3 contained the diaphragm and the fibre optic guide. The fibre optic cable need to be suitably secured and positioned either side the optical blade. It was also preferable that the fibre optic cables entering and exiting the enclosure were sited adjacent to each other making it easier to protect the fibre optics against possible damage and also allowing for a more compact detector.

Through using a fibre optic system and a moving blade to attenuate the light, there are several ways of positioning the fibres at either side of the blade and three methods are shown in figure 6.6; (a) bending the fibre optic so that the ends are opposed to each other, (b) the use of reflective surfaces to redirect the light, or (c) polishing the end of the fibre to make use of TIR. The methods (b) and (c) would allow the fibre optic cable to remain straight thus reducing optical losses which occur when optical fibres are bent. The possible problems with (b) are that the reflective surfaces may reduce in efficiency over time, and would require careful alignment. Method (c) is discussed further below.

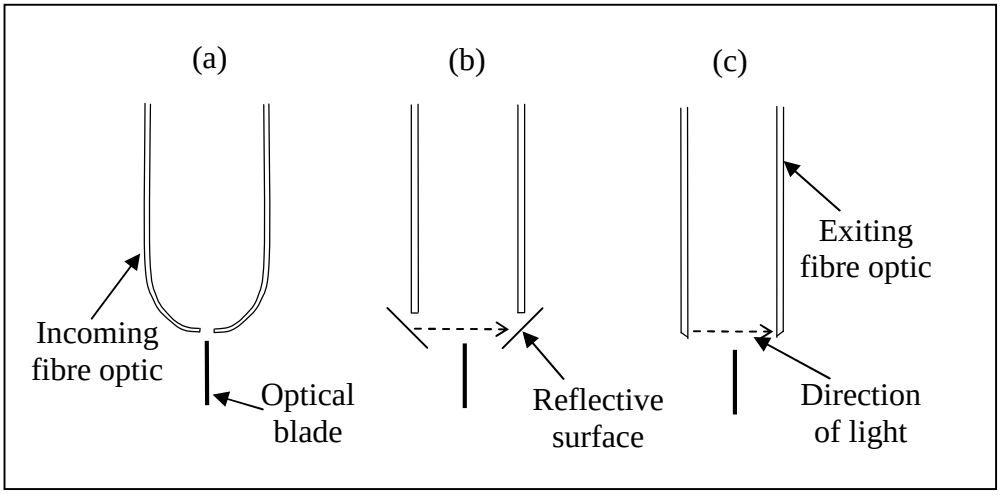

Figure 6.6. *Three methods of directing and collecting the light from the fibre optics; (a) bending the cable, (b) using reflective surfaces and (c) cutting the fibre optic ends to create TIR.*

The angle that permits TIR at the fibre end is dependant upon the refractive index of the core and the outside medium, in this case air. Cutting it an angle of 45° as shown in figure 6.7 (a), would reflect only a proportion of the light, whilst some of the extreme rays would still be transmitted through the end. To ensure that all the light was reflected, a minimum angle of 60° would be required, as shown in figure 6.7 (b), it would be desirable that the cut end was smooth and free from scratches. Using a cleaved angle of 60º the receiving fibre optic cable (with the same angle) would be required to be positioned at ~ 96° to the emitting optic fibre, as shown in (c). With this scenario, a small amount bending would still be required to enable the optic fibres to exit the enclosure adjacent to each other. By cutting the fibre optic at a 60° angle, the light from this multimode fibre would exit it at an angle ~ 90° (from θ_B to θ_C) as shown in figure 6.7 (b). The result would be that only a proportion of the emitted light would reach the receiving fibre optic cable with the ability to be transmitted back to the receiving detector. The consequential loss of optical signal would be quite large. It should also be noted that the cylindrical nature of the fibre optic gives a strong focusing effect in one axis. This further reduces the coupling across the required gap between the fibres. As a result this method was not used.

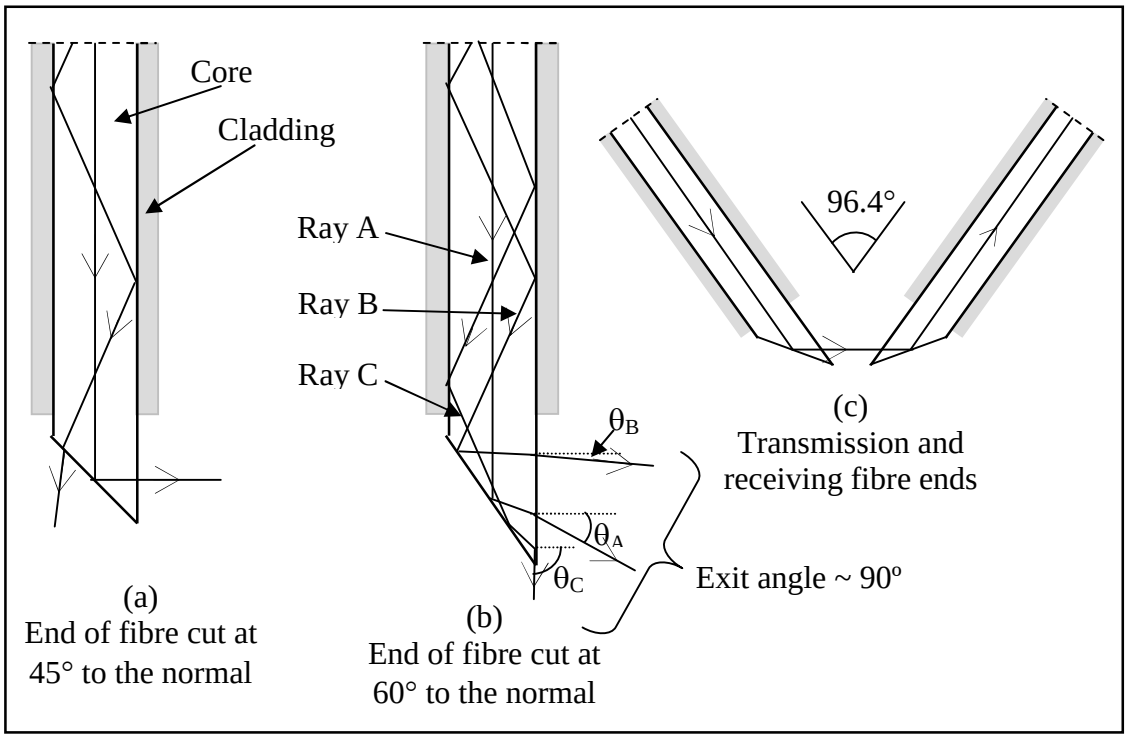

Figure 6.7. *Diagrams showing ray tracing (left and centre) for the ends of the fibre optic cable cut a 45º and 90º. Right, the angle of the cable required to recapture emitted light.*

Losses of optical power due to bending of the fibre (known as bending losses) result from the change in incident angle of the light rays between the core and cladding interface causing partial loss of TIR. This initially affects the more extreme rays but as the bending radius increases a larger proportion of the light passing along the fibre no longer experience TIR and is lost into the cladding. The fibre optic cable used had a recommended minimum bend radius of 50 mm. However, through the method of guiding the light as shown in figure 6.6 (a) and to keep the enclosure dimensions to a minimum it would be beneficial to have the bend radius less than 50 mm.

6.2.2 Design of the fibre optic holder

The fibre optic holder was constructed from PMMA, as discussed in section 6.1.2. The function of the guide was to firmly hold the fibre optic cable and securely place the cable ends near the optic blade. The inner dimensions of the enclosure limited the size of the fibre optic guide, which in turn dictated the maximum for the bending radius.

In order to examine optical power loss through bending the 1.0 mm core fibre optic cable, a mandrel was used to guide the optical fibre around different radii for 90° and 180° bends. The optical output from the emitter of the optical monitor No.1 was

connected to one metre of fibre optic cable. An optical power meter with a visible light detection head adjusted to detect at 660 nm was used to monitor the optical power output from the end of the fibre optic after it had passed around the mandrel.

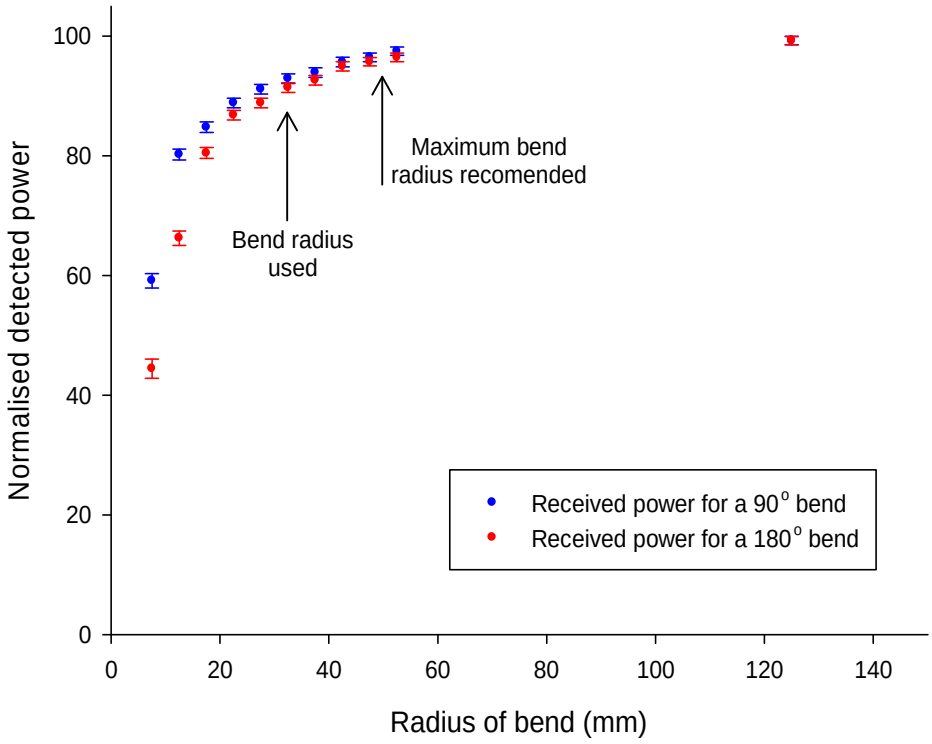

Figure 6.8. *Optical power received for a fibre optic cable at different bend radii through a 90° and a 180° bend. The bend radius used in the fibre optic guide is indicated.*

The results for bend radii from 7.5 to 125 mm are shown in figure 6.8, the error bars represent the range of results. The percent power received has been normalised to the power output where the fibre optic cable was straight. For the fibre optic guide a 90° bend was used, the results for a 180° were also added to indicate the effect of further bending.

A 90° bend with a 50 mm radius produced a loss of optical power of ~ 3% whereas a bend radius of 32 mm (which was to be used in the fibre optic guide) indicated a loss of ~ 7%. As two bends were required, one before the blade and another one after, the total power reduction by this system of light guiding would equate to approximately 13.5%. Any system of guiding light through 180° (via two 90° bends) to pass through an arrangement where the optical signal may be purposely interrupted would be expected

to be subject to some losses. This system of bending the cable indicates less loss of optical power than would be expected for a system of TIR shown in figure 6.6 (c).

The space at the centre of the fibre optic guide allowed the optic blade to move freely across the path of the light as it travels out of the emitting fibre towards the receiving fibre. Having a gap between the fibre optic cables which allowed space for the optical blade to travel again caused optical power loss, due to the divergent nature of the light exiting the fibre. The shape of the cone is dependant upon the NA of the fibre optic cable. Through placing a similar fibre optic cable opposite the emitting fibre to recapture the emitted light, losses dependant upon the separation distance were seen to be the major factor, reflections at the interfaces and scattering due to imperfections in the polished fibre ends having further effects.

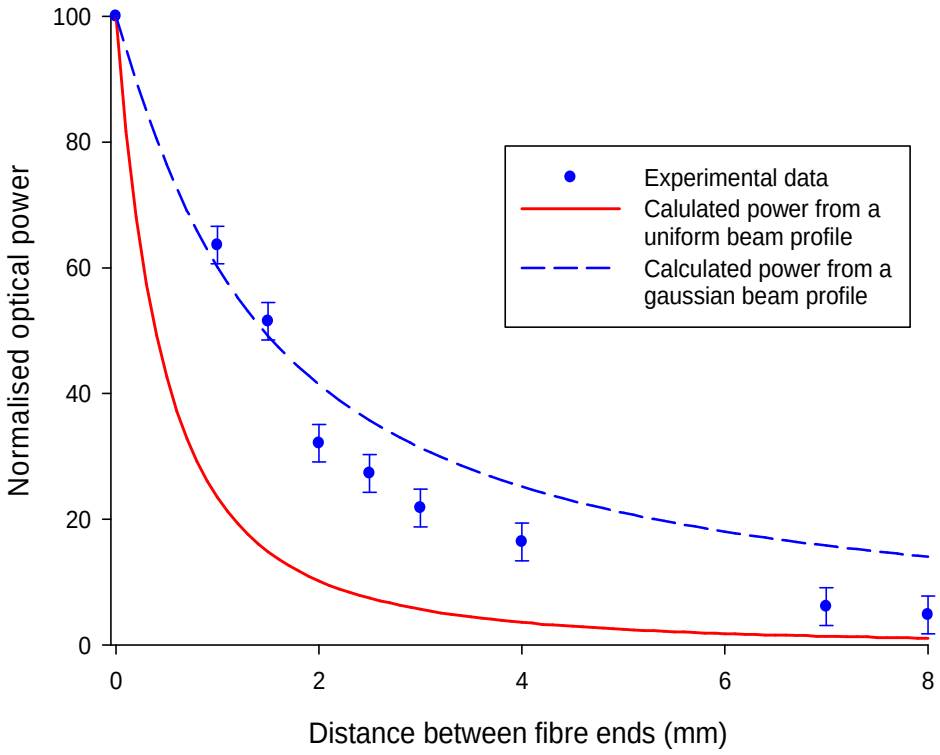

Figure 6.9. *Normalised optical power loss in the fibre optic cable as the cable ends are separated. The mean of six experiments are shown and the error bars showing the range of results.*

The graph in figure 6.9 shows experimental results for the power loss as the ends of the fibre optic are moved further apart. The power detected when the polished ends of the fibre optic cable were touching was normalised to 100. The error bars represent the range of results from six experiments. When placed into the fibre optic holder the

expected distance between the cable ends was to be between 1.5 mm and 2.0 mm, with a resultant reduced detected power of ~ 35% and ~ 50% respectively.

The solid line in the graph represents the calculated power loss which would have been expected from an emission cone of uniform radiant intensity and the broken line represents the power loss from a gaussian beam profile. The experimental data suggests that the actual beam profile was nearer to that of a gaussian beam.

6.2.3 Analysis of the beam emitted from the fibre optic

An Ophir Beamstar V-PCI CCD camera was used to measure the spacial profile of the optical intensity. In figure 6.10 the monitor display is shown; the intensity of the beam is shown in (a) as the different colours indicate an increase in intensity.

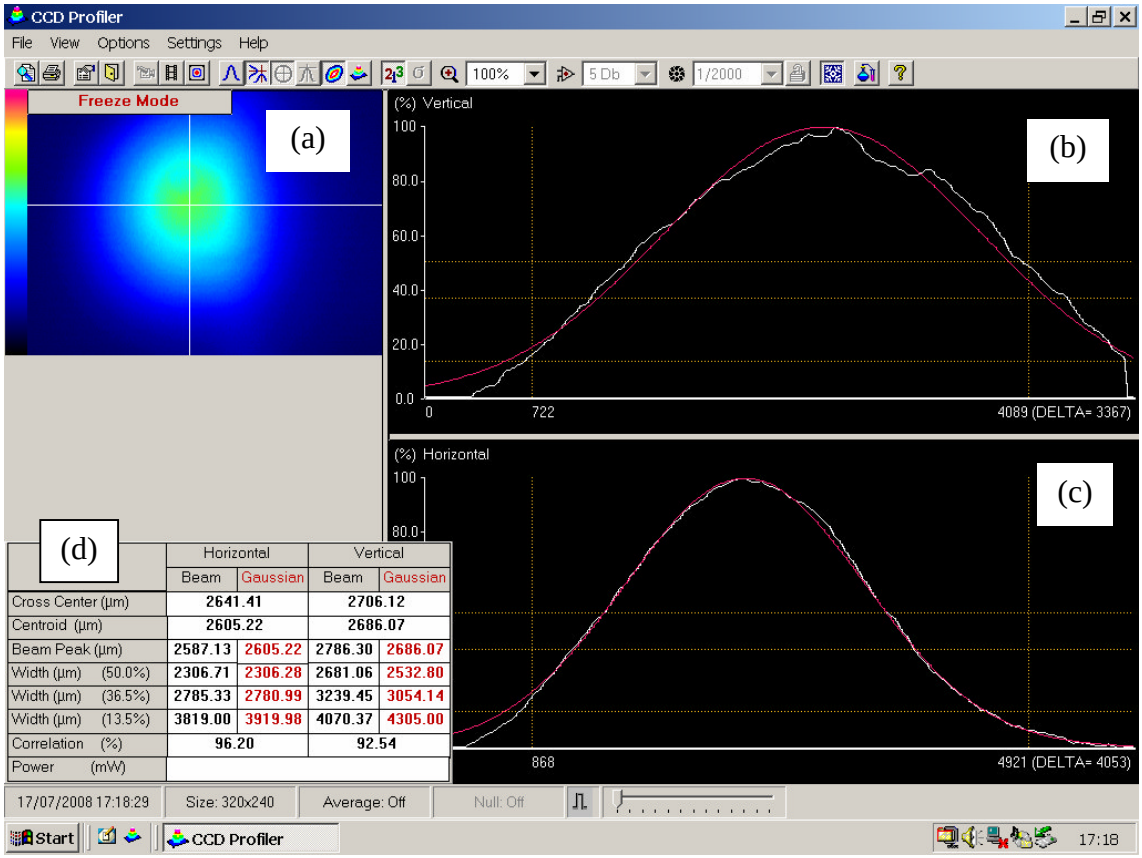

Figure 6.10. *Ophir Beamstar CCD beam profiler, showing the beam intensity (a), the vertical (b) and horizontal (c) profiles and data (d) of the emitted light from the fibre optic cable at a distance of 2.0 mm from the front of the camera.*

The two graphs (b) and (c) are the vertical and horizontal optical intensities across the centre of the emission, the white lines trace the profiles as indicated from the cross lines on the beam intensity (a) and the red lines in (a) and (b) are gaussian fits to the profiles viewed from the vertical and horizontal axes (all the graph traces are normalised). The

data in the figure (d) indicate the beam width and height. The distance of the end of the fibre optic to the front CCD camera was ~ 2.0 mm. The difference in the widths of the graphs in (a) and (b) may possibly be due to non uniformity in the cutting and polishing of the fibre end. However, the greatest intensity was in the centre of the beam, with a power drop off towards the edges.

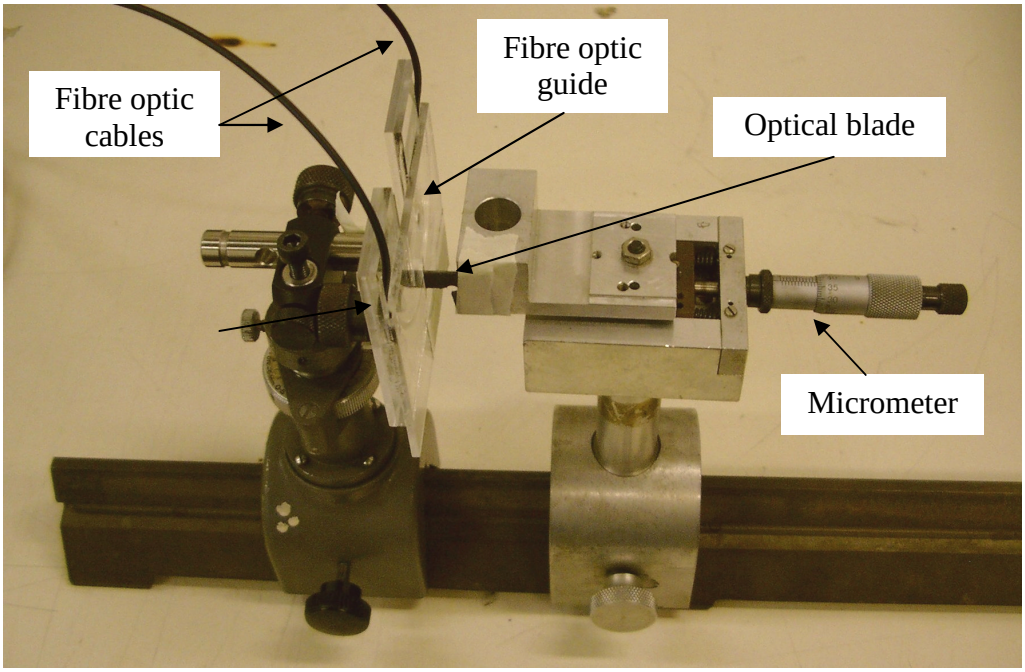

Figure 6.11. *Experimental set up to examine the change in light intensity as the optical blade cuts the beam.*

Further examination of the light intensity across the beam profile was seen through interrupting the transmission using an optical blade. A fibre optic guide was used to hold the fibre optic cables and an optical blade, made from stainless steel and painted in matt black paint (to reduce reflection), was mounted on a micrometer. The fibre optic cables were connected to the emission and detector of optical monitor No.2, as described previously, and the signal transmission response was monitored as a voltage. A gap of 2.0 mm was left between the fibre optic ends to allow the optical blade to freely travel. The experimental set up is shown in the photograph in figure 6.11 and the results from five experiments are shown in figure 6.12. Between each experiment the fibre optics were removed and re-aligned. The transmission intensity has been normalised and the error bars represent the range of results.

As the blade travelled between the fibres, the change in transmission intensity occurred over a 1.0 mm distance and the light transmission fell from its maximum intensity to zero. As expected, the cut off of the light intensity was not linear, with the greatest change in intensity occurring as the blade travelled across the central portion of the fibre optic. The calculated area of the fibre core, obscured by the blade, has been added to the graph in figure 6.12 (broken line) and can be compared to the actual reduction in transmission. A further curve (solid line) has been added. This reduction of light intensity, calculated as a gaussian beam profile based on the CCD camera data, closer represents the actual experimental data. However, small inconsistency between the experimental data and the solid line can be seen. This is due to the actual beam originating from a fixed aperture and a possible minor misalignment between the two fibre optics.

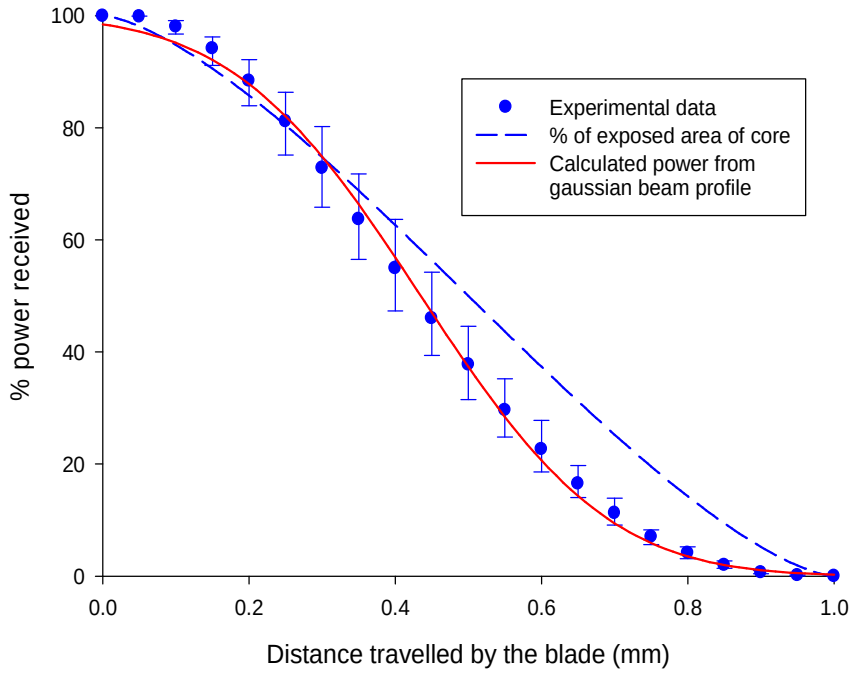

Figure 6.12 *Relative light intensity as optical blade interrupts the beam. The experimental data represents the mean from five experiments and the error bars show the range of results. The broken line shows the exposed core and the solid line is the expected intensity using the data from the CCD camera beam profile.*

As the blade travelled across the latter part of the fibre core the majority of the light transmission had been extinguished. Approximately 80% of the reduction in light transmission occurred as the blade travelled through the central ~ 0.55 mm. of the fibre core. The central part of the fibre core containing the greater part of the light intensities.

6.2.4 Design of the optical switch

In order to assess the response of a simple optical switch, where an optical blade partially modulates the transmitted light, the optical sensor No.1 was placed in the laboratory interceptor. Connecting optical monitor No.2 (where the detected light was proportional to the output voltage) to 10 m lengths of fibre optic cables, the interceptor was filled with water until it flowed out of the siphon. New motor oil was then poured in discrete quantities into the interceptor replacing the water. The voltage output from the monitor was noted as the oil depth increased. The change in voltage was due to movement of the diaphragm and therefore the blade as the pressure differential decreased. Once the oil passed the lower probe, no change in voltage occurred. Results for two experiments are shown in figure 6.13figure 6.12, it can be seen that the ~ 0.25 mm travel of the blade had only reduced the intensity of the transmitted light signal by about 20%.

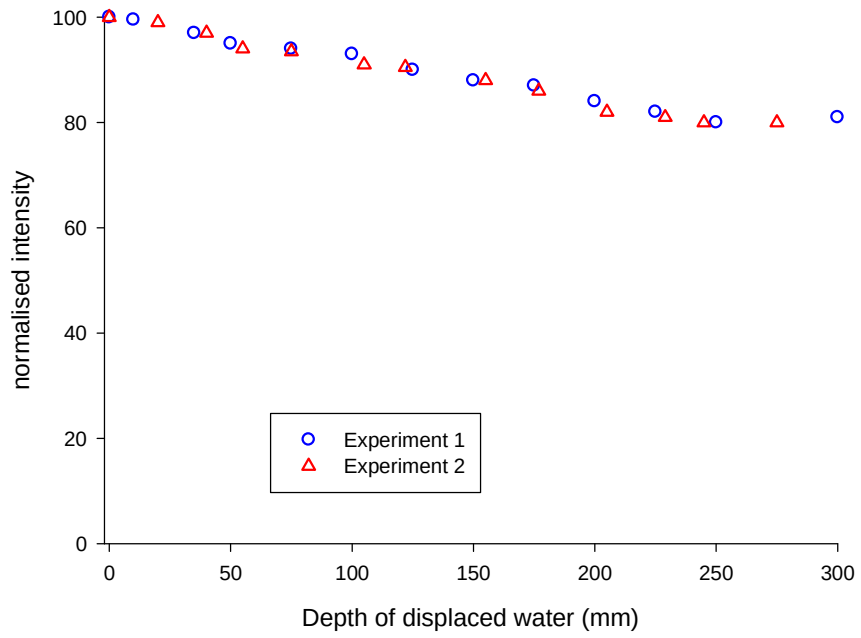

Figure 6.13. *Graph showing the change in light intensity using pressure diaphragm detector No1 as the oil level increased in the laboratory interceptor.*

This detector showed that the principle of using the pressure obtained from two positions (the upper and the lower probes) could be used to repeatedly reflect the pressure differential between these two points with the addition of oil. However, the major problem of using a detector which only slightly modified the transmitted light signal was that through moving or extending the length of the fibre optic cable the

detected optical power could be increased or decreased, which may mask the effect of the oil/water status, severely affect the accuracy of this detection system.

The limitations of using a solid blade were shown in the previous experiment. Using a solid blade, as shown by the diagrams in figure 6.14 (a), would interrupt the light as the diaphragm is inflated then as the pressure differential falls (through the presence of oil) the blade would move, allowing the transmission of light. However, the reverse occurs through using a blade with a slit, as shown in the lower diagrams (b). Here the light is transmitted through the blade only with a high pressure differential and blocked as oil level increases. By using the slit blade, the change from having an optical signal with water to the absence of a signal would not only be able to indicate the presence of oil but also in the event of a fault or failure by any of the components, such as the LED or the optic fibre cable, indicate that attention would be required. As such it has the further advantage of being fail safe. The blades were made from stainless steel, the dimensions of the gap in the slit blade were altered as development of the detector progressed.

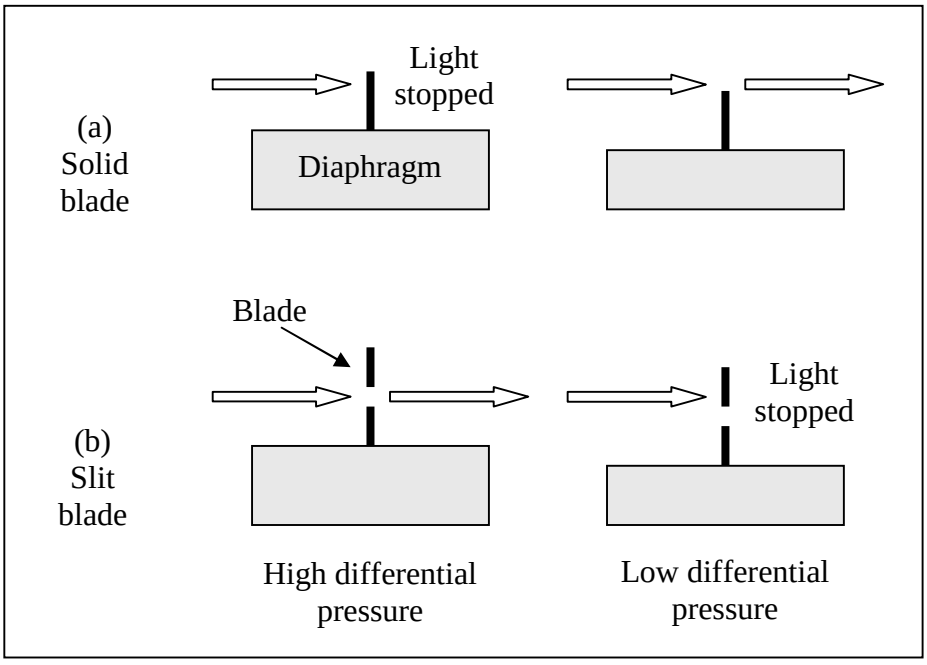

Figure 6.14. *Diagram showing diaphragm in two positions and how different blades stop the light.*

The pressure change in the diaphragm as the water was replaced by new motor oil was approximately 300 Pa and as previously discussed this would result in a movement in the diaphragm and in turn the movement of the blade by ~ 0.25 mm. This was not sufficient to eclipse the 1.0 mm diameter of the fibre optic core. Such a limited

movement of the blade would only produce a reduction in the optical signal as it passes across the gap between the two ends of the fibre optic cable. Alternatively, placing the blade to partially obscure the majority of the light, the change in the pressure differential as the water was replaced by oil would complete eclipse of the light transmission. Both of these scenarios would create an unsatisfactory situation; the first method which relies only upon a reduction in the optical signal could be prone to a misreading in circumstances where the optical signal was reduced through fluctuations in power supply or other variations caused by cable bending. The second method which has the advantage of totally blocking the light transmission, relies upon using the lower intensity light from the fringes of the emitted beam, reducing the maximum optical power transmitted to the receiver, producing a potentially reduced signal.

Two alternative methods were examined whereby the relatively small movement of the optic blade could be used to stop the transmission of the light whilst efficiently retaining the more intense optical power; the first used a lens to reduce the beam to a spot size ~ 0.25 mm and the second used a mask to clip the edges of the beam forming a slit of ~ 0.25 mm.

For a lens to reduce the beam size from 1.0 mm to create an image 0.25 mm, a magnification, m, of 0.25 would be required. To achieve this, the object distance, d_o, would need to be four times the image distance, d_i, as shown in equations (6.1) and (6.2).

$$m = 0.25 = \frac{d_i}{d_o} \tag{6.1}$$

$$d_o = 4d_i \tag{6.2}$$

If a desired distance of 1.0 mm was required between the lens and the image (to allow free movement of the optical blade), then a distance of four times that would be required for the objective distance. With a NA of the multimode fibre of 0.47, and an object distance at 4.0 mm, the diameter of the beam of light would be ~ 5.3 mm. The thickness of the lens would further increase the distance between the lens and the blade. Furthermore a similar lens system would be required to reintroduce the light into the receiving fibre optic cable. It was considered that the complexity and size of this

system, coupled with the required precision to set up this arrangement would take this beyond that required by Andel Ltd.

Through masking the edges of the beam and so restricting its width, the blade would need to travel a smaller distance from full clearance to fully eclipsing the beam and so cutting transmission. Several masks of different widths were assessed, these were adapted from stainless steel projection masks and again painted in a matt black paint to restrict reflection. A new optic guide was made with grooves capable of holding a mask. Shown in figure 6.15 (left) is an optic guide holding two masks and (right) a mask with a slit of 375 µm. Placing a single mask and two masks into the optic guide was assessed. It was found that a single mask placed adjacent to either the transmitting or receiving fibre optic produced similar results. Several different slit sizes were tried and these results are shown in figure 6.16.

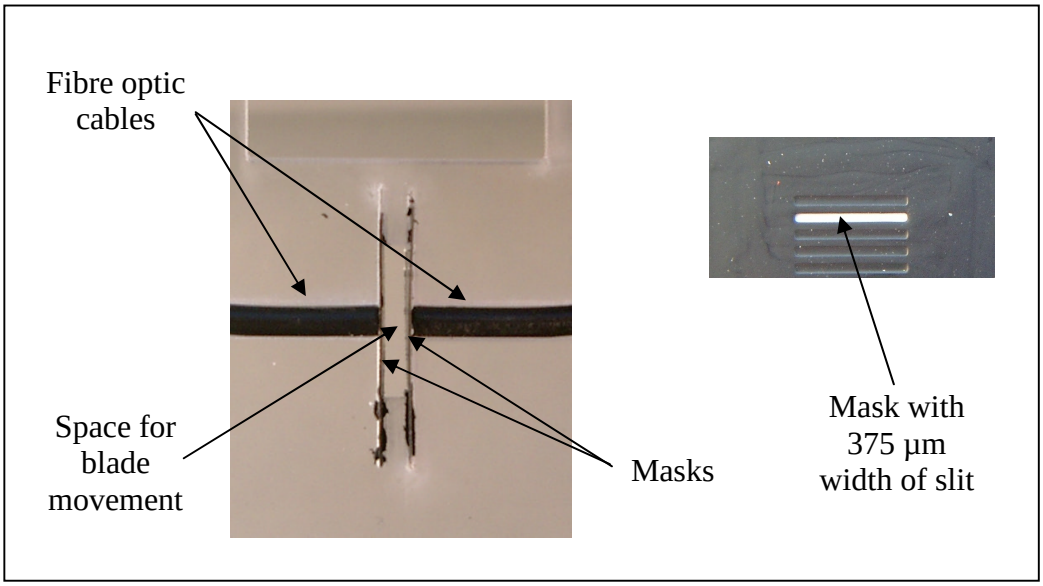

Figure 6.15 *Photograph of part of a fibre optic guide (left) showing fibre optic cables with two masks and (right) a mask with a 375 µm slit.*

As would be expected, the smaller the mask width the less distance the blade was required to travel to change the light transmission. Using only a single mask required the blade to travel a distance greater than the slit size to eclipse the light. This is particularly noticeable when using the single 200 µm mask.

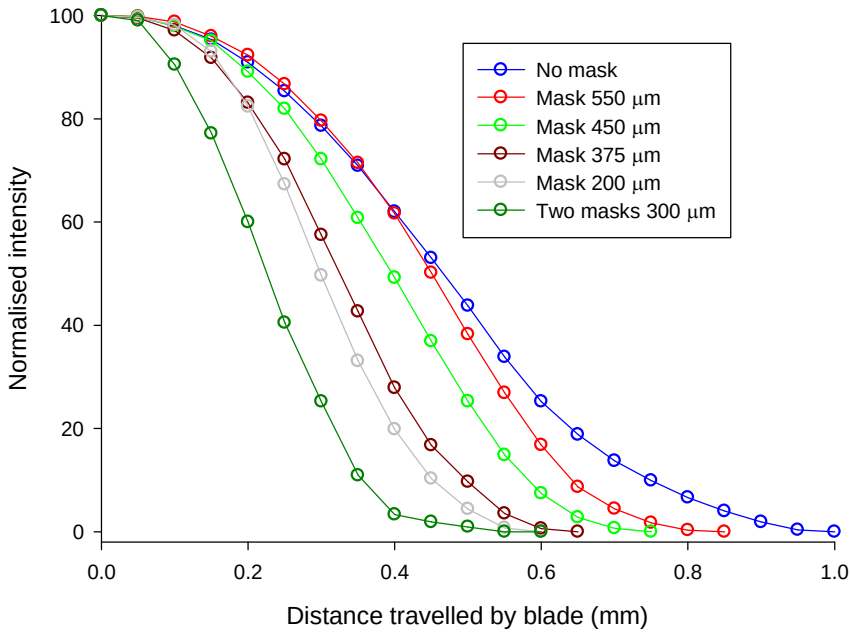

Figure 6.16. *Experimental results for several single mask and one experiment using two masks. A control with no mask is included.*

The consequence of using a mask to limit the blade movement was that the total amount of light being transmitted was reduced. The mask width affected the amount of light and as would be expected the smaller the mask width the greater the reduction in optical power. The 550 µm mask reduced the optical power transmission to ~ 62% compared to that with no mask and 300 µm and 200 µm producing ~ 40% and ~ 25% transmission respectively. Using the two 300 µm masks further takes the transmission to only 16% of the original value. However the effectiveness of using these masks needed to be balanced against the efficiency of being able to obscure the light transmission for the required movement of the optic blade. Once the two mask system had been decided upon as the appropriate option, the solid blade used in these experiments was replaced with a slit blade, as discussed earlier. The layout of which is shown in figure 6.17. This allowed light transmission with a high pressure differential but obscured the light as the pressure differential decreased. The slit in the blade had a width of 350 µm, wider than the mask widths, thus allowing fine-tuning via the adjustment screw (shown in figure 6.4), once the fibre optic guide had been attached to the pressure diaphragm.

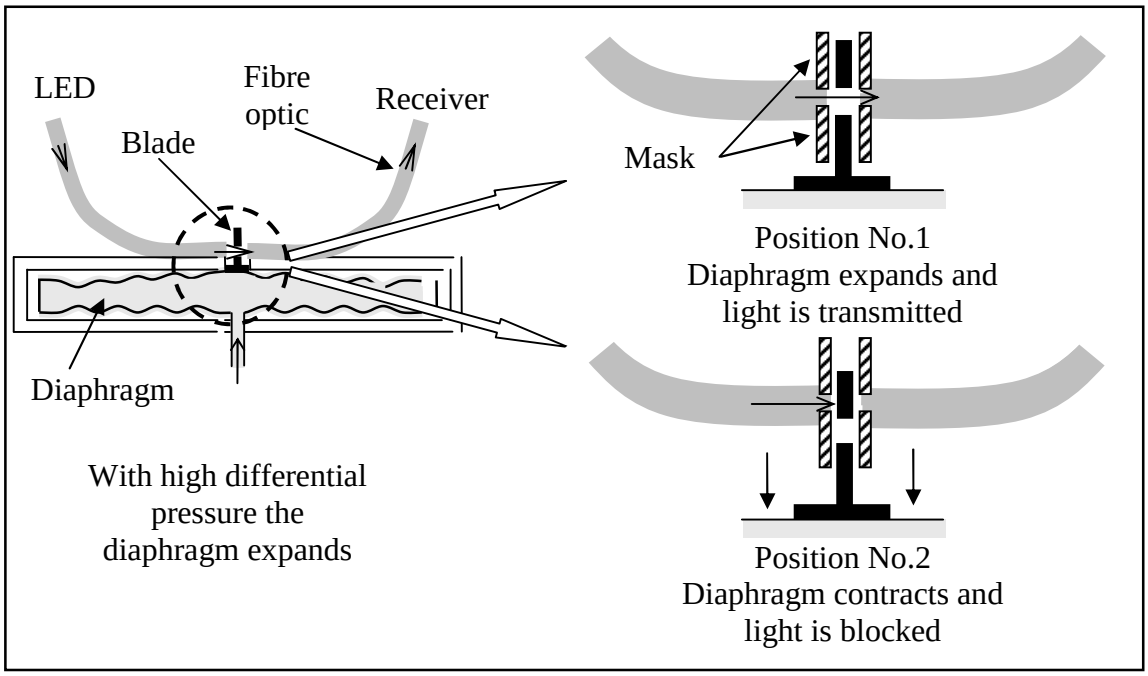

Figure 6.17. *Diaphragm, optic fibre and pressure activated blade, showing the relative positions of the mask and blade in position No.1 and No.2 as the pressure moves the diaphragm.*

Figure 6.17 shows a cross section of how this pressure activated sensor requires the movement from the diaphragm to operate a blade which is attached directly to the diaphragm. This has no secondary leverage or mechanism to create any retarding movement or associated friction that could be expected from such an arrangement and as such, the instrument would be durable and not deteriorate in efficiency over time; factors that could compromise the accuracy of such a system.

6.3 Evaluation of the pressure fibre optic detector

Two optical sensors were made, the diaphragm and probe dimensions being the same in each case. The pressure diaphragm sensor No.1, shown in figure 6.3, did not use a mask, simply relying upon a change in the light transmission as the blade moved across the gap between the emitting and receiving optical fibre. The fibre optic guide was limited inasmuch as it only held the fibres in position near the blade and did not guide them around a fixed radius. Whereas the optical sensor No.2 had a larger enclosure which allowed the fibre optic guide to have a larger bend radius (32 mm). Also the fibre optic cable exited the enclosure from the top making the detector easier to position without excessive bending of the fibre optics. The excess space within the enclosure that was not occupied by the diaphragm or the fibre optic guide, was filled using potting

compound, thus reducing the excess volume of the upper probe. It had been shown earlier in the pressure transducer chapter that a large or excess volume reduced the effective depth of the probe. In all of the following experiments and trials the upper and lower probe separation was set at 250 mm.

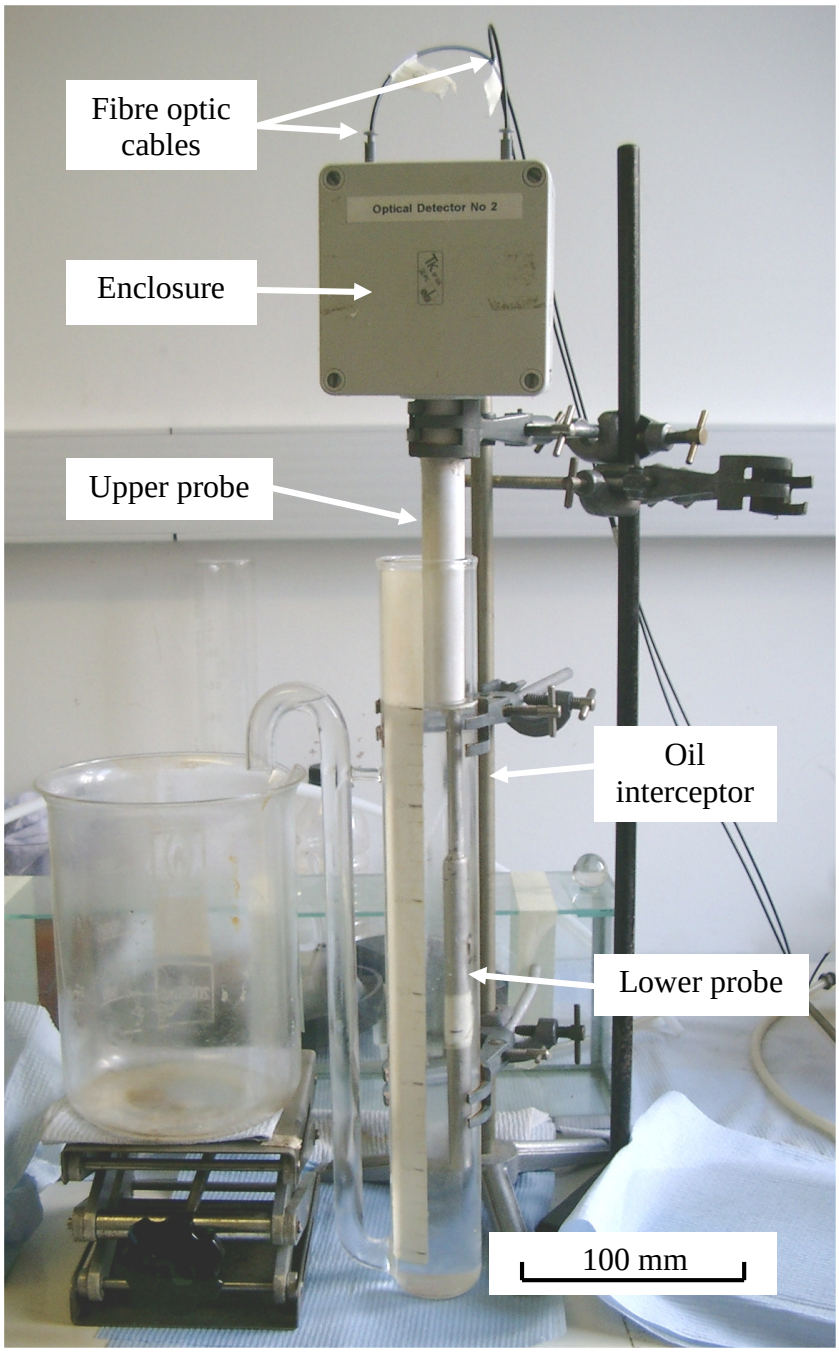

Figure 6.18. *Photograph of the optical sensor No.2, the probes are shown positioned in the laboratory oil interceptor.*

The optical sensor No.2, positioned in the laboratory oil interceptor is show in figure 6.18. This detector again was connected to optical detector No.2 (not shown) using

10 metre lengths of fibre optic cable and the reading taken using a voltmeter. To demonstrate the detector's sensitivity in determining the difference between water, new motor oil and DERV, the probes were lowered into each of these liquids. The position of the lower probe was noted and recorded against the voltage output and is shown in the graph in figure 6.19.

As the lower probe passed a depth of 250 mm the upper probe entered the liquid. For the DERV, the change in the differential pressure as the depth of the probes increased did not affect the optical transmission. The new motor oil showed a small increase in optical transmission as the upper probe was immersed, indicating that the relative positioning of the slit in the blade was allowing a small amount of light to be transmitted. However, immersing the probes into the water produced a distinct difference from that of the two oils. When the lower probe reached a depth of ~ 225 mm the change in the pressure differential moved the blade allowing the light to be transmitted, the signal intensity increased up to the point when the upper probe entered the water. What could be noted was that a small increase in the pressure differential continued to increase after both probes were further immersed.

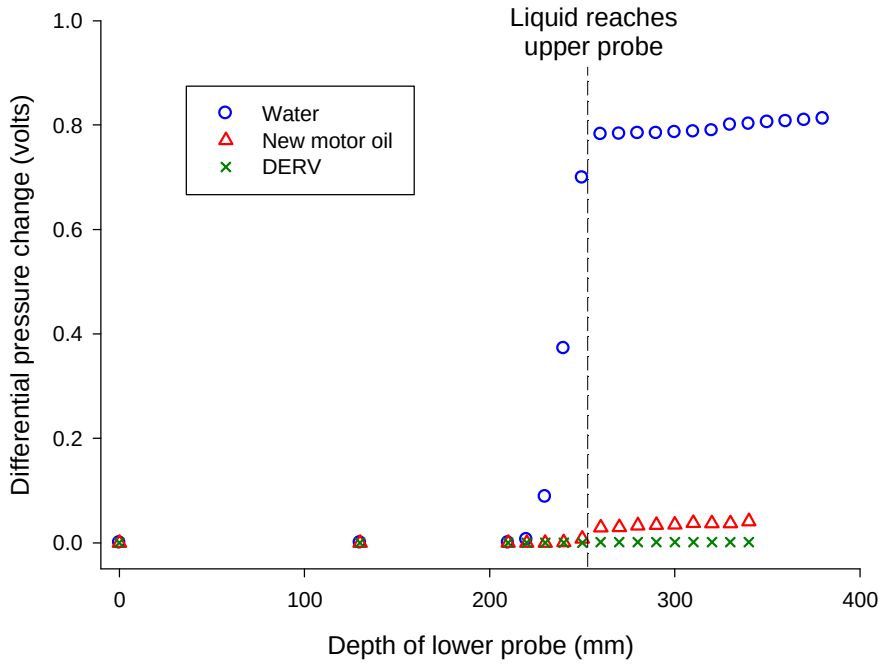

Figure 6.19. *Differential pressure change as the pressure diaphragm detector No.2 is immersed into water, new motor oil and DERV.*

The air volume to probe area for the upper probe was 140 cm^3 to 2.5 cm^2 producing a ratio of 56:1 and the lower probe having an air volume to probe area of 20.4 cm^3 to 0.78 cm^2 producing a ratio of 26:1. As discussed in the previous chapter, section 5.3, when the volume to probe area ratio is greater than ~ 53:1, a compromise in the ability of a probe to reflect the pressure at the base of the probe occurs. Here this is reflected when both the probes were further immersed, the upper probe pressure was not increasing at the same rate as the lower probe thus resulting in a small pressure differential increase.

To evaluate the optical sensor No.2 in the laboratory interceptor, the probes were placed in water until the upper probe was 5.0 mm below the surface and the lower probe 250 mm deeper. Oil was poured in discrete quantities into the interceptor displacing the water. Experiments using both the new motor oil and DERV were repeated several times. Four results, two for the new motor oil and two for DERV, are shown in figure 6.20, the detected light signal has been shown as a voltage.

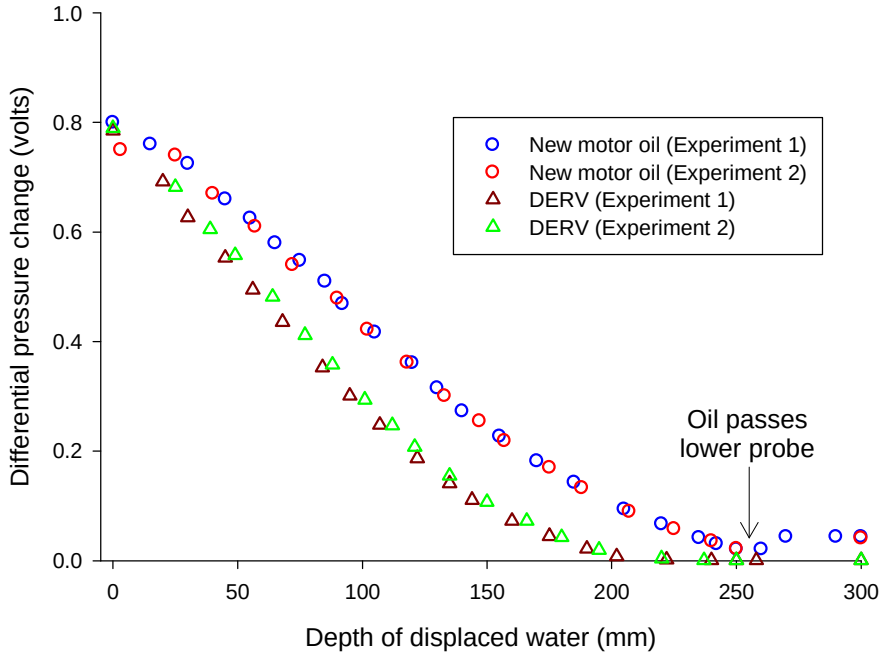

Figure 6.20. *Oil interceptor results for pressure diaphragm detector No2, displacing water with new motor oil and DERV.*

The outcome of using the less dense DERV as it entered the interceptor was that a larger volume was required to displace the water than was necessary for the new motor oil, approximately 5% more DERV (by volume) was needed. The result was that the depth (and resultant pressure) of DERV above the upper probe increases at a faster rate than for the new motor oil. The decrease in pressure differential, to a point where the blade

eclipses the light transmission, is reached at ~ 200 mm depth of water displacement as opposed to 250 mm for the new motor oil. It could be expected that if petrol was used, then the point where the light signal is extinguished would be reached earlier than that for the DERV.

The effect of the oil passing the lower probe can also be seen in figure 6.20. The small increase of the pressure in the lower probe creates a small increase in the pressure differential. A similar increase would also have occurred as the DERV passed the lower probe but here a similar pressure change in the lower probe would not have registered any change as the slot in the blade would have already been out of range to allow any light transmission to occur.

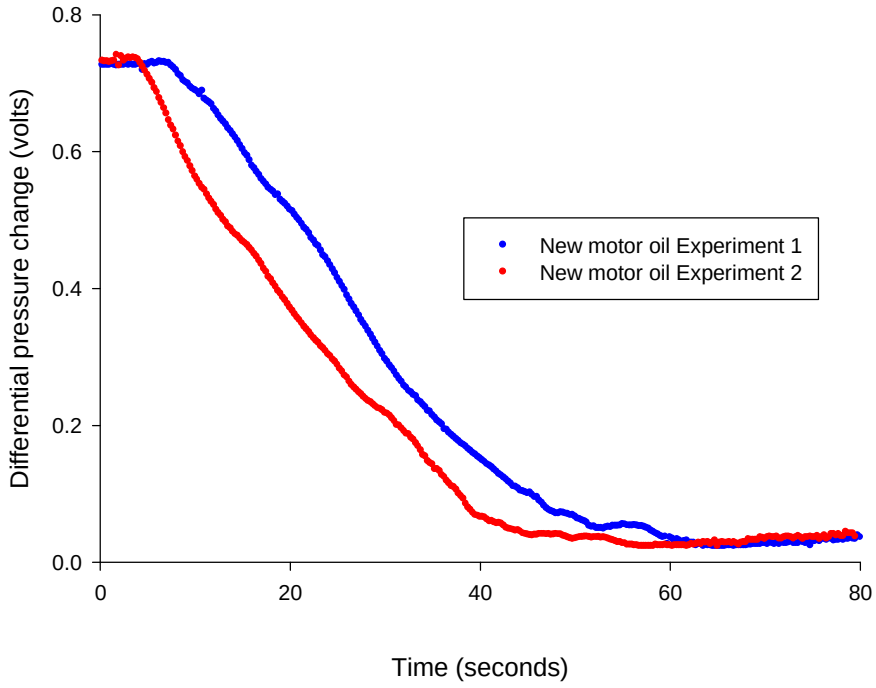

Figure 6.21. *Results from the data logger as new motor oil is freely poured into the oil interceptor.*

The experiments for both the new motor oil and DERV were repeated, this time the oils were freely poured into the interceptor and the output voltage was recorded via the Labjack data logger. The results for the new motor oil are shown in figure 6.21, with similar results being seen for the DERV. The speed at which the oil was poured into the interceptor effected the time it took for the monitor to eclipse the optical signal and reducing the output voltage to zero or near zero.

6.4 Trials at Andel Ltd

The diaphragm fibre optic detector was assessed at Andel Ltd. Again, as with the pressure tubing detector, the large 100 L interceptor was used. The probes of the diaphragm fibre optic detector were again placed at ~5 mm and 255 mm below the water/air interface for the upper and lower probes respectively. The detector was given an initial test by pouring oil into the interceptor, this recovered oil had a density of ~ 855-870 kg m^{-3}. Having demonstrated several times that the detector was set-up correctly an eight day trial was started. This trial reproduced a typical interceptor cycle, albeit shortened in time than would be expected. The sequence is shown below:

1. The interceptor has been emptied of all liquid.
2. Water was added.
3. Oil entered the interceptor.
4. The oil was removed from the interceptor.
5. Water was added.

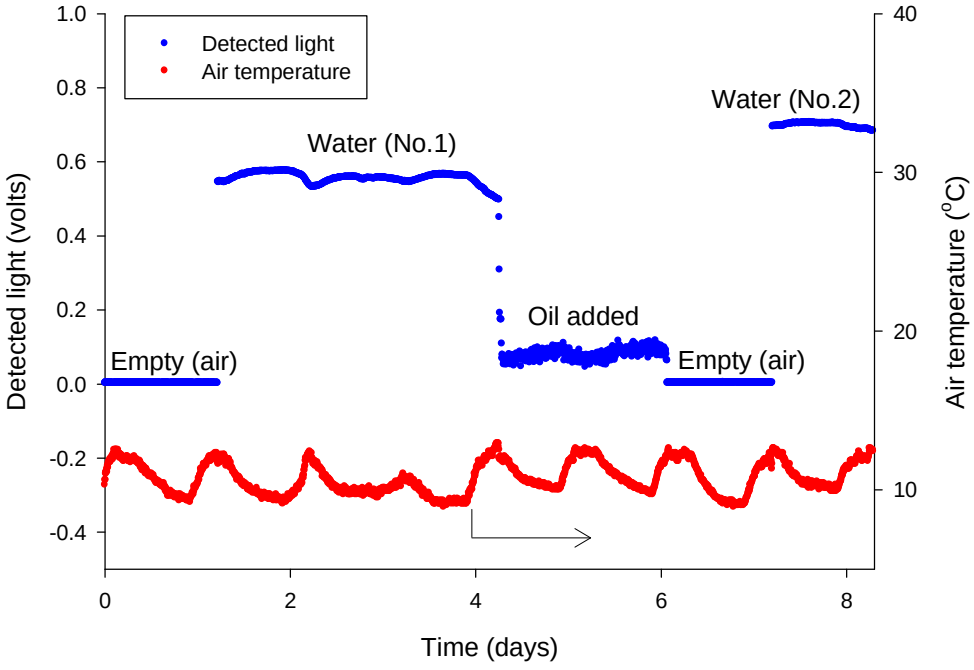

Figure 6.22. *Graph of an eight day trial of the diaphragm optical detector at Andel Ltd. This represents the events during the cycle of an interceptor, showing the response of the monitor. The air temperature is shown by the lower continuous line.*

Throughout the trial, the air temperature was also monitored. Of the two temperatures previously monitored with the pressure tubing detector, the air temperature was shown to vary over the larger range and was the most influential in affecting the detector. However, with the diaphragm fibre optic detector the daily fluctuation in the air temperature had little noticeable influence in the pressure readings. The results of this trial can be seen in figure 6.22.

This diaphragm fibre optic detector was capable of reporting one of two states:
1. The separator contains water only or water with some oil and the interceptor does not need further attention.

2 The oil level threshold has been reached and the interceptor requires the removal of the oil or that the liquid level is below the probes or a fault has occurred, these all requiring attention.

The detector response to the states of the interceptor is summarised in table 6.1. Here it can be seen that the response of the detector to the state of oil and that of air would produce the same warning. The situation of air around the probes would only occur if either the separation chamber had not been refilled with water once the oil had been removed or that there is a problem with liquid retention and the interceptor had a fault. With both these situations further attention would be required.

Medium around probes	Pressure differential	Light transmitted and detected	Warning required
Water	High	Yes	No
Part water/part oil	High/medium	Yes	No
Oil	Low	No	Yes
Air	Nil	No	Yes
Optic fibre/monitor fault	N/A	No	Yes

Table 6.1. *Summary of the various states occurring within the oil interceptor and the resulting response of the pressure diaphragm detector.*

This detector through the use of the upper and lower probes and similar to the double probe pressure tubing detector, has the ability to compensate for an unmatched liquid inflow to outflow. Thus, only the actual depth of oil within the interceptor is monitored.

6.5 Conclusions

The constant difference in the density between the oil and that of water, which was the basis of the oil detection methods in this chapter and the previous one, was able to produce repeatable results regardless of the oil types encountered. This was particularly noticeable in the trials at Andel Ltd where oil from unknown sources was used, both over short periods and through extended trials lasting several weeks.

The diaphragm fibre optic detector produced a distinct signal change in the presence of oil over that of water, which did not deteriorate with repetition. The diaphragm fibre optic detector does not have the complication of air leakage through the tubing. However, the diaphragm fibre optic detector was more complex to assemble than the equivalent pressure tubing detector, needing a higher level of precision for the alignment of components. In order to simplify construction, the possibility of utilising smaller core multimode fibre (e.g. 300 μm) should be considered. This would avoid the need for masks. Additionally, a larger diaphragm could be used to increase sensitivity if required.

Both of the detection methods which used the difference in density from water to that of oil to create a change in pressure complied with the constraints required by Andel Ltd. to produce an inherently safe oil detection technique.

7. Development of a portable microfluidic fluorimeter

The introduction of microfluidics over the last two decades has allowed chemistry to take place on a smaller scale than had been previously possible. Micro machining and other etching techniques have been used to produce micro-channels in glass and other substrates [104] and, coupled with the use of precision pumping mechanisms, small scale chemistry has been made possible. Microfluidics has enabled the synthesis of existing and new products in quantities smaller than through traditional methods, speeding up results and reducing wastage [105]. Similarly, assessment of small amounts of chemicals may also be scrutinised on a micro scale. Microfluidics may also be used to monitor other processes, here, they may be utilized to analyse other reactions or to assess ongoing environmental conditions. Microfluidics are often used within a laboratory in conjunction with existing equipment, with the microfluidic devices themselves requiring non-transportable or mains powered electrical supporting apparatus. In an analytical role, these reactions on this micro scale have the advantage of reducing the quantity of analyte and reagent consumed. Through the economic usage of chemicals, the use of more expensive reagents may be justified.

This research investigated the use of micro devices with regards to analytical systems where they can be used to monitor events as opposed to being used for the synthesis of materials. This chapter examines the requirements for a self contained, stand alone, analytical monitor. Such a system would be capable of studying the concentration change of particular individual species of analyte, found in water, through the regular analysis of samples drawn from that body of water. Here, the method of fluorescence has been specifically used for this automated portable monitor. The pheromone glutathione has been chosen as the model analyte for this research. Unlike the macro amounts of oil found within an interceptor, this amino acid which dissolves in water may be found at background levels of several nano moles and increases to concentrations of tens of micro moles once released as a pheromone from particular invertrabrates to stimulate mass spawning. Being able to detect this pheromone would lead to an indication of the imminent spawning event which would be of marine

ecological interest. It is the ability to detect this increase in concentration which is the goal of the development of a portable monitoring system incorporating microfluidics.

7.1 Glutathione

Glutathione has been used as a model compound for the fluorimeter within a microfluidic system, where the excitation wavelengths are in the UV region. As glutathione does not fluoresce without the addition of a fluorophore, experiments were carried out to determine the conditions that would be favourable for portable automated analysis. This section is an overview of the amino acid, glutathione, its synthesis, functions and detection. High levels of glutathione have been associated with the initiation of mass spawning of some marine invertebrates [106] and the use of an in situ analyser could help predict and monitor this occurrence. This study examines the use of *ortho*-phthalaldehyde as a reagent and its reaction with glutathione to form a fluorescent derivative as an indicator of increased concentrations of the thiol in water.

Glutathione is a low molecular weight amino acid, playing a major and varied role from a cellular to an organism level, serving a number of biological functions. Importantly this tripeptide molecule contains a thiol group (a sulphur and a hydrogen atom attached directly to a carbon atom) to help the cells in antioxidant defences. Glutathione ($_{L}$-γ-glutamyl-$_{L}$-cysteinyl-glycine, GSH) is present in animal cells, at concentrations up to 12 mM per cell [107]. Most of the cellular GSH being present in the cytosol, 85 - 90 % [108] and the rest being located in organelles, particularly the mitochondria. GSH is also present in bacteria and most plants cells [109]. GSH is found mainly in its reduced form, sometimes being referred to as reduced glutathione, but is also found in lower levels as oxidised glutathione (glutathione disulfide, GSSG). Collectively the GSH and GSSG are referred to as total glutathione. The determination of the concentration of GSH has been assessed through several methods including high performance liquid chromatography (HPLC), capillary electrophoresis (CE), nuclear magnetic resonance, chemiluminescence and fluorescence [110]. Levels of detection can be as low as pico moles [111], however many of these techniques are laboratory based methods which are not suited for portable systems.

7.1.1 GSH synthesis

The synthesis of GSH occurs within cells from three amino acids, Glutamate (glutamic acid, Glu), Cysteine (Cys) and Glycine (Gly). Cysteine contains a thiol group and can undergo redox reactions, when oxidised it can form cystine (two cysteine molecules joined by a disulphide bond). Glycine is a non-chiral amino acid and is the simplest of the 20 standard amino acids.

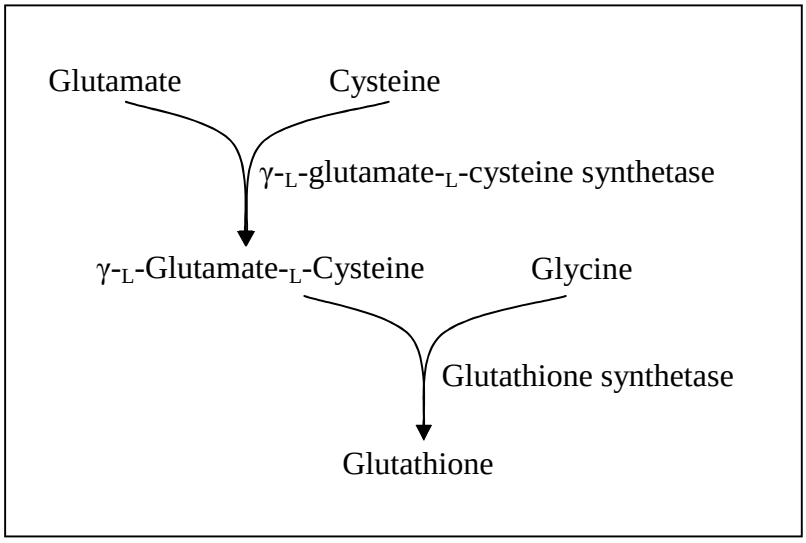

Figure 7.1. *The pathway for the synthesis of glutathione from three amino acid substrates.*

Two cytosolic enzymes are required to synthesise GSH in two separate sequential steps. The two enzymes γ-L-glutamate-L-cysteine synthetase and glutathione synthetase require the use of adenosine triphosphate (ATP) for each step and this is outlined in figure 7.1.

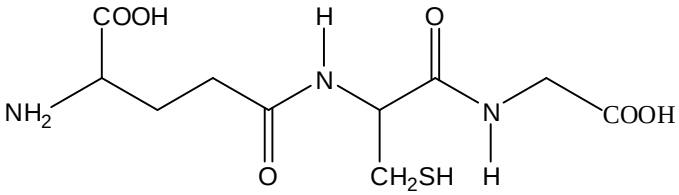

Figure 7.2. *Chemical structure of glutathione.*

The production of GSH occurs in virtually all cells. In the γ-L-glutamate-L-cysteine synthetase reaction, the γ-carboxyl group of the glutamate reacts with the amino group of the cysteine to form a peptide γ-linkage which protects the GSH from hydrolysis [108]. The product of the first step, γ-L-glutamate-L-cysteine, may also be a

substrate for other compounds but the cellular process favours the formation of GSH when it is required. Figure 7.2 shows the chemical structure of GSH [112].

7.1.2 Functions of GSH

The role of GSH is varied being intracellular, intercellular and also in the environment outside the organism, for purposes of cellular protection metabolism, transport and as a pheromone. Within the cell, GSH has the ability to reduce oxidative damage by acting as a redox buffer as oxidants and reactive oxygen species (ROS) can damage a range of cellular components. GSH also enhances the functional ability of other crucial antioxidants such as vitamin E and C [113]. Sources of these ROS can be from the cells own metabolic actions, particularly from the mitochondria or from xenobiotics.

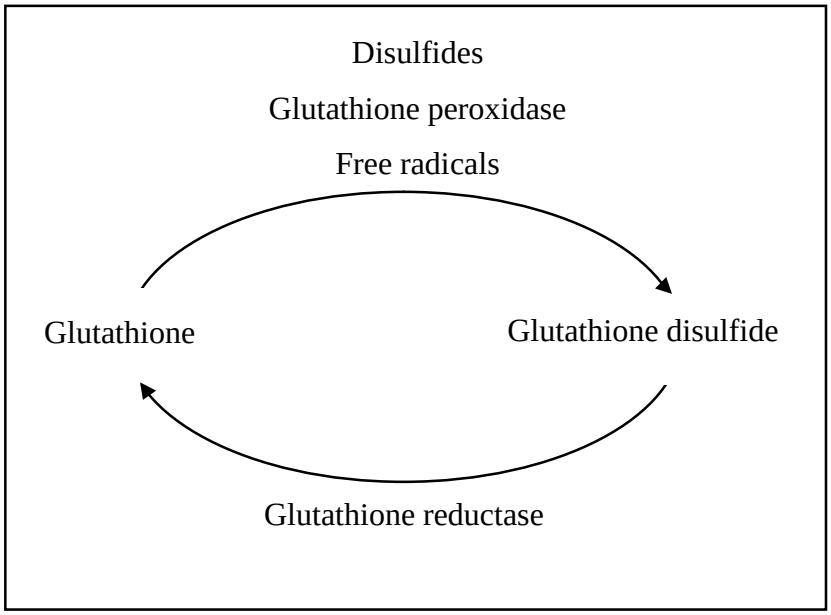

Figure 7.3. *The cycle of the oxidation of GSH and the reduction of GSSG.*

During detoxification of the ROS, the cells endogenous antioxidant, GSH, is oxidised to form GSSG. During this process GSH donates the thiol hydrogen from its cysteine component and so oxidizes the GSH, thereby GSH forms a disulfide link with either another molecule of GSH to form GSSG or with another protein thiol to form a mixed disulfide. These mixed disulfides may be also be reversible but in some instances may lead to irreversible oxidative inactivation of GSH and oxidative injury to the cell [114]. GSSG is converted back to GSH exclusively within the cell [109], GSH is not consumed during the process but recycled. The process is reversed by the enzyme

glutathione reductase with nicotinamide adenine dinucleotide phosphate (NADPH) acting as the electron donor.

Figure 7.3 shows the cycle of GSH and GSSG. Reduced GSH is a major thiol present in cells, with total cell concentrations of 0.5 to 12 mM, mainly found in the cell cytosol [108] but at the higher concentrations in the mitochondria [113]. GSSG can be around 1% of total glutathione [115], and can be an indicator of oxidative stress if levels are higher [109]. Figure 7.4 shows the chemical structure of GSSG [112]. In the cytosol the concentration of GSSG is around 1%, but may be in higher concentration in some of the organelles and can be found to be up to 25% in the mitochondria in granulocytes (a category of white blood cells) [115].

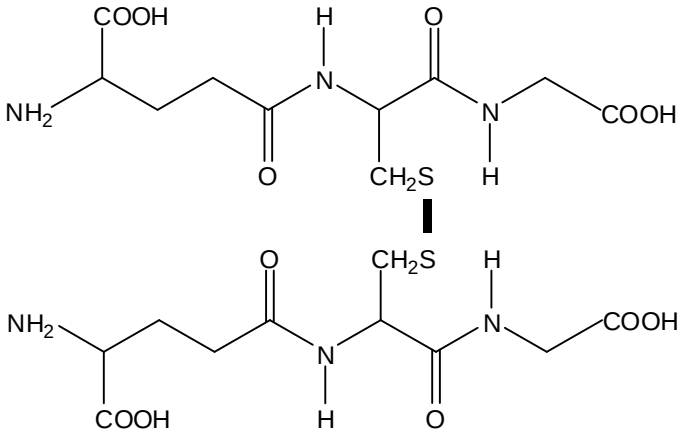

Figure 7.4. *Chemical structure of GSSG.*

GSH allows Cys, an important source of sulphur, to be stored and transported around the body, free Cys would otherwise be quite toxic [107]. Deficiency of GSH contributes to oxidative stress, which plays key roles in the pathogenesis of many diseases [108]. Outside the organism, GSH is used as a pheromone and it is this particular use on which the interest of this investigation centres.

7.1.3 Thiols as aquatic pheromones

The use of thiols as chemical signals has been studied for many years as they are known to be utilised by a number of species of marine invertebrates. Depending upon the species, pheromones can be used to attract an individual mate, or several of the opposite sex as well as sending out a general signal for synchronous spawning [106]. The signal for synchronous spawning may be used to trigger a single species of a local population or may activate mass multispecies spawning. These different types of sex pheromones

may well themselves be coordinated from environmental signals such as lunar periodicity, photoperiods (daylight lengths) or temperatures.

GSH is associated as one of these sex pheromones and is a precursor for another pheromone nereithione (cysteine-glutathione disulfide, CSSG), the latter being able to activate sperm release in *Nereis succinea,* at levels less than 1 µM [116-118]. Concentrations of CSSG along with GSH and GSSG in coelomic fluids are released by the females of this species during mass spawning.

Thiols are found at low background levels in all sea water. In coastal waters around the North Sea they range in concentrations from 0.70 to 3.60 nM [119] and may vary over relatively short distances. These thiols along with other dissolved organic carbon (DOC) are likely to be of marine origin rather than from terrestrial inputs. Of these thiols, glutathione occupies a large proportion of the total. Dissolved GSH concentrations can vary seasonally probably due to in-situ biological activity [120]. Thiols in water are released not only from invertebrates but are also from all biological marine life, however not necessarily as a pheromone. This is particularly the case for phytoplankton, which is abundant in shallow waters, accounting for a continuous and renewed background level of thiol.

Organic compounds, and in particular thiols, are photolyzed in the relatively shallow seas [121], possibly accounting for the higher levels of carbonyl sulphide in coastal waters [119], this being an important source for inorganic sulphur and part of the global sulphur biochemical cycle. Temperature, pH and oxygen levels also have an effect upon the process [122]. This photochemical oxidation of thiols by sunlight can produce a break down of 30-50% per day when exposed to sunlight and under incubator experimental conditions produce a half life of ~ 3 hours [123], thus emphasizing the need for field analysis of such chemicals.

7.2 Field deployable analytical systems

The use of in-field monitors allows real time data acquisition for events that would otherwise require post event analysis of the sample. Such a time delay allows the possibility of the analyte being subject to degradation, corrupting the results [124]. GSH for instance, would be subject to auto-oxidation without a blocking agent [110]. For a total analytical system (TAS) to be used as a detector to monitor environmental events, particular criteria need to be considered; analysis technique, location and length of operating time being major considerations. It follows that pressure on the power supply, chemical quantities and overall reliability of the system increases with extended detection time. Through miniaturising the analysis technique, less demand is placed on both of these, however miniaturisation can have its disadvantages, either through limits of detection [125] or dependability of the components. In addition, a robust and suitably packaged device would be needed for its own protection and also to provide access for service of the chemicals and data retrieval.

Several detection techniques have been used for in-field chemical investigations. Electrochemical techniques have detected thiols [126, 127] and GSH [128] through voltammetric measurements, these detection methods requiring high maintenance of the electrodes. However, such instruments have been used to collect data for up to several hours from coastal waters whilst measuring trace elements [129]. The reliability of the electrodes makes the voltammetric technique unsuited for long term detection.

Optical analysis can be a more dependable technique when the opportunity for maintenance is limited. GSH, similar to many short peptides, is not suited to absorption detection as detection at shorter wavelengths is feasible but less specific as other materials also absorb in this region [130], though the necessary purity of sample needed would be difficult to achieve in a portable system. However, fluorescence detection of GSH has the advantage of being both more selective and sensitive than UV absorption detection [131]. With no aromatic ring, GSH does not possess a strong chromophore and the introduction of a chromophore can improve analysis through fluorescence. For GSH detection specific chemicals that react with thiols, such as N-ethylmaleimmide and monoiodoacetic acid have, in laboratory conditions, obtained quantifiable analysis below µM concentrations [132].

When continuous assessment of an analyte is sought, flow injection analysis (FIA) can generate automated analysis through constant sampling. Such a technique has been used for several decades both in the laboratory [133] and for field monitoring [134] with various optical detection methods. Through the use of FIA, consumption of reagent will depend upon the set-up and may be as low as tens of µL per sample [135], however larger quantities are often required. Variations of FIA have been used, sequential injection analysis (SIA) offering several advantages such as lower frequency of maintenance and consuming less analyte and reagent [136, 137], other techniques have used fluid manipulation based on flow injection [138]. However, continuously drawing samples from open water to pass through a miniaturised reaction coil may reduce the unmanned deployment time due to a high demand upon the filtration system. Microfluidic devices aim to further reduce chemical consumption, reducing demand upon both analyte and reagent [13]. Microfluidics have been shown to be capable of producing in-field automated water monitor systems to generate results in a relatively short period of time, the tests also being able to be repeated as frequently as desired whilst using small quantities of reagent [139, 140].

The microfluidic device can be made from most appropriate materials that are inert to the liquid passing through and capable of having channels formed. Glass and plastics of various types are commonly used [13], providing low cost devices being suitable for disposable use [141]. The other considerations when using these devices with optical detection are that they are compatible with the optical spectra of both the excitation and emission wavelengths. For example, fluorescence analytical systems using UV excitation light may inadvertently generate fluorescence from the glass or plastic structures.

With any system that has been condensed to produce a portable package, there is a compromise between the qualities obtained from laboratory apparatus results against the convenience of transportable equipment. However, placed within its analytical range, a micro TAS (µTAS) would be capable of producing meaningful results.

7.2.1 Fluorescence detection of GSH

As the role of GSH is fundamental to most cells and other processes, consequently significant study of this amino acid has been made for many years. In different analyses of GSH both its presence and the concentration have been measured. As a result, a

variety of different methods have been established dependant upon requirements, however this particular compound is suited to detection through fluorescence techniques if attached to a chromophore.

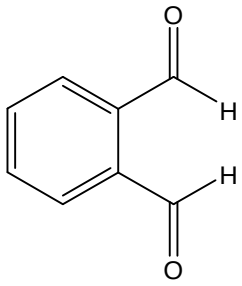

Figure 7.5. *Chemical structure of OPA*

GSH produces no fluorescence without adding an agent to form a fluorogenic derivative [130]. To study GSH a fluorophore group needs to be introduced, preferably one which reacts with the thiol group and is selective insomuch as it does not create auto-oxidation of the GSH during analysis. The compound *ortho*-phthalaldehyde (OPA), a dialdehyde attached to a benzene ring, is non-fluorescent was reported in 1966 [142] as a fluorometric technique being sensitive and highly specific for GSH. Figure 7.5 shows the chemical structure of OPA. OPA does not normally react efficiently with peptides, but in the presence of GSH, which provides both a thiol and an amine, will strongly fluoresce [143] and rapidly forms a fluorescent derivative [144]. For OPA analysis of amino acids, with the exception of GSH, tryptophan and tyrosine, the addition of a further chemical (2-mercaptoethanol [145, 146] and hydroxypropyl-β-cyclodextrin [147] being just two) is required to significantly enhance fluorescence [148]. For whole cell analysis, γ-$_L$-glutamate-$_L$-cysteine synthetase which also fluoresces with OPA can hamper the results for GSH determination [131]. Derivatization of GSH and OPA is pH dependant for maximum fluorescence, but with a pH that can vary from 9.5 to 12.0, a relatively broad range of pH can be used. Peak fluorescent response within this range is reasonably responsive [115, 149] and slowly decreases below pH 9.0. GSSG is destabilised below pH 12.0 and as such this pH can assess total glutathione [115]. Both GSH and GSSG have an optimum excitation wavelength (λ_{ex}) ~ 340 nm and a peak emission wavelength (λ_{em}) ~ 422 nm [143], but useful and consistent results have been achieved from broader excitation wavelengths [131]. GSH possess the sulfhydryl and amino groups that are able to react with the aldehyde groups of OPA to produce the fluorescent isoindole [150]. Fluorescence from the GSH OPA isoindole produced a

linear response between the concentration of GSH and the peak fluorescent intensity through the range of 0.1 pM to 10 nM GSH [111, 131, 151]. However, there have been indications of destabilising effects when excess OPA has been used [152].

Cysteine on its own, does not form an efficient fluorogenic derivative but the precursor of GSH, γ-$_L$-glutamate-$_L$-cysteine, reacts with OPA to form a cyclization structure to act as a fluorophore [153]. Figure 7.6 shows the tricyclic isoindole of GSH and OPA [130]. This derivative is reported as not being stable for the long term, being prone to hydrolysis in aqueous solution and attacked by excess OPA [147], although it is stable for several minutes. However, depending upon the detection method employed, such confines may be overcome. Limiting factors brought on about the quenching of the fluorophore can restrict the use of fluorometric techniques particularly where whole cell observations are carried out in certain organs [143]. Restricting interfering reactions or the use of buffer assays can avoid, limit or delay these inhibiting effects.

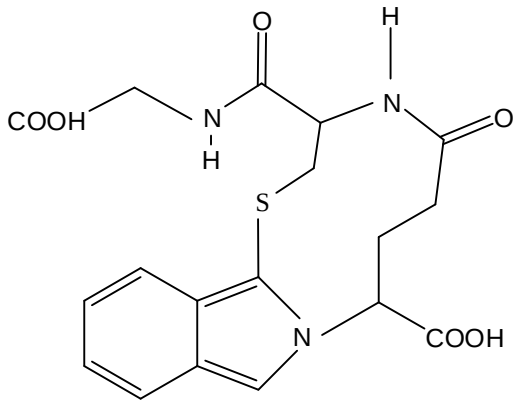

Figure 7.6. *Chemical structure of the tricyclic isoindole of GSH and OPA.*

Monochlorobimane (MCB) is a widely used fluorophore that is specific to amino acids with a thiol functional group, capable of detecting low concentrations of analytes to nano mole levels. For fluorescence, λ_{ex} 380 nm and peak λ_{em} 470 nm is at longer wavelengths to that of OPA [113]. There are several other fluorophores, however some require specific temperatures and are more suited to laboratory conditions. The use of a fluorimeter or fluorescence reader [148] necessitates the preparation of a purer analyte to avoid detecting other amino acids.

Both OPA and MCB are commonly used to assess GSH in a range of situations, each with their own suitability. For this study, OPA does appear to have several advantages over that of MCB, as follows; (i) Incubation of MCB is much longer, 15 minutes as

opposed to 1 minute for OPA, (ii) OPA is less pH sensitive. (iii) MCB is ~ 8 times more expensive, (iv) Photodegradation products of MCB can fluoresce, interfering with GSH determination. For these reasons, for the initial investigations, the choice of using OPA was made.

7.2.2 Mixing within the micro device

In a microfluidic device where the analyte is to be monitored indirectly, that is through a reaction with another chemical, the use of micro-channels can create conditions where two liquids can be brought together allowing mixing to occur. In the case where liquids are introduced separately and travel through the micro-channels, mixing through diffusion would be initiated at the junction where these chemicals meet. When mixing occurs through diffusion, these devices are generally referred to as micro-reactors, two such typical examples are shown diagrammatically in figure 7.7 and are usually several centimetres across.

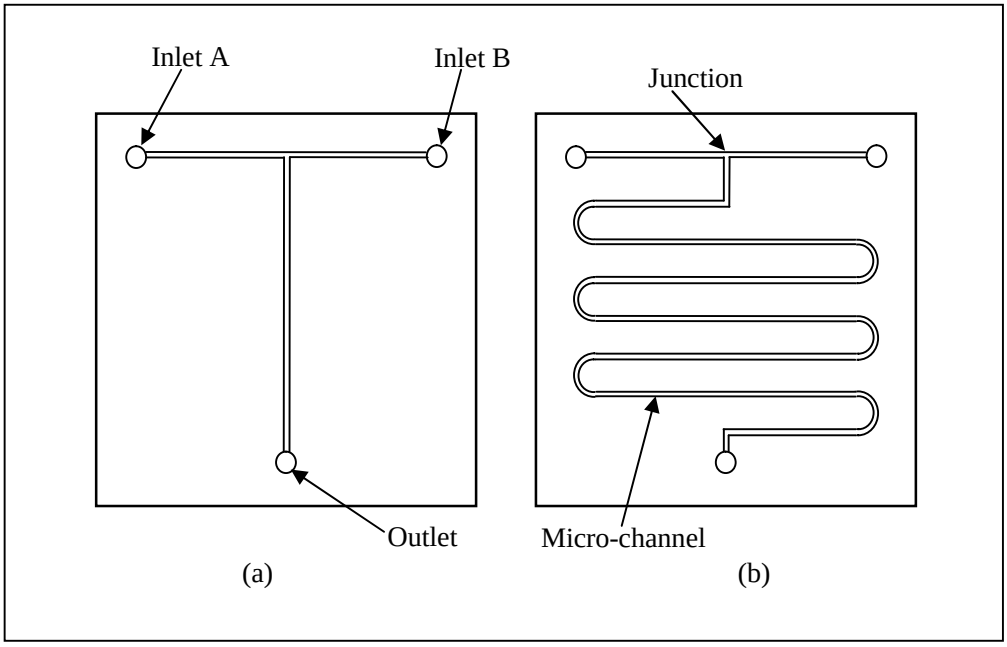

Figure 7.7. *Drawing of two micro-reactors with different channel path lengths; (a) straight and (b) serpentine.*

The channel designs are in general specific for each particular type of analysis. The length and path of the channel is determined by several factors; diffusion time required, profile dimensions and flow speed being the major ones. When the mixing time is fast or the flow rate is slow, a short channel, as in figure 7.7 (a) would be appropriate, whereas if the mixing time is slow or the flow rate was faster then a longer channel in

the shape of a serpentine (b), would allow a longer residence time within the channel. When the chemical is also analysed within the micro-reactor, the residence time may be increased so that after mixing the isoindole may be studied via fluorescence.

In macro-scale chemistry, mixing of chemicals is accomplished through turbulence (stirring or other motion) and diffusion. Within a micro-reactor, laminar flow dominates and turbulence is limited, the Reynolds number, Re, of the system is an indicator of the stability of the flow. The determination of whether the liquid flow within the channel is turbulent or laminar can be calculated through equation (7.1) [88], where D_c is the cylindrical diameter, ν the velocity, ρ the density of the liquid and η the dynamic viscosity of the liquid. The internal surface of the channel is presumed to be relatively smooth and regular in its profile. A Re of ~ 2300 is regarded as a benchmark where above this figure laminar flow begins to break down and turbulent flow begin [102].

$$\mathrm{Re} = \frac{D_c \nu \rho}{\eta} \tag{7.1}$$

In order to calculate a Reynolds number for a typical micro-channel where the cross sectional area is not round, an effective diameter can be used. This hydraulic diameter, D_h, derived from equation (7.2) [154] may replace D_c, to find Re.

$$D_h = \frac{4 \times \text{cross sectional area}}{\text{wetted perimeter}} \tag{7.2}$$

To find the Re for a micro-channel of dimensions 170 µm wide and 60 µm deep, and where the analyte and reagent are dissolved into water and where two similar solvents are mixed, is shown below:

$D_h = 88.7 \times 10^{-6}$ m
$\nu = 0.04$ m s^{-1}
$\rho = 999.1$ kg m^{-3} [78]
$\eta = 1.139 \times 10^{-3}$ N s m^{-2} [78] (last two figures at 15.0º C)

This results in a Re << 100, indicating that the liquid passing through the channel has a laminar flow and as such mixing would occur by diffusion. Figure 7.8 [154] shows a graph depicting the transition from laminar flow to turbulent flow. In this example, from stationary the flow rate along the pipe increases over time, it can be seen that the transition may not always be smooth. Other factors such as bends and connections will

contribute to turbulence. Turbulent flow will not decrease the mixing time, however, turbulence will make it unpredictable.

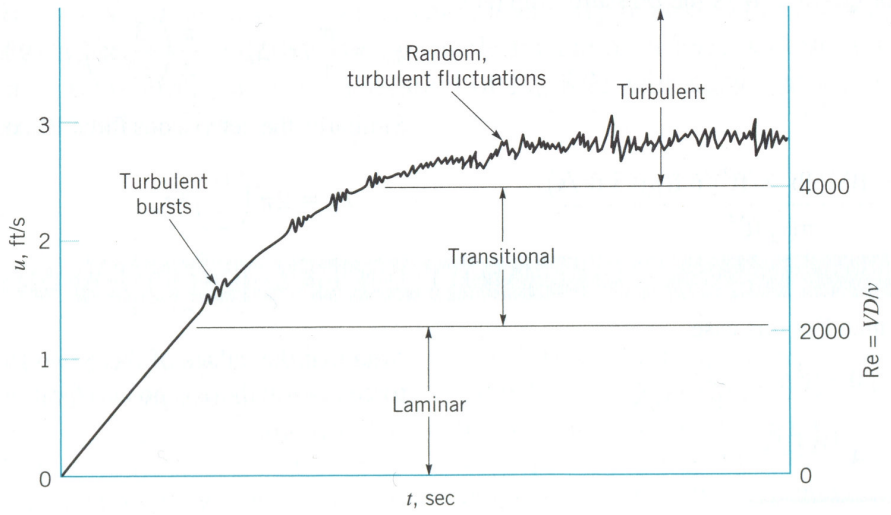

Figure 7.8. *Transition from laminar flow to turbulent flow in a pipe as the flow speed is increased over time. The two vertical axes indicate the flow speed and the Reynolds number. [154]*

The diffusion time, t, derived by equation (7.3) [155] is dependant upon L the distance (mean of half the width of the channel), see figure 7.9 and D the diffusion coefficient of the liquid. Initially the channel is filled by the two unmixed liquids, each occupying half the channel.

For diffusion to take place, molecules from each chemical are only required to travel half the channel width for full mixing to occur.

$$t = \frac{L^2}{2D} \qquad (7.3)$$

The diffusion coefficient of a solution is partially a function of the relative molecular mass of the diffusing substance and the solvent in which it is dissolved. In the case of glutathione (the larger of the molecules to be used) with a relative molecular mass of 307.33, is similar to sucrose (relative molecular mass 342) dissolved in water with a diffusion coefficient 5.7×10^{-10} m^2 s^{-1} [156]. Using this figure with a channel dimension L, at 52 µm, a diffusion time of ~ 2.4 seconds would be required. Thus with a flow rate of ~ 20 µL per minute (in this example it would result in a fluid speed of 44 mm s^{-1}), a travelling distance along the channel of ~ 100 mm would be needed to allow sufficient time for diffusion to occur. This would favour a serpentine channel configuration.

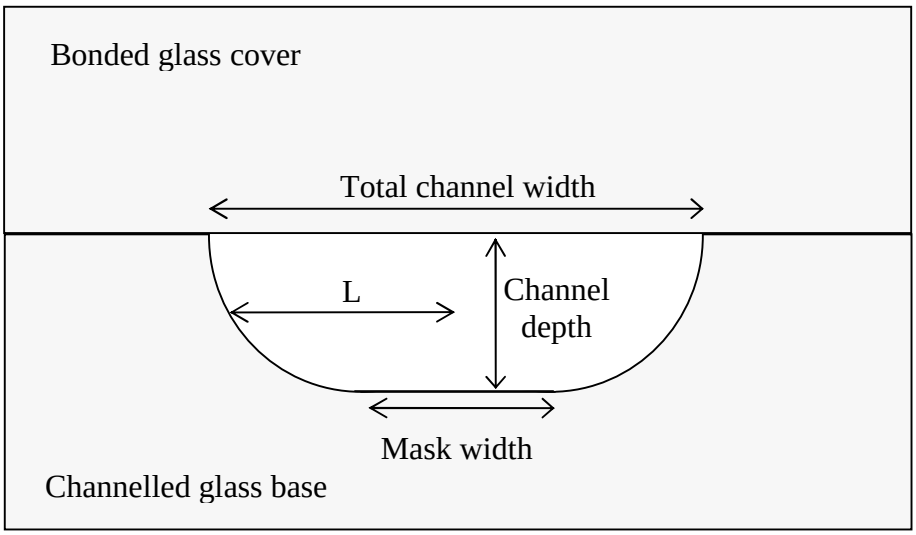

Figure 7.9. *Section through a micro-channel to show; the channel depth, total channel width, mask width and L, mean distance of half the width.*

7.2.3 Volumetric rate of flow and internal pressures

The fluid speed and channel dimensions are related to the volumetric flow rate. This flow rate affects the pressures within the tubing and micro-reactor, as such an increase in the flow rate will increase pressure gradient of the liquid within the tubing and channels. The consequence of high pressure is damaging to some types of tubing and may weaken joints that in turn can result in leaks. The pressure differential over the length of a circular tube of constant cross section can be expressed by the flow equation, commonly called Hagen-Poiseuille's law, and is given by equation (7.4) [154].

$$Q = \frac{\pi r^4 \Delta P}{8 \mu L} \qquad (7.4)$$

Where Q is the volume rate of flow ($m^3\ s^{-1}$), r is the radius of the tube, ΔP is the difference in pressure over the length of the tube, μ is the coefficient of viscosity and L is the length of the tube.

Ideally the flow rate should be adjusted so that the reagents achieve the residence time for diffusion to occur within the micro-reactor. However, there may be circumstances where the flow rate is required to be increased, such as when the tubing and channels need to be purged prior to performing a repeat analysis and it will be at these times when the pressure gradient surges. To achieve high flow rates whilst not unduly increasing the pressure gradient, larger channel dimensions would be needed. However, this would necessitate greater channel lengths to achieve mixing through diffusion,

which in turn would increase the volumes of analyte and reagent required. For a portable fluorimeter to maintain microfluidic capacities, tubing and channel dimensions need, where possible, to be kept to a minimum whereby chemical usage can be conserved.

7.2.4 Optical arrangement for light detection

In microfluidic devices the choice of optical components and the ancillary apparatus that is required to make the system work, creates the problem of how to position these parts into what would be a relatively small device but still achieving an efficient analytical tool. Many of these analytical detectors are laboratory based, whilst still examining the analyte within the chip, these detectors use adaptations of conventional equipment [157, 158], using non portable lamp and laser light sources [159]. Other systems have successfully replaced the large, expensive or complex bench top parts for compact, cheaper or more portable components [160]. The advantages of compact non laboratory equipment may inevitably have shortcomings as convenience has been traded against durability or detection limits. This section examines the various techniques used in micro-fluidics, with regards to optimising a system for portable detection.

To attain the most from the μTAS, the analysis of micro litre quantities of liquid requires an approach that optimises the whole analysis system by making efficient use of the limited reagent. It would be expected that for any analysis that requires a light source and in particular for fluorescence, then a relatively high powered light (as from a diode laser for example) would be preferred to that of a low intensity power source as may be found from an LED. Since, to a degree, the magnitude of the output signal is proportional to the absorbed excitation light and in turn that absorbed excitation light is proportional to the output power of that source. Thus, the significance of a high powered excitation light source is fundamental for detection at lower analyte rates. The fluorescence emission, F, is shown in equation (7.5) [17], is dependant upon the incident beam, P_o, the power of the incident beam after travelling through the medium, P, and the quantum efficiency of the analyte, K'.

$$F = K'(P_o - P) \qquad (7.5)$$

This simplified equation does not take into account such events as; saturation, bleaching and self absorption. However, a linear response may be obtained over a limited range,

which in turn will vary depending upon the detection technique and the particular set-up.

Simply shining the excitation light upon the analyte and place the detection system close by could well produce a usable result, however, this would not create the most resourceful use of the any system. Figure 7.10 [161] illustrates some of the on-chip detection configurations that can be accommodated for analysis.

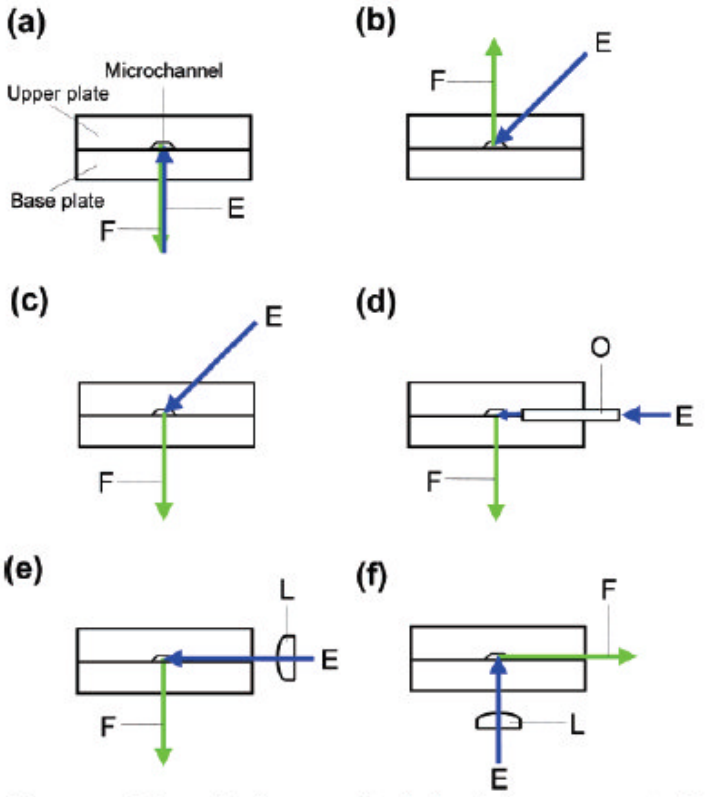

Figure 7.10. *Schematic diagrams of typical optical arrangements for microfluidic detectors: E, excitation source; F, detected fluorescence; L, lens; O, optical fibre*. [161]. *However, the lenses in (e) and (f) have been shown wrong way round.*

The position of the excitation light source will need to take into account the dimensions and shape of the channel or reservoir in which the analyte is situated. The excitation light may be delivered directly from the source, using if necessary mirrors or lenses or be delivered through fibre optics. Figure 7.10, (a) requires the use of a dichroic mirror to direct and ultimately separate the excitation and emitted light. Arrangement (b) and (c) both use off-axis excitation whereby the recovered emitted light can be detected without the use of a dichroic mirror. In (d), (e) and (f) an orthogonal approach is used with a similar advantage over (a). The micro-channels within a micro-reactor are generally positioned in a single plane and as such, directing the excitation light onto the micro-

channels from the side as in (d) and (e) would require imaging the light onto a 2-dimensional plane to optimise excitation light usage. Similarly, the positioning of (f) will only detect a small proportion of the emitted light.

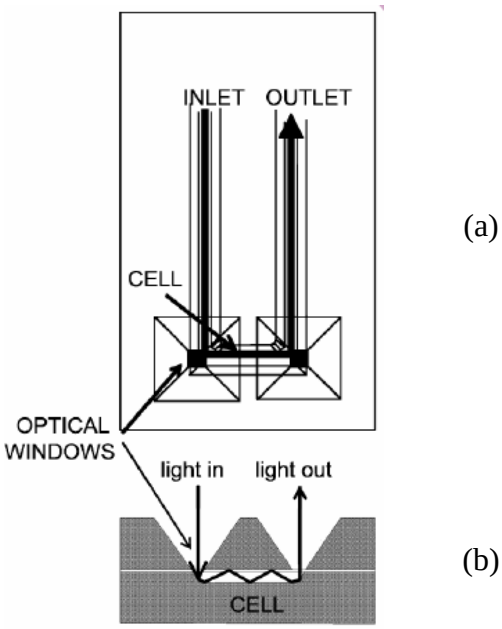

Figure 7.11. *Diagrams; (a) of a flow-though micro-channel used as a detection cell to determine absorbance of liquid, (b) is the cross section showing the channel as a light guide* [162]

In micro-fluidics where the analyte volume is limited, optimising the optical set-up for the restricted quantity of liquid is important in producing an improved response. Positioning the excitation light into a location that has the greatest path-length or by enlarging the path-length through which the beam passes, would allow a greater opportunity for the beam to be absorbed by the analyte (this is also concentration dependant). Through this, either a larger fluorescence response could be expected or a similar response from using a lower powered light source. The technique, shown in figure 7.11 [162], of increasing the path-length has been used to improve the sensitivity for absorption detection. The micro-channel itself can further enhance the efficiency of the excitation light by waveguiding the light along the channel through strategic positioning of the light source, directly or via fibre optics [163, 164]. Secondary advantages from this use of waveguide manipulation, for fluorescence, are that the excitation light is less likely to be scattered and inadvertently travel towards the detector.

Incorporating fibre optics into the micro-reactor can place the excitation light directly and accurately into position against the micro-channel [165, 166]. Similarly, fibre optics may also be used to transfer any resultant light to the detection system. The channels or grooves for these fibres can be incorporated into the manufacturing process of the micro-reactor. Other advantages of using fibre optics are that the excitation light source and the detector need not to be placed immediately adjacent to the micro-reactor [167] where space is restricted or the process requires particular conditions, such as high temperatures [168, 169]. Efficient use and collection of excitation and emission light has led to the use of integrated lenses [170, 171] but these greatly increase the complexity of micro-reactor manufacture and as such are not commonly used.

Light losses occur at interfaces through reflection and scattering [162], similarly light may be attenuated as it travels through lenses and filters. The use of optic components, whilst they are at times necessary to deliver an effective system, may ultimately be non-productive to the overall result. A close coupled system can be simpler to construct and where the optics and system allows this to be used it can prove be the most appropriate arrangement [21].

Whereas delivering the excitation light effectively to the required location through the use of a close coupling, lenses or fibre optics, the process of collecting the emitted light cannot always be achieved as efficiently. As fluorescence is emitted in all directions, to achieve a complete collection of the light into the detector is commonly unachievable. Efficient recovery of the emission light will improve the lower detection limit for any fluorescence system. Enhancement of emission light detection has been achieved through a reflective coating, creating a mirrored surface on the micro-reactor [172] increasing the recovered signal by over 100%. Such coatings can be produced through several techniques. Aluminium foil placed against the micro-reactor will redirect light that would otherwise be lost, however, there are more efficient techniques that are in direct contact with the micro-reactor, such as silvering the glass through the mirror reaction [173] or vacuum evaporation and deposition of aluminium.

In addition to optimising the optical arrangement of the light source and detector, further enhancement of the signal to noise ratio may be achieved through the use of a lock-in amplifier. Also called a phase sensitive detector, this system of signal enhancement can effectively reduce the effect of back ground noise. The source of

which can be from the electrical system itself, environmental or from unwanted stray light entering the detector. Through modulating the light source, either by chopping the beam or electrically switching the light on and off, at a fixed frequency (from several hundred to a thousand hertz) and with a synchronising reference, the detected signal can be isolated from the bulk of the background noise. LEDs are suited to electrical modulation without compromising their durability, allowing this type of signal enhancement to be incorporated into a system without adding to the overall size. This method has been used to produce an integrated detection system for an on-chip fluorescence detector under ambient light [160]. However, if the background noise was not detrimental and the fluorescence signal was low, then modulating the excitation light would inadvertently produce a lower emission response.

7.2.5 Pumps and filters

Within the μTAS low flow rates are needed, requiring pumps capable of delivering small quantities of liquid [141] and depending upon the analysis, microfluidic devices are normally expected to convey quantities from less than one to several tens of micro litres per minute [174].

Pumps can be classified into two groups; dynamic (such as centrifugal pumps) and displacement pumps. The latter being the most common used for micro-reactors [175]. Peristaltic pumps, which fall into this group, provide a relatively pulse free fluid flow and can continuously feed from a liquid reservoir, thus being suitable for sustained use. The rotary head, rollers and tubing are shown in figure 7.12. These pumps have the advantage that they can reverse the flow if required [176]. Syringe pumps which can accurately deliver liquids at various desired flow rates, are commonly used in laboratory based experiments, however these were considered to be unsuitable due to their limited capacity.

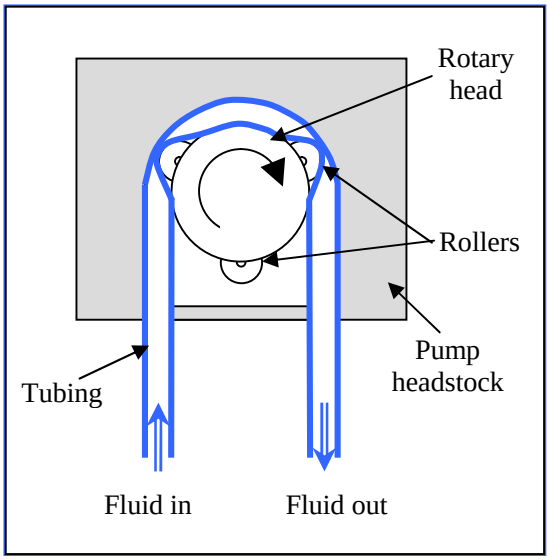

Figure 7.12. *Schematic diagram of a peristaltic pump, showing the rotary head, rollers, tubing and the direction of liquid flow.*

Collecting liquid samples from open water and pumping them through a micro-reactor requires a filtration system, not only to avoid blockages but also to reduce the organic particles which may inadvertently effect the reactions and results. Filters may be fabricated if needed for specific tasks [177], however cheaper mass produced purchased membrane filters have been extensively used to filter water for both flow injection [7, 178] and microfluidic analysis [179]. The choice of filtration cartridges, which are manufactured from several types of membrane material and with a number of pore sizes, will need to be suitable for both chemical compatibility and particle size filtration. Pore sizes from 0.2 to 0.45 µm have been incorporated for inline water filters [124, 179]. The life of such filters will depend upon both the amount of material to be removed and the water volume passing through them, a larger sized pre-filter would increase the useful lifetime of any final filter system.

7.3 Conclusions

This chapter discussed glutathione, its role as a pheromone and the use of fluorescence in its detection. The link between the release of the pheromone and the advent of spawning creates a means of detecting such events. This research concluded that the detection of GSH based on the technique of fluorescence would be appropriate in developing a portable detection system. Through the use of microfluidics, chemical consumption per analysis can kept to a minimum, further enhancing the duration for an automated system. The limitation of a self contained power supply upon the optical,

detection and pumping systems required it to be used efficiently. However, the balance between the liquid volumes and the flow rates required could potentially create problems due to pressure gradients along the tubing, which could be aggravated by a build up of debris within the micro-channels.

Whilst this monitor has been developed to assess glutathione, this being used as a model analyte, the process outlined a pattern of research that could be adapted to produce a monitoring system suited to other chemicals. The subsequent chapter follows the research for the μTAS.

8. Fluorimeter experimental and results

This chapter presents the experiments leading to the development of an automated portable fluorimeter, capable of detecting concentration changes for a specific analyte dissolved in water. The research starts with experiments which examined the analyte and reagent chemistry with regards to its fluorescence. After these initial findings, the research proceeded to the development of the liquid movement through the microfluidic system. This flow through technique needed to be capable of performing repeat analyses over a period of time, dealing with pumping of the various liquids, mixing of the chemicals and purging the tubing and channels in preparation for the following assessment. Finally the μTAS is tested using both prepared purified water samples and spiked sea water.

8.1 Instrumentation for the portable fluorimeter

During the development of the fluorimeter various combinations of components were used, including different arrangements for the pumps, valves, detection cell and microfluidic channels. These experimental arrangements led to the placement of the apparatus into a compact and portable unit. This section discusses the components that have been used in the experiments and the portable fluorimeter.

8.1.1 Microfluidic devices and detection cells

Several different micro-reactors were used in the experiments, these were made at the fabrication unit within the university, from borosilicate glass. This glass, as previously discussed, was unsuitable to be used with the UV excitation light, as such the fluorescence analysis was undertaken using fused silica cuvettes as samples holders, later to be replaced by purpose made, flow through, fused silica detection cells. The three micro-fluidic devices are shown in figure 8.1 and the dimensions are listed in table 8.1. The flow rate in μL min^{-1} for diffusion to occur is also shown, as expected, the longer channel lengths allow a faster volumetric flow rate.

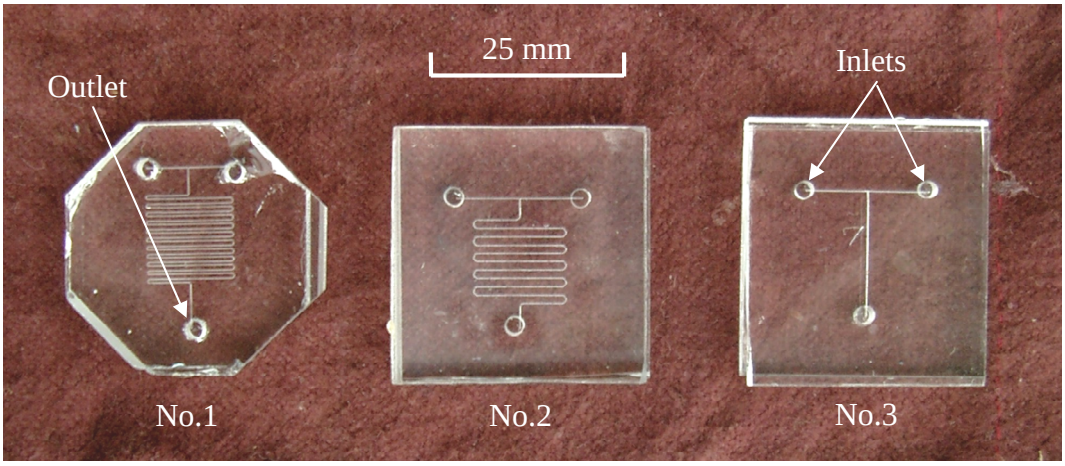

Figure 8.1 *Photograph of the three micro-reactor devices. No.1 and 2 have serpentine channels and No.3 has a Tee channel arrangement.*

The flow through detection cells, made from fused silica capillary tubes, had an ID 2.0 mm, OD 4.0 mm and were ~ 25 mm long, with an internal volume of ~ 78 µl. The analyte, after analysis, was removed by purging with water which flushed out the contents of the cell into the waste container.

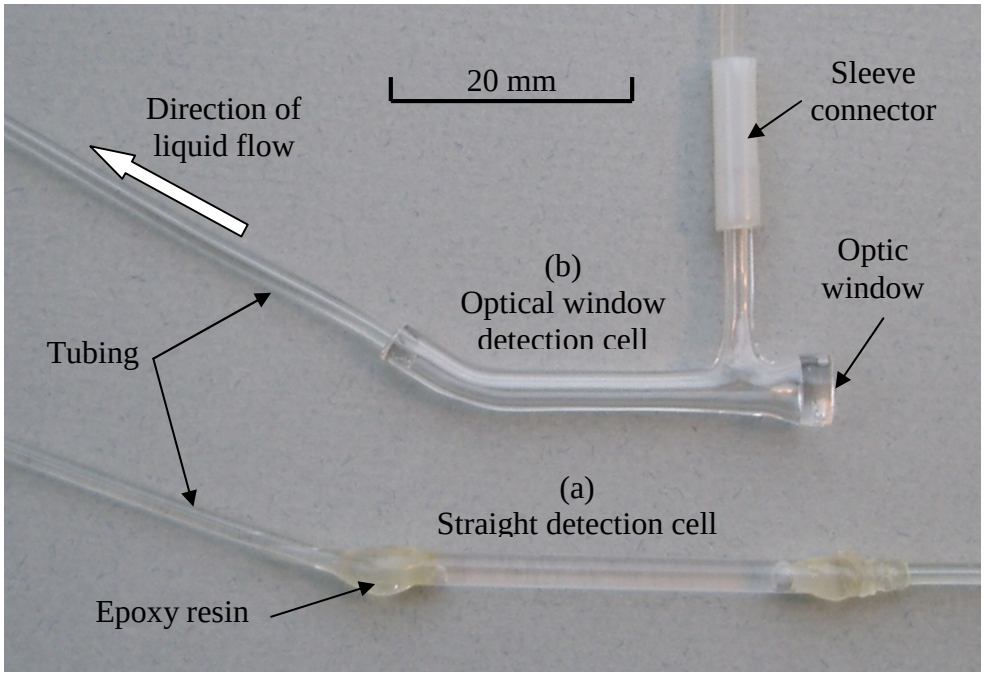

Figure 8.2. *Photograph showing two fused silica detection cells connected to tubing. The straight detection cell (a) has the tubing fixed with epoxy resin, the direction of flow is indicated for the optical window detection cell (b).*

Figure 8.2 is a photograph of the two flow through fused silica detection cells. The straight detection cell (a), was used for the majority of the experiments. The tubing was attached using epoxy resin. This cell was positioned so that the LED excitation light

illuminated the analyte from the side, whereas the optical window detection cell (b), was used later to assess improvements in the detected fluorescence signal. This was made so that the LED illuminated the detection cell from the end, via the optical window, thus increasing the illumination efficiency of the excitation light. However, this second cell was not fully explored due to time constraints.

8.1.2 Pumps and valves

Two pumps were used to transport the analyte and reagent, one of which was used to transfer liquid in both directions. The miniature peristaltic pumps, P625/275.143 were manufactured by Instech Laboratories Incorporated, PA, USA with a gear ratio of 275:1 which accommodated the volume range required and, through speed control, allowed a volumetric flow rate of 20 to 200 µL min^{-1}.

To assist the transfer of several chemicals needed, including water for flushing the system, three valve blocks were necessary. For this, two way miniature valves, LFYA1216032H manufactured by Lee Products Ltd. Buckinghamshire, UK, were used. These valves would work from a 12 volt DC supply and had a dead volume of 18 µL, suitable for the needs of this micro-fluidic system.

8.1.3 Tubing and connectors

Several types of tubing were used to connect the various components and detailed in table 8.1. The micro valves required specialised tubing with screw-in connections, these tubes TU/TC/12/26/9/50L were purchased from Lee Products Ltd., Buckinghamshire, UK. The liquid flow rate through the peristaltic pump was adjusted by both the pump rotation speed and the tubing type, of which three different types were used. Two from Instech; a single tube P625/TS020S with an ID of 0.020 inches (0.508 mm) and a dual tube P625/TS[D]015S with an ID of 0.015 inches (0.38 mm), and one from Elkay Laboratory Products Ltd., Basingstoke, UK. This PVC tubing, Accu-rated 116-0549-030, with an ID 0.3 mm, was less flexible than the Instech tubing. However, this increase in rigidity made it suitable for connecting to the micro-reactors. The use of the Instech dual tubing allowed a single pump to draw liquids from two sources equally, which was advantageous, however this was at the expense of being able to flush the microfluidic system from a single source (this is discussed later in 8.8.2).

The use of several types of different tubing types throughout the fluorimeter required a method of coupling. This was achieved through sliding the end of each tube into a nylon sleeve and fixing with epoxy resin. By butting the tubes together, any dead volume could be eliminated or kept to a minimum. A similar method of attachment was used to connect the tubing to the detection cells.

Tubing type or component	Tubing or component material	Tube or channel length (mm)	Internal dimensions (mm)	Maximum volumetric flow-rate for diffusion ($\mu L\ min^{-1}$)
Instech (single)	Silicone	various	0.50 ID	n/a
Instech (dual)	Silicone	various	0.38 ID	n/a
Elkay	PVC	various	0.30 ID	n/a
Lee	Nylon	various	0.27 ID	n/a
μ-reactor No.1	Glass	260	0.17 × 0.06	24.0
μ-reactor No.2	Glass	135	0.17 × 0.06	14.0
μ-reactor No.3	Glass	30	0.20 × 0.09	1.8
Tee connector	PEEK	20	1.27 ID	n/a
Detection cell	Fused silica	35	2.00 ID	n/a

Table 8.1. *Dimensions and material of the individual components used (ID refers to the internal diameter of the capillary tube). Also shown is the maximum volumetric flow rate for diffusion to occur within the different micro-reactors*

A Tee connector allowed the chemicals to be mixed, this was used in later experiments to replace the micro-reactors. This Upchurch Tee connector with compression fittings, made from PEEK (polyaryletheretherketone), an organic polymer, was purchased from Kinesis Ltd., St. Neots, UK.

8.1.4 Excitation light

The initial fluorescence experiments used a Shimadzu RF-1501 laboratory fluorophotometer. Following from these evaluations, a series of experiments were carried out to assess different components in the development of the portable system.

Prior to choosing a suitable portable excitation light, a 150 watt high pressure mercury lamp from Oriel Instruments was used in conjunction with a monochrometer manufactured by Edinburgh Instruments Ltd. Through varying the width of the entry and exit slits of the monochrometer, the bandwidth and the power of the excitation light could be adjusted. The eventual excitation source for the portable fluorimeter was an LED, which had a peak output at 340 nm, model T9H340C manufactured by Seoul Semiconductor Co. Ltd. and supplied by Roithner Lasertechnik GmbH, Austria. LEDs emitting at the shorter wavelengths tend to have a lower power output than those which emit in the visible to near IR region, however, in recent years, improvements in technology has meant that this power output has increased to provide a more useful fluorescence light source. This mid priced LED (~ €20) was supplied fitted with a hemi-spherical lens producing a small diverging beam, with an optical power output of ~200 µW from a 5 volt DC power source.

8.1.5 Light detector

A light detector able to respond to low light levels was required; for this task a metal packaged PMT, H5784-01 manufactured by Hamamatsu Photonics UK Ltd was chosen. This detector would adequately function from a battery power source, requiring + 15V and – 15V DC supply. With dimensions of 80 × 30 × 30 mm, this device was suited for both portability and compactness, with an 8 mm diameter circular optical window. This model of PMT had a peak radiant sensitivity at 400 nm and a gain of 10^5. In laboratory trials, detection limits of below a tenth of a nano watt were observed.

8.1.6 Light filters

For the development of this fluorimeter, the analyte GSH in combination with the reagent OPA had excitation and emission peaks in the regions of 340 nm and 440 nm respectively. To avoid unwanted excitation light interfering with the fluorescence signal and also to restrict the excitation light being detected by the PMT, a system employing two light filters was used. The first filter situated between the LED and the analyte and the second filter placed between the analyte and the photodetector. At the low light levels expected from small volumes of solutions with low analyte molarity, filters with a relatively high transmission level would be preferable. Although the LED which was used for the excitation source peaks at ~ 340 nm, the emission spectrum of LEDs may be much broader and for this device wavelengths as long as 600 nm could be detected.

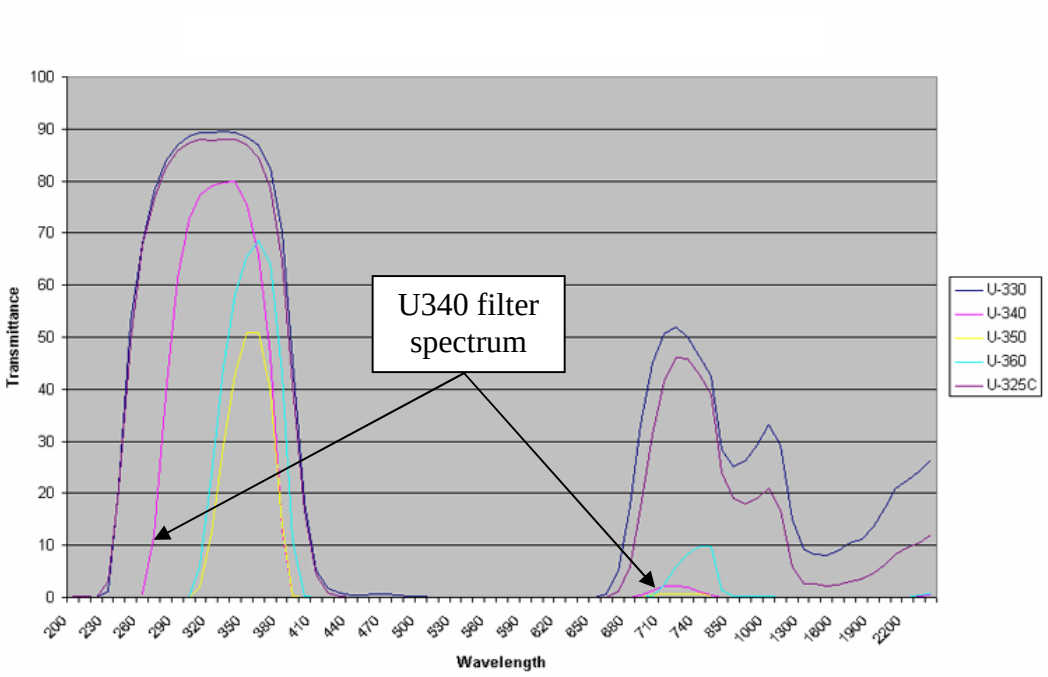

Figure 8.3 *UV bandpass transmission filters from Hoya Optics. The spectrum of filter U340 is depicted. [180]*

The first light filter was used to restrict the emission spectrum of the LED, a bandpass filter, a U340 produced by HOYA Optics [180], the transmission spectrum of which is shown in figure 8.3, here, for comparison, spectra from four other coloured glass bandpass filters are also shown. The U340 filter transmission peaks at 340 nm and has a FWHM ~90 nm, with 80% peak transmission. This relatively broad bandpass filter allowed the full width of the desired spectrum from the LED to pass. This filter blocked the emitted light longer than 400 nm, however up to 2% transmission was shown to occur from 700 – 850 nm but this posed no problem. Thus, through using this filter only the desired excitation light fell upon the analyte.

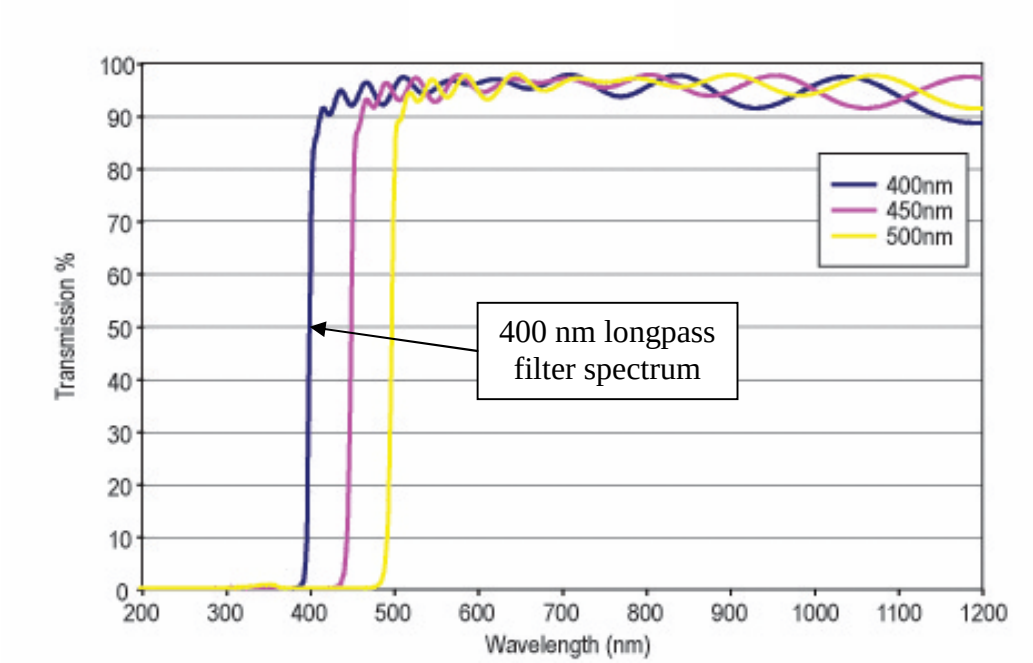

Figure 8.4. *Longpass filter from TECHSPEC Edmunds Optics. The spectrum of the 400 nm longpass filter is shown. [181]*

Having limited the emission spectrum from the LED, the second filter, which was placed between the detection cell and the PMT, eliminated the excitation light, thus allowing only the fluorescence light to reach the detector. For this, a TECHSPEC 400 longpass interference filter from Edmund Optics [181] was used, this is shown in figure 8.4, this graph produced by Edmund Optics also shows data from two other similar filters. This filter had a sharp cut-of slope factor and transmission above 400 nm of $> 85\%$. However, as there was a $< 1\%$ transmission below 400 nm, the system would still benefit from a careful arrangement of equipment to avoid excessive excitation light from entering the detector.

8.1.7 Liquid filters

The samples of sea water were filtered before they were analysed or before they were spiked with GSH. Millex GP filter units from Millipore, MA, USA, with a pore size of 0.22 μm, ensured that the micro channels stayed free from blockages due to particle contamination from the sea water.

8.1.8 Chemical storage

Chemical storage was required for the reagent, prepared standard, flushing water and waste. The chemicals were stored within the enclosure in 1.5 mL Eppendorf reagent

vessels from Star Lab GmbH, Germany. These vessels had caps in which a hole was drilled, thus allowing the tubing to enter whilst reducing spillage. The larger quantities of waste chemicals were stored in a 10.0 mL sealed specimen tube, again the lid was drilled to accept the tubing from the detection cell.

8.1.9 Electronic components and power supply

In addition to the components previously discussed, several other electronic items were used. A U12 Labjack data logger, manufactured by LabJack Corporation, Colorado, USA., was used to record data during experiments when continuous recording was required. When using the lower powered LED and to improve the sensitivity at the lower limit of detection, a lock-in amplifier was incorporated into the system, this required the LED to be modulated. The initial lock-in amplifier used was one which had previously been made within the department. Later, as the research progressed and the finalised components of the monitor were selected, a purpose built electronic controller, lock-in amplifier and data logger were assembled on a single PCB.

As the automated monitor was developed, the individual components were initially powered using separate mains power transformer units producing DC outputs. The final fluorimeter was powered from a 12 volt battery unit.

8.1.10 Portable instrument housing

The enclosure for the μTAS and all the analytical components was required to be light proof. The container with dimensions 232 × 212 and 143 mm deep was manufactured by Sarel Electrical Ltd., Swindon, UK. This was further adapted in the mechanical workshop, by adding a mechanical interlock so that the container could not be opened unless the PMT shutter was closed, thereby protecting the PMT from overexposure. The electronics and power pack were situated adjacent to the μTAS and contained within their own enclosure.

8.2 Preparation of the reagent and analyte

Reagents were prepared following procedures from previous research [146], which examined fluorescence reactions for amino acids. The borate buffer which was suitable for dissolving the OPA was prepared using di-sodium tetraborate ($Na_2B_4O_7$), supplied by Fisher Scientific UK Ltd, Loughborough, UK. A solution of 0.1 M was prepared using 19.07 g of di-sodium tetraborate, added to 500 mL of purified water and brought to a pH 9.5 with either 1.0 M of sodium hydroxide or 0.01 M of hydrochloric acid. Only small quantities of the buffer were required for each experiment and a preparation of 500 mL was stored at a cool temperature for future use.

The OPA was prepared using ortho-phthalaldehyde supplied by Fluka Chemicals Ltd. Dorset, UK. A solution of 5 mg mL^{-1} of OPA (with a relative molecular mass of 134.1, this equated to a 0.0373 molar solution) was initially used. Quantities of 25 mL were prepared by measuring 0.125 g of OPA, dissolving this in 1.25 mL of methanol and making up to 25 mL by adding the sodium tetraborate buffer. This was mixed freshly each time and was regarded as stable for one day when left at room temperature.

The GSH was required in µM quantities, however to achieve this, intermediate standards concentrations were made and the desired molarities were prepared through serial dilutions using purified water from 1 to 100 µM. The GSH was purchased in the form of L-Glutathione reduced (≥ 99%) from Sigma-Aldrich Co. Ltd. Poole, UK. The GSH was prepared freshly for each experiment. All purified water used was prepared through reverse osmosis using a Elgastat UHQ water purification system, with a purity of >18 MΩ cm.

8.3 Evaluation of the chemistry

This section examines the fluorescence excitation and emission spectra and the absorbance of the tricyclic isoindole, produced from the reaction of GSH and OPA (further referred to as the tricyclic isoindole). Although this fluorimeter was being developed to determine GSH in seawater, throughout its development for both convenience and repeatability purified water was used as a medium in which to dissolve the GSH. Only once the apparatus had been optimised was seawater spiked with GSH investigated.

8.3.1 Fluorescence of the tricyclic isoindole

The first examination of the tricyclic isoindole was for the fluorescence excitation and emission spectra. Equal quantities by volume of GSH and OPA were pre-mixed and placed into a fused silica cuvette with an internal optical path length through the liquid of 10 mm. The cuvette was placed into the Shimadzu RF-1501 fluorospectrophotometer. It was found that GSH molarities greater than 10 µM saturated the emission response of this fluorospectrophotometer.

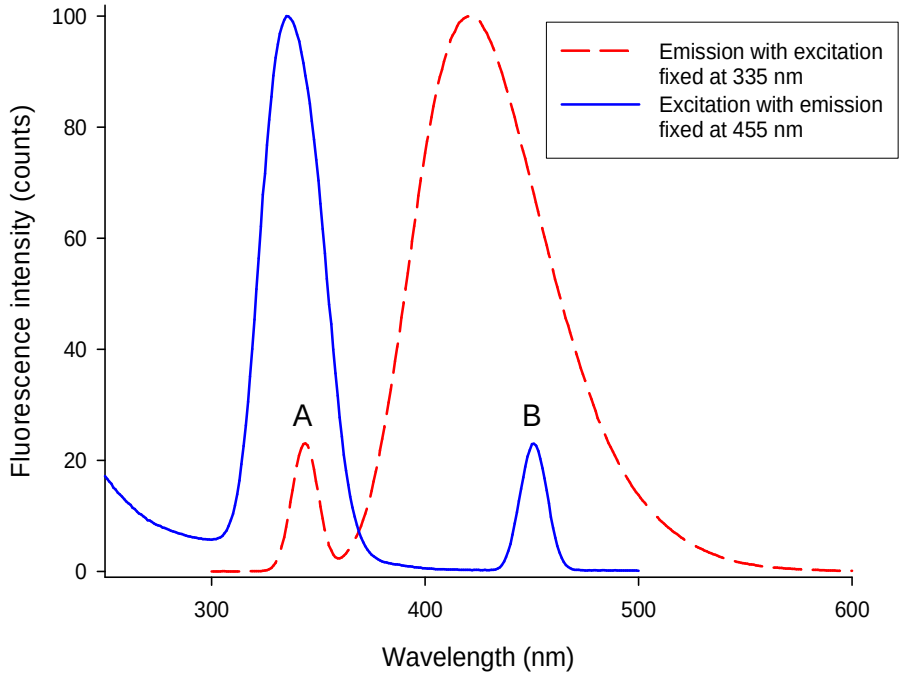

Figure 8.5. *Fluorescence excitation and emission spectra for the tricyclic isoindole. The major peaks in emission have been normalised. The minor peaks, A and B, are produced from the detection of scatter of the excitation light.*

Shown in figure 8.5 are two spectra. The broken line represents the spectrum for the fluorescence emission with the excitation fixed at 355 nm, indicating a peak emission at ~ 420 nm. The continuous line represents the spectrum of the effective excitation wavelengths with the emission fixed at 455 nm, showing peak excitation at ~ 330 to 340 nm, thus producing a Stokes shift of 80 to 90 nm. There is clearly a distinct separation between the excitation and the emission light with only a small overlap of spectra and would, through the use of a suitable longpass light filter to block the excitation light, have only a minimum reduction upon the detected fluorescence intensity.

8.3.2 Absorbance of the tricyclic isoindole

The absorbance of the tricyclic isoindole was examined using a Unicam 5625 UV/VIS spectrophotometer. Premixed concentrations of GSH and OPA were placed into a fused silica cuvette with a 10 mm path length, an empty cuvette was used as a baseline. The results are shown in figure 8.6, the absorbance of purified water has been added for comparison.

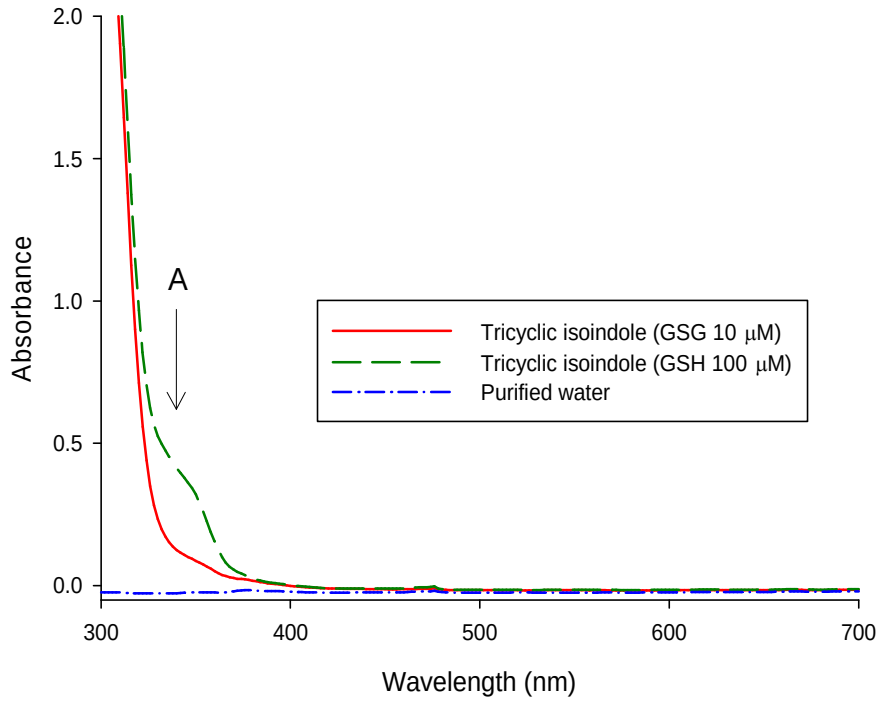

Figure 8.6. *Absorbance of the tricyclic isoindole using a 10 mm path length fused silica cuvette. Purified water has been added for comparison. The peak excitation wavelength has been highlighted by arrow A.*

The difference in the absorbance of the tricyclic isoindole with GSH at 10 µM and 100 µM occurs noticeably at the major fluorescence excitation wavelength, indicated by arrow A. Absorbance is low throughout the emission spectrum benefiting fluorescence light detection. Both samples of the GSH concentrations were highly absorbent at wavelengths shorter than 320 nm. An indicated absorbance, at 340 nm, of 0.125 and 0.414 was noted for GSH at 10 µM and 100 µM respectively, equating to absorption coefficients (correcting for the interface reflections as in chapter 3) for 10 µM GSH tricyclic isoindole of $\alpha_{\lambda 340} \sim 36\ m^{-1}$ and for 100µM GSH tricyclic isoindole of $\alpha_{\lambda 340} \sim 102\ m^{-1}$, which compares to water $\alpha_{\lambda 350} \sim 0.0436\ m^{-1}$ [95].

8.3.3 Influence of OPA concentration

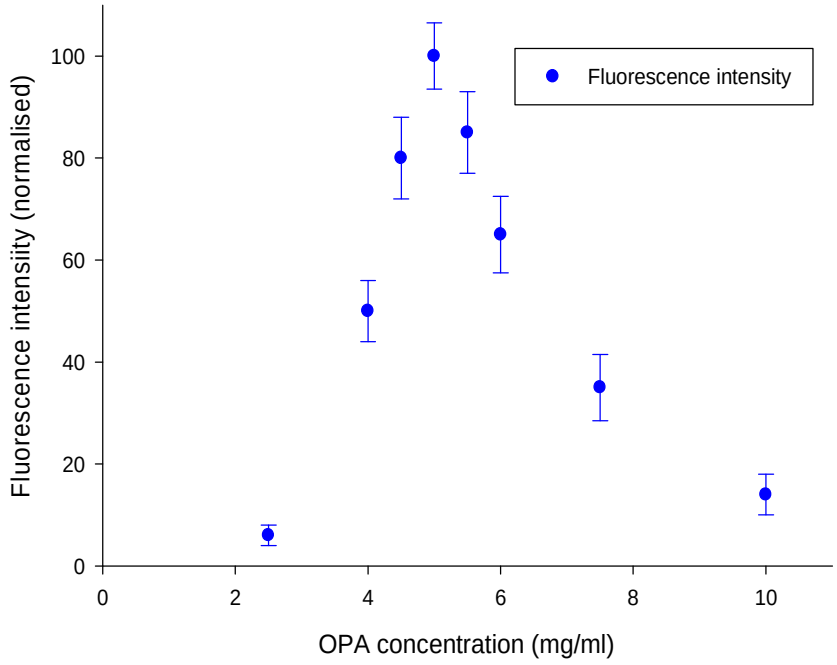

Figure 8.7. *Normalised peak fluorescence intensities resulting from various concentrations of OPA. GSH constant at 10 µM.*

Varying the OPA concentration from 2.5 to 10.0 mg mL^{-3} (0.0186 to 0.075 M) displayed a sharp rise and then fall in the fluorescence response, see figure 8.7. These experiments were carried out again with a GSH concentration of 10 µM. The graph was normalised to the peak emission which occurred at 5.0 mg mL^{-1} and the error bars represent the range and mean for three experimental results. The excitation was fixed at 340 nm and the figure for the peak fluorescence intensity, which occurred between 420 and 425 nm, was used to indicate the relative fluorescence response. Future preparations of OPA were fixed at 5.0 mg mL^{-1}.

8.3.4 Effect of buffer pH

The buffer pH was varied from 8.0 to 10.5 prior to the preparation of the OPA reagent. The OPA was mixed at a concentration of 5.0 mg mL^{-1} and the GSH was 10 µM. The excitation light was fixed at 340 nm and the peak fluorescence intensity was recorded which again occurred at 420 to 425 nm. The graph was normalised to the peak intensity and the error bars represent the range of results from three experiments.

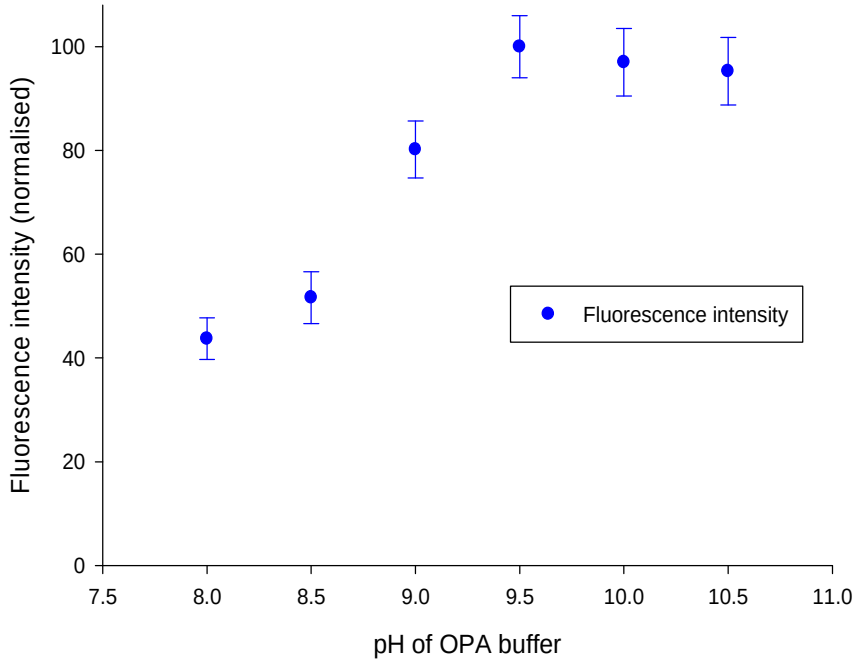

Figure 8.8. *Graph showing the normalised fluorescence intensity as the buffer pH of the OPA is varied.*

The results shown in figure 8.8 indicate an increase in fluorescence intensity as the pH was changed from 8.0 to 9.5, from this point there is little significant change in the response, similar to pH dependence previously found [142, 149]. Unlike the concentration of the OPA, the small change seen in the fluorescence response would allow a drift in the pH due either to the buffer or the solvent without greatly affecting the resultant fluorescence. Following the results from these experiments, the reagent was always prepared with a buffer at 9.5 pH.

8.4 Design of the optical system

The previous experiments had been executed using a laboratory bench-top fluorospectrophotometer. For a portable spectrometer the individual components needed were assembled allowing the separate parts to be assessed and changed as and when required. The major components consisted of a light source (and monochrometer as required), PMT, longpass filter and a fused silica cuvette to hold the analyte.

8.4.1 PMT response and calibration

The PMT was assessed for its response to various light intensities. A diode laser with an output at 405 nm manufactured by Power Technologies Inc was used as a light source. Combinations of several light filters were used to attenuate the light intensity. The different output powers were then assessed using the Fieldmaster light power meter manufactured by Coherent. With the PMT being more sensitive than the power meter, two neutral density filters were placed in front of the PMT, thus reducing the light entering into it by a factor of 2×10^{-6}.

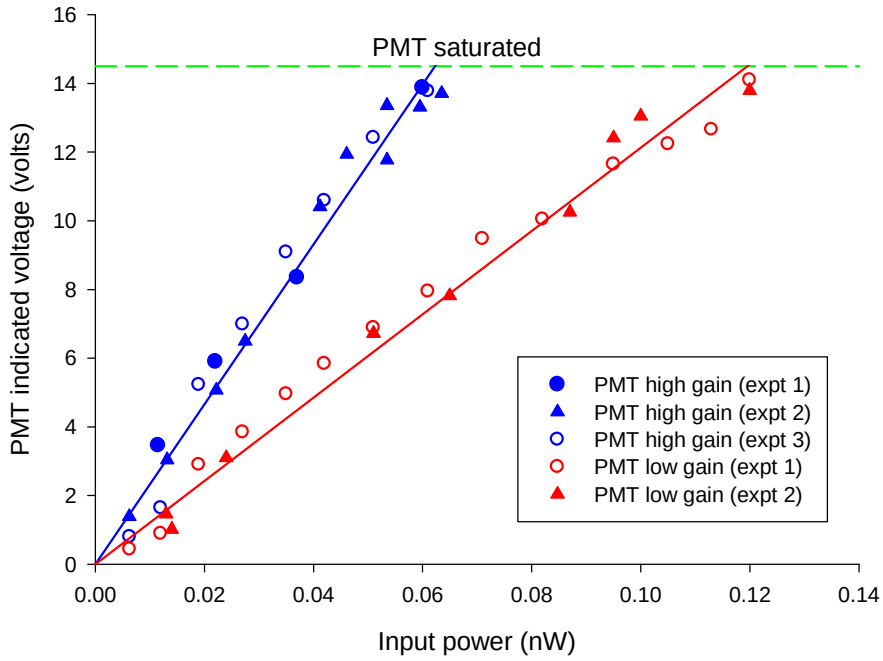

Figure 8.9. *Photomultiplier tube response to various light intensities from a light source at 405 nm. Results show the PMT output set to a high and low gain. The solid lines show a linear regression for each set of experiments.*

Through varying the gain of the PMT, two distinct output ratios from the PMT could be achieved, this is shown in figure 8.9. In both cases the maximum response from the PMT was ~ 14 volts and for both of the gain settings the input power produced a near linear response. With the gain set to high, an input of 0.07 nW was needed before saturating the PMT and with a low gain 0.12 nW was required.

8.4.2 Evaluation of light sources

Prior to choosing a suitable LED for use as fluorescence excitation, an interim light source was used to assess the required radiant power. The spectra of two light sources are shown in figure 8.10, a xenon flash light and a mains powered high pressure mercury lamp, captured using an Ocean Optics spectrophotometer. However, as the major part of each spectrum is in the visible region, there is poor overlap with the desired fluorescence excitation spectrum which is indicated by arrow A.

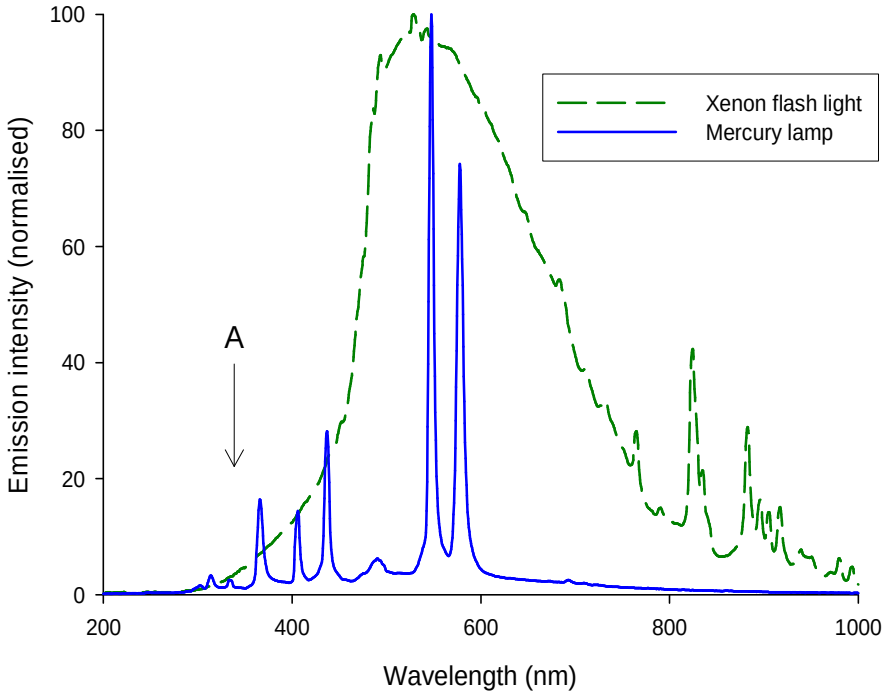

Figure 8.10. *Normalised optical output spectra from a camera xenon flash light and a high pressure mercury light. The peak excitation wavelength is indicated by arrow A.*

Both lights sources produced less than 1% of their total output in the desired 250 to 350 nm band. The mercury lamp light source, through producing a spiked spectrum was better suited to the demands needed of the fluorescence experiments and was used in conjunction with the monochromator. At this stage of the development of the fluorimeter, the only light filter required was the longpass filter, positioned between the

analysis cuvette and the PMT. Figure 8.11 shows the light exiting the monochromator at a peak emission of 340 nm using four different aperture settings. The graph shows the relative intensities which have been normalised to the peak output for aperture # 4. Where # 4 is the largest and # 1 is the smallest.

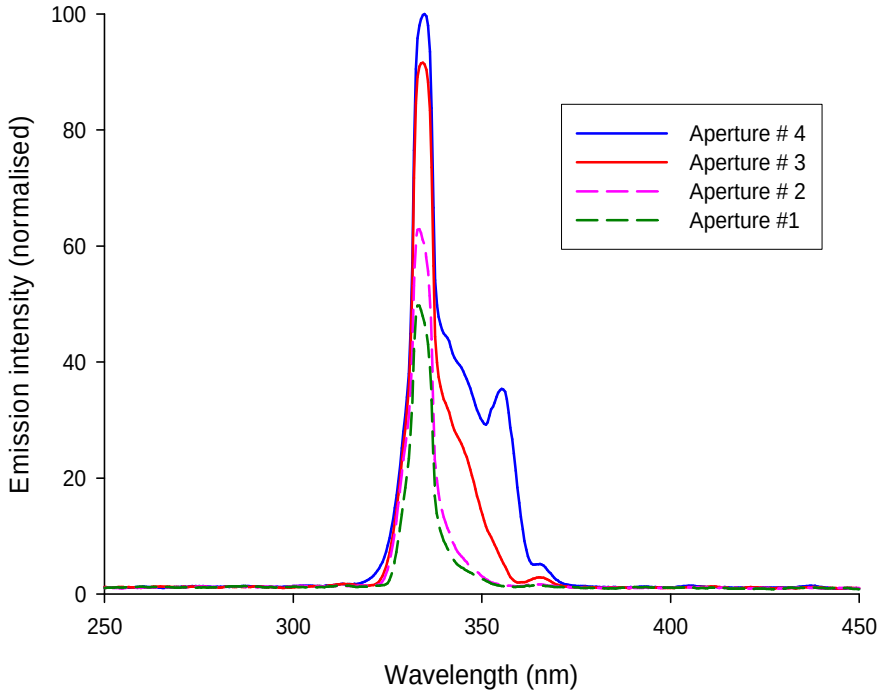

Figure 8.11. *Normalised optical output spectra from a high pressure mercury lamp after passing through a monochromator, four different aperture settings are shown.*

Each of these settings not only influences the bandwidth but also affects the optical power output. Measurements were made using the optical power meter and fitted with a UV detector adjusted to read at 340 nm. The optical power output from the mercury lamp after passing through the monochromator produced a range from 20 to 130 μwatts from aperture settings # 1 to # 4 respectively.

Prior to using the detection cell, a cuvette was used as a sample holder, this contained a much larger quantity of analyte. To limit the fluorescence signal, the excitation light was reduced through using an adjustable iris which was placed immediately after the monochrometer. This set-up was able to offer sufficient control of the excitation light so avoiding saturation of the PMT.

8.4.3 Sample holder

For the initial experimental set-up the analyte was still examined using a fused silica cuvette. For this the analyte and the reagent were premixed prior to being assessed. In these experiments a sample volume of ~ 2 mL was required.

8.4.4 Layout of optical components

Figure 8.12 shows the layout of the optical components making up the laboratory fluorimeter. For the detection of low levels of fluorescence the PMT was positioned adjacent to the analyte and orthogonal to the excitation light. With the fluorescence being emitted in all directions, placing the PMT close to the source of the fluorescence allowed a larger proportion of the light could be captured.

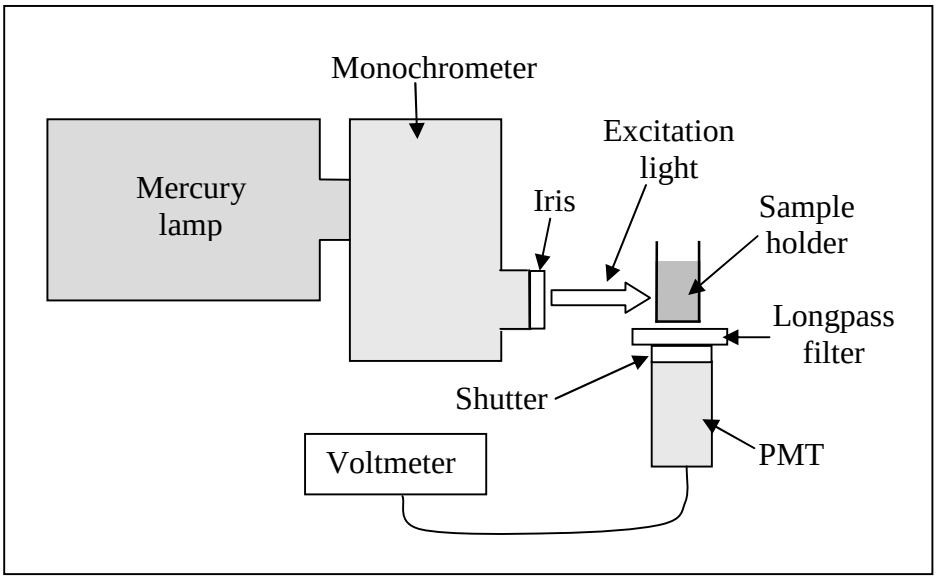

Figure 8.12. *Diagram showing the laboratory set-up of the apparatus to assess the fluorescence emission from the tricyclic isoindole located in the sample holder.*

To isolate the active components of the PMT from excessive light exposure, a shutter located before the optical window could be closed and is indicated in the figure. This was essential when the laboratory lights were switched on.

8.5 Evaluation of reagent concentration and stability

The laboratory set-up, as shown figure 8.12, was used to further evaluate the chemistry of the analyte, reagent and the tricyclic isoindole.

8.5.1 Effect of GSH molarity

Calibration standards of 1 to 10 μM of GSH were prepared to analyse their relative fluorescence intensity. These were pre-mixed with the reagent OPA at a ratio of 50:50 prior to analysis. A blank of purified water and OPA was also prepared. The upper limit of 10 μM GSH was used as this had previously been the maximum that the laboratory fluorospectrophotometer was able to assess. The intensity of the optical power from the mercury lamp needed to be adjusted to a level where the fluorescent emission produced a high response from the PMT without saturation. For this, the aperture was set at # 1 and the iris adjusted to produce a response by the PMT of ~ 12 volts, the optical excitation power of the mercury light after passing through the monochrometer was measured to be ~ 10 μW.

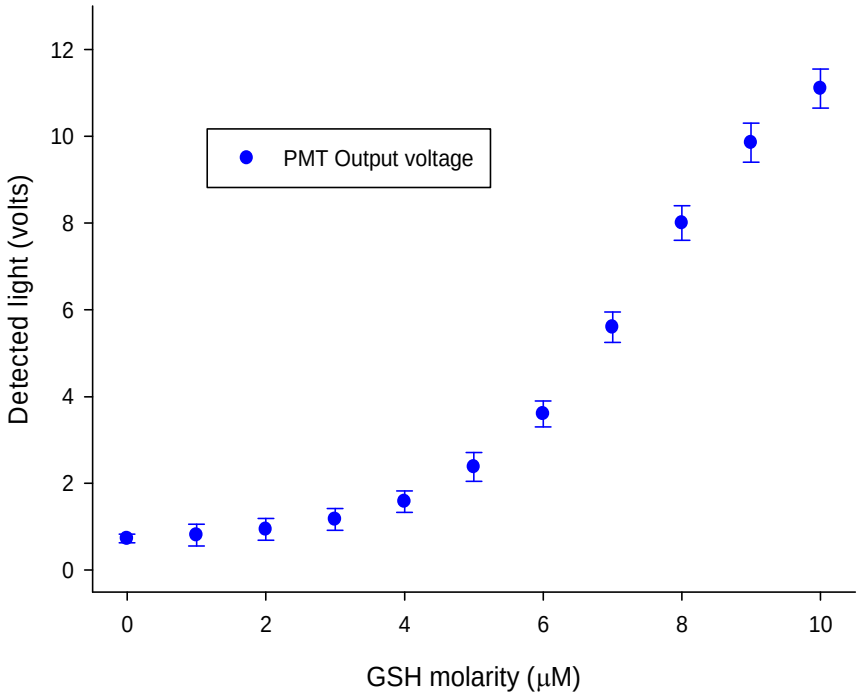

Figure 8.13. *The detected light, represented by the voltage output from the PMT, indicated an increase in fluorescence from the higher GSH molarities.*

The results from the experiments are shown in figure 8.13, the error bars representing the range of results from seven experiments. A reading of ~ 1 volt was produced from

the blank. This may be caused through a combination of several factors; scattered light from the excitation source may be entering the PMT of which part will pass through the longpass filter (with a blocking efficiency for this filter ≥ 99%, small amounts of stray light can create a large response by the PMT). Despite the use of a dark room, inadvertent light can still be entering the PMT, there may also be background electrical noise present. However, through closing the PMT shutter, the voltage reading was reduced to several mV, indicating that the background response was probably due to stray light. Nevertheless, a clear increase in fluorescence was observed and GSH at 10 μM was used for the following analyte and reagent experiments.

8.5.2 Stability of GSH

These experiments examined the stability of GSH once dissolved in water. The reagent OPA was prepared at 5 mg mL^{-1} and GSH was dissolved in water to make a solution at 10μM. A sample of GSH was immediately mixed with OPA to be used as a standard, the rest of the GSH was divided into two batches; one batch was placed in a refrigerator and the other was kept in the dark at room temperature.

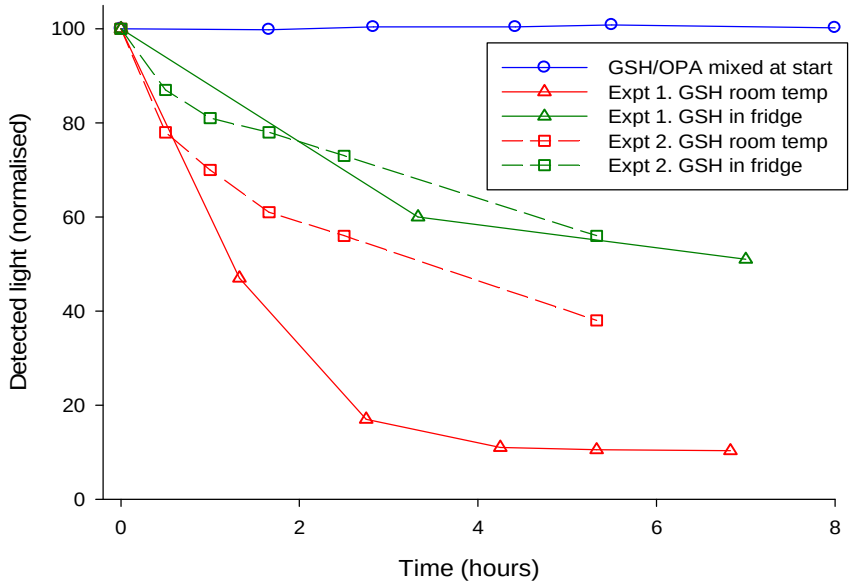

Figure 8.14. *Graph showing the effect of time and temperature upon GSH to form a fluorophore with OPA. This is compared to the premixed isoindole of GSH/OPA.*

The premixed standard was analysed in the fluorimeter, this response was normalised and used as the reference. Throughout a period of several hours, samples of GSH from the two batches were mixed with OPA and the fluorescence response tested. The results of two experiments are shown in figure 8.14. The effect of both time and temperature

upon the dissolved GSH reduced the fluorescence intensity of the freshly mixed tricyclic isoindole. The auto oxidation of the GSH was reduced by keeping the dissolved analyte at a lower temperature, in this case a refrigerator. The batches kept at room temperature, 19ºC and 16ºC for experiments 1 and 2 respectively resulted in rapid deterioration in the ability of the GSH to form a fluorophore. Such findings have been known and reported by other workers [119, 120, 132] and a half-life of ~ 3 hours [123]. These effects upon GSH became evident in later experiments.

8.5.3 Stability of the reagent OPA

Experiments to examine the durability of the reagent OPA were conducted for a period of six days. On each day that the OPA was assessed, a fresh GSH solution was prepared and mixed with the different dated OPA reagent samples. Between these daily assessments, the differently dated OPA reagents were kept in a refrigerator at a temperature ~ 4°C. The results of these experiments are shown in figure 8.15. Each day's results were normalised against a standard of the tricyclic isoindole that had been prepared each day from fresh batches of GSH and OPA.

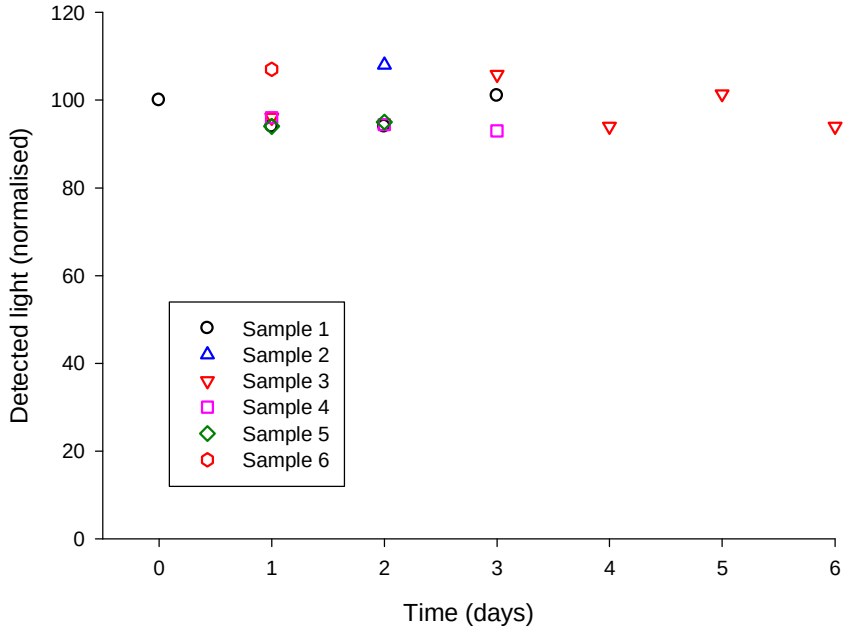

Figure 8.15. *Graph showing results from several experiments of the fluorescence response from mixing pre-prepared OPA with freshly prepared GSH.*

The range of the observed results was both higher and lower than the freshly prepared OPA by a factor of less than ± 10%, with most OPA batches varying over and under the normalised standard at some point throughout the experiment as a whole, possibly due

to preparation error. However, the stability of the OPA reagent through a six day period exhibited no significant deterioration in its ability to produce a fluorescence reaction with freshly prepared GSH.

8.5.4 Stability of the tricyclic isoindole

The tricyclic isoindole needed to be stable sufficiently long enough for the fluorescence analysis. To assess this, several experiments were undertaken. Here, the analyte and reagent were pre-mixed and placed into the cuvette and the fluorescence intensity was discretely analysed over a period of several hours.

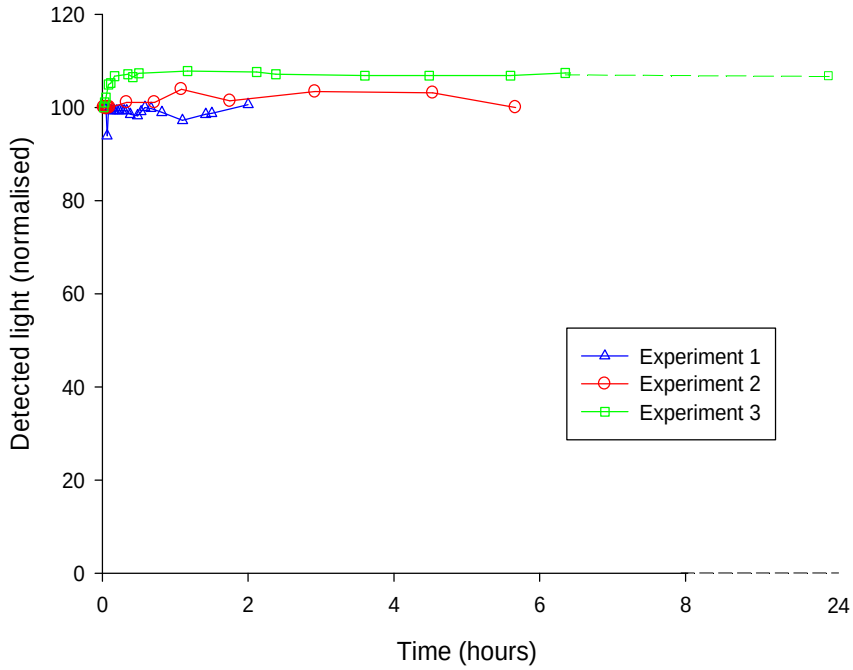

Figure 8.16. *Graph showing the stability of the GSH/OPA isoindole over time. The detected light indicates the intensity of the fluorescence response.*

For each experiment the results were normalised against the initial reading. The results can be seen for three experiments in figure 8.16. A small variation of the detected fluorescence was seen through the time period. An increase in detected light occurred in the third experiment, this may have been due to poor mixing when the first measurement was made, the subsequent readings being stable. The overall results indicated that the isoindole was stable for several hours, with the longest duration of 24 hours showing less than a 1% reduction in fluorescence and consistent with other findings [111, 147]. It was expected that once the GSH and the OPA were mixed, the fluorescence analysis would be made within several minutes.

8.6 Flow through detection cell

Up to this point, a fused silica cuvette had been used in analysing the tricyclic isoindole, which was filled and emptied manually, using 2 mL of solution each time. However, for an automated system involving only micro quantities of reagent, a different approach was needed. The manual filling and emptying was replaced by using a miniature peristaltic pump (previously discussed in section 8.1.2), where the analyte was propelled into a much smaller flow through detection cell, replacing the cuvette

8.6.1 Peristaltic pump tubing and flow rates

The flow rate of the water based solutions was dependant upon the speed of the pump, the tubing dimensions and tubing type (due the their ID and rigidity). In the different experiments either the Elkay or the Instech tubing was used. The various flow rates can be seen in figure 8.17, with the larger ID Instech tubing, as expected, producing the faster flow rate. The flow volume rate for the three tube types ranged from ~ 25 to 180 µL min^{-1} depending upon the pump speeds, with their flow rates being proportional to the pump speed, as seen in figure 8.17.

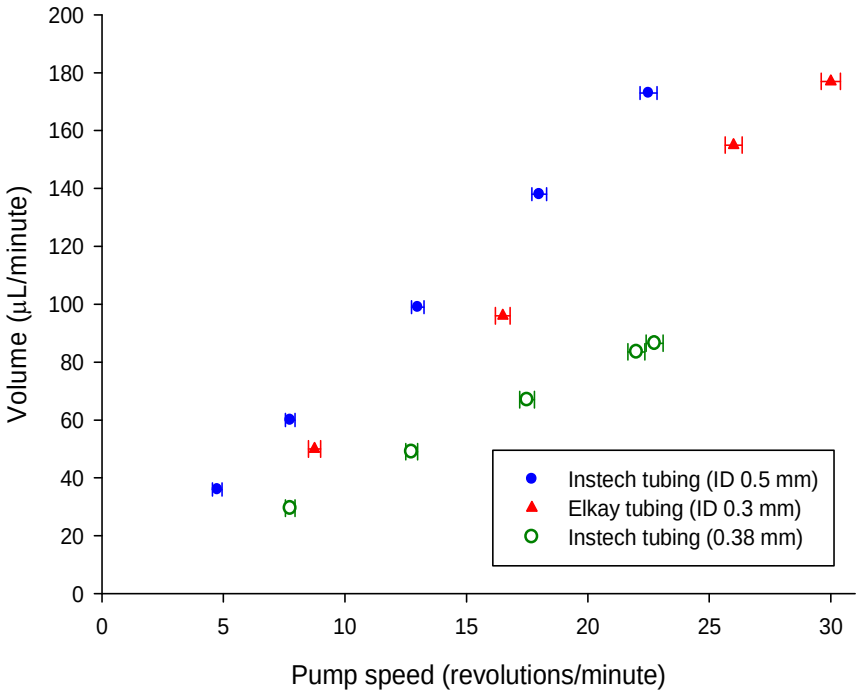

Figure 8.17. *Flow rates at different pump speeds using Instech and Elkay tubing. The three experiments show the effect of using different ID tubing and variation in tubing material.*

With all tubing types, problems were encountered with their continued performance; whilst using the more rigid Elkay tubing, the pump was unable to turn regularly at the slower speeds producing an uneven flow below ~ 8 revolutions per minute, whilst the flexibility of the Instech tubing allowed the pump to function at all speeds. The Instech tubing became, over time, weakened and was unable to cope with the high back pressure which was created at high flow rates when the system was used in conjunction with the small channelled micro-reactors. It was later found that the continuous movement of the peristaltic pump rollers affected the tubing and as such the flow of liquid along the tubing would cease entirely. It was also noted that leaving either type of tubing in a stationary pump for several days (under continuous pressure from the rollers) left the tubing both squashed and stretched, making it unusable for delivering accurate volumes.

8.6.2 Pumping GSH and OPA into the detection cell

The analyte and reagent were passed through, and were mixed in, the micro-reactor prior to entering the detection cell, as shown in the set up in figure 8.18. Micro-reactor No.1 (explained in section 8.1.1 and detailed in table 8.1) was initially used and the GSH and OPA had a diffusion time within these micro-channels of ~ 5.6 seconds (derived from equation 7.2 previously discussed in Chapter 7) requiring a volumetric flow rate of 24 µl min^{-1}

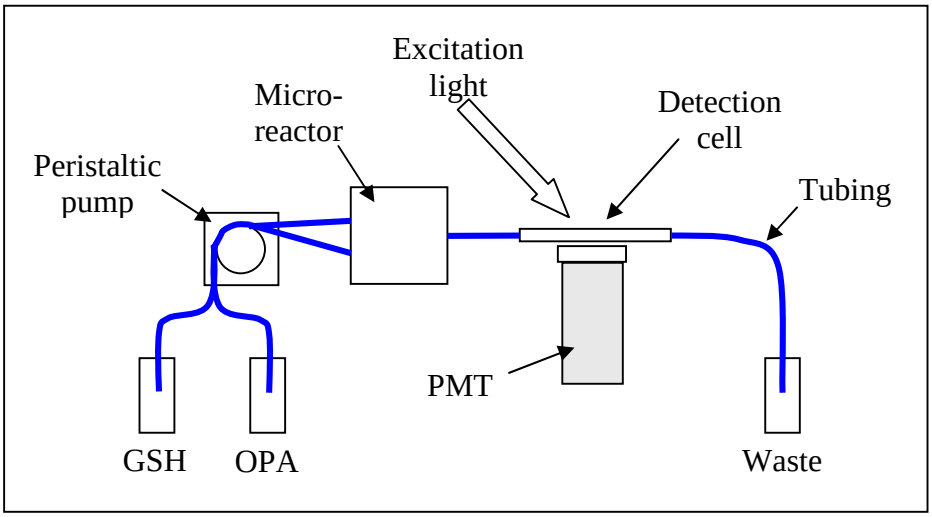

Figure 8.18. *Set-up of the peristaltic pump and flow through detection cell. Also shown is the position of the micro-reactor, excitation light and the PMT.*

Using the set-up as shown in figure 8.18, water was pumped through the system until the water was flowing out into the waste vessel. The flow of ~ 50 µL min^{-1} from each reagent vessel resulted in a total flow rate of ~100 µL min^{-1}, this flow rate was in excess of the target flow rate of 24 µL min^{-1} required for diffusion to occur.

Step	Time (minutes)	Pump	Task (indicated on graph)	Volume per task (µL)
1	2.00	On	GSH and OPA pumped	200
2	2.00	Off	Reaction monitored (A)	0
3	3.00	On	System flushed with water (B)	300
4	2.00	Off	Pump stopped (C)	0
5	2.00	On	Water continuously pumped (D)	200

Table 8.2. *Showing the different tasks and the time interval for each analytical run. The quantities of the liquid used for each task is also indicated.*

Nevertheless, the GSH at 10 µM and OPA were drawn from the separate containers and mixed within the micro-reactor before entering the detection cell and from there pumped into the waste container. The GSH and OPA were then replaced with water to flush the system, as had been required to rinse other detection systems [178]. During this time the UV excitation light continually illuminated the detection cell and the data logger recorded the PMT response. Results for three experiments are shown in figure 8.19. Each of the experiments followed the same timed sequence and is shown in table 8.2. Step 5 purged the tubing and detection cell with purified water prior to the following analysis cycle, this was shown to be necessary in some other systems.

These three experiments took place over a period of several hours and it can be seen that the fluorescence intensity from the second and third experiments decreased to ~ 85% and ~70% respectively, compared to the first experiment. These results indicate the instability of the GSH, this being broadly consistent with the findings in previous experiments, shown in figure 8.14.

With a flow rate of around 100 µL min^{-1} the residence time within the serpentine micro-reactor was insufficient to allow diffusion to occur across the entire cross sectional area. However, the liquid flow through the micro-reactor and into the detection cell would have allowed some degree of mixing. Once the pump stopped generating flow, the

detection cell containing the GSH and OPA permitted the analyte and reagent to mix, this may have been indicated by the increase in fluorescence over the period from just before A to immediately after B, as shown in the figure 8.19. When the pump was restarted, this time pumping water to flush the system, the fluorophore was exchanged for water and the detection of fluorescence declined.

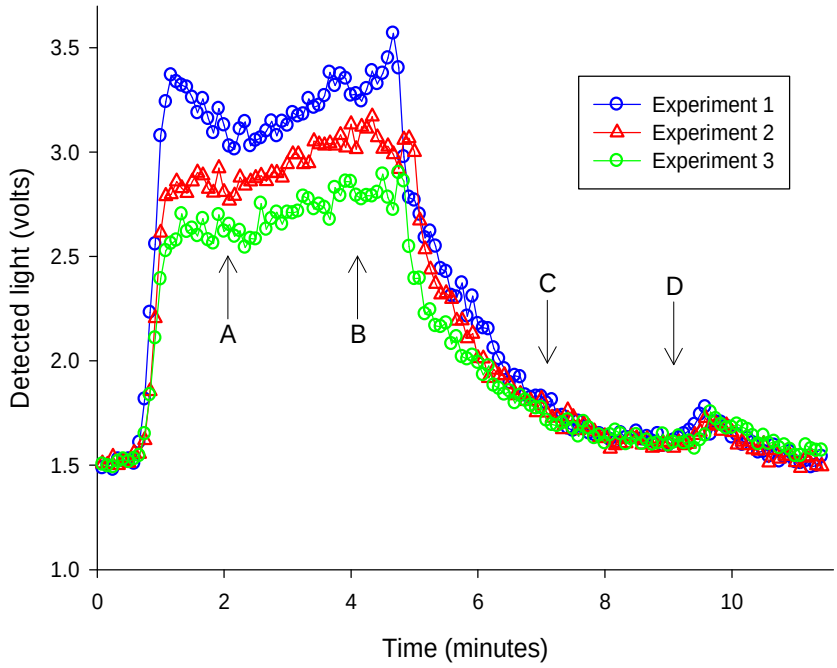

Figure 8.19. *Detected response during the cycles of the pumping and stationary phases. GSH and OPA was pumped up to point A. Point A to B is the reaction and analysis phase. Point B to C water was pumped through the system. Point C to D is the rest phase and point D onwards pumping water.*

A small increase in fluorescence can be seen following point D for the three experiments. Here it could have been expected that the fluorescence would have remained at a similar level before a further decline. However, due to the assembly of the detection cell and the tubing (which were attached by inserting the tubes approximately 5 mm into the detection cell) as shown in figure 8.20 (a), the differences in their internal dimensions created areas of dead volume where uneven flow may have occurred. These areas of uneven flow would in certain conditions create a separation bubble (area with limited flow) or a separation region (an isolated volume). The consequence of any separation in the flow would be to create an isolated region from the rest of the detection cell, see figure 8.20 (b). As such, the inflow of new liquid would not totally replace that which previously occupied the detection cell and a certain residue from the previous fluid would remain. Through stopping the pump this remaining liquid would

have the chance to diffuse into the bulk and in the case when the system is being purged, the tricyclic isoindole which remained in the detection cell would have the opportunity to create a small fluorescence signal from the diluted fluorophore. Likewise as the partially mixed GSH and OPA are drawn into the detection cell, the separation bubble of water would dilute the fluorophore. Such separation regions would account for the surge in fluorescence shown in figure 8.19 at point D and also for the time in which it took to purge the detection cell of the analyte.

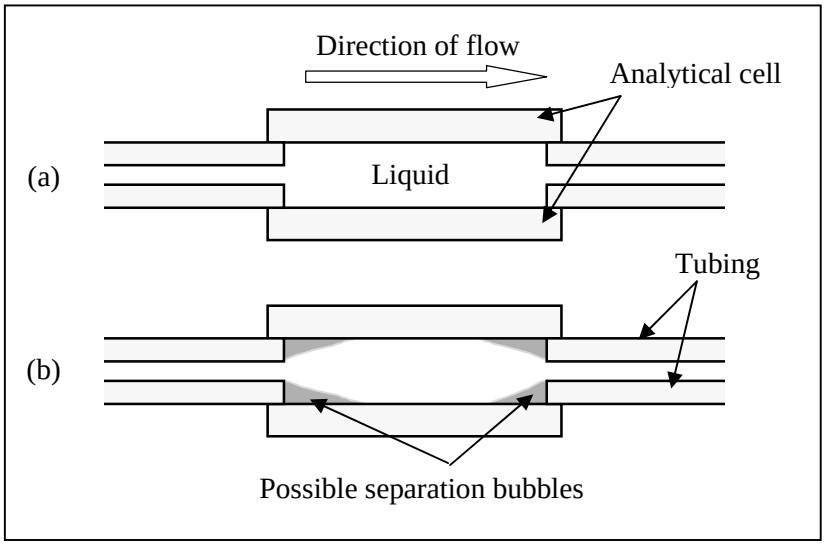

Figure 8.20. *Diagram of the detection cell with attached tubing. Showing (a) heterogeneous liquid fill and (b) possible separation bubbles.*

A different approach to purging the detection cell is shown in figure 8.21. Here, two further methods were tried; in the first water was pumped continuously until the system was thoroughly flushed through. The second method introduced air into the system (marked on the graph as B) this had the effect of forcing out the liquid in front of it. As the air bubble entered the detection cell, the bubble's air/water interface scattered the excitation light, creating the appearance of an increase in the fluorescence signal. At a volumetric flow rate of 100 μL min^{-1} this took ~ 50 seconds to pass along the detection cell.

As the detection cell filled with air, the scattered light decreased and as water was again pumped into the system at point C, this second air/water interface created a similar but smaller effect. After this, the system returned back to the original signal for that of water, demonstrating that it was possible to purge the system of the fluorophore within two minutes, as opposed to five or six minutes using only water. However, introducing

air into the system had on other occasions proved problematic both in the extra complication of its mechanism and in the difficulty of removing small incidental bubbles.

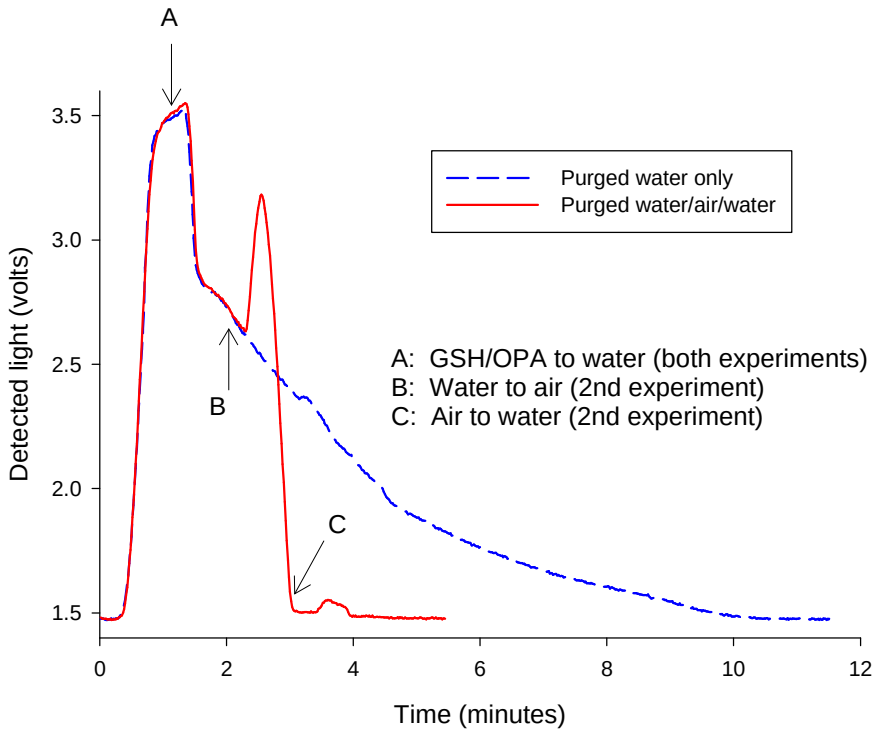

Figure 8.21. *Graph showing two methods of purging the detection cell of the fluorophore. The first method through continuously pumping water into the system and the second method through the introducing of an air bubble.*

8.6.3 Evaluation of the LED

The mercury lamp was replaced with the LED and set-up as shown in figure 8.22, the LED was ~ 25mm from the detection cell, which itself was placed above the centre of the PMT 8 mm diameter window.

To increase fluorescence emission from the tricyclic isoindole, the detection cell needed to be placed in the centre of the light projected from the LED. The emitted light from the LED was assessed using a CCD camera, this device, an Ophire Beamstar-V, by Ophire Optronics Ltd., was set-up in front of the LED which was mounted on an optical rail. From here, the distance between the CCD camera and the LED could be changed as the emission was monitored. The intensity of the LED beam profile was monitored at distances from 10 mm to 50 mm and displayed in both 2 and 3 dimensions, the results for 10 to 40 mm are shown in figure 8.23. The 2 dimensional displays represent an area of 6.4 mm by 4.8 mm and the colour is an arbitrary intensity, where red is the greatest

and blue the least. It can be seen that as the distance from the LED increases the beam diverges and the peak intensity decreases.

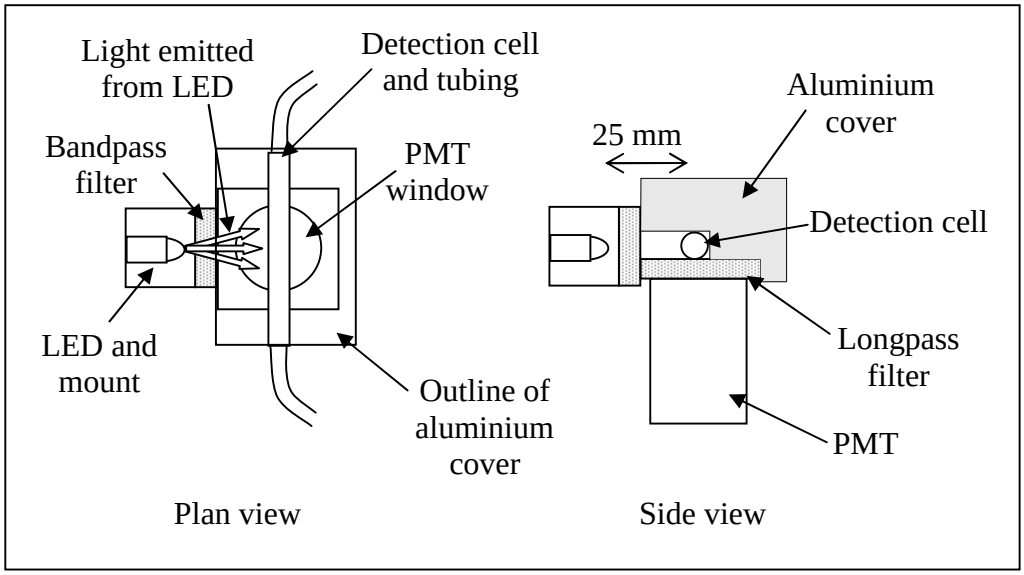

Figure 8.22. *The plan view and side view of the set-up showing the LED, filters, detection cell and PMT. The distance from the LED to detection cell is ~ 25 mm as indicated.*

To hold the detection cell in position and to assist in shielding the PMT from ambient light, an aluminium block was machined in the departmental workshop. This aluminium cover, indicated in figure 8.22, was made so that it sat over the PMT and a channel cut out to enable the detection cell to be securely held in position whilst allowing the light from the LED to illuminate the detection cell. The underside of this cover was painted matt black to reduce light scatter from the LED.

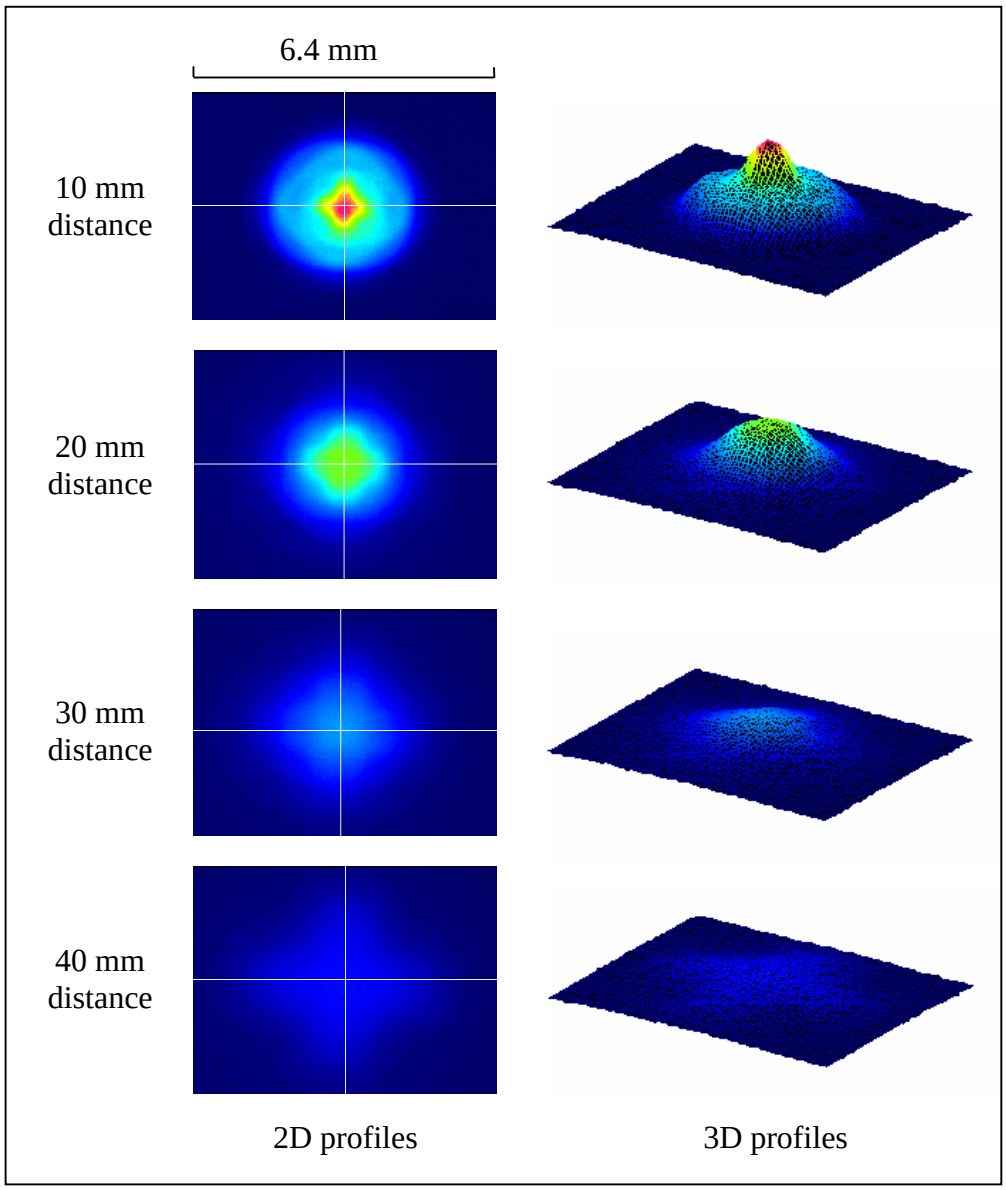

Figure 8.23. *CCD camera images of the light emission from the LED, at 10 – 40 mm distances from the LED to the camera. The colour shown in the two profiles represent an arbitrary intensity, where red is the highest intensity.*

Data from the CCD camera enabled the FWHM beam intensity for the LED to be measured, from this the beam was calculated to have a divergence half angle of 24 m rad. Due to the CCD camera distance at 40 and 50 mm from the LED, part of the LED been may have been too wide for the active area of the array, affecting the FWHM data and is shown in figure 8.24.

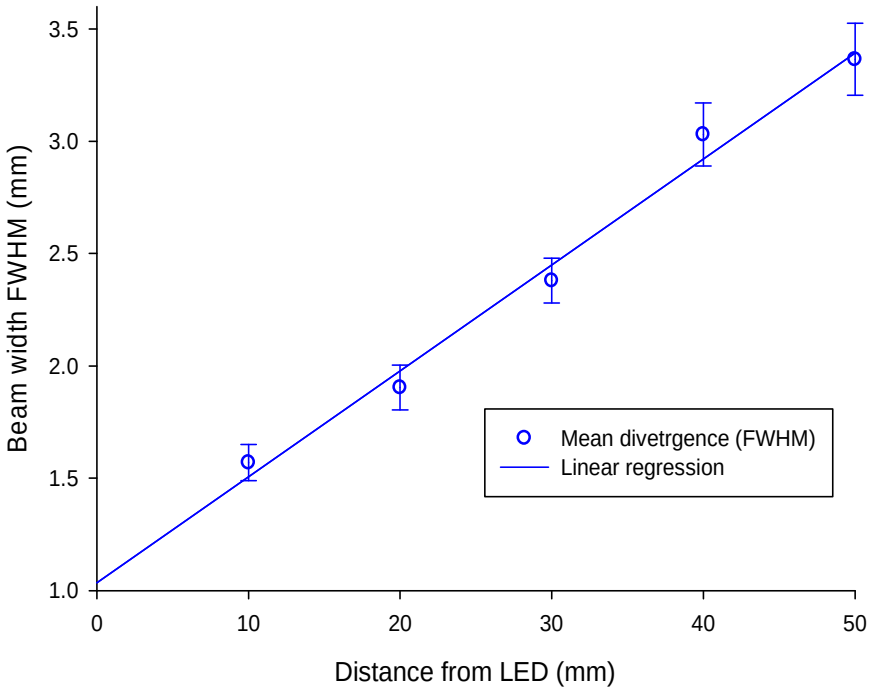

Figure 8.24. *Mean FWHM beam intensity for the LED. Half angle for emitted beam divergence 22.4 milli radians.*

The divergence of the beam at the distance of 25 mm would indicate a FWHM of ~ 2.25 mm. This light illuminated only a portion of the detection cell that was placed over the 8 mm diameter window of the PMT, this was not the most efficient use of the LED light. However the straight detection cell was used for the majority of the experiments.

8.6.4 Bandpass light filter

This coloured glass filter had the effect of also reducing the transmitted light by ~ 20% at 340 nm, the peak of the LED. However, the bandpass filter transmission width matched the required emission of the LED. The spectra from the LED in combination with the long pass and band pass filters are shown in figure 8.25, and assessed using an Avantes AvaSpec 2048 spectrophotometer. This normalised emission intensity shows a reduction in transmission of ~ 20% when using the bandpass filter, as indicated from the data sheet.

It can be seen in the spectrum of the unfiltered LED that there is some emission at wavelengths greater than 400 nm. Light in this region would, if allowed, mask to some degree the fluorescence emission from the tricyclic isoindole. The U340 bandpass filter can be seen to eliminate or at least reduce this to an acceptable level. Also shown on the

spectrum is the effect of placing the longpass filter between the LED and the spectrophotometer, both with and without the bandpass filter, showing the efficiency of the filter.

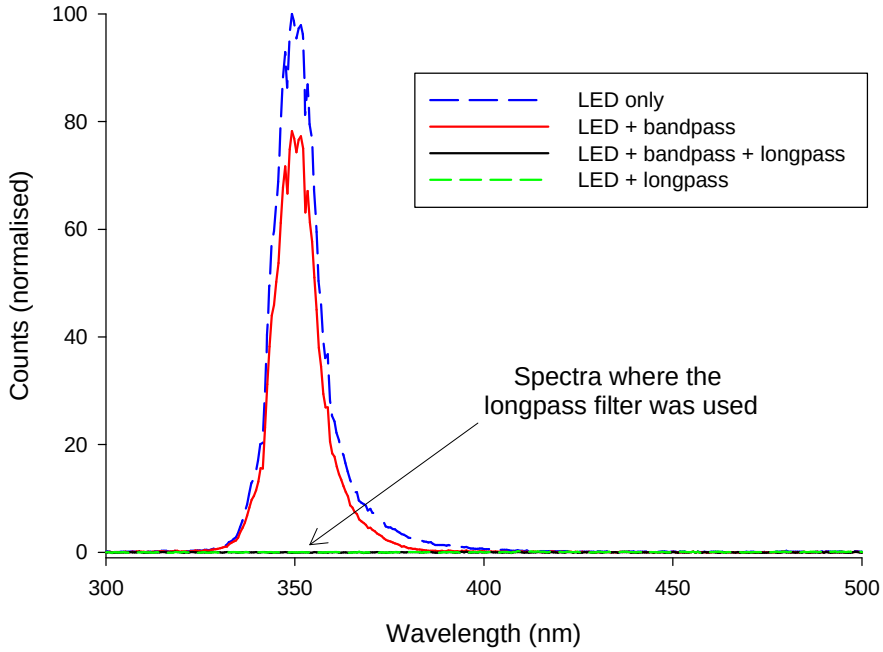

Figure 8.25. *Emission spectra of LED using different filter combinations captured using the Avantes AvaSpec 2048 photospectrometer. The emission intensity has been normalised to LED only.*

8.6.5 Modulating the LED

To reduce the effect of electrical background noise, a lock-in-amplifier (also called a phase sensitive detector) was incorporated, this had the secondary advantage of decreasing the effect of any ambient light which may enter the enclosure. For the lock-in-amplifier to operate the LED needed to be modulated, this was set at 1 kHz with a 50% duty cycle. The optical power of the modulated LED at a distance of 30 mm was measured, producing 35 µwatts without the bandpass filter and 27 µwatts with the filter, the filter reduced the power by ~ 23%, this power output being similar to the mercury lamp (this lamp being continuous wave) with the monochrometer at setting #1. However, the mercury lamp and monochrometer required the setting #4 (~ 130 µwatts) to produce the higher fluorescence response seen in figure 8.19.

8.7 Design of a portable system

After assessing the chemistry and apparatus, the components were assembled into the enclosure. The enclosure, described in the previous chapter, provided a platform to bring together the apparatus and afforded protection against the elements and at the same time acted as a barrier against the ingress of unwanted light. Within the enclosure all the chemicals could be housed, apart from the analyte which was introduced using one of the pumps. This allowed the analytical cycle to occur without having to breach the enclosure. For the initial experiments the pumps, valves, LED and PMT were controlled manually via external switches and the results recorded using a data logger. In the final experiments these were all automated through a pre-programmed computer controlled cycle.

For this automated portable fluorimeter to perform repeat analyses over a period of time, it was advantageous that five main criteria were met:

(i) The microfluidic system had the ability to be flushed through using purified water.

(ii) A pre mixed standard could be tested at desired times to validate of the system.

(iii) The microfluidic channels remained free from blockages.

(iv) Each analytical cycle could be performed within a limited time period.

(v) That the use of reagent and standard was kept to a minimum.

(vi) Air bubbles were kept out of the microfluidic system.

Several variations of enclosure set ups were tested and as difficulties were encountered with the earlier versions, rearrangements and changes to the components were necessary to fulfill the above criteria.

8.7.1 Instrument design No.1

The apparatus was organized into instrument design No.1, shown in figure 8.26. This allowed the use of two pumps which could be operated in tandem or separately, this in conjunction with valves could create several options for the pumping regime; mixing the analyte and OPA for analysis, testing the pre mixed standard and flushing part or all of the system with water.

However, despite the efficient speed control of the pump, an uneven flow still occurred. Although it was possible to match the speed of the two pumps at 5 revolutions per

minute (~ 30 µL min^{-1} for each pump), it was however found that the ratio of flow between the two pumps could vary in volumetric output by up to a ratio of ~ 60:40. Furthermore, at the higher flow rate required to purge the system with water, the liquid pressure increased. Principally due to the small channel size of the micro-reactor, this in turn affected the pumping efficiency of the more flexible silicone tubing. It was found that one pump could dominate, forcing its liquid not only through the micro-reactor but also back along through the tubing of the other pump and into the other vessels, cross contaminating the chemicals. This problem occurred with either both pumps on or with one on and the other stationary.

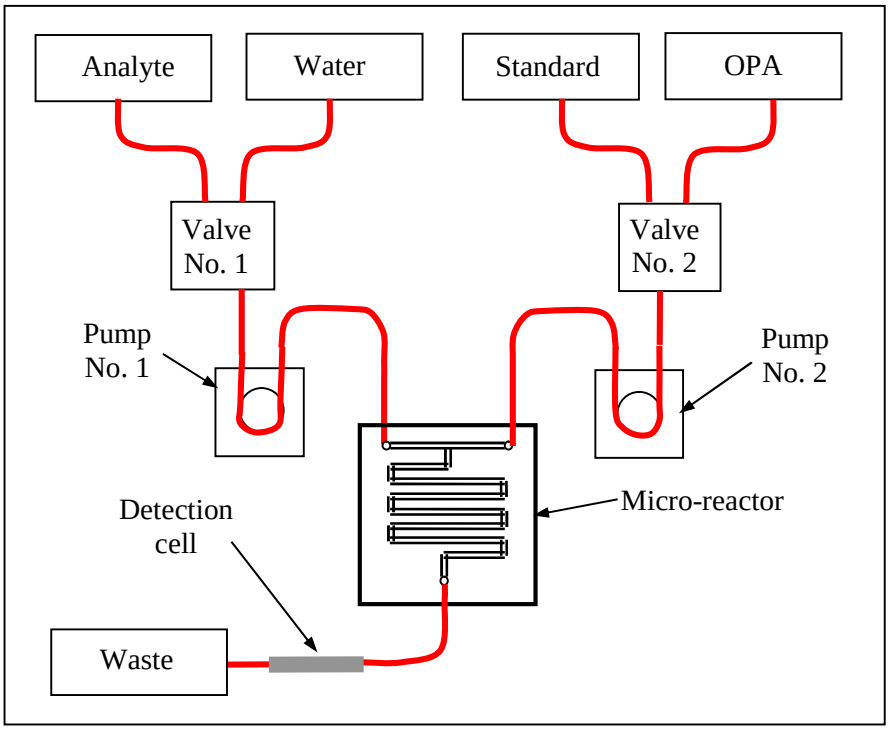

Figure 8.26. *Diagram of instrument design No.1 using two pumps, also illustrated are the locations of the valves and detection cell. The LED and PMT have been omitted for clarity.*

In this experiment and in previously ones, a serpentine micro-reactor (micro-reactor No.1, shown in figure 8.1) with a channel length of 260 mm was used, to ensure diffusion of the analyte and reagent. However to reduce the high pressure created by this length of micro-channel, this micro-reactor was replaced by one with a channel length of 135 mm (micro-reactor No.2, shown in figure 8.1), again with similar internal cross section. Having the same channel dimensions as the previous micro-reactor a similar diffusion time was required. To achieve diffusion within the micro-reactor, the volumetric flow rate needed to be slower at 14 µL min^{-1}. However, at the higher flow

rates required to flush the microfluidic system, similar problems of one pump dominating still occurred.

8.7.2 Instrument design No.2

To overcome the problems caused through using two pumps prior to the micro-reactor, the arrangement was altered. A single pump was placed after the detection cell so that the fluid was drawn through the system; the set-up is illustrated in figure 8.27 and referred to as instrument design No.2. This set up relied upon analyte and OPA being drawn through the microfluidic system in equal quantities. This in itself depended upon both parts of the tubing system being of equal length and free from flow restrictions, such as sharp bends in the tube.

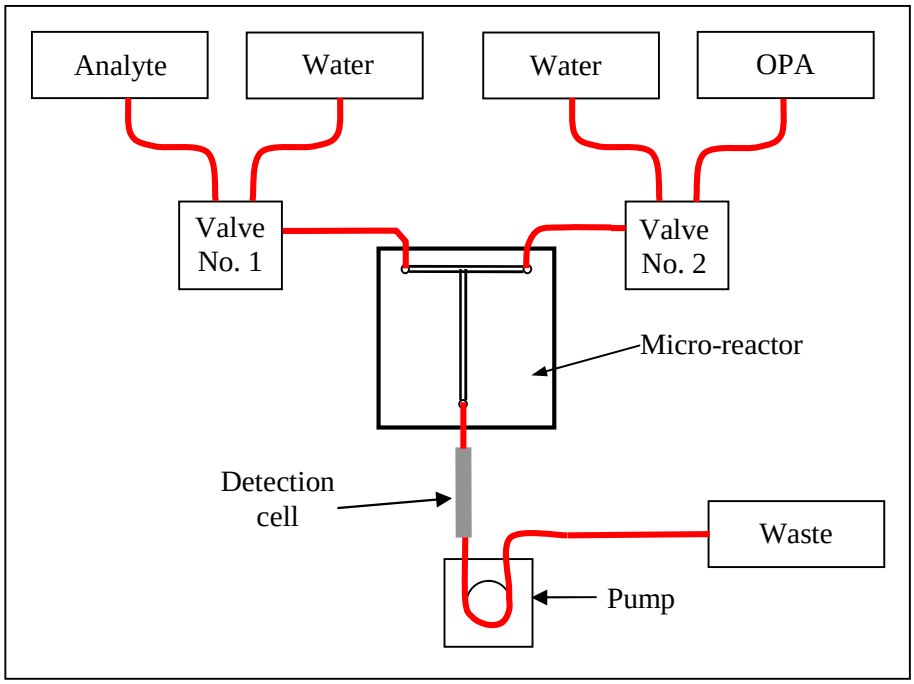

Figure 8.27. *Instrument design No.2, showing the pump positioned after the detection cell where the fluid is drawn through the system. Here the micro-reactor No. 3 is illustrated.*

With the micro-reactor No.2 being used, the pump was adjusted to deliver ~ 15 µL min^{-1} to achieve diffusion within the channels. The flow needed to purge the system was required to be at a faster rate, however, with this quicker flow, small air bubbles were found in the tubes, possibly entering through one of the tube connections. As these air bubbles reached the detection cell, the light detected by the PMT increased. As noted in previous experiments, light scatter from the air bubbles can produce a high background signal and as these new air bubbles became trapped within the detection cell the

fluorescence detection system was compromised. Similar problems with bubbles remaining in the optical cuvette had been noted by other workers [139].

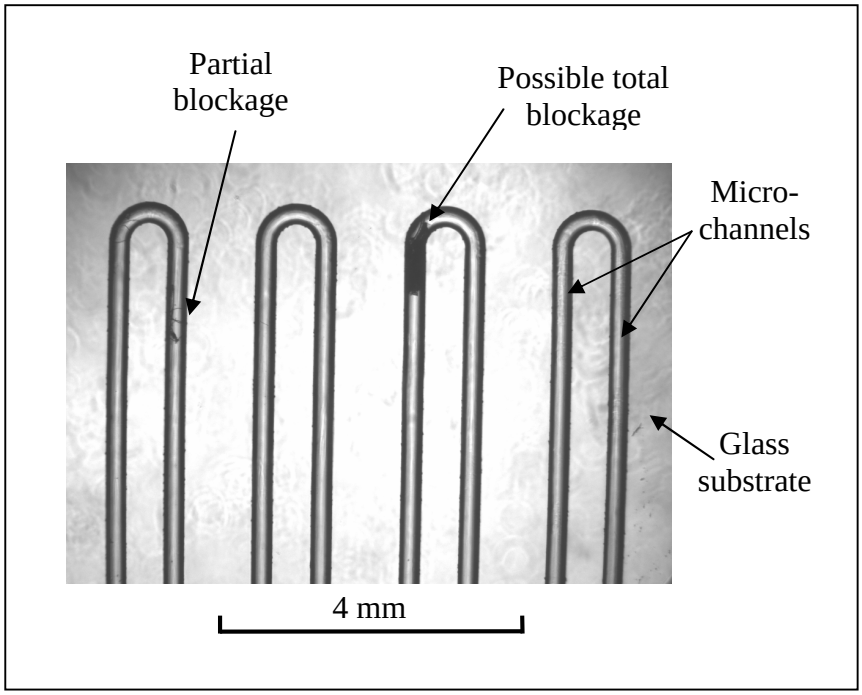

Figure 8.28. *Photograph of the micro-reactor No.2 showing a partial and total blockage of the channel. × 50 magnification.*

A secondary problem which occurred within the micro-channels was blockages, either partial or total. Over time, as liquid passed along the micro-reactor, materials can became trapped, though through regular cleaning these can be removed, avoiding the build-up of a major constriction. The photograph in figure 8.28 shows two obstructions within the micro-channel. Any partial blockage will affect the flow, increasing the resistance to the liquid movement, this in turn further distorts the volume pumped. A total blockage will stop the experiment entirely. As these blockages occurred whilst using purified water, drawing in water from the environment regardless of the filtration system would inevitably increase the possibility of blockages, particularly over prolonged periods of analysis and the use of micro-reactors for such a task appeared problematic for a reliable automated system.

Increasing the channel width and depth of the micro-reactor would reduce the occurrence of any blockages and decrease the pressure gradient. To this end a third micro-reactor was used, micro-reactor No.3 shown in figure 8.1. This had a straight mixing channel 15 mm long and a larger cross section, however a residence time

sufficient for diffusion to occur required a volumetric flow rate of 1.8 µL min^{-1}. This slow fluidic rate was unrealistically low to allow time for repeat analyses in a 15 minute analytical cycle and as such another approach was needed.

8.7.3 Moving away from the micro-reactor

The problem of the pressure gradient across the micro-reactor was created through the higher flow rates necessary to flush the microfluidic system. These pressures have been modelled, using equation (7.4), and are shown in figure 8.29. The calculated pressure gradients show the effect of two microfluidic systems, each using a different micro-reactor (No.1 and No.3), having different channel lengths and cross sectional areas. These were incorporated into a system at two flow rates, where the pump being situated at the beginning of the tubing and an open outlet at the end. It can be seen that the higher flow rate significantly increases the pressure when small micro channels are used. Increasing the channel cross sectional area (in the case of micro-reactor No.3), greatly reduces the pressure gradient at both flow rates. The reduction in back pressure has influenced flow rate for other systems [172].

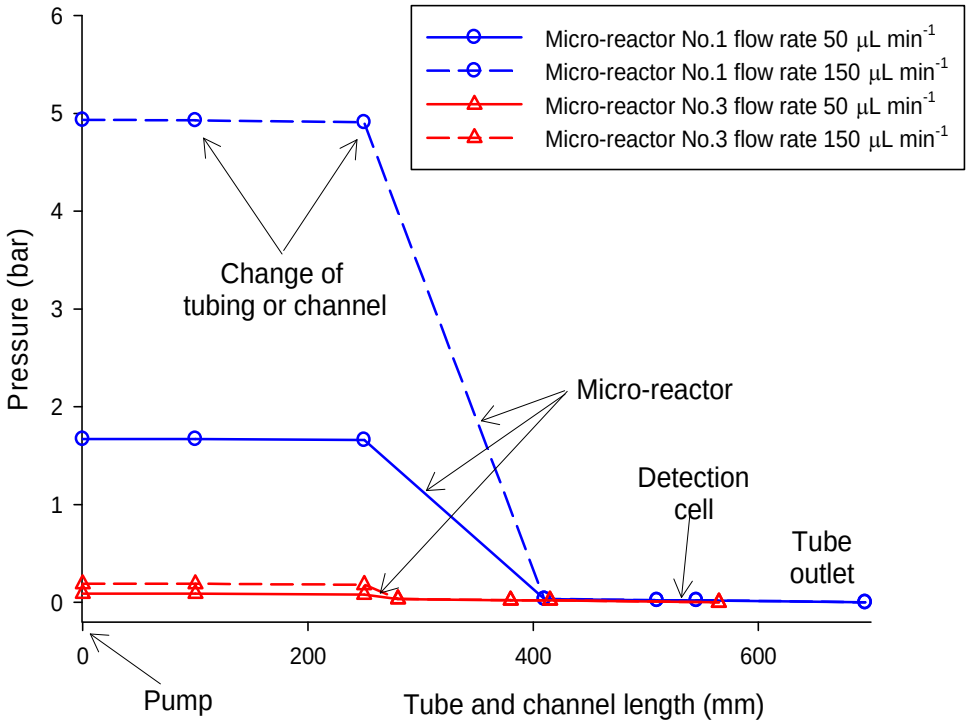

Figure 8.29. *Calculated pressure changes as liquid is pumped through the tubing and micro-reactor channel at volumetric flow rates of 50 and 150 µL min^{-1}. Dimensions of micro-reactors, detection cell are as in table 8.1.*

As a consequence of using a shorter channel length micro-reactor (with a larger cross section), there was insufficient time for total diffusion to occur within the micro-reactor, and therefore the reason to incorporate this particular component into the microfluidic system was no longer warranted. Combining the two tubes which carried the separate chemicals was achieved through the use of a Tee connector (discussed in 8.1.2).

The internal dimensions of the tubing and their material have been summarised in table 8.1 and the maximum flow rate required for diffusion to occur for the three micro-reactors is shown. It can be seen that the tubing dimensions are much greater than those of the micro channels of the micro-reactor with the consequence of reducing both the pressure gradient and the possibility of blockages. For diffusion to occur solely within the detection cell, a diffusion time of ~ 14 minutes would be required (using the parameters and equation 7.3 discussed in 7.2.2). The time needed for diffusion to occur was investigated and is discussed in the following section.

8.7.4 Instrument design No.3

Through replacing the micro-reactor with a Tee connector, a single pump could be placed immediately after the valves and before the joining Tee. By using the dual Instech tubing with pump No.1, the chemicals could be drawn through evenly. The layout for this arrangement is shown in figure 8.30 and referred to as instrument design No.3, this was to be the final arrangement needed. With the absence of a micro-reactor, the higher flow rates required to flush the system was possible. Using pump No.1 at 20 revolutions per minute created a combined flow for the analyte and reagent of 150 μL min^{-1} (75 μL min^{-1} per tube) producing a Reynolds number in excess of 5000. This high flow rate created mixing through turbulent flow.

Whilst the detection cell had a volume of 30 μL, it has been shown that a much larger volume was needed to purge this cell of the analyte. Using the flushing method of continuously pumping water, a volume ≥ 300 μL was needed, this has been shown in section 8.6.2. To be able to perform repeat analyses within a reasonable time limit, the volume needed to be pumped at a rate of 100 to 150 μL min^{-1}.

The consequences of using a single pump at this position meant that when the pump was activated, chemicals from two sources would always be drawn, reducing the selectivity that was originally desired from instrument design No.1. However, the

dependability of an equal quantity of chemicals and the ability to be able to pump at the flow rate required for flushing the system, compensated for the less predictable turbulence mixing times that occurred from using the Tee connector.

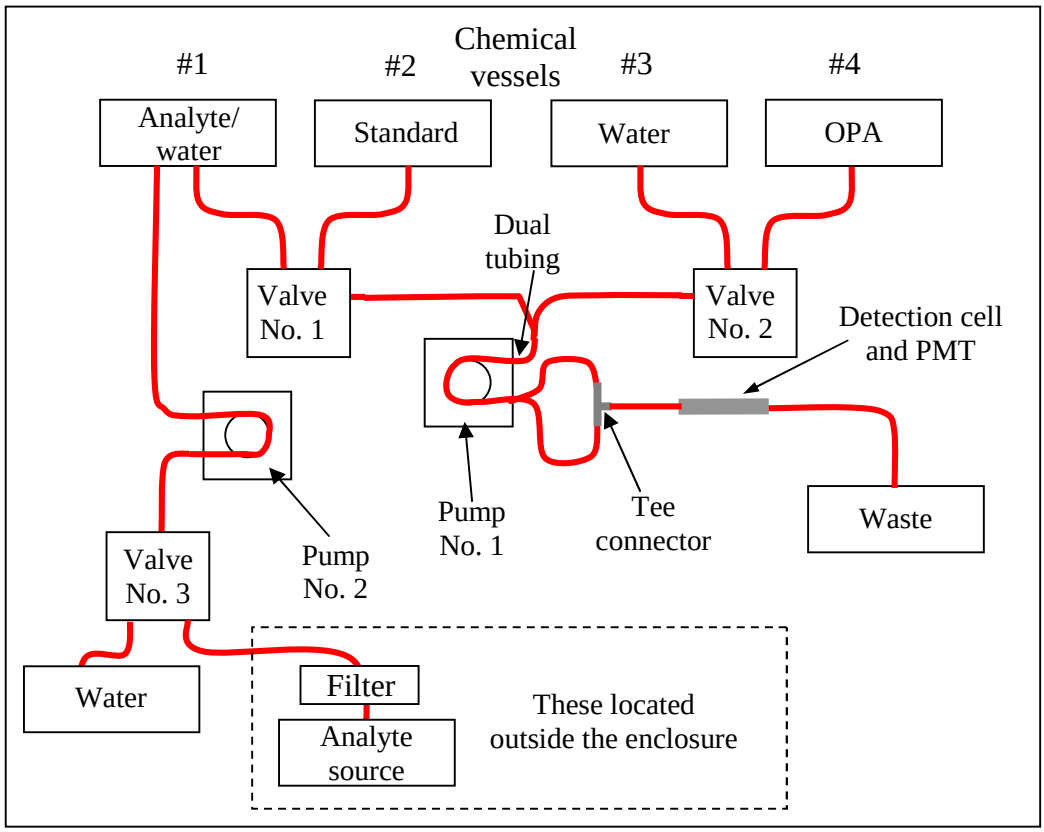

Figure 8.30. *Diagram of instrument design No.3 showing the pumps, valves and detection cell, the LED and PMT have been omitted for clarity. The tubing indicates the path of the chemicals.*

(i) Function of the pumps and valves

The functions of the pumps and valves and the sequence of analysis are described below:

At the start of each analytical cycle pump No.2 (positioned on the left of figure 8.30) was used to draw the analyte from outside the enclosure, passing it through a filter (positioned before valve No.3) and into the analyte chemical vessel #1. This pump, through using the larger ID Instech tubing at 22 revolutions per minute, would drive the liquid at ~ 150 µL min^{-1}. From this point pump No.1 propelled the analyte and OPA from chemical vessel #1 and #4, into the detection cell. A sufficient volume of analyte was required so that the tube which carried to the detection cell was immersed at all times during this pumping phase, this was to ensure that no air bubbles were drawn into the microfluidic system, the consequences of which have previously been discussed.

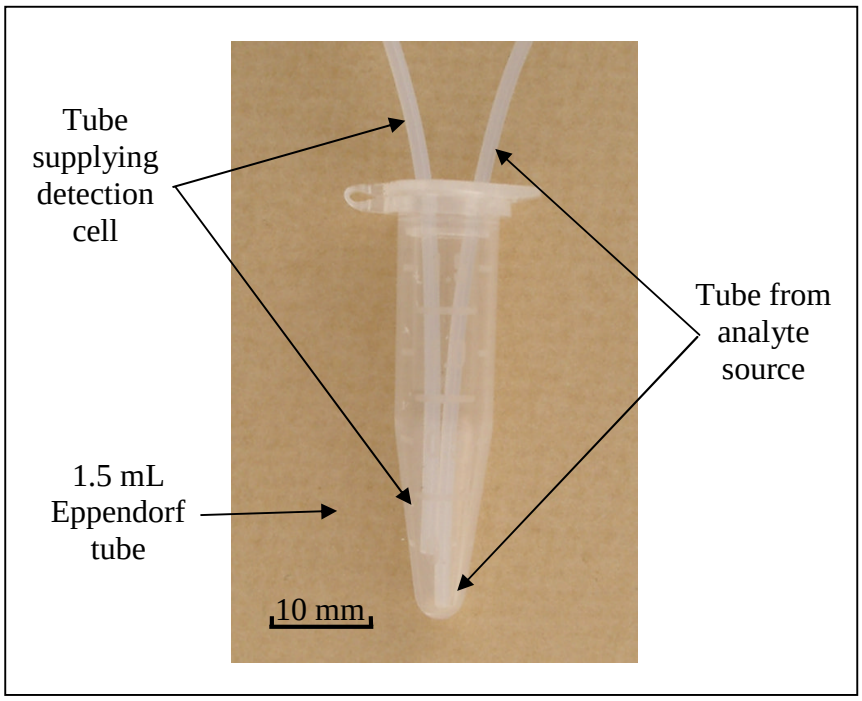

Figure 8.31. *Photograph of the tapered 1.5 mL Eppendorf tube, showing the positioning of the tubing used to deliver and remove the liquids.*

After the required analyte had been drawn into the detection cell, pump No.2 was then reversed and the remaining analyte was emptied back into the water source. Valve No.3 was switched and water was pumped by pump No.2 into the container previously used by the analyte. This water was used during the flushing process. Chemical vessel #1 (during the many analytical cycles) was repeatedly used to hold the different analyte samples. Through this arrangement, there was the possibility of cross contamination. However, by careful placement of the tubes within chemical vessel #1 and through using the flushing water to aid cleaning, no incidences of contamination were recorded, although a more sensitive analytical device may have found the contrary. Figure 8.31 shows the positioning of the tubes; the tube which supplied the detection cell was ~ 5 mm above the tube delivering and subsequently removing the surplus analyte and flushing water. By placing this tube at the base of the tapered 1.5 mL Eppendorf tube all the liquid could be removed. Air that entered the tubing of pump No.2 was of no consequence as it would not enter the analytical microfluidic system.

Once the analyte and OPA had been pumped into the detection cell and after a period to allowing mixing, the LED and PMT were activated and the results recorded. Following each analysis, the tubing and detection cell were flushed using water.

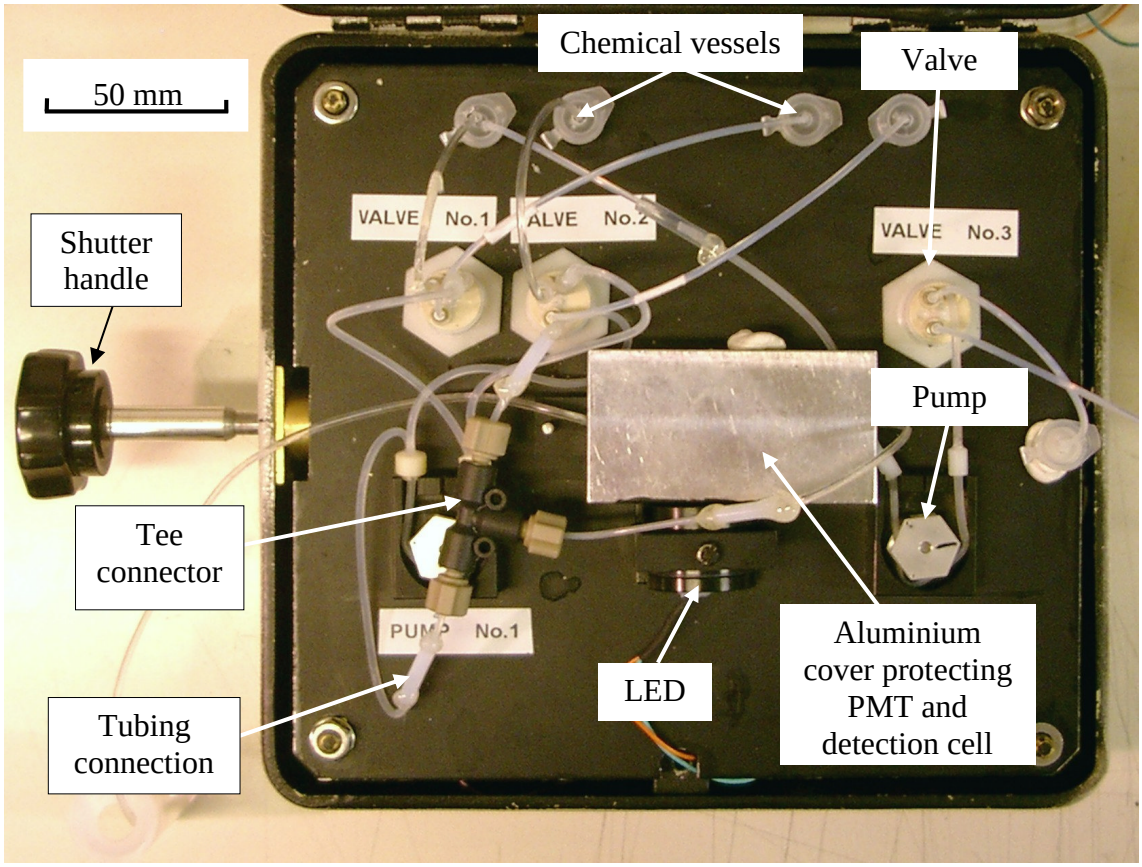

Figure 8.32. *Photograph of the instrument design No.3. The lid of the enclosure is open to show the pumps, valves, tubing and position of the LED and PMT.*

To validate and test the system was functioning correctly, the standard was periodically checked. This pre prepared standard of the tricyclic isoindole was pumped from chemical vessel #2 and water from chemical vessel #3, effectively diluting by half the molarity of the standard. Once the standard was assessed, the microfluidic system was again flushed with water in preparation for the next analysis. At this point, the excess flushing water in chemical vessel #1 was removed by reversing pump No.2.

A photograph of enclosure set up No.3 is shown in figure 8.32, here the lid of the enclosure is open. The handle on the left manually opens the shutter to expose the PMT, this was normally open during the analytical cycles. The lengths of tubing shown could eventually be reduced once the various experimental settings were finalised, however during the development process it was advantageous to leave these extended. One of the tubing connections is highlighted, the long term use of these connections gave reliability problems. Only one of the three valves and one of the two pumps is noted.

The importance of the internal volumes of the tubing and components is related to the timing of the pumps and, as such, the quantity of the chemicals used. The volumes of the tubing and components from instrument design No.3 are shown in table 8.3. The total volume of the analytical microfluidic system from the containers to the detection cell is ~230 μL. However the tubing may eventually be reduced in length once variations in the set up are finalised. The length of the sampling tube would eventually depend upon the system of sampling.

Position of tube or component	Tube type	Length (mm)	Volume of component (μL)
Chemical / valve	Lee	180	10.3 × 2
Valve/pump/Tee	Instech (dual)	300	34.0 × 2
Tee	PEEK	20	38.00
Tee/cell	n/a	140	9.9
Detection cell	Glass tube	30	94.2
		Total volume	230.7 μL

Sampling tube	Elkay/Instech	325 + 300	78.5
		Total volume	78.5 μL

Table 8.3. *This table shows the tubing and component dimensions and volumes and the total volume for the analytical microfluidic system and sampling tube system.*

(ii) Assessment of mixing time

To assess the time needed for mixing the analyte and reagent, the analyte and reagent were pumped into the detection cell and allowed to stand whilst the fluorescence intensity was monitored using the data logger. After four minutes the pump was restarted and the system was flushed using water, the results of which are shown in figure 8.33. The standing time is indicated on the graph, during this period the fluorescence intensity does not significantly alter, indicating that the analyte and reagent had mixed prior to or during entry into the detection cell. However, the peak intensity occurred once the pump was restarted, this was initially attributed to an isoindole, which produced higher fluorescence intensity, possibly through improved mixing within the tubing, was being pumped into the detection cell. This proved not to be the case (this phenomenon appearing to some degree in later experiments) but was a result of the

internal profile of the detection cell. The water which was in the detection cell prior to the analysis appeared not to be totally replaced by the incoming analyte and reagent and the effect of the separation bubble (previously discussed in 8.6.2) partially diluted the fluorophore.

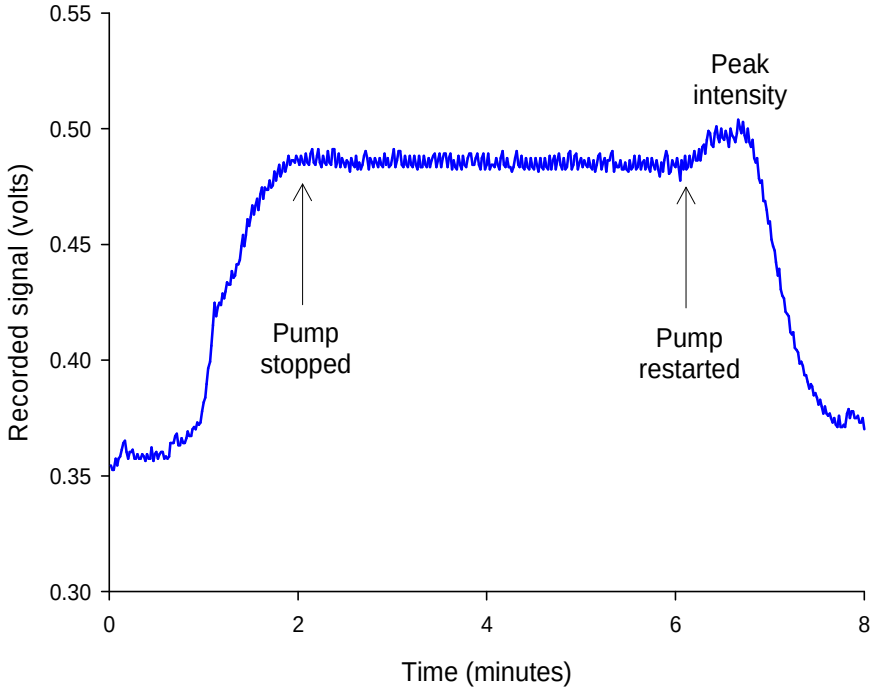

Figure 8.33. *Graph showing the results of the fluorescence as 100μM tricyclic isoindole is pumped into the detection cell. The peak intensity is indicated as the pump was restarted.*

Once the pump was restarted, the GSH and OPA which was residing in the tubing replaced the contents of the detection cell and produced a fluorescence intensity peak approximately 10% greater. After which the water flushing the system purged the detection cell of the fluorophore. From this experiment it was concluded that a standing time of ~ 30 to 60 seconds was sufficient prior to fluorescence analysis. The GSH used for this experiment had been prepared ~ one hour earlier to the analysis, accounting for the marginally reduced signal which would normally have been expected from a 100μM solution.

(iii) Manual control of analytical cycles

Having established the time for the analysis, further experiments were undertaken to confirm the viability of the set up. Pump No.1 and valves No.1 and 2 were manually controlled and the pump speed set to deliver 75 μL min^{-1} per tube (total rate 150 μL

min^{-1}). GSH was prepared with water at 10, 25, 50 and 100 μM and a standard solution was prepared using 100 and 200 μM GSH and OPA. The detection cycle is shown in table 8.4.

Step	Time (minutes)	Pump	Task (indicated on graph)	Volume per task (μL)
1	2.00	On	GSH and OPA pumped	300
2	1.00	Off	Reaction monitored	0
3	2.00	On	System flushed with water	300
4	-	Off	Change chemicals	0
5	Repeat analysis			

Table 8.4. *Showing the different tasks and the time interval for each analytical run. The quantities of the liquid used for each task is also indicated with the pump speed at150 μL* min^{-1}.

The results from the experiment recorded by the data logger are shown in figure 8.34. Between each analysis the LED and PMT were switched off (the fall in recorded signal is shown on the graph between each set of results). The analytical cycle can be seen as each of the analyte samples were mixed with OPA and entered the detection cell. This was followed by a period of no pumping, after which flushing with water reduced the light signal back to the original background intensity.

The abbreviations in the results shown in figure 8.34 are expanded in table 8.5. During the flushing process, water was drawn from both tubes.

Analysis abbreviation	Chemical passing through each tube	
	Tube 1	Tube 2
GSH# - OPA	GSH# = μM of GSH	OPA
ST100 – ST100	Standard using 100μM GSH	Standard using 100μM GSH
ST100 - water	Standard using 100μM GSH	Water
ST200 - water	Standard using 200μM GSH	Water
OPA - water	OPA	Water

Table 8.5. *Showing how the various combinations of analyte, OPA standards and water were drawn into the microfluidic system for fluorescence analysis.*

A blank sample of water and OPA was measured to show that only the addition of GSH produced a fluorescence response. Mixing the prepared standard of ST-200 with water simulated a mixture of 100µM GSH sample and reagent. This particular analysis not only tested whether the LED and PMT were working correctly but also assessed that each of the dual tubes were flowing at the same or similar rate, indicating that the tubing was free from blockages.

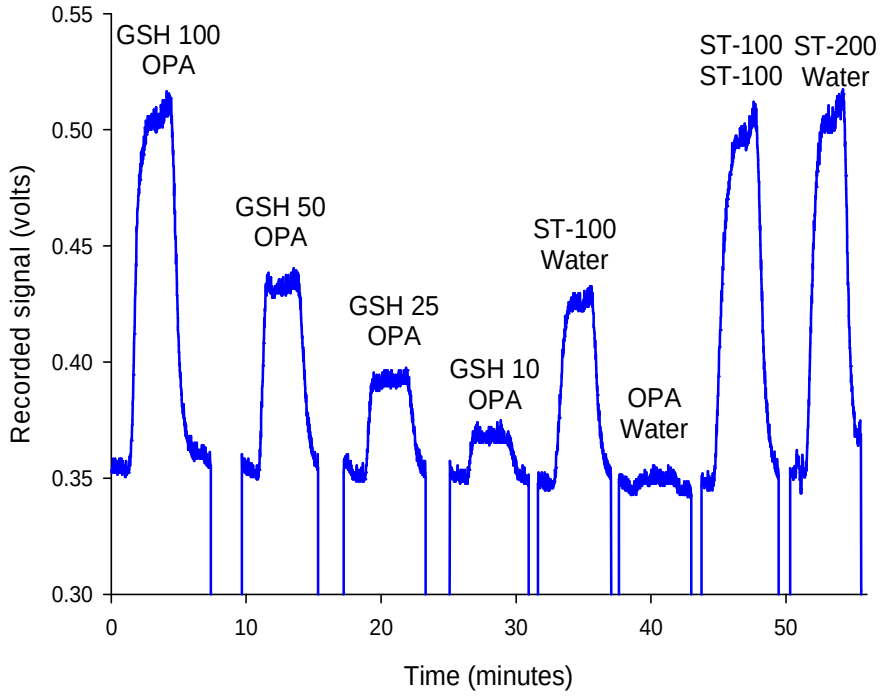

Figure 8.34. *Graph showing the fluorescence intensity signal recorded by a data logger as the different GSH molarities and standards were analysed.*

Any reading not in the 0.5 to 0.55 volt range for this particular analysis would have indicated a fault to the system, either in the microfluidics or the electronics. Whereas the fluorescence response of the standard ST-100 being pumped through both tubes would have only tested the electronic components, while a fault in the microfluidics (such as a blockage or disproportionate flow from each tube) would not have been identified. A 50:50 ratio flow rate through the two tubes was crucial for these experiments.

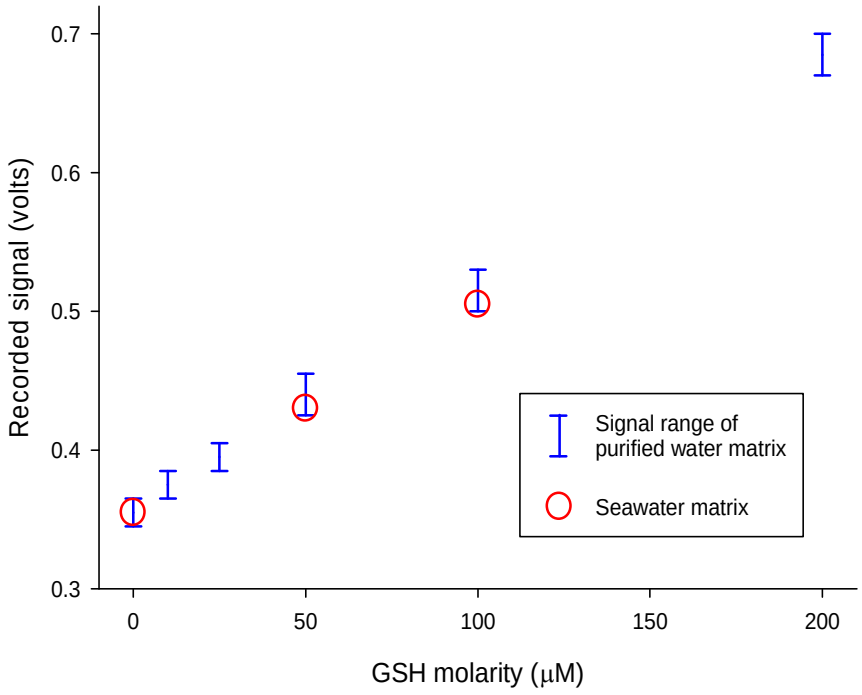

Figure 8.35. *Range of fluorescence intensities logged for the different GSH molarities in a purified water matrix from several experiments. Also results from a spiked and control seawater matrix.*

The fluorescence intensity for the last 30 seconds of the stationary phase was further analysed and the range of this signal is shown in figure 8.35 as purified water matrix. The response appearing linear over the molarity examined. The linearity of these 30 second analyses was the basis for the timings intended for an automated system.

(iv) Investigation of reproducibility of instrument design over 5 days

Following the experiment using the different GSH molarities, the fluorimeter was assessed for its viability over a five day period. On the first day OPA was prepared and divided into two samples; one stored at room temperature (~ 15°C) and the other stored in a refrigerator. Each day a fresh sample of GHS was made at 50 and 100 μM. On the first day a standard was prepared by mixing GSH at 200 μM and OPA, the resulting tricyclic isoindole was also stored at room temperature.

Each day several analytical cycles were performed to check the reproducibility of the fluorimeter. This was done by analysing the fluorescence response of the analyte and reagent against the standard. It was found through visual observation that the reagent OPA which had been stored in the refrigerator had crystallised, resulting in the corruption of the reagent. However, these crystals could be re-dissolved through

immersing the flask containing the reagent in warm water. After which the reagent worked correctly, this would reduce the lower working temperature of the system in the field. The reagent which had been stored at room temperature had not crystallised and functioned correctly. An electric device could be incorporated into the system to keep the reagent at a suitable temperature. The results for each day's experiments were found to lay within the range shown in Figure 8.35.

(v) Assessment of sample matrix

Up to this point the analyte had been prepared using purified water. For this fluorimeter to be deployed in a marine environment, an assessment of analyte prepared from sea water was required. Sea water collected from Filey Brigg on the East Yorkshire coast and brought back to the laboratory. The following day this was filtered using the Millex filter unit, described in 8.1.7. Samples of GSH were prepared in the usual way but instead of using purified water the filtered sea water was used. Molarities of 50 and 100 μM were made plus a non spiked control.

These samples were analysed in the fluorimeter with the reagent as described in table 8.4. The results are shown in figure 8.35 and labelled as seawater matrix. Each of the spiked samples and the control lay within the range previously seen in the results for the purified water experiments, indicating $\geq$ 95 % recovery.

Further to direct sampling of sea water, a quantity of water was taken from a tank in the Biology Department at Hull University, containing *Platynereis dumerilii*, a sea ragworm. This water sample, again after filtering and with no further conditioning, was investigated in the fluorimeter. This sample when mixed with the reagent produced no signal above the baseline, indicating no background presence of the analyte.

Task No.	Time (min-sec)		Pump No.1	Valve		Pump No.2	Valve No.3	LED/PMT analysis	Description	Chemical usage (µL) *±5%			
	Period	Total		No.1	No.2					Analyte	Water	OPA	Standard
1	1.30	1.30	Off	1	1	On	1	Off	Draw in analyte	-	-	-	-
2	2.00	3.30	On	1	2	Off	1	Off	Pump analyte/OPA	150	-	150	-
3	0.30	4.00	Off	1	1	Off	1	Off	Reaction time	-	-	-	-
4	0.30	4.30	Off	1	1	Off	1	On	Analysis	-	-	-	-
5	1.30	During 3/4	Off	1	1	Reverse	1	Off	Empty analyte	-	-	-	-
6	3.00	During 6/7	Off	1	1	On	2	Off	Add water	-	-	-	-
7	2.00	8.30	On	1	1	Off	1	Off	Purge system	-	300	-	-
8	2.00	10.30	On	2	1	Off	1	Off	Mix standard	-	150		150
9	0.30	11.00	Off	1	1	Off	1	On	Test standard/water	-	-	-	-
10	2.00	12.00	On	1	1	Off	1	Off	Purge system	-	300	-	-
11	1.30	14.30	Off	1	1	Reverse	1	Off	Empty water	-	-	-	-
12	0.30	15 min	All off							Totals			
Repeat cycle										150	750	150	150

Table 8.6. *Shown on the table are the sequence and timings for the pumps, valves and LED/PMT for analysis of the analyte and premixed standard. The quantities of chemical required are shown on the right (* variation found due to pump tubing). When only testing the analyte, tasks 8, 9 and 10 may be omitted and the 3 minutes of pumping in task 6 need only be 1 minute 30 seconds.*

(v) Sequencing and volumes for automated control of the analytical cycle

The tasks for the automated control of the fluorimeter have been listed in table 8.6, along with a time period and description for each event. These sequences and timings have been deduced from the experiments previously shown. The total volumes required for the cycle are, 150 µL each for the analyte and reagent and a further 300 µL of purified water. Testing the standard to confirm that the system is functioning correctly requires a further a 150 µL each of the premixed standard and purified water, this again would need 300 µL of purified water to purge the tubing and detection cell. However, testing the system would not be necessary for each analytical cycle, completing the analysis in 8 minutes and 30 seconds.

8.8 Conclusions

The steps involved in the development of this fluorimeter examined the chemistry of the GSH and the fluorescence reaction with the reagent OPA. First using laboratory equipment, then by replacing the light source and detector, the individual parts needed to be able to perform the detection in a portable system were introduced. Through manually controlling the components, analytical cycles could be run allowing the necessary assessment of the apparatus and pump speeds for controlling the flow rate; all this was necessary to produce the timing schedule which was required to automate the system. Changing the excitation light from the mercury lamp to the LED produced a lower fluorescence response when using the straight detection cell. However, the repeatability of the results from the analytical cycles could with confidence determine the GSH concentration within the range of molarities tested.

The problems encountered when joining the dissimilar tubing types which were required to match the different components proved to be a persistent source of leaks. The leaks which occurred regularly when using the micro-reactors were greatly reduced once that particular component was taken out of the system, being replaced by a much simpler tee connector. This allowed the liquid pressure inside the tubing to be lower and also eliminated the blockages which were occurring in the micro channels of the micro-reactor. When comparing the pre prepared standards with those mixed within the microfluidic tubing, this reduced system appeared not to have any effects upon the fluorescence analysis.

With the existing set up, the consumption of the reagent and analyte each, at 150 µL, may be reduced through decreasing the lengths of tubing between the valves, tee connector and detection cell. The tubes had been left at these lengths for the convenience of trying different configurations of the various instrument designs.

Both of the controls, the collected sea water and the tank sample, showed no fluorescence response. Whilst the spiked samples produced results similar to those prepared using the purified water, thus demonstrating that this method of fluorescence detection of GSH was suitable for deployment in a sea water environment.

9. Conclusions

This research resulted in the development of two types of environmental detectors, based around analysing a water/liquid medium in remote or unattended locations. Both of these detectors were designed to distinguish when pre-determined thresholds had been reached or exceeded. Reliability over the period of use was an important factor in their development, however the addition of failsafe and self checking components were able to promote confidence for their potential deployment. By the very nature of monitoring events in changeable settings, an awareness of the range of conditions encountered needed to be factored into the design to achieve reliability and consequently lead to trustworthy results, this being particularly important in automated systems.

The interceptor oil level detector was designed to certain specifications. The device had to be free from both electrical components within Zone 0 and of moving parts which could come into contact with the liquid inside the interceptor. Furthermore, the final device needed be able to be inexpensive. In producing a detector, capable of monitoring continuously for up to six months without attendance in a harsh demanding environment, the types of oils that could be encountered needed to be evaluated. Thereby when different detection methods were examined in the laboratory, an assessment of their suitability to function in the expected range of conditions could be made to discount the inappropriate techniques.

After reviewing the existing methods used for detection within the oil and other related industries, a number of possible techniques were decided upon where further investigation was worth pursuing. Several of these techniques were quickly dismissed as too expensive to automate, such as the viscosity method, or were unlikely to work throughout the range of oils likely to be encountered, as was the case with fluorescence. Additionally, other optical methods which had been successfully reported were found to be incompatible for use over long periods of time due to fouling of the optical windows. This accumulation of oil particles and other debris was a problem that was overcome though using the density and pressure detection technique.

Detection through pressure differential relied upon the variation in density between oil and water as the means of determining the accumulation of oil. The oil density ranged

from 13% to 25% below that of water. By using pressure probes, the problems previously encountered though a slow build up of a contaminating film was found to be insignificant. Relaying the pressure to the transducer and to the diaphragm through the use of air reduced the need of additional components, further simplifying the system. The lengths of tubing needed for the pressure transducer detector posed the only weakness of this particular method, however the small volume of gas lost through permeability through the walls of the tubing was adequately compensated for by an improved probe design. The robustness and simplicity of the double probe system was shown to work successfully during the extended trials. The optical diaphragm detector, through placing the detection of the differential pressure within the sensor head thus eliminating gas loss from permeability, relied upon fibre optic cables connected to the monitor to relay the state of the interceptor. The more delicate part of this method lay in the mechanism of the optical sensor, although once securely installed this did not prove to be problematic.

Both pressure detection techniques required the installation of tubing or cables to connect the monitor at a convenient and safe distance from the interceptor, to the sensor within the interceptor. Any disruption to these connections would, through the failsafe mechanisms incorporated in the detectors, be able to inform the operator of a fault. Similarly, through the design of the monitor system, the consequence of the interceptor not being refilled with water or experiencing a leak, the monitor would identify that the detected signal was out of the normal range and indicate attention required.

The oil interceptor detector was required to determine the presence of an immiscible liquid within a confined volume, in contrast, the portable fluorimeter was required to establish the presence of a substance dissolved in open or moving water. This was coupled with the fact that the analyte may rapidly deteriorate, thus requiring a regular sampling programme. Detecting a substance which would not readily separate required a detection method that was selective for the particular analyte.

The detection of GSH, which was used as a model analyte upon which to base the portable fluorimeter, has, due to its importance in control of biological systems, been well documented. The novel approach in this research took an existing detection method, which used OPA to produce a fluorophore, and incorporated this into a

microfluidic detection system capable of an automated analysis system that would be able to test samples unattended over several days.

Following the evaluation of the chemistry and assessing the optical spectra for the fluorescence process, the components required to miniaturise the system were chosen. The instruments were placed into an enclosure; this acted as a container to house the apparatus and also as a suitable dark box keeping out the ambient light. The problem of using an excitation light in the UV wavelength was that the material of the analytical cell and everything else within the immediate vicinity was particularly prone to fluorescing if made from an unsuitable material. The consequence of which would be to produce an unintended background signal, which would affect the lower limit of detection or totally masked the fluorescent signal entirely. With this in mind, the analytical cell was made from fused silica with the connecting tubing placed at a suitable distance. The aluminium cover which held the analytical cell in position above the PMT also served the purpose of shielding components from the UV light, whilst also providing extra protection to the PMT from incident illumination, this being in addition to the use of a lock-in amplifier.

To be able to perform repeat analyses within a specified period of time (and for this particular analyte around fifteen minutes was considered suitable), the system required a flow rate sufficient to fill the detection cell, with a capacity of ~ 90 µL, with the analyte and reagent, followed by flushing with water. This required a flow rate of sufficient volume to complete the cycle within the allotted time. In the earlier experiments, the analyte and reagent were mixed using a micro-reactor, incorporated within the microfluidic system. However, the tubing in conjunction with the micro-reactor proved to be quite problematic, insomuch as the flow rates required during part of the analytical cycle were restricted due to the size of the micro channels. The micro-reactor channels, where diffusion to occur during the slower flow rate, created a high pressure gradient within the tubing system at the faster flow rates. Using shorter channel lengths or larger channel dimensions were still insufficient to avoid the large increase in pressure and leakages or tube damage frequently occurred. The secondary problem of using the micro-reactor were blockages within the micro channels, which in a system expected to analyse samples of water from the environment and even with a filtration system, were not considered consistently dependable for incorporation into an automated detector expected to function for several days. Replacing the micro-reactor with a tee connector

allowed the high flow rates required during the flushing process and reduced the problem of obstructions in the fluidic system. As a result, the mixing of the analyte and reagent relied upon turbulent flow and diffusion as these liquids entered the detection cell, however, this proved not to be problematic.

This sensor, as with the interceptor detectors, incorporated the capacity to assess whether the components within the system are functioning correctly. Through testing a known prepared standard, the fluorescence signal received would either fall into the expected limits or fall outside this range, thus determining the state of the detector and the validity of the results.

The levels of excitation light from the LED were reduced compared to those from the mercury lamp, thus raising the limit of detection to 10 µM of GSH. However, the final analytical set-up produced results which were repeatable within the range of 10 to 100 µM and a linear response within this range was observed, providing a detection system capable of determining the threshold levels of the analyte which were sought.

Future work

The oil detector for use within an interceptor has been taken to a stage where it has been handed to Andel Ltd to develop into a commercial model. However, the construction of the fibre optic detector could be simplified by utilising a smaller core multimode fibre, which would avoid the use of a mask.

The portable fluorimeter would benefit from further development to two parts of the micro fluidic system. The pumping mechanism, which used the miniature peristaltic pumps to convey the liquid, may through the considering the incorporation of piston pumps, replacing the peristaltic pumps. As a consequence, increase the volumetric precision for the mixing of the two liquids and increase the reliability through not relying upon the tubing flexibility, which was shown to deteriorate over time. A secondary benefit of eliminating the tubing from this section of the micro fluidics would be to increasing the lifetime of the detector through the elimination of these wearing parts. The second area that requires further development is the analytical cell. Here an improved design was produced but not incorporated due to limitations in time.

10. Appendix A. Optical and physical properties of water and various oils

	Density kg m^{-3}	Boiling point ˚C	Refractive index *	Dynamic Viscosity N s m^{-2}	Dielectric constant F m^{-1}
Air	1.247 (10˚C) [78] 1.226 (15˚C) [78]	N/A	1.00 [78]	1.8×10^{-5} (18˚C) [78]	1.00 [78]
Pure water	1000 (4˚C) [78] 999 (15˚C) [78] 998 (20˚C) [78]	100 [78]	1.33 [182]	1.569×10^{-3} (4˚C) [78] 1.139×10^{-3} (15˚C) [78] 1.002×10^{-3} (20˚C) [78]	80.37 (20˚C) [78]
Diesel (DERV)	820 (15˚C) [183]	180-390 [183]	1.462 [58] 1.460 **	2.7×10^{-3} [183]	2.1 [184]
Red diesel	As for DERV	As for DERV	1.478 **	As for DERV	As for DERV
Gas oil	820 (15˚C) [185]	180-390 [185]	1.436 [58]	As for DERV	2.1 [184]
Petrol	750 (15˚C) [186]	25-215 [186]	1.419 [58]	$0.4\text{-}1.1 \times 10^{-3}$ [92]	2.0-2.2 [184]
Paraffin	800 [79]	Not determined	1.43 [79] 1.44 [182]	1.6×10^{-3} [187]	1.6 2.5 [184]
New motor oil	870 [188]	Not determined	1.477 **	224×10^{-3} [99]	2.1-2.4[189]
Used motor oil	850 - 870 **	Not determined	No result	175×10^{-3} [99]	Not determined
Samples from Andel Ltd	845 - 855 **	Not determined	No result	Not determined	Not determined

*Refractive index at wavelength 589.3 nm, at or near 293K.

** Determined in the laboratory

11. Appendix B. Pressure conversion table

Units	Pascal (Pa)	Bar (bar)	milliBar (mbar)	Pound/sq.inch (psi)	Atmosphere (atm)	Torr (mm Hg)	*Metres depth/unit	**Units per metre
1 Pa	≡ 1 N/m^2	0.00001	0.01	1.45038×10^{-4}	9.8692×10^{-6}	7.5006×10^{-3}	0.000102	9806.6
1 bar	100 000	≡ 10^6 dyn/cm^2	1000	14.50377	0.98692	750.06	10.197	0.9806
1 mbar	100	0.001	≡ 10^3 dyn/cm^2	1.45038×10^{-2}	9.8692×10^{-4}	0.75006	0.0102	98.066
1 psi	6894	0.06894	68.947	≡ 1 lbf/in^2	0.068046	51.715	0.703	1.422
1 atm	101 325	1.01325	1013.25	14.6959	≡ 1 atm	760	10.332	0.0968
1 torr	133.322	1.3332×10^{-3}	1.3332×10^{-6}	19.337×10^{-3}	1.3158×10^{-3}	≡ 1 mm Hg	0.0136	73.529

Pressure from the pascal to the bar converts exactly, the others are given in approximate terms.
*Depth for 1 unit, in metres of water (at 1000 kg m^{-3}).
**Units per metre of water (at 1000 kg m^{-3}).
At sea level, 30 m of altitude ≈ 350 Pa ~ 3.5 mbar

12. References

[1] R. A. Bailey, H. M. Clark, J. P. Ferris, S. Krause, and R. L. Strong, eds., *Chemistry of the Environment*, 2nd Ed, Academic Press, New York, (2002).

[2] R. Reeve, *Introduction to Environmental Analysis*, John Wiley and Sons, Ltd., Chichester, UK, (2002).

[3] R. M. Harrison, ed., *Pollution: Causes, Effects and Control*, 3rd Ed, The Royal Society of Chemistry. Cambridge, (1996).

[4] M. K. Hill, *Understanding Environmental Pollution*, Cambridge University Press, Cambridge, (1997).

[5] J. W. Kirchner, X. Feng, C. Neal, and A. J. Robson, *Hydroligical Processes*, **18,** 1353 (2004)

[6] D. MacDougall, W. B. Crummett, and et al, *Guidelines for Data Acquisition and Data Quality Evaluation in Environmental Chemistry, Analytical Chemistry*, **52,** 2242 (1980)

[7] P. C. F. C. Gardolinski, H. Grady, E. P. Achterberg, M. Gledhill, A. D. Tappin, W. A. House, and P. J. Worsfold, *Water Res*, **35,** 3670 (2001)

[8] G. Hanrahan, S. Ussher, M. Gledhill, E. P. Achterberg, and P. J. Worsfold, *Trends in Analytical Chemistry*, **21,** 233 (2002)

[9] C. E. Lenehan, N. W. Barnett, and S. W. Lewis, *The Analyst*, **127,** 997 (2002)

[10] N. W. Barnett, C. E. Lenehan, and S. W. Lewis, *Trends in Analytical Chemistry*, **18,** 346 (1999)

[11] S. J. Haswell, *The Analyst*, **122,** 1R (1997)

[12] A. Manz, N. Graber, and H. M. Widmer, *Sensors and actuators B*, **1,** 244 (1990)

[13] L. Marle and G. M. Greenway, *Trends in Analytical Chemistry*, **24,** 795 (2005)

[14] F. R. Connor, *Noise*, 2nd Ed, Edward Arnold, London, (1992).

[15] T. Coor, *Journal of Chemical Education*, **45,** A533 (1968)

[16] R. Blanc, A. González-Casado, A. Navalón, and J. L. Vilchez, *Analytica Chimica Acta*, **403,** 117 (2000)

[17] D. A. Skoog, F. J. Holler, and T. A. Nieman, *Principles of Instrumental Analysis*, 5th Ed, Brooks/Cole USA, (1998).

[18] M. J. Nahorniak and K. S. Booksh, *Analyst*, **131,** 1308 (2006)

[19] L. A. Currie, *Analytical Chemistry*, **40,** 586 (1968)

[20] T. Coor, *Journal of Chemical Education*, **45,** A583 (1968)

[21] J. R. Webster, M. A. Burms, D. T. Burke, and C. H. Mastrangelo, *Analytical Chemistry*, **73,** 1622 (2001)

[22] J. R. Lakowicz, *Principles of fluorescence spectroscopy*, Springer, New York, (2006).

[23] D. A. Skoog and J. J. Leary, *Principles of Instrumental Analysis*, 4th Ed., Saunders College Publishings, Orlando, (1992).

[24] E. Hecht, *Optics*, 4th Ed., Addison-Wesley, Reading, (2002).

[25] B. Herman, *Fluorescence Microscopy*, 2nd Ed., BIOS Scientific Publishers Ltd., Oxford, (1998).

[26] D. Meschede, *Optics, Light and Lasers*, Wiley-VCH, Weinheim, (2004).

[27] P. K. Dasgupta, I.-Y. Eom, K. J. Morris, and L. J, *Analytica Chimica Acta*, **500,** 337 (2003)

[28] R. W. Cattrall, *Chemical Sensors*, Oxford University Press, Oxford, (1997).

[29] M. J. Usher and D. A. Keating, *Sensors and transducers : characteristics, applications, instrumentation, interfacing*, Macmillan, Basingstoke, (1996).

[30] D. A. Krohn, *Fiber Optic Sensors Fundamentals and Applications*, Instrument Society of America, NC, USA, (1988).

[31] E. Udd, *Fiber Optic Sensors. An Introduction for Engineers and Scientists*, John Wiley and Sons, Inc. New York, (1991).

[32] M. D. Marazuela and M. C. Moreno-Bondi, *Analytical Bioanalytical Chemistry*, **372,** 664 (2002)

[33] T. O. Myers and I. M. Bell, *IEEE 14th International Mixed-Signal, Sensor and Systems Test Workshop. IMS3TW2008.*, (2008)

[34] Safety of laser products, PD AEC TR 60825-14:2004, (2004).

[35] Environment Agency, Pollution Prevention Guidelines, PPG3, (2005).www.p2pays.org/ref/16/15218.pdf (accessed 18/10/2005)

[36] Andel Ltd., New Mills, Broughham Road, Huddersfield, West Yorkshire. HD7 6AZ.

[37] EU Waterframe Directive, Waterframe Note 2, (2000).http://ec.europa.eu/environment/water/water-framework/index_en.html, (accessed 07/09/2008)

[38] C. L. B. Guedes, E. Di Mauro, V. Antunes, and A. S. Mangrich, *Marine Chemistry*, **84,** 105 (2003)

[39] R. M. Garratt, I. J. Pickering, C. E. Haith, and R. C. Prince, *Environmental Science and Technology*, **32,** 3719 (1998)

[40] M. D'Auria, R. Racioppi, and V. Velluzzi, *journal of Chromatographic Science*, **46,** 339 (46)

[41] R. F. Lee, *Spill Science Techology Bulletin*, **8,** 157 (2003)

[42] R. C. Prince, R. M. Garratt, R. E. Bare, M. J. Grossman, T. Townsend, J. M. Suflita, K. Lee, E. H. Owens, G. A. Sergy, J. F. Braddocks, J. E. Lindstrom, and R. R. Lessard, *Spill Science Techology Bulletin*, **8,** 145 (2003)

[43] T. K. Dutta and S. Harayama, *Environmental Science and Technology*, **34,** 1500 (2000)

[44] The International Tanker Owners Pollution Federation Ltd (ITOPF), Technical information paper, (2002). http://www.itopf.com/fate.html, (accessed 21/4/2006).

[45] R. M. Harrison, ed., *Pollution : Causes, Effects and Control*, 3rd Ed., The Royal Society of Chemistry, Cambridge, (1995).

[46] European Union Water Framework Directive 2000/60/EC, (2000).http://ec.europa.eu/environment/water/water-framework/index_en.html, (accessed 15/01/2008)

[47] Environment Agency, Pollution Prevention Guidelines, PPG1, (2005).www.p2pays.org/ref/16/15218.pdf (accessed 18/4/2006)

[48] Environment Agency, Pollution Prevention Guidelines, PPG2, (2004).http://www.environment-agency.gov.uk/commondata/acrobat/ppg02feb04_126893.pdf, (accessed 08/09/2008)

[49] Environment Agency, Water quality, (2006).http://www.environment-agency.gov.uk/subjects/waterquality/?lang=_e, (accessed 18/4/2006)

[50] C. Vázquez, A. B. Gonzalo, S. Vargas, and J. Montalvo, *Sensors and Actuators A*, **116,** 22 (2004)

[51] Environment Agency, Pollution Prevention Guidelines, PPG19, (2005).www.p2pays.org/ref/16/15218.pdf (accessed 18/4/2006)

[52] ATEX Guidelines, Directive 94/9EC, (2005).http://europa.eu.int/comm/enterprise/atex/guide/guidesec_en.pdf, (accessed 20/11/2005)

[53] M. Milani, F. P. Pucillo, M. Ballerini, M. Camatini, M. Gualtieri, and S. Martino, *Materials Characterization*, **52,** 283 (2004)

[54] Afriso Euroguage Ltd., East Grinstead, West Sussex. England, (2005). http://www.eurogauge.co.uk/, (accessed 22/11/2005).

[55] P. Raatikainen, I. Kassamakov, R. Kakanakov, and M. Luukkala, *Sensors and Actuators A*, **58,** 93 (1997)

[56] Kobold Instruments,(2005).http://www.koboldmessring.com/_uk/index.htm (accessed 18/11/05).

[57] F. Pérez-Ocón, M. Rubiño, J. M. Abril, P. Casanova, and J. A. Martínez, *Sensors and Actuators A*, **125,** 124 (2006)

[58] S. Roy, *Sensors and Actuators B*, **55,** 212 (1999)

[59] E. Musayev and S. E. Karlik, *Sensors and Actuators A*, **109,** 21 (2003)

[60] Heron Instruments, (2005). http://www.heroninstruments.com/interface_meters/Sm-Oil_meter.html (accessed 18/11/05).

[61] Solinst,(2005).http://www.solinst.com/Prod/122/122d2.html (accessed 18/11/05)

[62] Sandia National Laboratories,(2005).http://www.sandia.gov/news-center/news-releases/2005/optics-lasers/lightsimple.html (accessed 18/11/05).

[63] Optek,(2005).http://www.optek.com/Product_Detail.asp?ProductID=10 (accessed 18/11/05)

[64] T. Hengstermann and R. Reuter, *Applied Optics*, **29,** 3218 (1990)

[65] C. E. Brown and M. F. Fingas, *Marine Pollution Bulletin*, **47,** 477 (2003)

[66] Proceedings of EARSeL-SIG-Workshop LIDAR, Dresden/FRG, June 16-17, 2000. eProceedings No, 1., Dresden/ FRG, 2000.

[67] M. F. Fingas and C. E. Brown, *Spill Science Techology Bulletin*, **4,** 199 (1997)

[68] S. Patsayeva, V. Yuzhakov, V. Varlamov, R. Barbini, R. Fantoni, C. Frassanito, and A. Palucci,Proceedings of EARSel-SIG-Workshop LIDAR, Dresden/FRG, 2000.

[69] M. L. Pascu, N. Moise, and A. Staicu, *Journal of Molecular Structure*, **598,** 57 (2001)

[70] P. Karlitschek, F. Lewitzka, U. Bünting, M. Niederkrüger, and G. Marowsky, *Appl. Phys. B*, **67,** 497 (1998)

[71] Turner Designs,(2005).http://www.oilinwatermonitors.com/ (accessed 18/11/05)

[72] Sigrist Process-Photometer,(2005).http://www.photometer.com (accessed 18/11/05)

[73] J. Bublitz, M. Dickenhausen, M. Grätz, S. Todt, and W. schade, *Applied Optics*, **34,** 3223 (1995)

[74] Laser-Laboratorium Göttingen e.V. ,(2005).http://www.llg-gmbh.de/english/products/fluorimeter_en.htm (accessed 18/11/05)

[75] D. Patra and A. K. Mishra, *Analytica Chimica Acta*, **454,** 209 (2002)

[76] J. L. Beltrán, R. Ferrer, and G. J., *Analytica Chimica Acta*, **373,** 311 (1998)

[77] D. M. Rayner and A. G. Szabo, *Applied Optics*, **17,** 1624 (1978)

[78] D. R. Lide, ed., *CRC Handbook of Chemistry and Physics*, 83rd Ed., CRC Press Inc., (2002).

[79] R. M. Tennant, ed., *Science Data Book*, 25th Impression, Oliver and Boyd, Essex, (2004).

[80] *Filtration and Separation*, **44,** 13 (2008)

[81] Gems Sensors and Controls, Basingstoke. Hampshire, UK, (2008). www.gemssensors.com, (accessed 22/08/2008).

[82] A. S. Morris, *Measurement and Instrumentation Principles*, Butterworth-Heinemann, Oxford UK, (2001).

[83] Impress Sensors and Systems, Thatcham, Berkshire, England, (2005). http://www.impresssensors.co.uk/, (accessed 25/11/2005).

[84] Arjay Engineering Ltd., (2000). http://www.arjayeng.com/, (accessed 25/11/2005).

[85] D. C. Giancoli, *Physics for Scientists and Engineers*, 4th Ed., Pearson Education Inc. N.J. USA, (2008).

[86] K. H. Chang and Y. J. Lee, *Metrologia*, **41,** S95 (2004)

[87] J. A. Ibáñez-Mengual, R. P. Valerdi-Pérez, and J. A. García-Gamuz, *European Journal of Physics*, **29,** 53 (2008)

[88] A. Tomiyama, G. P. Celata, S. Hosokawa, and S. Yoshida, *International Journal of Multiphase Flow*, **28,** 1497 (2002)

[89] D. A. Krohn, *Fiber optic sensors - fundanentals and applications*, Instrument Society of America, NC. USA, (1988).

[90] E. Udd, *Fiber Optic Senors - An Introduction for Engineers and Scientists*, Jonh Wiley and Sons Inc., New York, (1991).

[91] M. H. Majles Ara, S. H. Mousava, E. Koushki, S. Salmani, A. Gharibi, and A. Ghanadzadeh, *Journal of Molecular Liquids*, **142,** 29 (2008)

[92] ConocoPhillips, MSDS, Unleaded Petrol, (2006). http://www.conocophillips.co.uk/fuels/specs/msds/index.htm (accessed 3/5/2006),

[93] R. T. Morrison and R. N. Boyd, *Organic Chemistry*, 6th Ed., Prentice Hall Inc., New Jersey, (1992).

[94] A. Barbaro, G. Cecchi, and P. Mazzinghi, *Applied Optics*, **30,** 852 (1991)

[95] R. C. Smith and K. S. Baker, *Applied Optics*, **20,** 177 (1981)

[96] D. W. Green, J. O. Maloney, and R. H. Perry, *Perry's Chemical Engineers' Handbook*, 6th Ed., McGraw-Hill, New York ; London, (1984).

[97] M. Krzan, K. Lunkenheimer, and K. Malysa, *Colloids and Surfaces A: Physicochemical and Engineering Aspects*, **250,** 431 (2004)

[98] P. V. O'Neil, *Advanced engineering mathematics*, 5 th. Ed., Thomson Brooks/Cole, Pacific Grove, Calif. ; London, (2003).

[99] National Park Service, Nature and Science. U.S. Department of the Interior,(2003).http://www.nature.nps.gov/hazardssafety/toxic/list.cfm,(accessed 11/10/2005).

[100] F. A. Jenkins and H. E. White, *Fundamentals of Optics*, 4th. Ed., McGraw-Hill International Book Co., New York, (1981).

[101] National Physical Laboratory (2006) Historic Barometric Pressure Data, Online Barograph,(2006).http://www.npl.co.uk/pressure/pressure-history.html (accessed 11/12/2006).

[102] R. W. Fox, A. T. McDonald, and P. J. Pritchard, *Introduction to fluid mechanics*, Wiley, New York, N.Y. ; London, (2004).

[103] Cole-Palmer (Catalogue 2007/08). Hanwell, London.

[104] D. J. Harrison, A. Manz, Z. Fan, H. Lüdi, and H. M. Widmer, *Analytical Chemistry*, **64,** 1926 (1992)

[105] R. J. Holmes, P. Summersgil, T. Ryan, B. J. T. Brown, A. Mockbil, B. D. Grieve, and P. R. Fielden, *Journal of Food Science*, **74,** N37 (2009)

[106] G. J. Watson, M. G. Bentley, S. M. Gaudron, and J. D. Hardege, *Journal of Experimental Marine Biology and Ecology*, **294,** 169 (2003)

[107] E. Camera and M. Picardo, *Journal of Chromatography B*, **781,** 181 (2002)

[108] G. Wu, Y.-Z. Fang, S. Yang, J. R. Lupton, and N. D. Turner, *The Journal of Nutrition*, **134,** 489 (2004)

[109] A. Meister, *Science*, **220,** 472 (1983)

[110] A. R. T. S. Araujo, M. L. M. F. S. Saraiva, and J. L. F. C. Lima, *Talanta*, **74,** 1511 (2008)

[111] B. A. Neuschwander-Tetri and F. J. Roll, *Analytical Biochemistry*, **179,** 236 (1988)

[112] K. Havel, K. Pritts, and t. Wielgos, *Journal of Chromatography A*, **853,** 215 (1999)

[113] W. Kamencic, A. Lyon, P. G. Paterson, and B. H. J. Juurlink, *Analytical Biochemistry*, **286,** 35 (2000)

[114] J. C. Deutsch, C. R. Santhosh-Kumar, and J. F. Kolhouse, *Journal of Chromatography A*, **862,** 161 (1999)

[115] K. J. Lenton, H. Therriault, and J. R. Wagner, *Analytical Biochemistry*, **274,** 125 (1999)

[116] J. L. Ram, C. T. Müller, M. Beckmann, and J. D. Hardege, *The FASEB Journal*, **13,** 945 (1999)

[117] E. Zeeck, C. T. Müller, M. Beckmann, J. D. Hardege, U. Papke, V. Sinnwell, F. C. Schroeder, and W. Francke, *Chemoecology*, **8,** 33 (1998)

[118] J. D. Hardege, H. Bartlets-Hardege, C. T. Müller, and M. Beckmann, *Peptides*, **25,** 1517 (2004)

[119] R. Al-Farwati and C. M. G. Van Den Berg, *Environmental Science and Technology*, **35,** 1902 (2001)

[120] D. Tang, M. M. Shafer, D. A. Karner, J. Overdier, and D. E. Armsrtong, *Environmental Science and Technology*, **38,** 4247 (2004)

[121] R. F. Whitehead, S. de Mora, S. Demers, and M. Gosselin, *Limnology and Oceanography*, **45,** 278 (2000)

[122] T. Almgren and I. Hagström, *Water Research*, **8,** 395 (1974)

[123] L. M. Laglera and C. M. G. van den Berg, *Marine Chemistry*, **101,** 130 (2006)

[124] A. R. Bowie, E. P. Achterberg, P. N. Sedwick, S. Ussher, and P. J. Worsfold, *Environmental Science and Technology*, **36,** 4600 (2002)

[125] X. Xu, L. Li, and S. G. Webster, *Trends in Analytical Chemistry*, **26,** 68 (2007)

[126] R. R. Moore, C. E. Banks, and R. G. Compton, *The Analyst*, **129,** 755 (2004)

[127] P. C. White, N. S. Lawrence, J. Davis, and R. G. Compton, *Electroanalyst*, **14,** 89 (2002)

[128] A. Salimi and S. Pourbeyram, *Talanta*, **60,** 205 (2003)

[129] K. A. Howell, E. P. Achterberg, C. B. Braungardt, A. D. Tappin, P. J. Worsfold, and D. R. Turner, *Trends in Analytical Chemistry*, **22,** 828 (2003)

[130] M. Koller and H. Eckert, *Analytica Chimica Acta*, **352,** 31 (1997)

[131] C. C. Yan and R. J. Huxtable, *Journal of Chromatography B*, **672,** 217 (1995)

[132] J. Zhang, Z. Hu, and X. Chen, *Talanta*, **65,** 986 (2005)

[133] N. Yamashiro, S. Uchida, Y. Satoh, Y. Morishima, H. Yokoyama, T. Satoh, and R. Yamada, *Journal of Nuclear Science and Technology*, **41,** 890 (2004)

[134] P. C. F. C. Gardolinski, A. R. J. David, and P. J. Worsfold, *Talanta*, **58,** 1015 (2002)

[135] S. Gabmann, I. Ibendorf, and L. Pagel, *Sensors and Actuators A*, **133,** 231 (2007)

[136] S. Lee, O. Sohn, Y. Yim, K. Han, G. W. Hyung, S. H. Chough, and J. I. Rhee, *Talanta*, **68,** 187 (2005)

[137] A. Economou, *Trends in Analytical Chemistry*, **24,** 416 (2005)

[138] G. Marshall, D. Wolcott, and D. Olson, *Analytica Chimica Acta*, **499,** 29 (2003)

[139] C. M. McGraw, S. E. Stitzel, J. Cleary, C. Slater, and D. Diamond, *Talanta*, **71,** 1180 (2007)

[140] C. R. Koch, J. D. Ingle, and V. T. Remcho, *Twelfth International Conference on Miniaturized Systems for Chemistry and Life Sciences, San Diago, USA*, (2008)

[141] M. Sequeira, M. Bowden, E. Minogue, and D. Diamond, *Talanta*, **56,** 355 (2002)

[142] V. H. Cohn and J. Lyle, *Analytical Biochemistry*, **14,** 434 (1966)

[143] A. P. Senft, T. P. Dalton, and H. G. Shertzer, *Analytical Biochemistry*, **280,** 80 (2000)

[144] M. C. G. Alvarez-Coque, M. J. M. Hernandez, R. M. V. Camanas, and C. M. Fernandez, *Analytical Biochemistry*, **178,** 1 (1989)

[145] J. R. Benson and P. E. Hare, *Proc. Nat. Acad. Sci. USA*, **72,** 619 (1975)

[146] M. Roth, *Analytical Chemistry*, **43,** 880 (1971)

[147] B. D. Wagner and G. J. McManus, *Analytical Biochemistry*, **317,** 233 (2003)

[148] K. Lewicki, S. Marchant, L. Matoub, J. Lulek, J. Coulon, and P. Leroy, *Talanta*, **70,** 876 (2006)

[149] C. Cereser, J. Guichard, J. Drai, E. Bannier, I. Garcia, S. Boget, and A. Revol, *Journal of Chromatography B*, **752,** 123 (2001)

[150] R. N. Puri and R. Roskoski, *Analytical Biochemistry*, **173,** 26 (1988)

[151] P. J. Hissin and R. Hilf, *Analytical Biochemistry*, **74,** 214 (1976)

[152] W. A. Jacobs, M. W. Leburg, and E. J. Madaj, *Analytical Biochemistry*, **156,** 334 (1986)

[153] O. Orwar, H. A. Fishman, N. E. Ziv, R. H. Scheller, and R. N. Zare, *Analytical Chemistry*, **67,** 4261 (1995)

[154] B. R. Munson, D. F. Young, and T. H. Okiishi, *Fundamentals of Fluid Mechanics*, 5th Ed., John Wiley & Sons, Inc., NJ. USA, (2006).

[155] P. Watts and C. Wiles, *Chem Commun*, **5,** 443 (2007)

[156] K. J. Laider, J. H. Meiser, and B. C. Sanctuary, *Physical Chemistry*, 4th Ed, Houghton Mifflin Company, Boston, (2003).

[157] G. L. Duveneck, A. P. Abel, M. A. Bopp, G. M. Kresbach, and M. Ehrat, *Analytica Chimica Acta*, **469,** 49 (2002)

[158] T. Kamei, B. M. Paegel, J. R. Scherer, A. M. Skelley, R. A. Street, and R. A. Mathies, *Analytical Chemistry,* **75,** 5300 (2003)

[159] B. Kuswandi, Nuriman, J. Huskens, and W. Verboom, *Analytica Chimica Acta*, **601,** 141 (2007)

[160] L. Novak, P. Neuzil, L. Pipper, Y. Zhang, and S. Lee, *Lab on a Chip,* **7,** 27 (2007)

[161] J.-L. Fu, Q. Fang, T. Zhang, X.-H. Jin, and Z.-L. Fang, *Analytical Chemistry*, **78,** 3827 (2006)

[162] E. Verpoorte, *Lab on a Chip*, **3,** 42N (2003)

[163] F. S. Ligler, M. Breimer, J. P. Golden, D. A. Nivens, J. P. Dodson, T. M. Green, D. P. Haders, and O. A. Sadik, *Analytical Chemistry*, **74,** 713 (2002)

[164] G. Gauglitz, *Anal Bioanal Chem*, **381,** 141 (2005)

[165] L. Malic and A. G. Kirk, *Sensors and actuators A*, **135,** 515 (2006)

[166] O. Leistiko and P. F. Jensen, *Journal of Micromechanics and Microengineering*, **8,** 148 (1998)

[167] B. H. Welgl and O. S. Wolfbels, *Analytical Chemistry*, **66,** 3323 (1994)

[168] G. M. Greenway, S. J. Haswell, and P. H. Petsul, *Analytica Chimica Acta*, **387,** 1 (1999)

[169] G. M. Greenway, L. J. Nelstrop, and S. N. Port, *Analytica Chimica Acta*, **405,** 43 (2000)

[170] J.-C. Roulet, R. Völkel, H. P. Herzig, E. Verpoorte, N. F. Rooij, and R. Dändliker, *Analytical Chemistry*, **74,** 3400 (2002)

[171] S. Camou, H. Fujita, and T. Fujii, *Lab on a Chip*, **3,** 40 (2003)

[172] L. Marle and G. M. Greenway, *Analytica Chimica Acta*, **548,** 20 (2005)

[173] Y. Saito, J. J. Wang, D. A. Smith, and D. N. Batchelder, *Langmuir*, **18,** 2959 (2002)

[174] C. R. Koch, V. T. Remcho, and J. D. Ingle, *Sensors and Actuators B*, **135,** 664 (2008)

[175] D. J. Laser and J. G. Santiago, *Journal of Micromechanics and Microengineering*, **14,** R35 (2004)

[176] P. Woias, *Sensors and Actuators B*, **105,** 28 (2005)

[177] B. He, L. Tan, and F. Regnier, *Analytical Chemistry*, **71,** 1464 (1999)

[178] A. R. Bowie, E. P. Achterberg, S. Ussher, and P. J. Worsfold, *Journal of Automated Methods and Managemment in Chemistry*, **2,** 37 (2004)

[179] J. Cleary, C. Slater, D. Kim, W. S. Yerazunis, and D. Diamond, *Twelfth International Conference on Miniaturized Systems for Chemistry and Life Sciences, San Diago, USA.*, (2008)

[180] HOYA,Optics Division, HOYA Corporation, USA,(2007).http://www.hoyaoptics.com/color_filter/index.htm (accessed 17/12/2007)

[181] Edmund Optics, York, UK,(2007).http://www.edmundoptics.com/UK/ (accessed 17/12/2007)

[182] A. M. James and M. P. Lord, *Macmillan's chemical and physical data*, Macmillan, London ; Basingstoke, Hants, (1992).

[183] ConocoPhillips, MSDS Auto Diesel DERV, (2003). http://www.conocophillips.co.uk/fuels/specs/msds/index.htm, (accessed 20/2/2006).

[184] (2005).http://www.asiinstr.com/technical/Dielectric%20Constants.htm (accessed 18/11/05),(accessed 18/11/05).

[185] ConocoPhillips, Material Safety Data Sheet, Gas Oil, (2002). http://www.conocophillips.co.uk/fuels/specs/msds/index.htm, (20/2/2006).

[186] AZ, MSDS, Unleaded Gasoline, (2003).

[187] *Measuring Equipment (Liquid fuel and Lubrication) Regulations 1995*, National Weights and Measures Laboratory, Middlesex, UK., (1999).

[188] Castrol(UK)Ltd., Safety Data Sheet, Castrol GTD Magnatec 10W-40, (2002). http://www.conocophillips.co.uk/fuels/specs/msds/index.htm, (accessed 20/2/2006).

[189] (2005).http://www.compsys.com/enews/knewspro.nsf/v/RGAY-52PN9Y (accessed 18/11/05)